

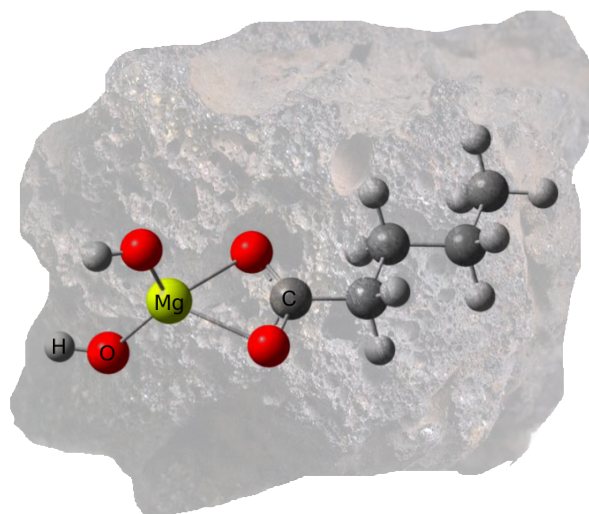
TECHNISCHE UNIVERSITÄT MÜNCHEN



Previously unknown organomagnesium compounds in astrochemical context

Alexander Ruf

Dissertation



TECHNISCHE UNIVERSITÄT MÜNCHEN

Fakultät Wissenschaftszentrum Weihenstephan für Ernährung, Landnutzung und Umwelt
Lehrstuhl für Analytische Lebensmittelchemie

Previously unknown organomagnesium compounds in astrochemical context

Alexander Ruf

Vollständiger Abdruck der von der Fakultät Wissenschaftszentrum Weihenstephan für Ernährung, Landnutzung und Umwelt der Technischen Universität München zur Erlangung des akademischen Grades eines

Doktors der Naturwissenschaften (Dr. rer. nat.)

genehmigten Dissertation.

Vorsitzender: Prof. Dr. Erwin Grill

Prüfer der Dissertation:

1. apl. Prof. Dr. Philippe Schmitt-Kopplin
2. Prof. Dr. Michael Rychlik
3. Prof. Eric Quirico, PhD (Université Grenoble Alpes)

Die Dissertation wurde am 06.12.2017 bei der Technischen Universität München eingereicht und durch die Fakultät Wissenschaftszentrum Weihenstephan für Ernährung, Landnutzung und Umwelt am 18.01.2018 angenommen.

Do we feel less open-minded, the more open-minded we are?
A tribute to sensitivity and resolution...

Acknowledgments

This work has been prepared at the Helmholtz Zentrum München in the research unit Analytical BioGeoChemistry of apl. Prof. Dr. Philippe Schmitt-Kopplin, in collaboration with the Chair of Analytical Food Chemistry at the Technical University of Munich. In the course of these years, I have relied on the courtesy and support of many to which I am grateful. The success of this PhD thesis would not have been possible without help and support of many wonderful people.

First of all, I would like to thank the whole research group Analytical BioGeoChemistry for a very friendly, informal, and emancipated working atmosphere that formed day-by-day an enjoyable period of residence - it has felt like freedom! Small issues like having stimulating lunch discussions or going out into a bar, friendly people could be found herein to setting up a balance to scientific work. I am thankful for enabling travels to conferences and meetings. I am fulfilled, this level of expanding mindsets is priceless and crucial, both on a scientific and a personal level. However, a couple of people, deserve a mentioning by name to express them my deep gratitude.

Philippe - as my PhD supervisor with always open doors to my issues. To me, it was an ideal degree of balancing inspiration, guidance, support and "letting me do my things". I am very grateful for the matter of trust into my work, e.g. at representations on conferences or at Munich SFB OLIM project meetings. In addition, thanks for "embedding" me into a huge scientific network, on which bases for many ideas on future projects have been created (e.g. Paola Caselli from observational and modeling astrochemistry in space, Dieter Braun from origin(s) of life research or Dirk Schulze-Makuch and Nancy W. Hinman from the field of astrobiology). Last but not least, Post Doc positions were thus enabled. One example, I want to highlight, is the successful story of the PNAS publication. Publishing in PNAS as a PhD student is hard to believe and simple amazing. This work was a product of multidisciplinary, collaborative science, to which you introduced me so well! On a face-to-face level, thanks also for having instantaneously a sympathetic ear at all

times for all kinds of problems, including private issues. I enormously acknowledge this incredible degree of flexibility. I am aware that this is not always an easy job to get into short discussions with me. Nevertheless, to me, these feeling of comfortability made me being creative and let science to be pushed forward. Interactions have felt barrierless, more like a friendship than a strict professor-student relationship. This kind of freedom is the spore of scientific success! Thanks, Philippe, for this hardly describable atmosphere. I am looking forward to the future !

Franco - daily work atmosphere was enhanced in quality due to our interactions. Thanks for having countless discussions and creative input on mass spectrometric data analysis, graph-theoretical problems, quantum chemistry, philosophy, politics, girlfriends, either in the office or at Isar. Those were always barrierless, open-minded discussions - discussions "über den Tellerrand hinaus". It has always felt to be self-explanatory to help each other - a good feeling! Creative ideas regarding visualization, graphs, etc. helped me a lot during various kinds of studies. Additionally, while writing this thesis at the moment, I am highly looking forward on your secret quotation, you will present during my PhD defense party. Additional thanks for proof-reading of this thesis.

Basem - helpful discussions, creating new ideas regarding theoretical and experimental background helped a lot during this doctoral time period. Your experience and gut feeling regarding quantum chemical computations is priceless! Additionally, I am highly grateful for your personal availability whenever I had problems or questions.

Jenny, Astrid - thanks for all the "krims krams", which HAS to be done. Whatever, if bureaucratic issues or personally questions bothered me, you were always instantaneously willing to help.

Anja - thanks a lot for every kind of help regarding administrative issues. In particular, reimbursement issues for travels and conferences went really smoothly thanks to your active and enthusiastic help. Eventhough, also these things HAVE to be checked rather than someone WANTS to do them, you created a convenient atmosphere including nice little words, also when working off these necessary points from our lists.

Norbert - thanks for "hardcore", fundamental discussions on basic chemistry issues regarding coordination compounds, especially during the period of detection and verification of dihydroxymagnesium carboxylates. Suggestions from NMR side helped to dig deeper in mechanistic understanding. Critical input always helps to optimize solid arguments and move further to feel confident of fundamentally new scientific knowledge! Additional thanks for numerous discussions on astrophysical, astrochemical and astrobiological topics, including their philosophical consequences. Not to forget: an amazing week in Paris together with Juliana in our shared flat - I highly enjoyed it! Additional thanks for proof-reading of this thesis.

Marianna - thanks for priceless help on multivariate data analytical problems. Dealing with our daily-life multi-dimensional data complexity, it would have been not possible to extract meaningful information without dealing with statistical data analysis.

Daniel - thanks for always having a "helping hand", especially with R programming issues.

Ryan - thanks for introducing me to "the grammar police".

Nancy - thanks for open discussions on astrobiological, geochemical issues. Your experienced insights from NASA astrobiology background helped a lot in setting up hypothesis.

Benedicte - thanks for constructive and efficient collaboration on astrobiological and geobiological problems. By discussing via email instantaneously or via lab exchanges, fruitful hypothesis were born. I am looking forward on their realizations in near future.

Rainer (Augart) - herein, I don't want to forget to mention people, who supported me during "science kindergarten". Rainer, you were the initial motivator during my apprenticeship as a chemical lab assistant, forcing me to go deeper into theoretical chemical science. Sadly, I don't have the opportunity anymore to express my deep gratitude personally to you, but I want to use this medium as an alternative. Without setting the basis, paths cannot be followed! This should never be forgotten.

Christian (Neusüß), Dirk Flottmann - in addition to previous words, I want to thank both of you for support during my BSc studies. Nonrestricted, open scientific discussions and stimulations to move forward into theoretical chemical science pushed me actually forward. An important issue, I don't want to forget here, is the initiated contact by you, Christian, with Philippe in Munich. This connection set my scientific basis!

Eric (Quirico), Michael Rychlik - thanks for flexible support and spontaneity while finishing this PhD thesis.

Lee - highly deep gratitude for long ongoing friendship, which cannot be expressed by any language. Our close interactions since over 20 years shaped my character as a person. I think, shared passion for various kinds of science (maths, physics, astronomy, chemistry, philosophy) or music issues (as the toco-jungs period) fixed us together and gave me inspriation in several areas all over the years. At a certain point, friendships are so deeply well-grounded that you don't question them anymore. THANKS, beyond words..

Mama, Papa, Thomas - thanks for EVERYTHING ! Unconditional support in all kinds of situations or daily issues gave me freedom to have life as easy as possible. But not everything's easy in daily life. Thank you also for supporting me when having had hard times in my life. In general, I feel grateful because of continuous interest in things I am doing. Thanks for listening for hours, when I am talking about science or other things, I am curious about. Even if scientific background diverges, you never quit in listening and show your interest in my issues. That's a wonderful feeling! For this, I want to quote Johann Wolfgang von Goethe: "Alles, was den einen Menschen interessiert, wird auch in dem andern einen Anklang finden". Without your support, I would not be at the level where I am now !

Marie - over the past years, you became the spore of my inspiration and creativity. Many thanks for our ongoing philosophical journey ! Additional thanks for open my mind regarding connections between arts and science - a powerful and more convergent combination, as one would think on a first sketch. Continuously, you opened my mind step by step. Exemplarily, thoughts on distinguishability of terms "Arbeit, Urlaub, Reisen, Freizeit" (work, vacation, spare time) made me being more conscious within daily life. In addition, thanks also on a practical level. Constructive suggestions and advices on (re-)orientation during "Wackelmomenten",

which brought stability to me. Herein, one important issue was the fact of finishing projects. Thoughts and discussions on sense of projects, goal definitions and relative time periods of projects inspired me a lot. Additional thanks for proof-reading of this thesis.

In conclusion, I am deeply happy to be part of a group of lovely people, surrounding and inspiring me, day-by-day - THANKS !

Acknowledgments according to sections

Regarding section 2, I gratefully acknowledge the co-authors Basem Kanawati, Norbert Hertkorn, Qing-Zhu Yin, Franco Moritz, Mourad Harir, Marianna Lucio, Bernhard Michalke, Joshua Wimpenny, Svetlana Shilobreeva, Basil Bronsky, Vladimir Saraykin, Zelimir Gabelica, Régis D. Gougeon, Eric Quirico, Stefan Ralew, Tomasz Jakubowski, Henning Haack, Michael Gonsior, Peter Jenniskens, Nancy W. Hinman and Philippe Schmitt-Kopplin and additionally, we thank Rainer Bartoschewitz, Maria Elizabeth Zucolotto, Ansgar Greshake, Herbert Raab, Michael Farmer, Greg Hupé, André Moutinho, Sonny Clary, Fabien Kuntz, Valery Bogdanovsky, Aid Mohamed, Ismailly Sidi Mohamed, Abdel Fattah Gharrad, and the National Institute of Polar Research for providing meteorite samples. We also thank the reviewers for their open-mindedness regarding our concept and their constructive comments, which substantially improved the quality of the manuscript, and Matthew Sanborn for proofreading the manuscript. This work was supported by NASA Cosmochemistry Grant NNX14AM62G and Emerging Worlds Grant NNX16AD34D (to Q.-Z.Y.).

Regarding section 3, I gratefully acknowledge the co-authors Basem Kanawati and Philippe Schmitt-Kopplin and additionally, we thank Daniel Hemmler for data analytical support and discussions hereof.

Regarding section 4, I gratefully acknowledge the co-authors Basem Kanawati and Philippe Schmitt-Kopplin and additionally, we thank Franco Moritz for data analytical support and constructive discussions hereof. Additional thanks to Jenny Uhl for server hardware support.

Munich, March 2018

A handwritten signature in black ink, appearing to be 'Q.-Z.Y.', written in a cursive style.

Abstract

Astrochemical probes, such as the interstellar medium or meteorites, show an enormous richness of complex organic molecules. This huge molecular diversity of extraterrestrial organic matter, especially in carbonaceous chondrites, represents a chemodiversity hotspot. The co-existence of this manifold organic chemical space and the history of exposure to high astrophysical energies of meteorites during their formation has given rise to many questions in the field of recent organic astrochemistry. Mechanisms for forming and preserving organic molecules within chemical evolution have been proposed. In this context, metalorganic species are supposed to selectively preserve certain organic compounds, in particular prebiotically relevant, surface-active molecules like fatty acids. Here, we describe the detection of dihydroxymagnesium carboxylates (CHOMg) in astrochemical context. CHOMg compounds were detected in meteorites via ultrahigh-resolving mass spectrometric techniques (FT-ICR-MS analysis). Ultrahigh mass spectrometric resolution was necessary to enable unambiguous detection of CHOMg molecules in complex organic mixtures. High resolving power $R > 10^6$ and high mass accuracy < 200 ppb enabled to resolve mass peaks, which differ in mass differences by less than the mass of an electron (CHOMg-CHO isobaric problem). Mass spectra of many ten thousands of detected mass signals resulted. These results underline the power of data-driven astrochemical research for in-depth studies of meteoritic (metal)organic matter composition. We demonstrate the occurrence and remarkable diversity of dihydroxymagnesium carboxylates within meteoritic soluble (metal)organic matter and discuss their chemical properties/reactivity. The huge organic molecular diversity makes meteorites ideal samples to elucidate fundamental organic chemical reactivity. Additionally, CHOMg signatures can be related to meteoritic thermal history and fractionation processes. Furthermore, dihydroxymagnesium carboxylates represent a novel chemical class, which has not been documented in chemical databases to date. Thus, we probed chemical stability of these novel CHOMg chemical compounds. Quantum chemical studies gained fundamental insights into chem-

ical properties of CHOMg molecules, as assessed by means of both second-order Møller–Plesset perturbation theory (MP2) and density functional theory (DFT) methods. Chemical stability was studied by targeting two molecular regimes, (i) the polar head group and its resistance towards release of CO₂; (ii) the apolar alkyl chain for charge-remote fragmentation. CO₂ release out of dihydroxymagnesium carboxylates results in formation of Grignard-type dihydroxymagnesates. Fragmentation probability and chemical characteristics of putatively formed Grignard-type molecules are discussed. In addition, dihydroxymagnesium carboxylates were found to release methylene (CH₂) and ethylene (C₂H₄) via alkyl chain fragmentation, as probed via experimental MS/MS and computational DFT studies. CHOMg compounds and their corresponding CHO molecules (e.g. fatty acids) showed increased relative abundances of even over odd carbon-bearing alkyl chains. This implies potential selective preservation of amphiphilic CHOMg-derived life-relevant molecules, with might has direct consequences on chemical evolution in general and capacity for vesicle formation in particular. The finding of dihydroxymagnesium carboxylates in meteorites proposes ongoing studies in future to deeper elucidate the role of CHOMg molecules in context of early complex organic molecule formation and their implications on chemical evolution.

Zusammenfassung

Astrochemische Analysen vom interstellaren Medium oder von Meteoriten zeigen einen enormen Reichtum an komplexen organischen Molekülen. Die große molekulare Vielfalt extraterrestrischer organischer Materie, in kohligen Chondriten im Speziellen, ist ein Hotspot für Chemodiversität. Die Koexistenz dieses mannigfaltigen organischen chemischen Raums und die vorangegangene Exposition von Meteoriten gegenüber hoher astrophysikalischer Energien während deren Entstehung hat viele Fragen auf dem Gebiet der jüngsten organischen Astrochemie aufgeworfen. Mechanismen zur Erzeugung und Konservierung organischer Moleküle innerhalb der chemischen Evolution wurden vorgeschlagen. In diesem Zusammenhang sollen metallorganische Spezies bestimmte organische Verbindungen, speziell präbiotisch-relevante oberflächenaktive Moleküle, wie Fettsäuren, selektiv konservieren. Hier beschreiben wir den Entdeckung von Dihydroxymagnesiumcarboxylaten (CHOMg) im astrochemischen Kontext. CHOMg-Verbindungen wurden in Meteoriten mittels ultrahochauflösender, massenspektrometrischer Methoden detektiert (FT-ICR-MS-Analyse). Sehr hohe Massenauflösung war notwendig, um CHOMg-Moleküle in komplexen organischen Mischungen eindeutig nachzuweisen. Hohes Auflösungsvermögen $R > 10^6$ und hohe Massengenauigkeit < 200 ppb ermöglichten, Massensignale eindeutig aufzulösen, die sich in Massendifferenzen um weniger als die Masse eines Elektrons unterscheiden (isobares CHOMg-CHO-Problem). Es resultierten Massenspektren, die mehrere zehntausend detektierte Massensignale enthielten. Diese Ergebnisse unterstreichen die Leistungsfähigkeit der datengetriebenen astrochemischen Forschung für grundlegende Studien der Zusammensetzung meteoritischer (metall)organischer Substanzen. Wir zeigen das Vorkommen und die bemerkenswerte Diversität von Dihydroxymagnesiumcarboxylaten in meteoritischen, löslichen (metall)organischen Substanzen und diskutieren deren chemische Eigenschaften/Reaktivität. Die große organische molekulare Vielfalt macht Meteoriten zu idealen Proben, um fundamentale organisch-chemische Reaktivität aufzuklären. Darüber hinaus konnten CHOMg-Signaturen mit meteoritischen thermischen Verlaufs- und

Fraktionierungsprozessen in Beziehung gebracht werden. Desweiteren stellen Dihydroxymagnesiumcarboxylate stellen eine chemische Substanzklasse dar, die bisher in chemischen Datenbanken nicht dokumentiert wurde. Daher haben wir die chemische Stabilität dieser neuartigen chemischen CHOMg-Verbindungen untersucht. Quantenchemische Studien lieferten grundlegende Einblicke in die chemischen Eigenschaften von CHOMg-Molekülen, die sowohl mittels Møller-Plesset-Störungstheorie zweiter Ordnung (MP2), als auch mittels Dichtefunktionaltheorie (DFT) studiert wurden. Die chemische Stabilität wurde getestet, indem zwei molekulare Regimes beprobt wurden, (i) die polare Kopfgruppe und ihre Resistenz gegenüber der Freisetzung von CO_2 ; (ii) die unpolare Alkylkette hinsichtlich der ladungsgetrenten Fragmentierung. Die CO_2 -Freisetzung von Dihydroxymagnesiumcarboxylaten führt zur Bildung von Grignard-ähnlichen Dihydroxymagnesaten. Fragmentierungswahrscheinlichkeit und chemische Eigenschaften von hypothetisch gebildeten Grignard-artigen Molekülen werden diskutiert. Darüber hinaus wurde durch experimentelle MS/MS und theoretische DFT-Studien gefunden, dass Dihydroxymagnesiumcarboxylate Methylen (CH_2) und Ethylen (C_2H_4) über eine Alkylkettenfragmentierung freisetzen. CHOMg-Verbindungen und ihre entsprechenden CHO-Moleküle (z. B. Fettsäuren) zeigten erhöhte relative Häufigkeiten von geradzahligen über ungeradzahligen Kohlenstoffketten. Dies beinhaltet eine potentiell selektive Konservierung amphiphiler CHOMg-abgeleiteter lebensrelevanter Moleküle mit direkten Konsequenzen für die chemische Evolution im Allgemeinen und die Fähigkeit zur Vesikelbildung im Besonderen. Die Entdeckung von Dihydroxymagnesiumcarboxylaten in Meteoriten schlägt weitere Forschungsprojekte in der Zukunft vor, um die Rolle von CHOMg-Molekülen im Kontext der Entstehung früher komplexer organischer Moleküle und deren Auswirkung auf die chemische Evolution tiefgründig zu studieren.

Scientific contributions

Publications

Publications, which are directly related to this PhD thesis

- Data-driven astrochemistry - on step further in resolving the astrobiological puzzle, submitted for publication.
- Ruf, A., Kanawati, B. and Schmitt-Kopplin, P., The role of organomagnesium species within chemical evolution, submitted for publication.
- Ruf, A., Kanawati, B. and Schmitt-Kopplin, P., Do dihydroxymagnesium carboxylates form Grignard-type reagents? A theoretical investigation on decarboxylative fragmentation, *Journal of Molecular Modeling*, accepted.
- Bischoff, A., Barrat, J. A., Bauer, K., Burkhardt, C., Schmitt-Kopplin P., Ruf, A., ... and Heinlein, D. (2017). The Stubenberg meteorite—An LL6 chondrite fragmental breccia recovered soon after precise prediction of the strewn field. *Meteoritics & Planetary Science* 52(8), 1683–1703.
- Ruf, A., Kanawati, B., Hertkorn, N., Yin, Q. Z., Moritz, F., Harir, M., ... and Schmitt-Kopplin P. (2017). Previously unknown class of metalorganic compounds revealed in meteorites. *Proceedings of the National Academy of Sciences*, 114(11), 2819-2824.
- Bartoschewitz, R., Appel, P., Barrat, J. A., Bischoff, A., Schmitt-Kopplin P., Ruf, A., ... and Hochleitner, R. (2017). The Braunschweig meteorite - a recent L6 chondrite fall in Germany. *Chemie Der Erde-Geochemistry*, 77(1), 207-224.

Other publications within the time period of these doctoral studies

- Fundamental experimental studies on easy ambient sonic spray ionization, in preparation for publication.
- Dihydrogenphosphate dopants in electrospray ionization mass spectrometry, in preparation for publication.
- Roullier-Gall, C., Witting, M., Tziotis, D., Ruf, A., Gougeon, R. D., and Schmitt-Kopplin, P. (2015). Integrating analytical resolutions in non-targeted wine metabolomics. *Tetrahedron*, 71(20), 2983-2990.

- Roullier-Gall, C., Witting, M., Tziotis, D., Ruf, A., Lucio, M., Schmitt-Kopplin, P., and Gougeon, R. D. (2015). Combined Nontargeted Analytical Methodologies for the Characterization of the Chemical Evolution of Bottled Wines. In *Advances in Wine Research* (pp. 13-27). American Chemical Society.

Talks

- Solar-System symposium, Sapporo, Japan, 2018, title: Novel metalorganic compounds revealed in meteorites.
- Invited talk at Kyushu University (Department of Earth and Planetary Sciences/Research Center for Planetary Trace Organic Compounds, H. Naraoka), Fukuoka, Japan, 2018, title: Ultrahigh-resolving analytics in meteoritic soluble (metal)organic matter.
- Symposium "2nd Annual Workshop of the Deutsche Astrobiologische Gesellschaft e.V. (DAbG)", Potsdam, Germany, 2017, title: Novel metalorganic compounds revealed in meteorites.
- Conference "Paneth Kolloquium 2017", Nördlingen, Germany, 2017, title: Novel metalorganic compounds revealed in meteorites.
- Conference "Goldschmidt2017", Paris, France, 2017, title: Novel metalorganic compounds revealed in meteorites.
- Invited talk at Aix-Marseille Université (Physique des Interactions Ioniques et Moléculaires/Astrochimie, Spectroscopie, Théorie, Réactivité, Origine, G. Danger), Marseille, France, 2017, title: Novel metalorganic compounds revealed in meteorites.
- Seminar on emergence of the origin of life, coordinated by D. Braun, Munich, Germany, 2017, title: Profiling of meteoritic organic matter and the role of metalorganic compounds.
- Invited talk at Max Planck Institute for Astronomy/Uni Jena (Laboratory Astrophysics and Cluster Physics Group, T. Henning/C. Jäger), Jena, Germany, 2017, title: Novel metalorganic compounds revealed in meteorites.
- Conference "Evolution of Chemical Complexity: From simple interstellar molecules to terrestrial biopolymers", Liblice, Czech Republic, 2016, title: Ultrahigh-Resolving Analytics in Meteoritic Soluble Organic Matter.
- Seminar on emergence of the origin of life, coordinated by D. Braun, Munich, Germany, 2016, title: Ultrahigh-Resolving Analytics in Meteoritic Soluble Organic Matter.

Poster

- Conference "Paneth Kolloquium 2017", Nördlingen, Germany, 2017, title: Ultrahigh-Resolving Analytics in Meteoritic Soluble Organic Matter.
- NIM Conference "Molecular Origins of Life", Munich, Germany, 2016, title: Ultrahigh-Resolving Analytics in Meteoritic Soluble Organic Matter.
- 79th Annual Meeting of The Meteoritical Society, Berlin, Germany, 2016, title: Ultrahigh-Resolving Analytics in Meteoritic Soluble Organic Matter.

Contents

1. Introduction	1
1.1. Astrochemistry	2
1.1.1. Interstellar medium and circumstellar environments	2
1.1.2. Molecular complexity	2
1.1.3. Chemical evolution	4
1.1.4. Comet chemistry	5
1.1.5. Laboratory astrophysics	6
1.2. Meteorites	6
1.2.1. Classification of meteorites	7
1.2.2. Chondrules, CAIs, cosmochemistry	8
1.3. Organic material in meteorites	9
1.3.1. Insoluble organic matter	9
1.3.2. Soluble organic matter - amino acids and beyond	10
1.3.3. High-resolving chemical analytics - data-driven astrochemistry	12
1.3.4. Targeted versus nontargeted analysis	16
1.3.5. Comprehensive chemical profiling of meteoritic organic matter	18
1.3.6. Combining experimental and computational techniques	18
1.4. Organometallics in astrochemistry	19
1.5. Relevance of (metal)organic astrochemistry - astrobiological implications	20
1.6. Motivation and objectives of the thesis	23
2. Previously unknown class of metalorganic compounds revealed in meteorites	25
2.1. Introduction/motivation	26
2.2. Evaluating the CHOMg Chemical Space	28
2.3. Dihydroxymagnesium Carboxylates: A Previously Unreported Chemical Class	32
2.4. Chemosynthesis of organomagnesium compounds and the link to thermal history	37
2.5. Conclusions/outlook	43
3. Do dihydroxymagnesium carboxylates form Grignard-type reagents?	45
3.1. Introduction/motivation	46
3.2. Decarboxylation of dihydroxymagnesium carboxylates - probing the potential energy surface	47
3.3. Chain length dependence of $[(\text{OH})_2\text{MgO}_2\text{CR}]^-$ decarboxylation	49
3.4. Insights into the decarboxylation-type fragmentation mechanism	50
3.5. Properties of putative Grignard-type OH-bearing molecules	51
3.6. Conclusions/outlook	52
4. The role of organomagnesium species within chemical evolution	55
4.1. Introduction/motivation	56
4.2. Odd/even alternation within meteoritic (metal)organic matter	57
4.3. Methylene and ethylene release from dihydroxymagnesium carboxylates	58

4.4. Why is there odd/even alternation? Insights from pseudocyclic conformations	60
4.5. Implications for fatty acid chemical evolution	62
4.6. Conclusions/outlook	63
5. Conclusions and outlook	65
A. Appendix Chapter 2	67
A.1. ICP-MS Experiments	67
A.2. SIMS Experiments	68
A.3. ESI-FT-ICR-MS experiments	69
A.4. Computations	69
A.5. Correlation Between the Experimental and Computed Fragmentation Energies	70
A.6. Calculation of the Measured Equilibrium Constant K'	70
A.7. Mass Difference Network Reconstruction	71
A.8. Statistical Evaluation of Meteorite Samples	71
A.9. Mg Isotope Measurements	72
A.10. Information on 61 meteorite samples, used in the statistical analysis	74
A.11. Mass list of significantly enriched compounds in thermal processed meteorites	77
A.12. Coordinates of the relaxed, computed geometry of C ₁₆ -dihydroxymagnesium carboxylate	94
A.13. Coordinates of the relaxed, computed geometries - C ₁₆ -carboxylate .	95
A.14. Coordinates of the relaxed, computed geometries - C ₅ -dihydroxymagnesium carboxylate	96
B. Appendix Chapter 3	99
B.1. Computational methods	99
B.2. Coordinates of computed structures regarding the potential energy curve	100
B.3. Natural bond orbital analysis - coordinates of the computed C ₅ -dihydroxymagnesium carboxylate transition state geometry	105
B.4. Natural bond orbital analysis - coordinates of the computed OH- and Cl-bearing putative Grignard-type molecules	106
C. Appendix Chapter 4	109
C.1. ESI-FT-ICR-MS experiments	109
C.2. Computational methods	112
C.3. Coordinates of representative computed pseudocyclic organomagnesium structures	114
C.4. Coordinates of representative computed structures regarding thermodynamic fragmentation energy simulations	116
Bibliography	121
List of Figures	131
List of Tables	133

Eidesstattliche Erklärung	135
Curriculum vitae, contact	137

1. Introduction



Astrochemistry represents a manifold scientific field, including various disciplines. Here, special emphasis should be placed on data-driven methods, such as ultrahigh-resolving analytics and their interplay with quantum chemical computations. These methods enable remarkable insights into complex chemical spaces in meteorites and allow to extract even previously unknown chemistry. By considering the title of this thesis, "Previously unknown organomagnesium compounds in astrochemical context", we will first introduce basic terms within this field of research. Clarifications on astrochemistry, meteoritic research with respect to organic chemistry and their implications towards astrobiology will be given. In addition, special care is taken with respect to molecular complexity and chemical evolution. Questions on chemical evolution scratch philosophical problems. Finally, the motivation and objectives of this thesis are outlined.

1.1. Astrochemistry

"Astrochemistry is the science devoted to study of chemical processes within different astrophysical environments, including the interstellar medium, comets, circumstellar and circumplanetary regions" [1]. This scientific field combines many aspects from different disciplines, which profit from different ways of thinking. Roughly spoken, it includes "everything", as considering the need for tracking the origin of the universe up to implications on astrobiology. The latter disciplines focus on questions on the origin of life or asking for habitability on planets other than Earth. Inspiration, "language", scientific techniques from astronomy, astrophysics and chemistry (physical/theoretical/analytical chemistry) are combined to investigate molecular information in space. Additionally, biologists complement this manifold area of research for tracking astrobiological problems, as tracking the origin of life or habitability on outer Earth planets. Even interests for philosophers are set in these topics. Evolution, transport and transformation of molecules are monitored, from molecular clouds and diffuse interstellar medium (ISM) to their incorporation into solar system material such as comets and meteorites.

1.1.1. Interstellar medium and circumstellar environments

Probing molecules within ISM and circumstellar environments is achieved via radio astronomy. For a long time, scientists suspected that the interstellar medium would be too harsh for organic species and that only a few simple molecules could be formed under such extreme conditions. However, since the 1970s, millimeter and submillimeter observations have detected ≈ 200 interstellar and circumstellar molecules to date, including hydrocarbons, alcohols, acids, aldehydes, ketones, amines, ethers, and other organic molecules (Table 1.1) [2]. In addition, 62 extragalactic molecules were detected [2]. Molecular spectroscopy studies led to the detection of this huge number of molecules in astrophysical environments. Most of them have been discovered via their rotational signature from radio to far-infrared frequencies. In addition, some have also been observed in the visible and near-infrared domains.

Technically, infrared ground-based, airborne, and space-based spectroscopic observations have found evidence of complex organic molecules (COMs) with aromatic and aliphatic structures in space. As a striking example, the Atacama Large Millimeter/submillimeter Array (ALMA) ground-based observatory from European Southern Observatory (ESO) should be mentioned here [3]. Exemplarily, powerful scientific results such as studies on cosmic dust [4], comae of comets [5] or protoplanetary disk surrounding star images [6] were obtained. A second break-through example in radio astronomy is the Herschel Space Observatory, a space observatory from European Space Agency (ESA), collaborating with National Aeronautics and Space Administration (NASA) [7]. Striking results on planet formation could be reported by help of Herschel detection [8].

1.1.2. Molecular complexity

This observed and increasing manifold diverse astrochemistry is necessarily connected with the term of molecular complexity [1]. Generally, the problem of complexity can be tracked by two differently motivated approaches, namely via a bottom-up approach or a top-down approach. First, the bottom-up approach considers pre-

1.1 Astrochemistry

cise description of fundamental building blocks and their interactions towards each other. In terms of astrochemistry, characteristics of simple diatomic species and their formation to more complex small-scale polyatomic molecules are studied. The top-down approach starts with exploring present highly complex molecular spaces. Putative precursors are targeted out of complicated and complex molecular networks. Obviously, these two strategies converge and try to describe problems on astrochemical molecular complexity as comprehensive as possible.

Atom number	Molecules
2 atoms	H ₂ ; AlF; AlCl; C ₂ **; CH; CH ⁺ ; CN; CO; CO ⁺ ; CP; SiC; HCl; KCl; NH; NO; NS; NaCl; OH; PN; SO; SO ⁺ ; SiN; SiO; SiS; CS; HF; HD; FeO?; O ₂ ; CF ⁺ ; SiH?; PO; AlO; OH ⁺ ; CN ⁻ ; SH ⁺ ; SH; HCl ⁺ ; TiO; ArH ⁺ ; N ₂ ; NO ⁺ ?
3 atoms	C ₃ *; C ₂ H; C ₂ O; C ₂ S; CH ₂ ; HCN; HCO; HCO ⁺ ; HCS ⁺ ; HOC ⁺ ; H ₂ O; H ₂ S; HNC; HNO; MgCN; MgNC; N ₂ H ⁺ ; N ₂ O; NaCN; OCS; SO ₂ ; c-SiC ₂ ; CO ₂ *; NH ₂ ; H ₃ +(*); SiCN; AlNC; SiNC; HCP; CCP; AlOH; H ₂ O ⁺ ; H ₂ Cl ⁺ ; KCN; FeCN; HO ₂ ; TiO ₂ ; C ₂ N; Si ₂ C ₂₀₁₅
4 atoms	c-C ₃ H; l-C ₃ H; C ₃ N; C ₃ O; C ₃ S; C ₂ H ₂ *; NH ₃ ; HCCN; HCNH ⁺ ; HNCO; HNCS; HOCO ⁺ ; H ₂ CO; H ₂ CN; H ₂ CS; H ₃ O ⁺ ; c-SiC ₃ ; CH ₃ *; C ₃ N ⁻ ; PH ₃ ; HCNO; HOCN; HSCN; H ₂ O ₂ ; C ₃ H ⁺ ; HMgNC; HCCO ₂₀₁₅
5 atoms	C ₅ *; C ₄ H; C ₄ Si; l-C ₃ H ₂ ; c-C ₃ H ₂ ; H ₂ CCN; CH ₄ *; HC ₃ N; HC ₂ NC; HCOOH; H ₂ CNH; H ₂ C ₂ O; H ₂ NCN; HNC ₃ ; SiH ₄ *; H ₂ COH ⁺ ; C ₄ H ⁻ ; HC(O)CN; HNCNH; CH ₃ O; NH ₄ ⁺ ; H ₂ NCO ⁺ (?); NCCNH+2015; CH ₃ Cl ₂₀₁₇
6 atoms	C ₅ H; l-H ₂ C ₄ ; C ₂ H ₄ *; CH ₃ CN; CH ₃ NC; CH ₃ OH; CH ₃ SH; HC ₃ NH ⁺ ; HC ₂ CHO; NH ₂ CHO; C ₅ N; l-HC ₄ H*; l-HC ₄ N; c-H ₂ C ₃ O; H ₂ CCNH(?); C ₅ N ⁻ ; HNCHCN; SiH ₃ CN ₂₀₁₇
7 atoms	C ₆ H; CH ₂ CHCN; CH ₃ C ₂ H; HC ₅ N; CH ₃ CHO; CH ₃ NH ₂ ; c-C ₂ H ₄ O; H ₂ CCHOH; C ₆ H ⁻ ; CH ₃ NCO ₂₀₁₅ ; HC ₅ O ₂₀₁₇
8 atoms	CH ₃ C ₃ N; HC(O)OCH ₃ ; CH ₃ COOH; C ₇ H; C ₆ H ₂ ; CH ₂ OHCHO; l-HC ₆ H*; CH ₂ CHCHO(?); CH ₂ CCHCN; H ₂ NCH ₂ CN; CH ₃ CHNH; CH ₃ SiH ₃ ₂₀₁₇
9 atoms	CH ₃ C ₄ H; CH ₃ CH ₂ CN; (CH ₃) ₂ O; CH ₃ CH ₂ OH; HC ₇ N; C ₈ H; CH ₃ C(O)NH ₂ ; C ₈ H ⁻ ; C ₃ H ₆ ; CH ₃ CH ₂ SH (?); CH ₃ NHCHO ? ₂₀₁₇
10 atoms	CH ₃ C ₅ N; (CH ₃) ₂ CO; (CH ₂ OH) ₂ ; CH ₃ CH ₂ CHO; CH ₃ CHCH ₂ O ₂₀₁₆
11 atoms	HC ₉ N; CH ₃ C ₆ H; C ₂ H ₅ OCHO; CH ₃ OC(O)CH ₃
12 atoms	c-C ₆ H ₆ *; n-C ₃ H ₇ CN; i-C ₃ H ₇ CN; C ₂ H ₅ OCH ₃ ?
>12 atoms	HC ₁₁ N ?; C ₆₀ *; C ₇₀ *; C ₆₀ +*

Table 1.1: Molecules in the Interstellar Medium or Circumstellar Shells (as of 10/2017) [2]. All molecules have been detected (also) by rotational spectroscopy in the radiofrequency to far-infrared regions unless indicated otherwise. * indicates molecules that have been detected by their rotation-vibration spectrum, ** those detected by electronic spectroscopy only. Tentative detections, which have a reasonable chance to be correct, are indicated by "?". Depicted dates represent the year most relevant to the detection (including isotopic species or vibrationally excited states) is given for recent results – the past two to three years.

Astrochemical molecular complexity can be probed both in interstellar/circumstellar medium or in meteoritic systems. Sampling the ISM can be compared to gas-phase physical chemistry and tracks mostly gas-phase reactions or grain-surface reactions [1]. Methodologically, molecular complexity in terms of mostly <10 atom molecules is tracked with chemical reaction networks, including basic molecular transformations (e.g. e⁻ or H transformations) [1]. Therefore, fundamental reaction pathways within formation of complex organic molecules can be understood within this bottom-up approach. Sampling meteorites revealed a significantly higher number of involved components within a chemical network of diverse and complex organic

1.1 Astrochemistry

molecules [9, 10]. This comprehensive top-down approach provides complementary insights on global chemical processes.

1.1.3. Chemical evolution

When speaking about diversity and complexity of organic molecules, one simultaneously asks for the origin and temporal evolution of these complex organic species [11]. The term chemical evolution is ambiguously discussed nowadays [12]. Originally, Calvin introduced this term to describe "the conversion of simple organic or inorganic molecules to assembled, complicated, partly polymeric chemical compounds, which eventually became capable of reproduction including mutation and metabolism" [12]. Nevertheless, the term is also interpreted and used to denote processes of astrophysical element/molecule synthesis [13]. Herein, chemical evolution is used to combine a general concept of formation and evolution of chemical molecules, starting from astrochemical synthesis within interstellar environments towards their interactions/transformation within prebiotic chemical systems. The transformation of (abiotic) molecular systems towards prebiotic and finally biotic systems can be expressed by a decrease in chemical complexity and a convergence of the molecular set towards local stability minima. One brief example is the convergence out of the amino acid chemical space and its decrease from ≈ 159 amino acid isomeric structures, as found in meteorites [14, 15], towards primarily 20 proteinogenic amino acids within biochemical systems on Earth [16]. A need for future aspects underlies in deeper learning on mechanisms of convergence of abiotic towards biotic chemical spaces. More data on astrochemical organic diversity and its transition towards a less diverse set of organic molecules within biospheres will enable more precise descriptions of molecular convergence within geological time scales. **What are the driving forces to select only $\approx 13\%$ of amino acids for biotic organized systems? What makes these 20 proteinogenic amino acids special? Is chemical convergence towards biochemical spaces stochastic or deterministic?**

Fig. 1.1 sketches chemical evolution in terms of molecular diversity and molecular complexity. Starting within interstellar and circumstellar medium with simple organic precursor molecules (e.g. H_2O , NH_3 or CH_3OH), chemical evolution and transformation towards rather complex biomolecules is triggered by highly diverse and multiparametric circumstances [17]. Chemical evolution goes "hand in hand" with material aggregation of astronomical/celestial bodies. A molecule's life-time is highly dependent on the following parameters:

- astrophysical energy gradients
- combinatorial effects of molecular synthesis, influenced by local element abundances
- intrinsic life-times of molecules (chemical stability)
- encapsulation within changed molecular motifs to increase chemical stability (early molecular preservation)
- molecular assembly potential (primitive chemical communication systems)
- molecular environments as compartmentalized systems (different energetic conditions, possibility of preservation)

1.1 Astrochemistry

1.1.4. Comet chemistry

Next to molecular sampling within interstellar or circumstellar space, comets represent states being one the step further within chemical evolution. Comets originate either from the Kuiper belt or from the Oort Cloud, as formed in the outer regions of the solar system. The Kuiper belt is a disc-shaped collection of icy debris at a distance of around 100 astronomical units (AU) just outside the orbit of Neptune. The Oort Cloud is located at a distance as much as 50,000 AU that may contain a significant mass of material left over as a remnant of the formation of the solar system. Generally, chemical composition of a present-day comet is a good marker to study the composition of the outer solar system and, more interestingly, the early solar nebula [18].

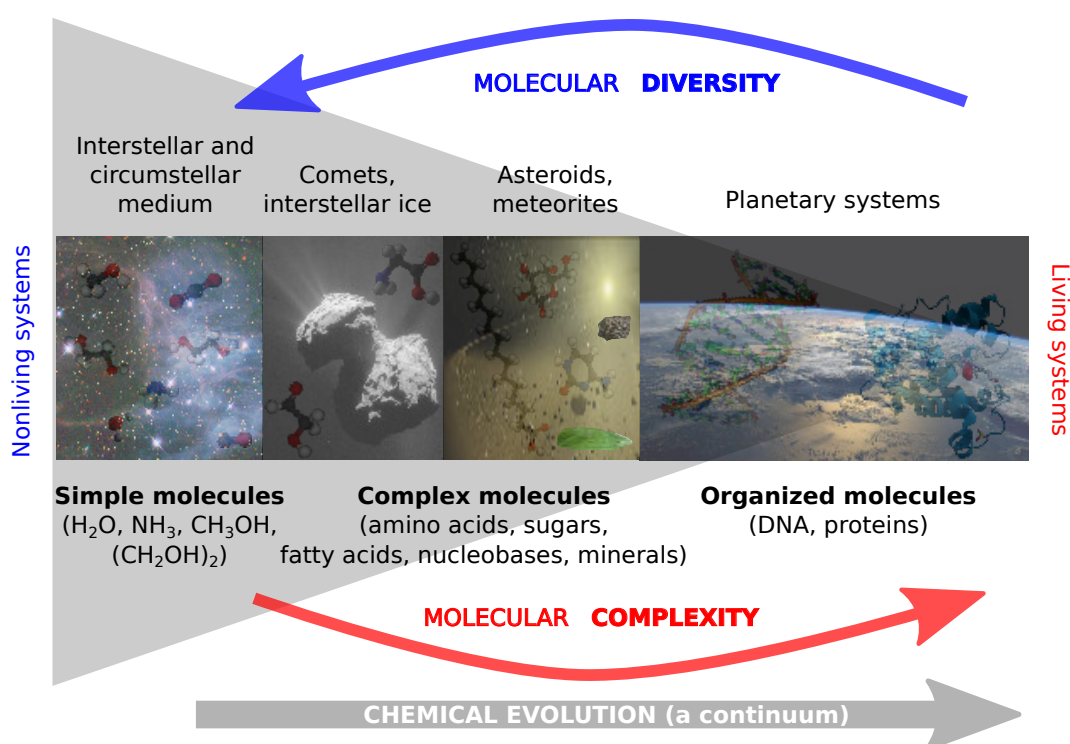


Figure 1.1: Sketching chemical evolution in terms of molecular diversity and molecular complexity. Molecular transformation within time and space are illustrated. Simple molecules within interstellar and circumstellar medium evolve to highly oriented, complex macromolecules on planetary systems, enabling the potential of living systems.

A milestone in probing comet chemistry was Rosetta, a space probe built by ESA, along with its lander module Philae [19]. The comet 67P/Churyumov–Gerasimenko was visited. This mission was named charmingly "Rosetta - rendezvous with a comet", launched from 2 March 2004 until 30 September 2016. In astrochemical context, special focus was set on the search for organic molecules on 67P/Churyumov–Gerasimenko. Philae's COSAC instrument (Cometary Sampling and Composition Experiment, gas chromatograph, GC and a time-of-flight mass spectrometer, TOF-MS) was designed to identify organic compounds in the material from the nucleus of the comet. Second, ROSINA (Rosetta Spectrometer for Ion and Neutral Analysis) was used to

1.2 Meteorites

study organic compounds within the comet's atmosphere and ionosphere. ROSINA consists of two mass spectrometers, a double focusing magnetic mass spectrometer (DFMS) and a reflectron-type time-of-flight mass spectrometer (RTOF). Especially, the DFMS data are of high interest because of its high mass resolving power ($R = 3,000$), which allows for differentiating $^{12}\text{C}^{16}\text{O}$ from $^{14}\text{N}_2$ or ^{13}C from ^{12}CH within a mass range of 1 - 150 amu (atomic mass units). Successfully, various organic molecules, including prebiotic chemicals, such as the smallest amino acid glycine [20], or suggested high-molecular-weight organic compounds were detected [21].

1.1.5. Laboratory astrophysics

Laboratory astrophysical studies are a contemporary important tool to "solve puzzles" in the field astrochemistry, in complement to observational radio astronomy, astrophysical modeling and state-of-the-art chemical analysis of meteoritic samples [22]. Technical detection problems within observational approaches can be overcome by simulating e.g. interstellar ice analogs in the laboratory (e.g. spectroscopic interference by brightness of sampling molecular species close to stars). This enables a better understanding of formation mechanisms of complex organic molecules [23], predicting reactive intermediate species [24], overcoming spectroscopic detection challenges [25] or understanding celestial body evolution [26].

Digging one step further in chemical evolution is realized via probing meteorites, possessing mineral components and even rocky materials. This brings meteoritic bodies closer towards planetesimal characteristics, in terms of geology. Next to comets, meteorites represent astronomical objects that are thought to have survived from the very beginnings of the solar nebula some 4.5 billion years ago [18]. The analysis of meteorites is revealing to probe astrochemical complexity, as it will be further discussed within the next sections. We will see further benefits of laboratory chemical analysis.

1.2. Meteorites

Hot cores in giant molecular clouds collapse to form young stellar objects, the birth of stars via protostars. Formed stellar objects include their own cloud or nebula around them. Analogously, the solar nebula was nothing more than an average collection of dust and matter that had achieved critical mass. Molecular cloud collapses may have been triggered by shock waves, perhaps from a supernova, accelerating the rate of collapse so that above a critical mass the collapse was inevitable. Shock waves are mainly believed to be collisionless plasma instabilities including extremely high energy particles, travelling through space [27, 28]. Meteoroids are aggregated dust particles as derived from a giant molecular cloud. The early composition of solar nebula was fundamentally responsible for the composition of the Sun and, with some processing, the chemistry of the planets. In other words, early composition of solar nebula is directly connected to our contemporary "chemical household", including the evolution and origin of life.

Together with comets, meteorites may as well be called as fossils or children of our solar system. Meteorites are thought to have survived from birth of solar nebula some 4.5 billion years ago [16, 18]. These stony samples profit from many aspects relative to other types of extraterrestrial materials. As meteorites land on Earth, these types of samples can be analyzed in chemical laboratories using

1.2 Meteorites

high-end analytical instrumentations. A high degree of analytical precision allows for sensitive probing on e.g. early solar system or planetary history information [29, 30]. Many more powerful channels of information are provided by analyzing meteorites, such as profiling of astrochemical complexity.

First, we want to clarify terminology on meteor, meteoroid and meteorite [18].

meteor	an object entering Earth's atmosphere that burns up completely during its passage through the upper atmosphere - a 'shooting star'
meteoroid	the name given to a meteorite or a meteor before it enters Earth's (or any other planetary) atmosphere
meteorite	an object entering Earth's atmosphere that survives the fall to Earth's ground and can be sampled

1.2.1. Classification of meteorites

Meteorites are of special interest for some already mentioned reasons (e.g. laboratory analysis, accessible information on solar system history). This makes those objects special for human scientific research and classification schemes of meteorites were invented. Basically, meteoritic classification terminology follows geological mineral grouping. Meteorite mineralogy is complicated since 275 mineral species were reported so far [18]. Nevertheless or exactly therefore, this proxy is diagnostic of the origin of the sample. Broadly screened, meteorites are classified into three major classes [18]:

iron	composition principally of pure metallic nickel-iron (sensitive to oxidation)
stony	principally silicates or rocky meteorites (requires careful laboratory analysis to determine extraterrestrial origin)
stony-iron	a mixture of the previous two classes

In addition, meteorites are grouped into falls and finds. Falls refer to an observed landing and a find is a meteorite discovery. A more detailed scheme of classification of meteorites is sketched in Fig. 1.2. Special emphasis is taken on undifferentiated chondrites, especially carbonaceous chondrites (C chondrites) to study organic chemistry within these types of meteorites. CI chondrites are thought to be the most primitive meteorites in terms of mineralogy [31]. C chondrites contain ≈ 2 wt% (percentage by weight) carbon-bearing organic matter [15]. Additional help on classification is provided from cosmochemical meteoritic isotopic analysis [32]. Bulk H, C and N abundances were determined, as assessed mostly by organic material. Lability of organic matter by aqueous alteration suggests analysis on organic matter to be a more sensitive probe for classifying meteorites.

An important issue within meteoritic research is the question of its parent body, as meteoroids are generally formed by collision of two celestial bodies. Meteorites are well-described, which originate from asteroidal parent bodies (e.g. HED meteorites or Chelyabinsk), from planets (e.g. Mars) or from moon (e.g. or lunar meteorites) [16]. To the best of my knowledge, no meteorite was ever directly found

1.2 Meteorites

with cometary origin, although studies probed properties of putative meteorites with cometary origin [33–36]. Nevertheless, interstellar dust particles were observed in the Earth’s atmosphere [37]. These results could be relevant since interstellar dust is directly connected to cometary material [38]. Furthermore, dynamical studies and meteor observations indicate a continuum between dark asteroids and comets and conclude that there should be a small fraction of the $\approx 30,000$ meteorites that originate from comets [39]. Differences between CI1 chondrites and cometary nuclei could be ascribed by recent space missions, which were recorded basically from star-dust data [39]. It has been suggested that type 1 (and maybe type 2) C chondrites are best candidates for being cometary meteorites. In direct comparison, the D/H ratio of CI1 chondrites is lower than that of comets.

A meteoritic composition is influenced by shock processes (e.g. by impact, collision during meteoroid formation), thermal metamorphism (e.g. by radionucleic heat) or aqueous alteration effects.

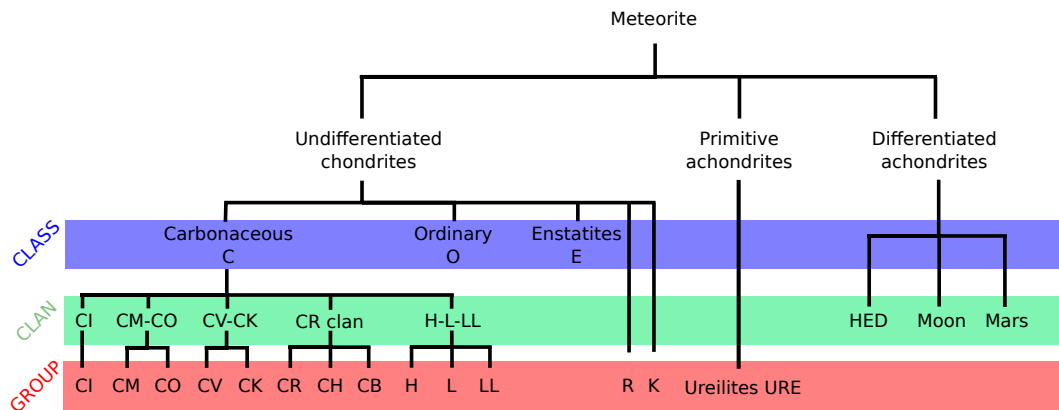


Figure 1.2: Classification of meteorites. This figure is adapted from the classification scheme, as shown by Weisberg, McCoy and Krot [40]

1.2.2. Chondrules, CAIs, cosmochemistry

The chondrite subclass of stony meteorites is characterized by globules of once-molten material that quickly solidified. These globules are called chondrules and are remnants of the early protoplanetary disc. Their composition is usually similar to that of the Sun and contain silicate minerals, e.g. olivine $(\text{Mg,Fe})_2\text{SiO}_4$. Chondrules are attractive, weakly processed probes for isotopic ratio determinations. Secrets on the early solar system may be unlocked or this measure is used to get insights on composition of interstellar dust, as both chondrules and dust originate from the protoplanetary disc. Putatively even older are calcium-aluminium-rich inclusions (CAIs), submillimeter- to centimeter-sized light-colored calcium- and aluminium-rich inclusions, which are found within C chondrites. Probing CAIs via lead (Pb-Pb) isotope radiometric dating (using radioactive clocks) represents a sensitive measure for geological time scales. For the Northwest Africa 2364 (NWA 2364) meteorite, an age of 4568.22 ± 0.17 million years has been determined, which was inferred as the beginning of the formation of the planetary system, meaning this time could be interpreted as the age of the solar system [41]. This field of tracking meteoritic isotopic signatures is known as cosmochemistry or chemical cosmology. Chemical cosmology

1.3 Organic material in meteorites

can be interpreted as tracking the formation of the universe/solar system by help of chemical probes. Cosmochemistry is also used to track the spatial/astronomical origin of a meteoritic sample within the solar system, e.g. via determination of the deuterium/hydrogen ratio (D/H) [42]. Generally, it is important to match data from different techniques (radioastronomy, meteoritic laboratory analysis, computational modeling). One example for doubtful astronomical origin due to lack of underlying data is the NWA 7325 meteorite, which has been discussed to putatively originate from Mercury [43–45].

In addition, chondrules might also be a source of interstellar molecules, as processed in ice layers of dust particles in giant molecular clouds. **What are astrochemical origins and how are these complex organic molecules formed? Did they form within a meteoritic body? Are there any interactions between organic molecules and minerals?** However, the source of organics within chondritic compartments and their interaction with minerals is not fully understood yet. Further studies both from analytical meteoritic chemistry and laboratory studies on interstellar ice analogs are needed to understand better the origin and formation of ancient complex organic molecules.

1.3. Organic material in meteorites

Searching for organic matter within meteorites is mainly motivated by tracking carbon-bearing compounds within carbonaceous chondrites (C chondrites). C chondrites contain ≈ 2 wt% organic matter carbon [15]. This field of research is connected by astrobiological/origin of life questions. The Murchison meteorite, an observed fall of ≈ 100 kg of in 1969 in Australia, influenced significantly studies on meteoritic organic material [46]. Early investigations on Murchison meteorite by well-equipped laboratories was motivated that time also in the context of return samples from Apollo missions, a NASA program dedicated for manned lunar landing. Over almost 50 years, Murchison has become a valuable extraterrestrial organic reference material, which has been probed by modern analytical techniques.

Organic material in meteorites is known to be present in various forms. Meteoritic organic matter can be roughly grouped into soluble and insoluble organic matter (SOM and IOM). Soluble organic matter represents small free molecules, including prebiotically-relevant compounds, such as amino acids or fatty acids. The major part (≈ 70 %) of meteoritic organic matter is entitled as being insoluble, which is referred to a highly cross-linked aromatic chemical network or macromolecules [47].

1.3.1. Insoluble organic matter

Studying insoluble organic matter requires extensive analytical sample preparation. A meteoritic specimen will be suspended to a HF/HCl mixture with considering the residue as insoluble organic matter. Subsequently, IOM is thermally and chemically degraded (via pyrolysis and RuO_4 oxidation to release aromatic and aliphatic moieties). Remaining organic compounds are analyzed via gas chromatography mass spectrometry (GC-MS) [48]. Alternatively, nuclear magnetic resonance spectroscopy (NMR) [47, 49] or Raman spectroscopy [50, 51] are used to elucidate meteoritic IOM. IOM is generally characterized as a highly macromolecular chemical network of high chemical aromaticity. Derenne and Robert proposed a chemical

1.3 Organic material in meteorites

model structure for insoluble organic matter of Murchison [52]. Despite a high degree of unsaturation/aromaticity, incorporation of heteroatoms (oxygen, nitrogen, sulphur) can be observed. Chemical parameters were described as $H/C = 0.70$, $O/C = 0.22$ and $N/C = 0.03$ [52]. Additionally, Raman spectroscopy studies on IOM provide information on thermal metamorphism of meteorites [53, 54].

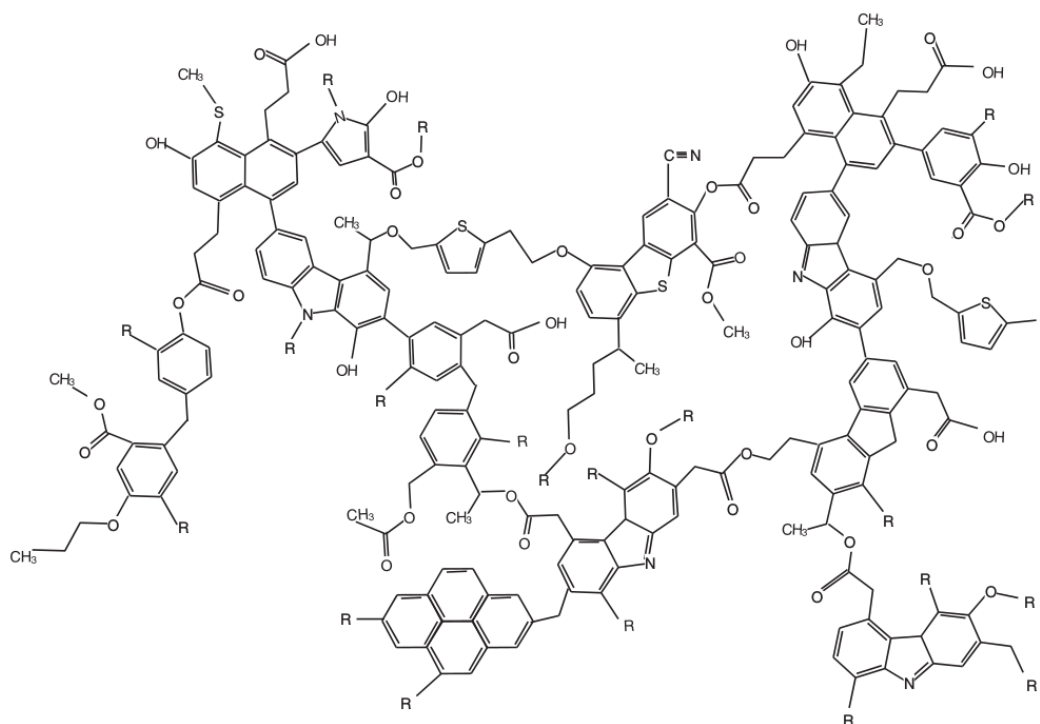


Figure 1.3: Model of molecular structure of Murchison insoluble organic matter. Figure is adapted with permission from John Wiley & Sons, Inc. [52].

1.3.2. Soluble organic matter - amino acids and beyond

Soluble organic matter in meteorites, often entitled as free organic compounds [15], is of high interest, especially in prebiotic focus of origin of life questions [55]. Herein, amino acids are perhaps the most often discussed compound class in carbonaceous chondrites. Special care is taken with the issue of terrestrial contamination [56–58], e.g. on carbon and nitrogen stable isotope composition [59]. Carbon isotopic measurements are routinely used to test organic target molecules for extraterrestrial origin [60].

Amino acids. Amino acids are building block for life within proteins. In addition, these molecules were found within astronomical environments, namely comets [20]. The Martian meteorite Allan Hills 84001 (ALH 84001) attracted intense media attention in 1996. U.S. president Bill Clinton gave a speech about potential life on Mars [61]. Interpretations based on studies on ALH 84001, which was examined for organic material and fossils [62]. Subsequent conclusions deciphered the detected fossils and polyaromatic hydrocarbons are probably artefacts or terrestrial contamination, respectively [63]. Isotopic measurements of ^{14}C amino acid measurements of ALH84001 could be related to antarctic terrestrial contamination [18]. Nevertheless,

1.3 Organic material in meteorites

the search for amino acids, building blocks of life, are an ongoing highlight within general meteoritic research. Analysis on fresh Murchison meteorite samples revealed the presence of both proteinogenic and non-proteinogenic amino acids, in concentration ranges of ≈ 60 ppm [15, 64]. ≈ 159 amino acid isomeric structures could be found in meteorites to date [14, 15].

Nucleobases. Moving one step further on the prebiotic ladder, nucleobases were found in Murchison meteorite, as well [60]. The nucleobases pyrimidine and purine are essential for terrestrial organisms, which depend on nucleic acids (RNA and DNA) to encode genetic information, a crucial biotic process in all known forms of life. In addition to Murchison, nucleobases were found later in other eleven meteorites, mostly carbonaceous chondrites [65]. Interestingly, Almahata Sitta #4, an ureilite meteorite, was reported to contain the nucleobase adenine, as well [65].

Sugars. Additionally, other prebiotically-relevant molecules were probed within meteorites. Studies on the carbonaceous chondrites Murchison and Murray revealed the presence of polyols (sugars and derivatives) [66], in comparable amounts to amino acids. Sugars are together with nucleobases two out of three essential building blocks of nucleic acids, the probably most important biomolecules. Only phosphorylation reactions keep the puzzle of astrochemical nucleic acid formation still alive to date [67–71].

Carboxylic acids. Next to proteins or nucleic acids, carboxylic acids are of significant biochemical importance. Vesicle formation, membrane bilayer structures and finally the built-up of biological minimal cells are mainly dependent on amphiphilic molecules, like carboxylic acids/fatty acids. Fatty acids represent a compact store of energy in cell membranes. Therefore, attraction was focussed on the analysis of carboxylic acids within meteorites [72, 73]. Carboxylic acids are known to reach concentrations of ≈ 300 ppm within carbonaceous chondrites and represent the most abundant organic species in meteorites [16].

Chirality. The concept of chirality is an important probe for living systems by differentiating L and D form enantiomeric conformers. In other words, homochirality represents a signature of life. To present-day knowledge, nature uses almost exclusively L-amino acid and D-sugar enantiomers to incorporate these biomolecular building blocks into protein or nucleic acid chemical machineries within living systems [74]. This phenomenon attracted many people within the field of origin of life studies. Enantiomeric excess of both amino acids [75] and sugars [76] were studied within meteorites. L-isovaline was found to have $\delta^{13}\text{C}$ values of $\approx +18\%$ [75]. Nevertheless, the origin of homochirality is still under debate [77–80]. Many theories have been presented, ranging from "by chance" versus "determinism", including chemical models like autocatalysis or physical models like enantiomeric amplification as triggered via circularly polarized electromagnetic radiation.

Generally spoken, soluble free organic compounds can be analyzed by two different analytical approaches, by means of targeted or nontargeted analytical strategies. Above described examples represent targeted analyses, in which a precisely defined goal exists, as the search for amino acids within a Martian meteorite to gain insights on the probability of existence of Martian life. Within this fairly rigid hypothesis-driven research, putatively important latent analytes may be overlooked. As following, motivations for nontargeted analytical methodologies and their manifold power within meteoritic organic matter studies will be given.

1.3.3. High-resolving chemical analytics - data-driven astrochemistry

A critical parameter within studying in-depth meteoritic organic matter is analytical instrumentation. A significant increase in instrumental quality has been observed over the last decades. Huge steps forward in terms of sensitivity and resolution have been done, caused by analyzing extraterrestrial samples by help of state-of-the-art analytical techniques. Special emphasis is set here on high-resolving chemical analytics. Modern equipment, like high-resolution mass spectrometry (MS), nuclear magnetic resonance spectroscopy (NMR) pushed organic astrochemistry significantly forward. Increase of sensitivity, accuracy and resolution by orders of magnitude within analytical instrumentation enabled previously "unseen" astrochemical insights, like the observation of ribose within interstellar ice analogs by two dimensional gas chromatography coupled to mass spectrometric detection (GCxGC-MS) [81].

In-depth compositional profiling - ultrahigh-resolving MS. Mass spectrometers are fine scales that weigh precisely masses of molecules. Ultrahigh-resolving analytics, like Fourier transform ion cyclotron resonance mass spectrometry (FT-ICR-MS) mass spectrometry, represent one of the most powerful tools to allow holistic insights into complex chemical spaces. FT-ICR mass spectrometry offers highest resolving power and mass accuracy among all types of mass spectrometers [82, 83]. In addition, high sensitivity is provided to enable the study of complex mixtures. Frequency-based measurements, like in FT-ICR-MS, result in extremely high mass resolving power ($R > 10^6$) and mass accuracy (< 200 ppb). This enables the differentiation of mass differences less than the mass of an electron. Measured m/z signals are assigned to molecular compositions.

In addition to ultrahigh-resolving FT-ICR-MS techniques, Orbitrap instrumentation is used more and more in astrochemical studies. In comparison to FT-ICR-MS, Orbitrap is lower in resolving power and mass accuracy by \approx one order of magnitude ($R \approx 10^5$ and mass accuracy ≈ 2 ppm) [84, 85]. Investigations on refractory carbonaceous components of comets [86], interstellar ice/pre-cometary ice analogs [87] or on meteorites were performed [88–90]. Striking results like the detection of nucleobases in meteorites were reported using high-end analytical methods [65]. Additionally, orbitrap mass analysers were also suggested as space mission instruments to characterize *in situ* planetary environments [91].

A disadvantage of mass spectrometry is that only molecular formulas are provided. No direct structural information is provided on a first hint. Nevertheless, data-analytical methods were developed to gain insights into chemical structural properties. Senior reported in 1951 graph-theoretical derivations (cyclomatic number) to elucidate chemical structural information out of molecular formulae [92]. Basic assumptions here are the similarity between molecules and graphs (networks). This mathematical concept allows for applying graph-theoretical rules on molecular systems. Based on Senior's work, many applications were reported to describe structural characteristics for given elemental compositions, e.g. the seven golden rules of Kind and Fiehn [93]. In addition, Pellegrin presented in 1983 a second, similar approach to Senior's, on the nitrogen rule and degree of unsaturation of organic molecules [94]. This approach has been applied further to describe chemical properties on aromaticity via the aromaticity index [95] or aromaticity equivalent approach [96].

1.3 Organic material in meteorites

Data-driven astrochemistry. Ultrahigh-resolving chemical analytics is directly connected to high-dimensional data sets. Schmitt-Kopplin et al. reported high chemical diversity and complexity within meteorites. Chemical information of thousands of individual components out of a complex organic mixture was assessed from diversely-classified meteorites [9, 97–100]. Tens of thousands of different molecular compositions and likely millions of diverse structures were observed in solvent extracts of pristine carbonaceous meteorites [9].

Data analytical tools are required to extract information out of these complex and diverse chemical data sets. Dealing with thousands of detected signals, visualizing data is a crucial first step to evaluate chemical analysis. A moderately simple, but powerful approach to plot data is a van Krevelen diagram [101]. Atomic ratios, mostly oxygen/carbon versus hydrogen/carbon, are plotted to gain information on complex high-dimensional compositional spaces. Fig. 1.4 shows a van Krevelen diagram of Murchison soluble organic matter, highlighting presence of a manifold number of organic molecules. $\approx 15,000$ molecular formulae are visualized. This representation enables to extract information regarding chemical classes at first sight [9].

Fatty acids/lipids, aromatic hydrocarbons, amino acids or sugar compounds were observed. In addition, this representation depicts information on homologous series, as revealed from experimental FT-ICR mass spectrometric data. Differentiation of the complex organic mixture into chemical spaces CHO, CHNO, CHOS and CHNOS is enabled. Variability in degree of unsaturation (via H/C ratio) and oxygenation (O/C ration) can be deciphered. van Krevelen diagrams enable also visual comparison of different samples regarding their chemical similarities.

Another data-driven analytical approach to get insights into complex organic chemical spaces is mass difference network analysis [102–104]. Herein, nodes represent experimental m/z values and edges (connections within the network) represent exact mass differences, which are equivalent to a net molecular formula of a chemical reaction. Holistic chemical diversity is visualized. Mass difference networks allow for studying unknown chemical substances (chemical dark matter). Additionally, chemical pathways can be studied within reaction sequences only by help of molecular formulas [105]. Fig. 1.5 shows a mass difference network of soluble organic matter

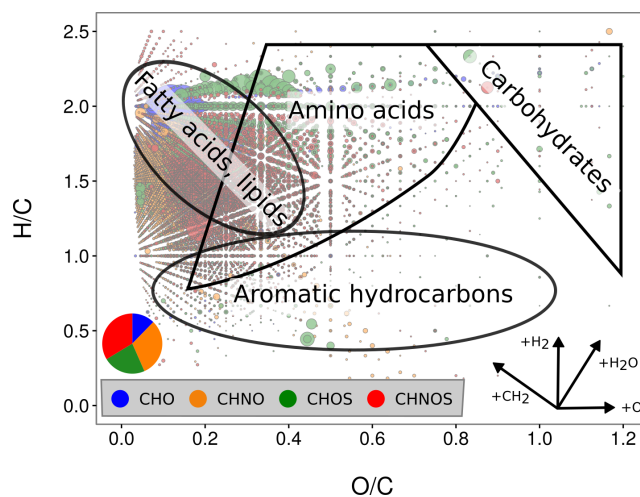
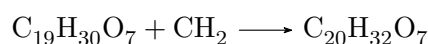


Figure 1.4: van Krevelen diagram of Murchison soluble organic matter. O/C versus H/C is plotted for negative ionization ESI-FT-ICR-MS methanolic soluble organic matter of Murchison. The bubble size is normalized to mass spectrometric intensity. Chemical subspaces: CHO (blue), CHNO (orange), CHOS (green), CHNOS (red). $\approx 15,000$ molecular formulae are shown [9].

1.3 Organic material in meteorites

of Murchison, as computed from negative ionization ESI-FT-ICR-MS experiments. $\approx 15,000$ molecular formulae are depicted to extract information on the global distribution of chemical spaces CHO, CHNO, CHOS and CHNOS [9]. In this analysis, edges (reaction-equivalent mass differences) are represented by fundamental astrochemical building blocks (e.g. H_2 , CH_2 , N_2 or SO_2). 66% of all mass differences are C-, H-, O-bearing molecular formulas. Thus, interconnections among heteroatomic chemical subspaces (e.g. CHO-CHNO transitions) are not widespreadly present and heteroatomic chemical spaces remain to be fairly separated. A zoomed-in picture of CHO-bearing molecules, including their respective connected mass differences, are depicted. This compartment within the complex chemical network illustrated exemplarily basic aliphatic carbon chemistry within Murchison soluble organic matter. Herein, an exemplary chemical reaction is:



Data-driven mass difference network analysis is highly sensitive to experimental mass accuracy. Routinely, mass accuracy ranges of ± 0.1 - 0.2 ppm are required to accurately perform valid results via mass difference network analysis. This makes this method still challenging for broadly adapted Orbitrap experimental data. Nevertheless, FT-ICR mass spectrometry enables valid experimental data for studying comprehensive chemical characteristics out of high-dimensional chemical space data sets [103, 104].

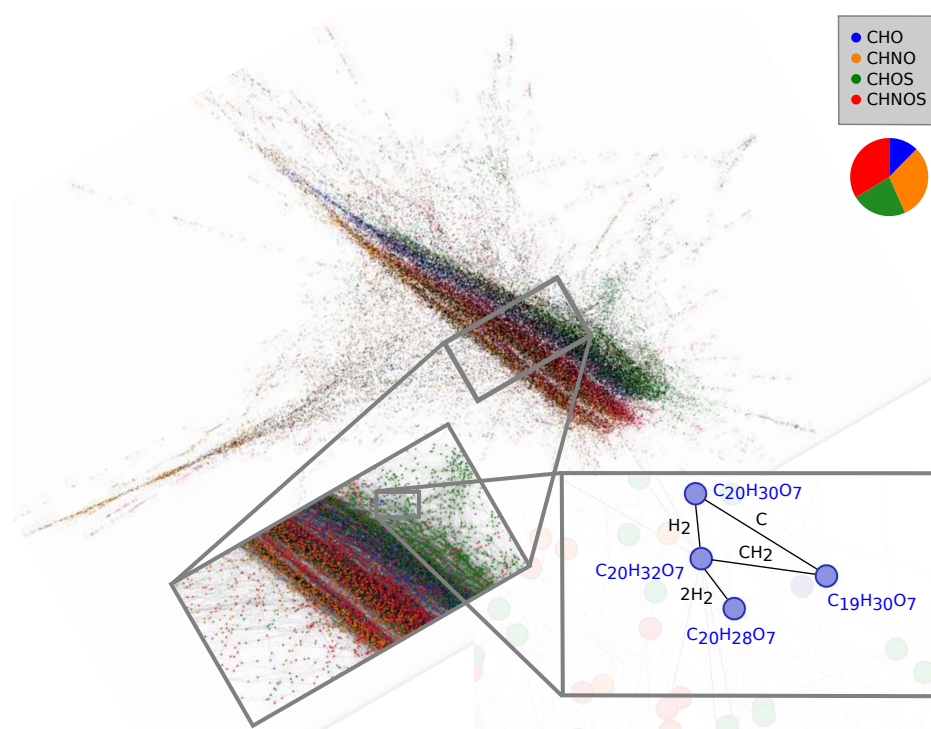


Figure 1.5: Mass difference network of Murchison soluble organic matter. Mass difference network of negative ionization ESI-FT-ICR-MS methanolic soluble organic matter of Murchison. The network was visualized via Gephi software [106], using the Force Atlas2 layout algorithm. Chemical subspaces: CHO (blue), CHNO (orange), CHOS (green), CHNOS (red). $\approx 15,000$ molecular formulae are shown [9].

1.3 Organic material in meteorites

Data science profits from global holistic data analysis by implementing statistical, ensemble-related data treatment to understand and analyze general phenomena with data [107]. A major aspect of motivation in data-driven science is that results and subsequent interpretations of scientific problems should be independent of the experimenter's hypothesis, but only be based on observed data [108]. High-resolving chemical analytics of meteorites, including thousands of data per sample, allow for moving forward in analyzing meteoritic organic matter by help of data-driven methods, such as network approaches or machine learning techniques [9, 109].

The application of multivariate statistical methods (e.g. principal component analysis, PCA or partial least squares analysis, PLS) will allow to extract significant features out of a multiple complex feature spaces with thousands of compounds each and further increase the disposable resolution [110, 111]. Therefore, discriminant molecules can be extracted, which differ in relative abundance between several samples, even out of complex chemical spaces.

Structural chemical information - organic spectroscopy.

Complementary to comprehensive compositional information, spectroscopic techniques, like NMR, infrared (IR) or Raman spectroscopy provide insights into chemical functionalities. IR spectroscopy studies revealed the presence of carbonyl compounds (aldehydes, ketones) in solvent extracts of Murray [113] or Orgueil meteorite [114]. Compositional diversity in meteoritic IOM was also revealed by IR spectroscopy [115]. Additionally, Raman spectroscopy represents an important tool within characterization of insoluble organic matter [50, 51]. NMR spectroscopy was used to characterize both insoluble [47, 52] and soluble organic matter [112]. Hertkorn et al. proposed in a nontargeted NMR approach a model for soluble organic matter for Murchison [112]. Aliphatic methyl, methyl in β -position to carboxylic groups and carboxylic groups were reported in a ratio 12 : 2 : 7.

Insights on chemical isomers - chromatography. In addition to compositional and structural information, differentiation of chemical isomers is probed via analytical separation techniques. Capillary electrophoresis (CE) analyses revealed insights on amino acid chirality [116]. Gas chromatographic studies (GC-MS) detected sugars [117], diamino acids [118] or nucleobases [60] in meteorites. Results from two-dimensional GCxGC-MS methods revealed the challenging detection of ribose out of a complex mixture including various conformers within interstellar ice analogs [81] and suggest a pathway for prebiotic ribose formation, the central molecular subunit in RNA.

By combining state-of-the-art chemical analytical techniques, probing composi-

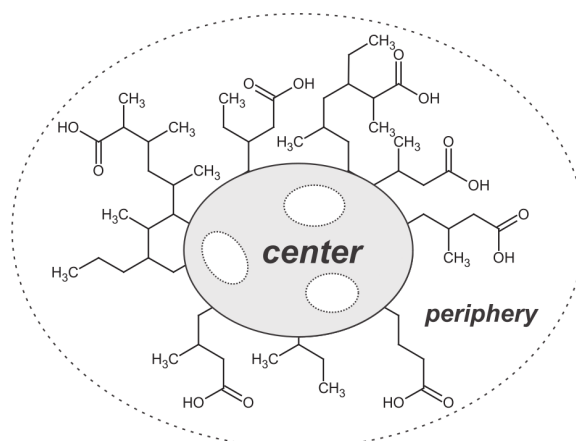


Figure 1.6: Model of molecular structure of Murchison soluble organic matter. Figure is adapted with permission from John Wiley & Sons, Inc. [112].

tional complexity, chemical structural information and isomeric specific data, chemical complexity can be studied in great detail. The Schmitt-Kopplin lab developed and optimized for more than a decade ultrahigh-resolving compositional FT-ICR-MS [9], structural NMR spectroscopic [112] and chromatographic [9] analyses on complex meteoritic organic matter in a holistic nontargeted analytical approach. It could be shown that coupled high-resolving analytics in combination with sophisticated data analytical methods (e.g. molecular networks) helps in expanding our knowledge in astrochemistry towards higher molecular masses and complex molecular structures [10, 97].

1.3.4. Targeted versus nontargeted analysis

The molecular diversity of extraterrestrial organic matter in carbonaceous chondrites represents a chemodiversity hotspot. As shown numerous times for Murchison, which is considered as carbonaceous meteoritic reference material, a manifold set of organic compounds were found. Chemical analysis were performed by means of both targeted [55, 117–119] and nontargeted [9, 112, 120] methodologies. Both approaches complement each other and converge in combination for gaining as much information on the studied scientific system as possible. On a first sight, the nontargeted methodology can be seen as a top-down profiling/screening approach, which profits from targeted complementary results (and vice versa), whereas the targeted approach elucidates specific systems in-depth in a bottom-up manner. In a nontargeted approach, all analytes are globally profiled within maximum analytical possibilities without biased or constrained hypothesis in order to gain comprehensive information in top-down manner. As such, holistic nontargeted analyses of meteoritic soluble organic matter revealed a much higher degree of molecular diversity than that found in any organic matter of terrestrial origin, as observed in Murchison [9, 112].

Thoughts on comprehensive chemical analysis. Every analytical chemical method starts with defining a hypothesis prior analysis. Targeted analysis mostly fix these hypotheses with respect to a set of defined molecules, which should be detected or quantified. Nontargeted approaches define the analytical goal by describing chemical processes, seeking for more global chemical description of a sample or studying interactions within a complex chemical network including all analytes. In short, the term *target* is synonym to chemical compounds within a sample. Nontargeted methods profit from not overlooking specific analyte molecules, which were not focussed during the hypothesis formation prior analysis [121]. Fig. 1.7 illustrates the power of curiosity-driven research, motivated for not defining too strictly analytical targets. In contrast, targeted methods are able to dig deeper for mechanistic studies of single analyte molecules. Therefore, both analytical strategies enable a powerful complementary set for analyzing chemical mixtures.

Generally spoken in abstract manner, the appropriate choice of an analytical method to probe a sample of interest is not so trivial - it can even become a philosophical problem. Probing a sample is motivated by a specific interest of an analyst. For example, one is interested into the absolute or relative abundance of one specific molecule in a sample, e.g. the absolute abundance of a specific amino acid within a Martian meteorite. Another type of analyst's interest could be the probing of intensity distributions of fatty acid homologues series within a sample of interest. On this second level, confounding effects for a set of single fatty acid molecules can be

1.3 Organic material in meteorites

tracked due to the simultaneous detection of chemically similar molecules. When moving one abstract layer forward, the interest of an analyst can be described as a comprehensive, holistic probing of a certain sample of interest. Herein all molecules of a sample are defined as actual analytes. In fact, in the third case samples will be studied, including its ingredients' interactions in total. Analytes are not treated as isolated systems *within* the sample of interest. A general sketch of different fundamental analytical strategies can be summarized as following.

- targeted Analytes are single molecules
→ Quantification/monitoring of single molecules/studying molecules on a mechanistic level
- semitargeted Analytes are a set of molecules
→ Relationships of chemically similar molecules
- nontargeted Analytes are all present molecules (in theory)
→ Information on as many as molecules and their in-between interactions/screening of global molecular spaces

Nontargeted analysis in practice.

The analytical scenario of a global, holistic screening of both, analytes and analytes' interactions represents an ideal, which cannot be realized practically. It is obvious that *all molecules* cannot be sampled simultaneously within one analytical method. Instrumental constraints limit the coverage of analytical targets within an experiment. For instance, in mass spectrometry, certain number of molecules are discriminated by the ionization mode (e.g. apolar molecules in electrospray ionization - ESI). Another example is the analytical technique gas chromatography, which specifically focusses on volatile chemical compounds.

When thinking on targeting a chemical sample as holistic as possible, the analytical matrix sets the role of the chemical analytes, which goes in hand with several problems. In targeted analysis, the interfering effect which can confound a target peak is called matrix effect [121]. Methods were developed to balance out the matrix when targeting single compounds, e.g. the standard addition method [121]. However, in nontargeted strategies, the matrix effect cannot be tracked such easily and represents a present-day problem within this kind of analytical approach [123]. Therefore, the intention of holistically probing a chemical system is a fundamental problem of experimental research. Results and interpretations are always dependent on "what you see", meaning scientific conclusions are dependent on detection specificity and sensitivity. **So, what is actually a global chemical profile?** In practice, nontargeted, comprehensive analysis is dominated by high-dimensional big

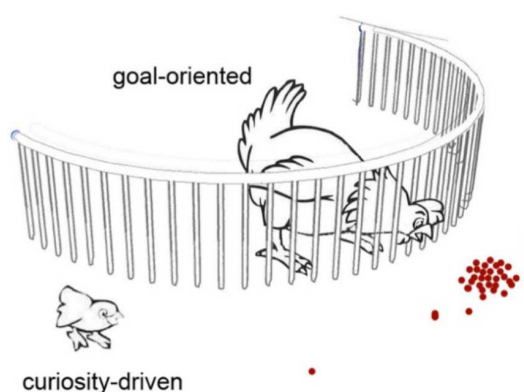


Figure 1.7: Curiosity-driven research This figure is adapted with permission from ©The Nobel Foundation, nobel lecture of Laureate Theodor W. Hänsch, Stockholm, Dec. 8, 2005 [122].

1.3 Organic material in meteorites

data experiments (data-driven astrochemistry), which are discussed above.

1.3.5. Comprehensive chemical profiling of meteoritic organic matter

Studying meteoritic soluble organic matter via nontargeted analytical strategies (data-driven astrochemistry), represents a powerful tool to probe astrochemical complexity in a broad molecular range (100 - 1,000 amu, atomic mass units). To date, thousands of individual components were profiled within complex organic mixtures from diversely-classified meteorites [9, 112]. Likely millions of diverse structures were observed in solvent extracts of pristine C chondrite meteorites [9, 112]. This suggests that interstellar chemistry is extremely active and rich.

The extreme richness in chemical diversity of meteoritic soluble organic matter offers information on the meteoritic parent body history. Hints on heteroatom incorporation and its chronological assemblies, shock and thermal events can be extracted by advanced data analytical methods of these correlated high-dimensional data sets [10]. Heteroatomic organic and metalorganic molecules (e.g. N-, S- or Mg-bearing compounds) play an important role in the description of chemical evolution. It could be shown that coupled high-resolving analytics in combination with sophisticated data analytical methods (e.g. molecular networks) helps in expanding our knowledge in astrochemistry towards higher molecular masses and complex molecular structures [10].

Nitrogen chemistry. Heteroatomic organic molecules were found to play an important role in the description of chemical evolution. The thermally and shock-stressed Chelyabinsk (LL5 chondrite) [98] showed high numbers of nitrogen atoms within CHNO molecular formulas, relative to other L-type meteorites with lower shock grades, especially in the melt region. Analogous concordance could be also observed for Soltmany (L6 chondrite) [97] Novato (L6 chondrite) [124], Braunschweig (L6 chondrite) [125]. L and LL ordinary chondrite meteorites are similar in their petrologic composition

Sulphur chemistry. The extremely thermally altered Sutter's mill (C-type) reflects a loss in the organic diversity, but an increase in the polysulphur domain, as compared to other CM2-analyzed falls [10, 126]. Sutter's mill soluble organic matter specifically exhibit many signals in mass range 318.75 - 319.0 amu, corresponding to oxygen-rich and multiple sulphur-containing molecules

1.3.6. Combining experimental and computational techniques

Astrochemistry deals with molecular complexity and diversity [1]. The presence of ≈ 200 molecules to be detected in interstellar and circumstellar medium was not always expected by the scientific community [2]. This remarkable chemical space is not trivial to understand regarding the formation and stability of its consisting organic molecules under highly energetic (gradual) conditions in astronomical environments. The combination of quantum chemical simulations with observational results is powerful to understand astrochemical systems [127]. With significant increase in computational power over the past years, large molecular systems could be realized to probe via molecular simulations.

As an example, interstellar grain prebiotic chemistry was computed by means of interactions of glycine and alanine on polycyclic aromatic hydrocarbon flakes [128].

1.4 Organometallics in astrochemistry

Enhanced stability of the carboxyl group by chemisorption could be found and implications on enantioselection were proposed. This work is one example for putatively important results in prebiotic chemical evolution in absence of experimental data. Nevertheless, the power of quantum chemistry herein is to help laboratory experimental modeling and observational studies by suggesting theoretical data, like here on adsorption energies within this relevant interstellar prebiotic system. As another example, quantum chemical studies could shed insights into the lack of detection of interstellar anions [129]. This work underlines the importance of valence and dipole-bound excited states in the detection of anionic species in ISM. These results may help in addition to laboratory data future work on the detection of interstellar anions.

In terms of computational methods, specific emphasis should be taken on density functional theory (DFT) and second-order Møller–Plesset perturbation theory (MP2). These two quantum chemical methods were mainly used in this work.

Density functional theory (DFT) is the current workhorse in theoretical chemistry determining electronic structures. In difference to traditional *ab initio* quantum chemistry concepts like Hartree-Fock theory (HF), DFT replaces Ψ by the electron density function ρ to describe the quantum mechanical system and its energy [130]. DFT often succeeds in computational costs over *ab initio* quantum chemical methods and can be therefore adapted to medium-large molecular system (<50 atoms). Sensitive to accuracy of DFT results is majorly the choice of the functional and the basis set regarding the respective chemical system to compute.

Møller–Plesset perturbation theory (MP2) represents an *ab initio* quantum chemical method, describing a system's energy by the many-body wave function Ψ . In advantage to Hartree-Fock theory (HF) routines, MP2 computations include electron correlation effects, which increases the accuracy in describing electronic properties of a chemical system [131]. Practically, MP2 computations are more accurate than DFT simulations, but are also computationally much more expensive. Therefore, MP2 simulations on moderately large molecular systems are not fully practicable.

In conclusion, the interplay between experimental and computational methods are powerful within organic astrochemistry studies. Sparse observational data or the degree of complexity of targeted chemical network require help from quantum chemistry methods. Increasing computational power enables nowadays a quantum-mechanical description of challenging complex molecular systems, including fairly high number of atoms.

1.4. Organometallics in astrochemistry

Organometallic molecules are rarely discussed in astrochemistry yet [132, 133]. Scientists focussed mainly on studying either organic material (discussed above) or minerals [134] within astronomical environments. Interestingly and contradictory to the lack of research, they are supposed to represent key intermediates for organic evolution.

Particularly as reported for interstellar medium reactions, iron interactions with polyaromatic hydrocarbons (PAH) are discussed. The formed Fe-PAH complexes have been proposed to influence the growth of PAH in evolved star envelopes and influence therefore the formation of aromatic organic molecules within these as-

1.5 Relevance of (metal)organic astrochemistry - astrobiological implications

tronomical environments [135, 136]. Additionally, Fe^{n+} has been proposed to be involved in the destruction/formation of CO [137] and formation of HCO [137].

In meteoritic context, few work was done on mineral-organic spatial associations, e.g. interactions between aromatics and carboxylic functional groups with phyllosilicates for Renazzo meteorite (CR2 chondrite), Murchison (CM2 chondrite) and Orgueil (CI chondrite) [138], suggesting modification of organic matter by clay-mediated reactions [139]. Additionally, associations between aliphatic CH and OH in phyllosilicates in Tagish lake meteorite (C2-ung chondrite) were found [140].

Generally, organometallic species are well-known from classical organic laboratory to efficiently catalyze various reactions [141]. This stimulates research on astrochemical molecules within astrochemical environments. As indicated above, the origin and formation of early complex organic molecules within meteoritic chondrules is still unknown. One putative pathway might be the formation via organometallic intermediate states. Studies on the hypothesis that the formation of soluble organic matter in meteorites is related to mineral aqueous alteration were performed previously [142]. Nevertheless, the problem of primordial complex organic molecule formation still remains largely unsolved. **Thus, more extensive research on complex organic molecules formation and the role of organometallic species therein has to be done.**

1.5. Relevance of (metal)organic astrochemistry - astrobiological implications

Research on complex organic molecules within astrochemical environments is often connected to astrobiological questions, like the search for building blocks of life [143–145]. When searching for building blocks of life, one would need to define life first. This represents an intrinsic problem within this scientific question itself, since the definition of life is a long ongoing manifold challenging task [146]. Many prominent scientists, e.g. Erwin Schrödinger, have done research on the question of definition of life [147]. While digging deeper into a guess to strictly define life in a physical manner, many problems rose up [147–149]. As an example, Schrödinger reported the problem of negative entropy within a rigorous physical definition [147].

Generally, life can certainly be defined through a collection of characteristics. Due to enormous physical and chemical complexity, this methodology would be more profitable rather than a concept of definition via strict mathematical derivations. Many definitions are biologically-oriented, including basically four characteristics, as proposed by Schulze-Makuch and Irwin [146].

- metabolism
- growth
- reproduction
- adaptation to environment

Benner, Ricardo and Carrigan asked for "a common chemical model for life in the universe" [150]. For an astrochemistry community, a chemical way of defining life might be more intuitive. Benner, Ricardo and Carrigan listed the following parameters as fundamental requirements for life.

1.5 Relevance of (metal)organic astrochemistry - astrobiological implications

- | | |
|------------------------------------|--|
| • thermodynamic disequilibrium | assuming Darwinian evolution to be a progressive process and that "that life actually does something" |
| • bonding | covalent bond, e.g. C-C |
| • isolation within the environment | Darwinian cycle can proceed only if it replicates itself in preference to others; compartmentalization |
| • carbon-like scaffolding | "machinery's nutrients" |
| • energetic patterns in metabolism | no equilibrium, but energy transfer |
| • solvent | efficiency of chemical reactions within liquid phase |

Independent of the exact definition of life, a common aspect is the need for organic molecules (nutrients) within a living environment. Therefore, the search for organic molecules in putative habitable environments is required as one fixed criterion for life. Second, energetic conditions (temperature, pressure, electromagnetic radiation) are also important to be profiled, since energetic patterns in metabolism are needed for living systems. In conclusion, the search for organic compounds as building blocks of life is necessarily related to their surrounding energetic conditions to ask for molecular local stability and energetic reaction patterns within a found local chemical network.

Organic molecular diversity in meteorites likely reflects an integrated temperature history of the respective bodies [98, 124–126]. Cometary systems and primitive bodies are conserved at lower temperatures (both CM2 primitive meteorites, keeping their original chemical complex signature and CM2 meteorites that have been altered with temperature and/or aqueous alteration) [16]. Since most meteorites undergo high energy gradients within astrophysical environments, especially during the formation of a meteoroid body, high energy local surface temperatures and pressures are involved when two celestial bodies collide. The presence of highly diverse extraterrestrial meteoritic organic matter seems to be in contradiction on a first glance. Therefore, thermolabile organic molecules (e.g. carboxylic acids [153]) must be operative under a wide range of conditions. The following questions thus arise:

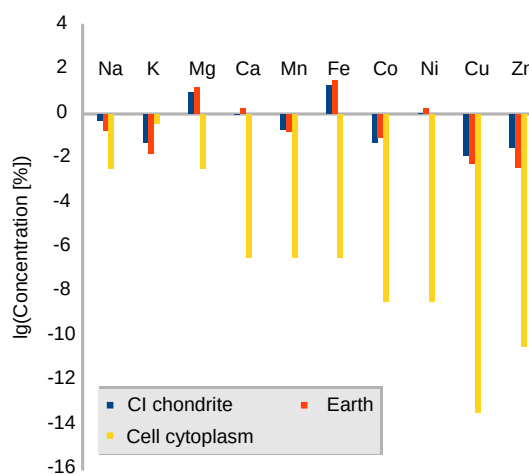


Figure 1.8: Metal distributions for meteorites, Earth and a biological system. Data are adapted from Lodders for CI chondrites [31], McDonough for Earth [151] and Williams for cell cytoplasm [152]

1.5 Relevance of (metal)organic astrochemistry - astrobiological implications

- Are intermediate states within chemical evolution required to preserve organic compounds?
- Can minerals stabilize organic molecules within geological time scales?

The interaction of organic matter and minerals, especially clay minerals, is known to play an important role in organic chemical evolution via catalytic effects in meteorites [139]. The importance of metal ions within chemical evolution has been previously suggested numerous times [154–156]. Metal ions may drive prebiotic reactions via free-radical reactions. In particular, their role in peptide formation was studied in clay environments by polymerization of alanine and glycine [157].

In biological, living systems (end-members of chemical evolution), metal ions play essential roles in about one third of enzymes [158]. Therein, metal ions are significantly involved in biochemical electron flow processes in a substrate or enzyme or change substrate molecular conformations via specific bindings [159].

Metal abundance distributions for several environments following the time line of chemical evolution (meteorites - Earth - biological system, Fig. 1.8) give insights on the relevance of different elements. Magnesium Mg and iron Fe are most abundant species for all three chemical systems, meteorites, Earth and biological cell cytoplasm. In parallel, the significance of magnesium in traditional organometallic chemistry has been broadly studied and well-known [141]. Both abundance and organometallic affinity motivate for probing magnesium-organic compounds within context of chemical evolution. The finding of magnesium-bearing species (MgCN [160]) in proto-planetary nebulae argues for studying this research topic.

1.6. Motivation and objectives of the thesis

The co-existence of manifold organic chemical diversity and high astrophysical energy history of meteorites sets the basic motivation of this work. Organometallic species are supposed to preserve organic compounds, especially prebiotically-relevant molecules like fatty acids within chemical evolution. The role of intermediate organometallic chemistry is asked and studied by help of experimental ultrahigh-resolving chemical analytics of meteoritic samples, combined with quantum chemical computations on chemical stability of metalorganic molecules. Both abundance and organometallic affinity of magnesium-bearing molecules motivate for probing magnesiumorganic compounds within astrochemical context. The outline of this work is illustrated in Fig. 1.9. As a coarse guide, section 2 describes the detection of previously unknown organomagnesium compounds, dihydroxymagnesium carboxylates $[(\text{OH})_2\text{MgO}_2\text{CR}]^-$ (CHOMg) in meteorites. Section 3 and section 4 study fundamental chemical properties of dihydroxymagnesium carboxylates. In addition, their chemical stability is discussed on both experimental and theoretical levels.

Section 2 describes the detection of CHOMg in meteorites. Dihydroxymagnesium carboxylates represent an unreported chemical class, which has not been reported to date in chemical databases (e.g., ChemSpider, SciFinder, and PubChem). We demonstrate the occurrence and remarkable diversity of CHOMg compounds within meteoritic soluble metalorganic matter and present discussions on chemical properties and reactivity of dihydroxymagnesium carboxylates. Molecular diversity makes meteorites ideal samples to elucidate fundamental organic chemical reactivity. Additionally, CHOMg signatures can be related to meteoritic thermal history and fractionation processes.

In a next step, we ask for the chemical stability of these novel chemical compounds, dihydroxymagnesium carboxylates. Quantum chemical studies gained insights into decarboxylation fragmentation mechanisms (section 3). Computations were performed by means of both second-order Møller–Plesset perturbation theory (MP2) and density functional theory (DFT) methods. Release of CO_2 from dihydroxymagnesium carboxylates enables formation of Grignard-type dihydroxymagnesates. Fragmentation probability and chemical characteristics of putatively formed Grignard-type molecules will be discussed.

Section 4 studies chemical stability of dihydroxymagnesium carboxylates regarding alkyl chain fragmentation. Odd/even alternation effects were observed within the stability of CHOMg molecules. In addition, chemical properties of CHOMg-related fatty acid compounds were discussed. Amplification of even carbon-bearing CHO and CHOMg molecules were observed and their implications on chemical evolution will be discussed.

1.6 Motivation and objectives of the thesis

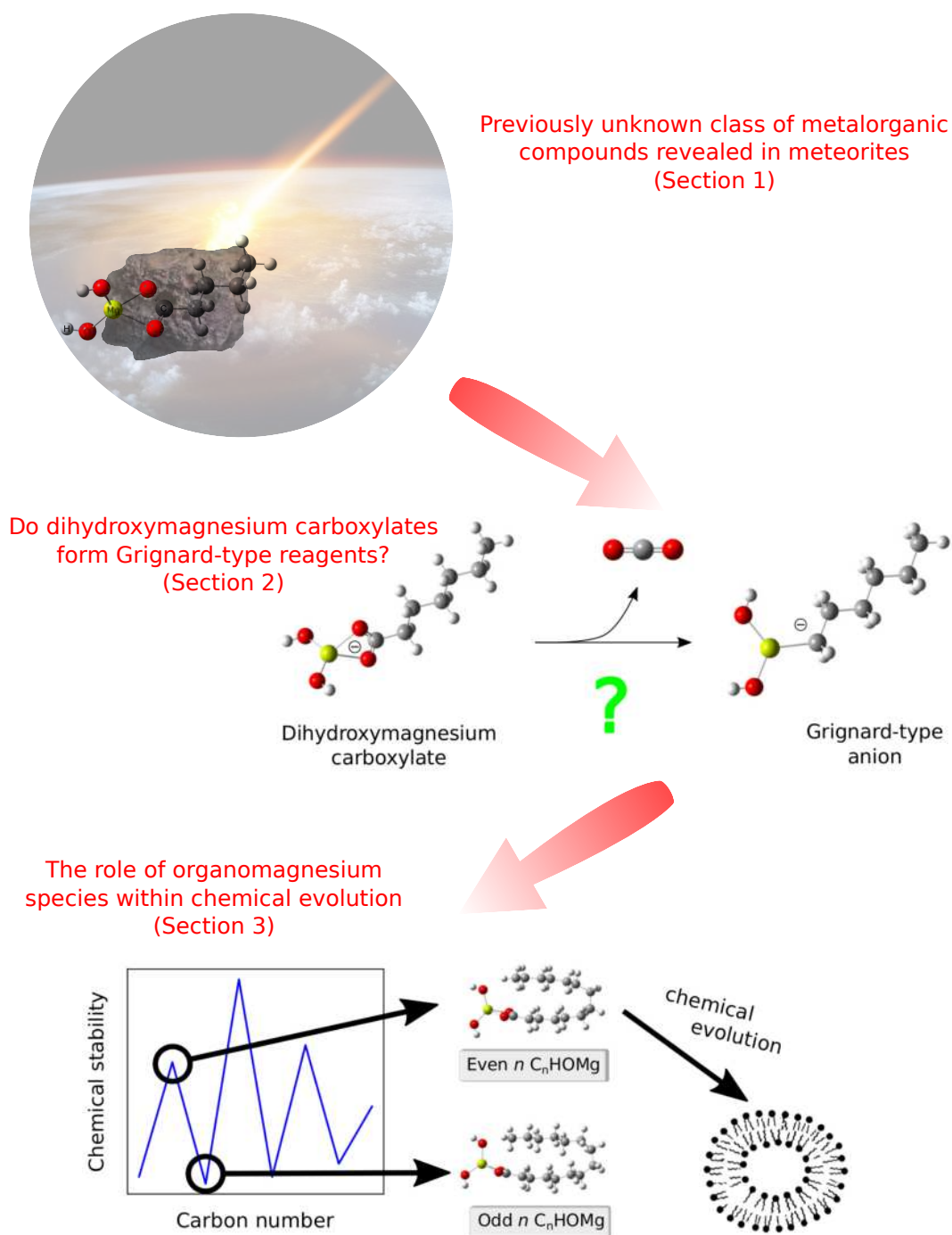
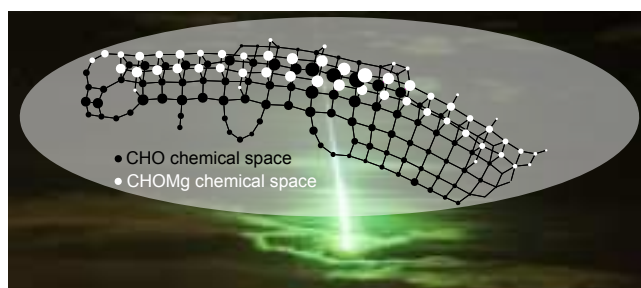


Figure 1.9: Outline of this thesis.

2. Previously unknown class of metalorganic compounds revealed in meteorites



The rich diversity and complexity of organic matter found in meteorites is rapidly expanding our knowledge and understanding of extreme environments from which the early solar system emerged and evolved. Here, we report the discovery of a hitherto unknown chemical class, dihydroxymagnesium carboxylates $[(\text{OH})_2\text{MgO}_2\text{CR}]^-$, in meteoritic soluble organic matter. High collision energies, which are required for fragmentation, suggest substantial thermal stability of these Mg-metalorganics (CHOMg compounds). This was corroborated by their higher abundance in thermally processed meteorites. CHOMg compounds were found to be present in a set of 61 meteorites of diverse petrological classes. The appearance of this CHOMg chemical class extends the previously investigated, diverse set of CHNOS molecules. A connection between the evolution of organic compounds and minerals is made, as Mg released from minerals gets trapped into organic compounds. These thermostable compounds might have contributed to the stabilization of organic molecules on a geological time scale, which emphasizes their potential astrobiological relevance.

2.1. Introduction/motivation

The molecular diversity of extraterrestrial organic matter in carbonaceous chondrites has been studied by means of both targeted [55, 117–119] and nontargeted [9, 112, 120] analytical methodologies, which are complementary to each other. The targeted approach focuses on molecules of biological/prebiotic interest in greater detail, such as amino acids, nucleobases, or carbohydrates [162], overlooking other analytes. In the nontargeted approach all analytes are globally profiled to gain comprehensive information. As such, holistic nontargeted analyses of meteoritic soluble organic matter revealed a much higher degree of molecular diversity than that found in any organic matter of terrestrial origin, as observed in Murchison [9, 112]. The Murchison meteorite (CM2 type, where CM refers to Mighei-type carbonaceous chondrite) is the most investigated meteorite, typically seen as an example of abiotic organic complexity and a model of the processes that occurred inside its asteroid parent body [9].

Few metalorganic compounds have hitherto been described in the meteoritic context [133], despite the close proximity and intercalation of the mineral and organic phases in meteoritic materials. Fioroni predicted the identification of metalorganic species in measureable quantities; however, these have not been detected yet, either by spectroscopic techniques or upon meteorite analyses. Carbonaceous meteorites, such as Murchison (CM2) or Orgueil (CI1), are heterogeneous in organic molecular species and their abundances [138, 163]. These organic materials, including carboxylic compounds, are known to be mixed with Mg-rich phyllosilicates [138]. The interaction of organic matter and minerals, especially clay minerals, plays an important role in the evolution of meteoritic organic matter via catalytic effects [140]. Mg is one of the most abundant elements in the solar system [31] and is an important component in many common rockforming minerals. Furthermore, relative to other elements in the first three groups of the periodic table, Mg offers the highest propensities of forming metalorganic compounds [164], for example chlorophyll or Grignard reagents. Classical metalorganic compounds with a covalent Mg–C bond exhibited high binding energies with a distinct thermal robustness and an appreciable photostability [165].

Mg commonly occurs as a divalent cation that is coordinated to six water molecules or other oxygen-containing ligands [166]. Meteorites contain Mg-rich minerals (Fig. 2.1) [167] and complex organic compounds [9, 55], which are thought to evolve chemically, not simultaneously, in the early solar system [142, 168]. For example, Fischer–Tropsch-type (FTT) reactions are believed to play an important role in providing pathways to form (complex) organic molecules. The reacting molecules in FTT reactions are CO, H₂, and inorganic minerals as catalysts [169]. Another hypothesis for organic matter formation is the mineral alteration by aqueous alteration (18). In both cases, minerals, including those that bear Mg [170], have a potential consequence on the organic chemistry in space.

Here, we demonstrate the occurrence and remarkable diversity of previously unrecognized CHOMg compounds within meteoritic soluble organic matter and present the chemical class of dihydroxymagnesium carboxylates, followed by a discussion of their chemical properties and reactivity. CHOMg signatures will be shown to relate to meteoritic thermal history and fractionation processes.

2.1 Introduction/motivation

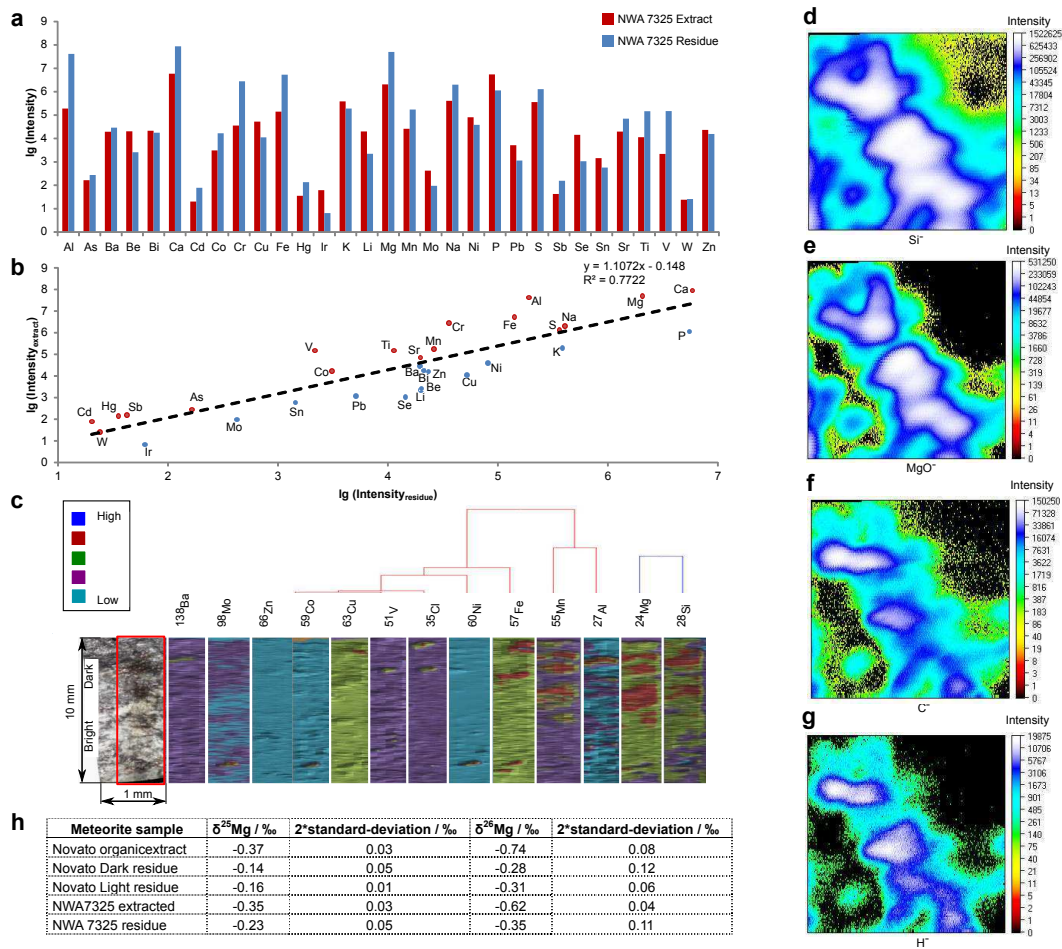


Figure 2.1: Elemental analysis. Element abundances in the methanolic extract and the residue sample of the NWA 7325 meteorite are shown, as obtained from ICP-MS data. (A) A bar graph with the decimal logarithm of the measured element's intensities, provided for 31 elements in the extract (red) and in the residue (blue). (B) A linear regression between the extract's intensity and the residue's intensity, both expressed in the decimal logarithm, is presented to reflect the solubility potential of the measured elements. The red data points represent elements enriched in extracts, and the blue-labeled elements remain in residue. High abundances for Al, Ca, and Mg and volatile elements are enriched in the extract, with exceptions, mainly observed at trace levels. Spatially resolved elemental distribution of the Novato meteorite surface is depicted, as gained from LA-ICP-MS measurements, for the dark and the bright site of the specimen (C). HCA of 13 element profiles reveals extensive concordance of the abundant elements Mg and Si, which is in agreement with dominant magnesium silicates in the solid-state phase. SIMS analyses results of a glassy vein of the LL5 ordinary chondrite Chelyabinsk specimen are shown with the mapped intensities of Si^- , MgO^- , C^- , and H^- (D–G) This supports that the analyzed specimen is rich, both in C^- and H^- (likely organic matter), next to congruent areas of Si^- and MgO^- (magnesium silicates). (H) Mg isotope results of organic extract and whole-rock residues for Novato and NWA 7325.

2.2 Evaluating the CHOMg Chemical Space

2.2. Evaluating the CHOMg Chemical Space

Our methods and processes for conducting electrospray ionization Fourier transform ion cyclotron resonance mass spectrometry (ESI-FT-ICR-MS) on soluble organics in meteorites are described in the Appendix A.3. To understand the nature of previously unassigned peaks, we studied 61 meteorites with different petrologic types, covering a wide range of meteorite classes (Table S1). The selected representative meteorites include achondrite Northwest Africa 7325 (NWA 7325, ungrouped [171]), ordinary chondrites Novato and Chelyabinsk [98, 124], and carbonaceous chondrite Murchison (CM2 [9]).

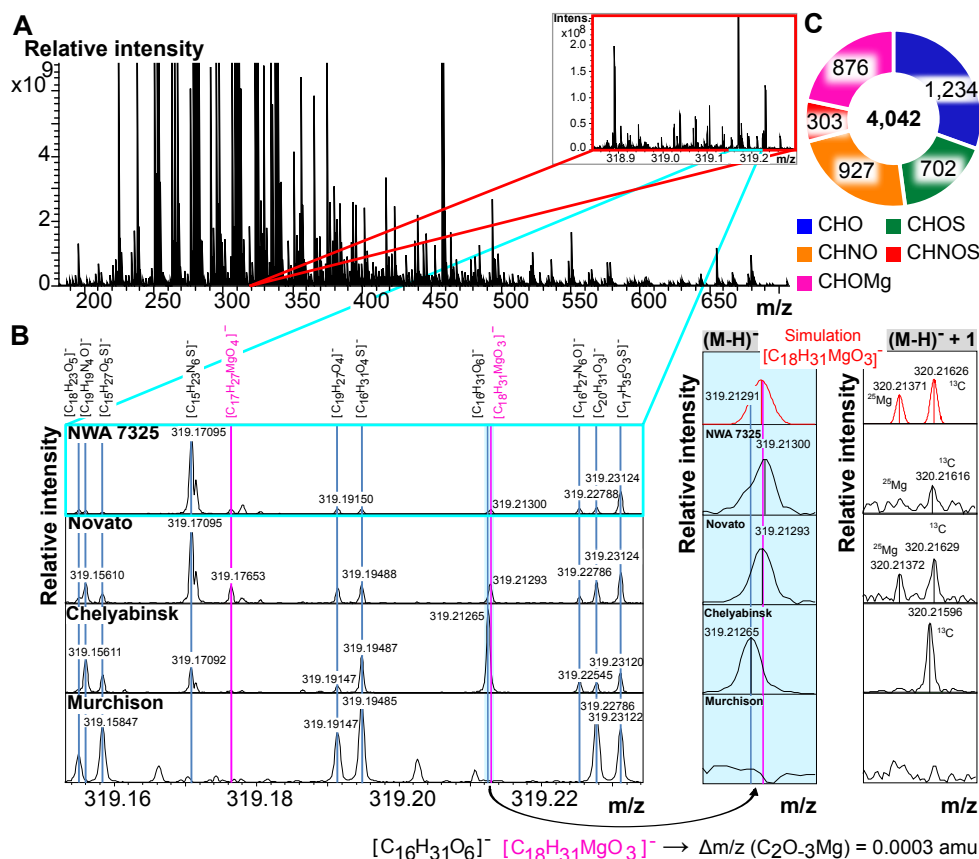


Figure 2.2: Detection of the CHOMg chemical space. Negative ionization mode ESI-FT-ICR mass spectrum of an ungrouped achondrite (NWA 7325) is shown (A). It is aligned together with two ordinary chondrites (Novato and Chelyabinsk) and a carbonaceous chondrite meteorite (Murchison) by CHNOS compounds (B). Some distinct mass peaks were detected that are nonaligned and represent CHOMg compounds (pink labels). Less than one electron mass difference ($\Delta m/z = 0.0003$ amu) between the isobaric molecule ions $[C_{16}H_{31}O_6]^-$ and $[C_{18}H_{31}MgO_3]^-$, with the corresponding mass difference of $C_2O_{-3}Mg$, requires an ultrahigh mass resolving power and high mass accuracy to enable unambiguous differentiation between the CHNOS and the CHOMg chemical spaces. The second most abundant CHOMg isotopologue, here at $m/z = 320$, consists of two peaks (^{25}Mg and ^{13}C) of comparable amplitude. The specific presence of $[C_{18}H_{31}MgO_3]^-$ is confirmed in NWA 7325 and Novato but excluded in Chelyabinsk and Murchison meteorites, which only display the single ^{13}C -based peak and no second isotopologue mass peak at $m/z = 320$. (C) Relative abundances of NWA 7325 chemical species are depicted.

2.2 Evaluating the CHOMg Chemical Space

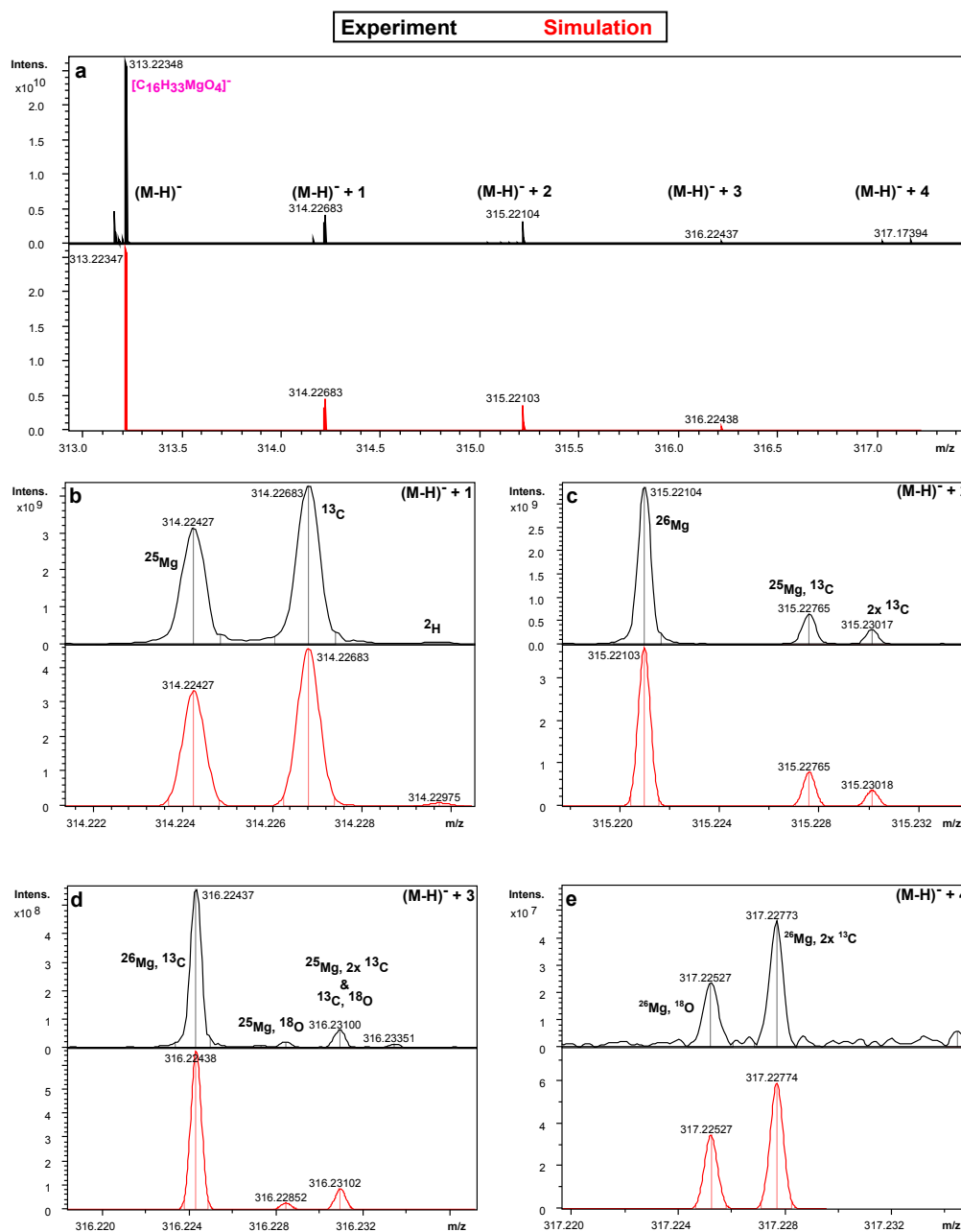


Figure 2.3: Isotopic fine structure for the $[\text{C}_{16}\text{H}_{33}\text{MgO}_4]^-$ molecule ion. (A–E) $[\text{C}_{16}\text{H}_{33}\text{MgO}_4]^-$ was identified via its isotopologues in the Novato methanolic extract, as seen in ESI-F T-ICR mass spectra. The black spectrum is the experimental mass spectrum from Novato extract, and the red profile represents the theoretically computed isotopic pattern at natural abundance of C, H, O and Mg. The observed isotopic distribution is primarily caused by the isotopes $^{24}/^{25}/^{26}\text{Mg}$, $^{12}/^{13}\text{C}$, $^{16}/^{18}\text{O}$ and $^{1/2}\text{H}$. To separate each isotopologue at FWHM, a minimum mass resolving power of $R \approx 125,000$ at $m/z = 313$ is required. Beyond CHOMg, the total combinatorial molecular complexity within the sample set includes N and S compositions. The mass resolving power of $R \sim 500,000$ helps to exclude more complex combinatorial formula solutions, which contain, for example, nitrogen and sulfur and discriminates unambiguously the CHOMg from the CHNOS chemical compositions.

2.2 Evaluating the CHOMg Chemical Space

The mass spectra of the ungrouped achondrite NWA 7325 show a very dense CHNOS space of soluble organic compounds, comparable to ordinary chondrites (Fig. 2.2). Recurrent patterns of 876 unassigned mass peaks were discovered to which we assigned CHOMg formulas (Fig. 2.2). These mass peaks accounted for 22% of peaks in the soluble organic matter of NWA 7325, 26% in Novato, and 24% in Chelyabinsk, all of which underwent significant heating during petrogenesis, but only 2% in the comparatively primitive meteorite Murchison; absolute quantities are not directly accessible via ESI. Nevertheless, CHO and CHOMg compounds are observed in almost equal mass peak counts n for thermally stressed meteorites [$n(\text{CHO}) : n(\text{CHOMg}) \approx 1:1$]. CHO compounds represent the major soluble organic compounds in ordinary chondrites, ranging up to ~ 300 ppm [55]. Thus, CHOMg compounds are expected to be in a similar concentration range.

The unambiguous distinction between the CHNOS and the CHOMg chemical spaces requires an extremely high mass resolving power ($R > 10^6$) and mass accuracy (< 200 ppb, Fig. 2.2) to differentiate mass differences less than the mass of an electron. At lower mass resolving power, CHOMg compositions would be largely occluded by merging with the CHNOS compositional space. To avoid any alignment error due to this m/z overlap, CHNOS compounds are shown to reveal the precise internal calibration (Fig. 2.2). The $^{24/25/26}\text{Mg}$ isotopic fine structure analysis validated the existence of C-, H-, O-, Mg-based compositions (Fig. 2.2 and Fig. 2.3).

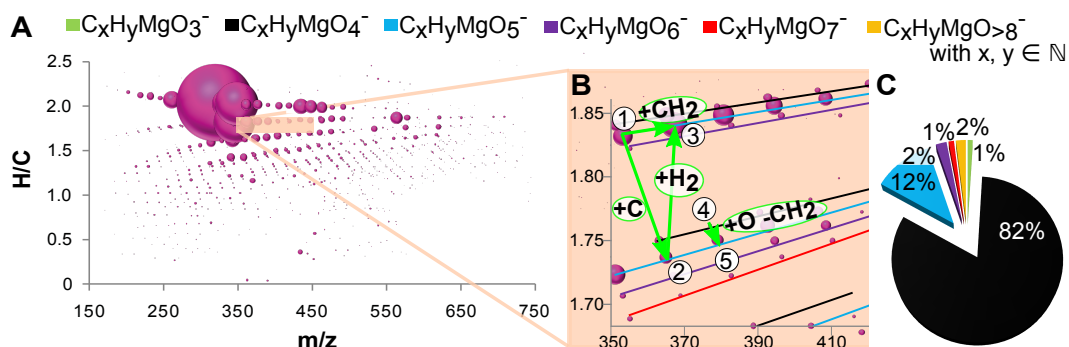


Figure 2.4: Characteristics of the CHOMg chemical space. CHOMg chemical compositions of NWA 7325 soluble organic matter are depicted by massed H/C ratio, for the complete A) and zoomed-in compositional space (B), illustrating the density of fairly complete homologous series within the CHOMg compositional space. The bubble size represents the relative intensity of the mass peaks. The detailed arrangement of CHOMg compounds allows visualization of nominal elemental/molecular transformations, with examples provided (circled numbers: ①, $\text{C}_{18}\text{H}_{33}\text{MgO}_5^-$; ②, $\text{C}_{19}\text{H}_{33}\text{MgO}_5^-$; ③, $\text{C}_{19}\text{H}_{35}\text{MgO}_5^-$; ④, $\text{C}_{21}\text{H}_{37}\text{MgO}_4^-$; and ⑤, $\text{C}_{20}\text{H}_{35}\text{MgO}_5^-$). (C) Relative abundances of these Mg-metalorganics, shown in different colors (B and C), demonstrate the dominance of the MgO_4R^- molecular subspace, with $\text{R} = \text{hydrocarbon } \text{C}_x\text{H}_y$ and $\{x,y\} \in \mathbb{N}$.

2.2 Evaluating the CHOMg Chemical Space

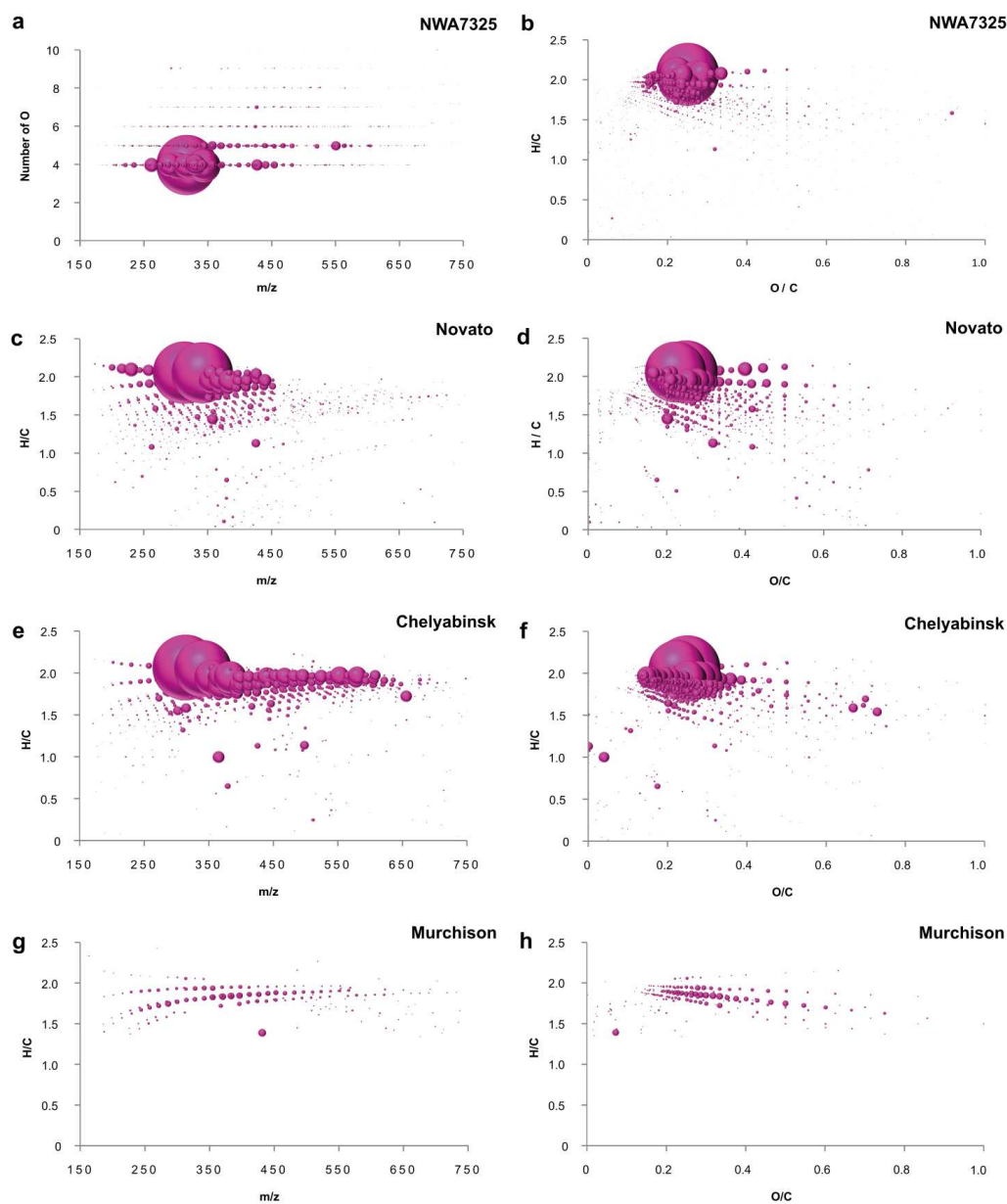


Figure 2.5: Complexity of the CHOMg chemical space. (A) The dominance of CHOMg molecules possessing four oxygen atoms compared with the whole CHOMg chemical space for the soluble organic matter of NWA 7325. H/C vs. O/C for NWA 7325 (B), H/C vs. O/C and H/C vs. m/z representations of CHOMg chemical compositions for Novato (C and D), Chelyabinsk (E and F), and Murchison (G and H) meteorite samples illustrate the chemical complexity of their organic extracts. The bubble size represents the relative intensity of the mass peaks. The mass-edited H/C ratio diagram of NWA 7325 is shown in Fig. 2.4A in the main text.

2.3 Dihydroxymagnesium Carboxylates: A Previously Unreported Chemical Class

CHOMg chemical compositions of NWA 7325 soluble organic matter are depicted by massed H/C ratio, for the complete (A) and zoomed-in compositional space (B), illustrating the density of fairly complete homologous series within the CHOMg compositional space. The bubble size represents the relative intensity of the mass peaks. The detailed arrangement of CHOMg compounds allows visualization of nominal elemental/molecular transformations, with examples provided (circled numbers: ①, $C_{18}H_{33}MgO_5^-$; ②, $C_{19}H_{33}MgO_5^-$; ③, $C_{19}H_{35}MgO_5^-$; ④, $C_{21}H_{37}MgO_4^-$; and ⑤, $C_{20}H_{35}MgO_5^-$). (C) Relative abundances of these Mg-metalorganics, shown in different colors (B and C), demonstrate the dominance of the MgO_4R^- molecular subspace, with $R = \text{hydrocarbon } C_xH_y$ and $\{x,y\} \in \mathbb{N}$.

The diversity of CHOMg species within soluble organic matter of NWA 7325 highlights the complex chemical space that is occupied by these metalorganic compounds (Fig. 2.4 and Fig. 2.5). This van Krevelen-type representation shows several extended, methylene-based fairly complete homologous series (Fig. 2.5). The absence of odd-even preferences in alkyl chains testifies to a nonbiological origin of CHOMg compounds [172]. Biological synthesis of fatty acids or general aliphatic chain molecules is usually a C_2 unit propagation process [173]. Therefore, the extraterrestrial origin (C_1 step chemosynthesis) can be distinguished from a terrestrial synthesis environment. Compounds bearing four oxygen atoms (MgO_4R^- , with $R = \text{hydrocarbon } C_xH_y$ and $\{x,y\} \in \mathbb{N}$) dominate the CHOMg chemical compositions (>80%, Fig. 2.4C and Fig. 2.5A) with a prevalence of nearly saturated aliphatics R , including long alkyl chains, which is uncommon for meteoritic soluble organic matter [112]. The sequential traces of the CHOMg compositional space of the other three meteorites, Novato, Chelyabinsk, and Murchison, demonstrate their wide molecular ranges and diversity (Fig. 2.5).

2.3. Dihydroxymagnesium Carboxylates: A Previously Unreported Chemical Class

To establish the chemical structure responsible for those peaks, the most intense mass peaks of MgO_4R^- compounds ($R = \text{hydrocarbon } C_xH_y$ and $\{x,y\} \in \mathbb{N}$) were subjected to collision-induced dissociation tandem mass spectrometry (CID-MS/MS) to initiate fragmentation. These CHOMg compounds were found to be highly thermostable. High collision energies (>10 eV, 965 kJ/mol) were necessary to observe $Mg(OH)_2$ abstraction [$\Delta m/z = 57.99052$ atomic mass units (amu), Fig. 2.6] from the parent ions. Fragmentation patterns were characteristic of long-chain aliphatic compounds [$\Delta m/z = 2.01565$ amu for H_2 loss and $\Delta m/z = 28.03130$ amu for C_2H_4 elimination [174], Fig. 2.6]. Acidification of the samples caused Mg-metalorganics (organomagnesium complexes) to hydrolyze. The precipitation of $Mg(OH)_2$ substantiates the idea that the observed CHOMg molecules are $[(OH)_2MgO_2CR]^-$ anionic complexes (Fig. 2.6), namely dihydroxymagnesium carboxylates, which have not been reported to date in chemical databases (e.g., ChemSpider, SciFinder, and PubChem).

Thermodynamic properties of dihydroxymagnesium carboxylates were elucidated both experimentally and theoretically. Mass spectrometric and computed fragmentation energies are in agreement, indicating a remarkable stability of CHOMg molecules as well as a strong (covalent) binding between $Mg(OH)_2$ and the carboxyl group (Eqs. S1 and S3 and Table S2). The $[(OH)_2MgO_2CC_{15}H_{31}]^-$ anion approaches a tetrahedral coordination geometry with Mg as coordination center (Fig.

2.3 Dihydroxymagnesium Carboxylates: A Previously Unreported Chemical Class

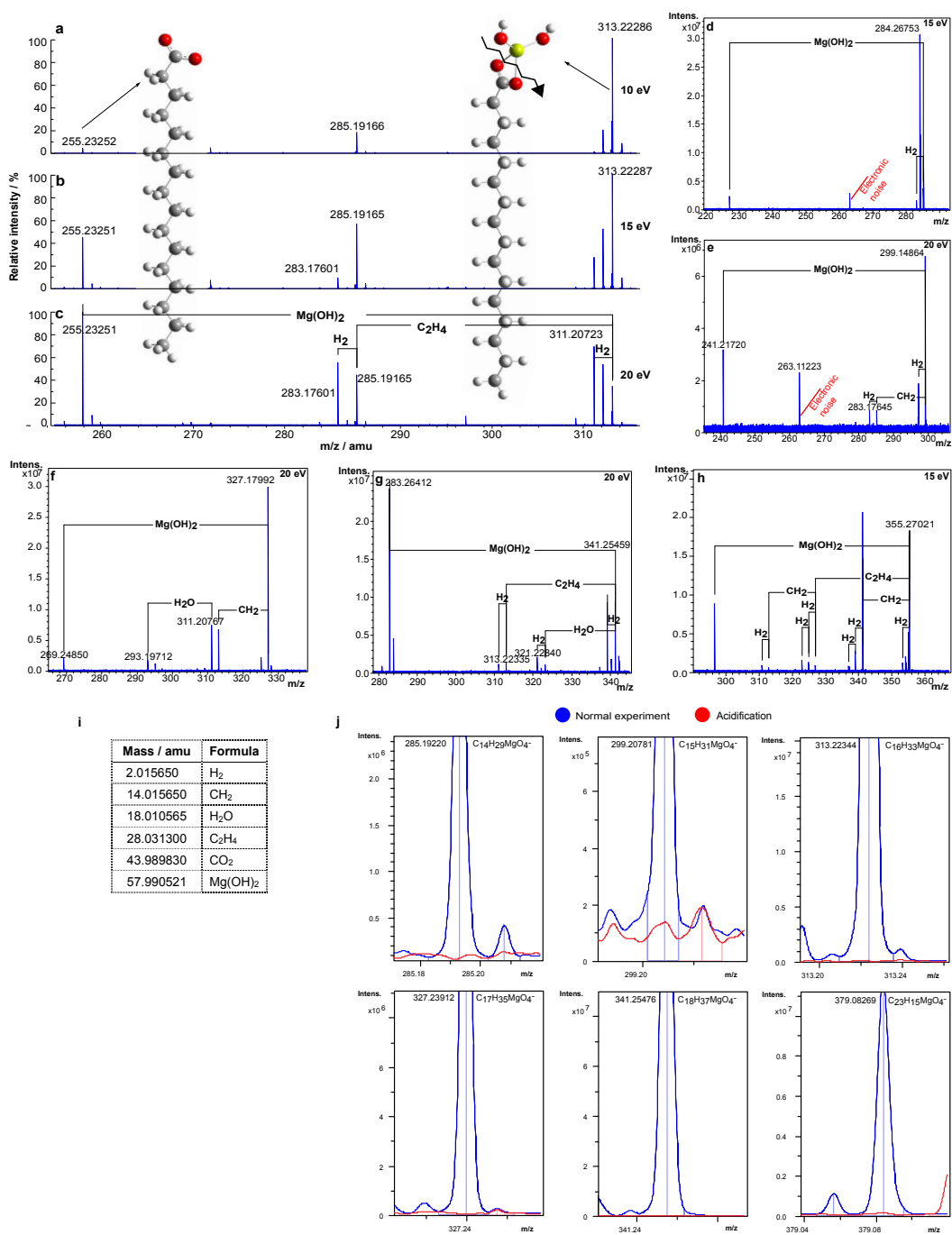
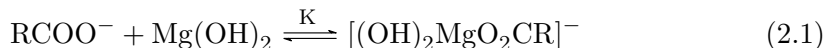


Figure 2.6: Fragmentation experiments to characterize dihydroxymagnesium carboxylates. (A–C) CID mass spectra of NWA 7325 of C₁₆-dihydroxymagnesium carboxylate [C₁₆H₃₃MgO₄][−] complex are shown at collision energies of 10 eV, 15 eV, and 20 eV. Additionally, five precursor molecular ions, ranging from C₁₄ to C₁₉ show fairly congruent fragmentation patterns of dihydroxymagnesium carboxylates. The computed coordinates of the depicted structures are presented in Table S2. (I) Exact masses of the fragmented molecules. (J) (−)-ESI-FT-ICR mass spectra of selected dihydroxymagnesium carboxylates in the NWA 7325 methanolic extract are shown, where the standard extract is labeled blue and the red signal is the extract in presence of formic acid (HCOOH). The complex is hydrolyzed in the presence of formic acid and Mg(OH)₂ is precipitated. The peaks were smoothed via the Gauss smoothing algorithm, as implemented in Bruker Compass DataAnalysis 4.2 SR1, with a smoothing width of 0.001 amu (2.1 points).

2.3 Dihydroxymagnesium Carboxylates: A Previously Unreported Chemical Class

2.7). Interestingly, Mg atoms seem to occur in a rarely observed fourfold coordination [175]. The reactivity of dihydroxymagnesium carboxylates as a function of chain length was assessed by determining Gibbs free energies ΔG for the reaction, shown in Eq. 2.1; ΔG was computed both by means of density functional theory (B3LYP-DFT) and by second-order Møller–Plesset perturbation theory (MP2):



The measured equilibrium constant K' [$K' \sim K \cdot c(\text{Mg}(\text{OH})_2)$, Eqs. S2 and S3] of the complex formation, following Eq. 2.1, relates to Gibbs free energy ΔG via Eq. 2.2:

$$\Delta G = -RT \ln K' \quad (2.2)$$

Eq. 2.2 provides a negative correlation of ΔG with K' (Fig. 2.7 and Fig. 2.8). The tendency of carboxylate complex formation continually decreases with increasing alkyl chain lengths R, as a result of two opposite effects. The inductive, bond-polarizing +I effect increases with higher numbers of alkyl carbons, making the carboxyl groups better nucleophiles, thereby shifting the equilibrium toward complex formation. However, the inverse effect of chain length on the acidity or the deprotonation potential of the ligand dominates. Here, longer alkyl chain carboxylates have higher potential to remain in their protonated form (RCOOH), which makes them weaker nucleophiles. Consequently, a higher coordination tendency for short-chain organic acids results (Fig. 2.7), which was verified for various homologous series (Fig. 2.8).

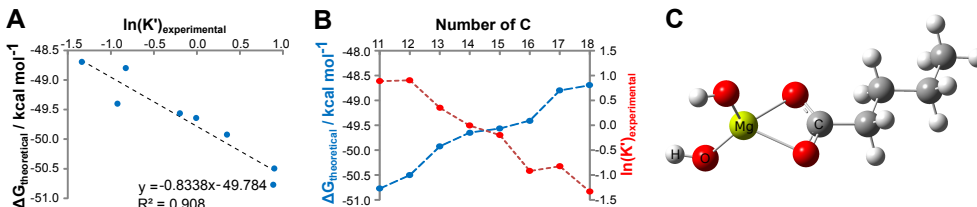


Figure 2.7: Characterization of dihydroxymagnesium carboxylates. (A) The negative correlation between the experimental equilibrium constant, expressed as $\ln K'$, and the computed Gibbs free energy ΔG of the $[(\text{OH})_2\text{MgO}_2\text{CC}_n\text{H}_{2n+1}]^-$ complex formation with $n \in \mathbb{N}$ for different linear alkyl chain lengths between C_{11} and C_{18} , as computed with density functional theory (DFT). (B) The dependency of $\ln(K')$ (experimentally via MS) and ΔG (theoretically via DFT) on different alkyl chain lengths is displayed to illustrate the reactivity of dihydroxymagnesium carboxylates, whereas the optimized computed geometry for the representative ion dihydroxymagnesium-n-pentanoate $[(\text{OH})_2\text{MgO}_2\text{CC}_4\text{H}_9]^-$ is depicted in C (see Table S2 for the computed coordinates of relaxed geometry of C_5 -dihydroxymagnesium carboxylate complex anion.)

2.3 Dihydroxymagnesium Carboxylates: A Previously Unreported Chemical Class

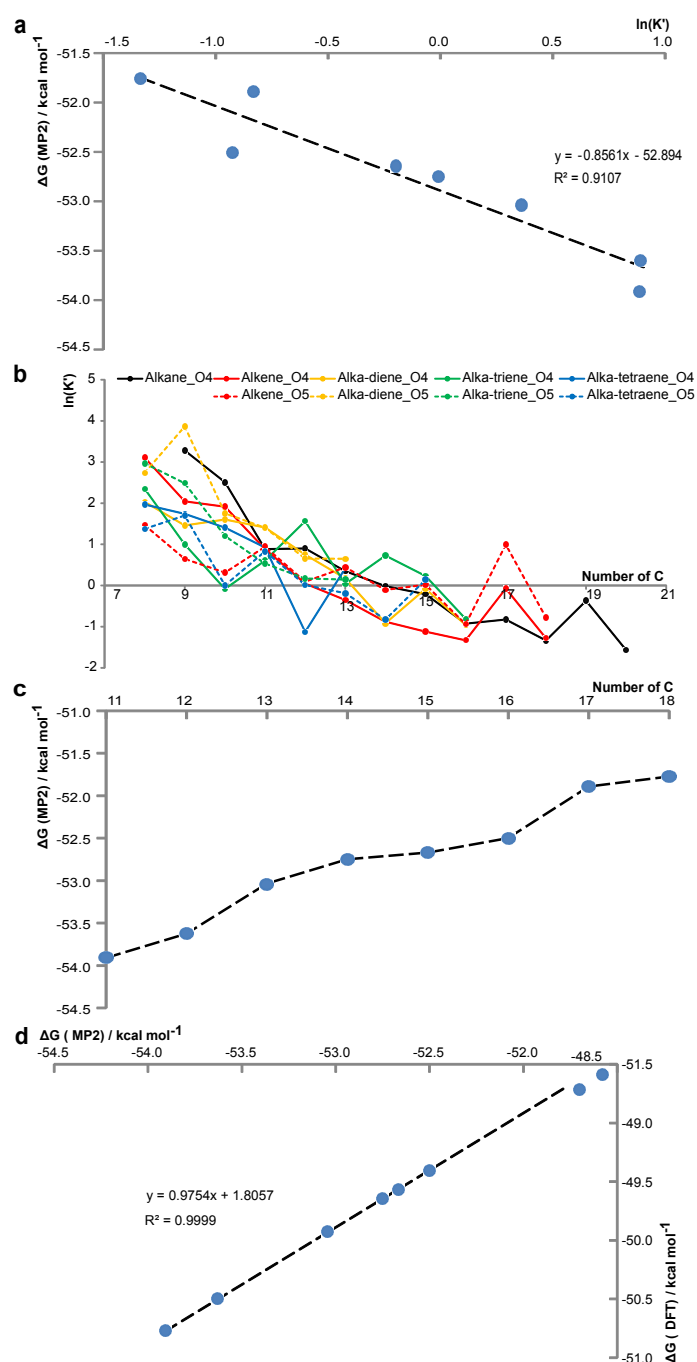


Figure 2.8: General CHOMg reactivity and verification of DFT simulations with MP2 level of theory. (A) Negative correlation of the Gibbs free energy ΔG with $\ln(K')$, following Eq. 2.2 for different linear alkyl chain lengths between C_{11} and C_{18} , computed with MP2 extracts (discussed in the main text). (B) $\ln(K')$ is plotted vs. the number of carbon atoms for several homologous series, varying by alkyl saturation and number of oxygen atoms in the aliphatic chain. A general decreasing trend with increasing numbers of C atoms is observed, indicating that smaller alkyl chain CHO molecules are more reactive to form CHOMg compounds, relatively longer aliphatic chain molecules. Additionally, local reactivity anomalies are highlighted by functional fluctuations. (C) ΔG is plotted vs. the number of carbon atoms in linear alkyl chain lengths of the $[(OH)_2MgO_2CC_n]^-$ complex formation with $n \in \mathbb{N}$, as computed on MP2-level of theory. (D) Correlation between the DFT-B3LYP and MP2 methods, which illustrates the accuracy of DFT, describing this complex formation reaction properly.

2.3 Dihydroxymagnesium Carboxylates: A Previously Unreported Chemical Class

Mass difference network analysis visualizes holistic chemical diversity of CHOMg in detail. In this data driven analytical approach, nodes represent experimental m/z values (here, FT-ICRMS data of NWA 7325 soluble organic matter) and edges (connections within the network) represent exact mass differences, which are equivalent to a net molecular formula of a chemical reaction [102]. The chemical complexity/reactivity of the CHOMg space (pink-coded nodes) and its regular connection to certain CHO compositions (blue-coded nodes, Fig. 2.9 and Fig. 2.11) is revealed.

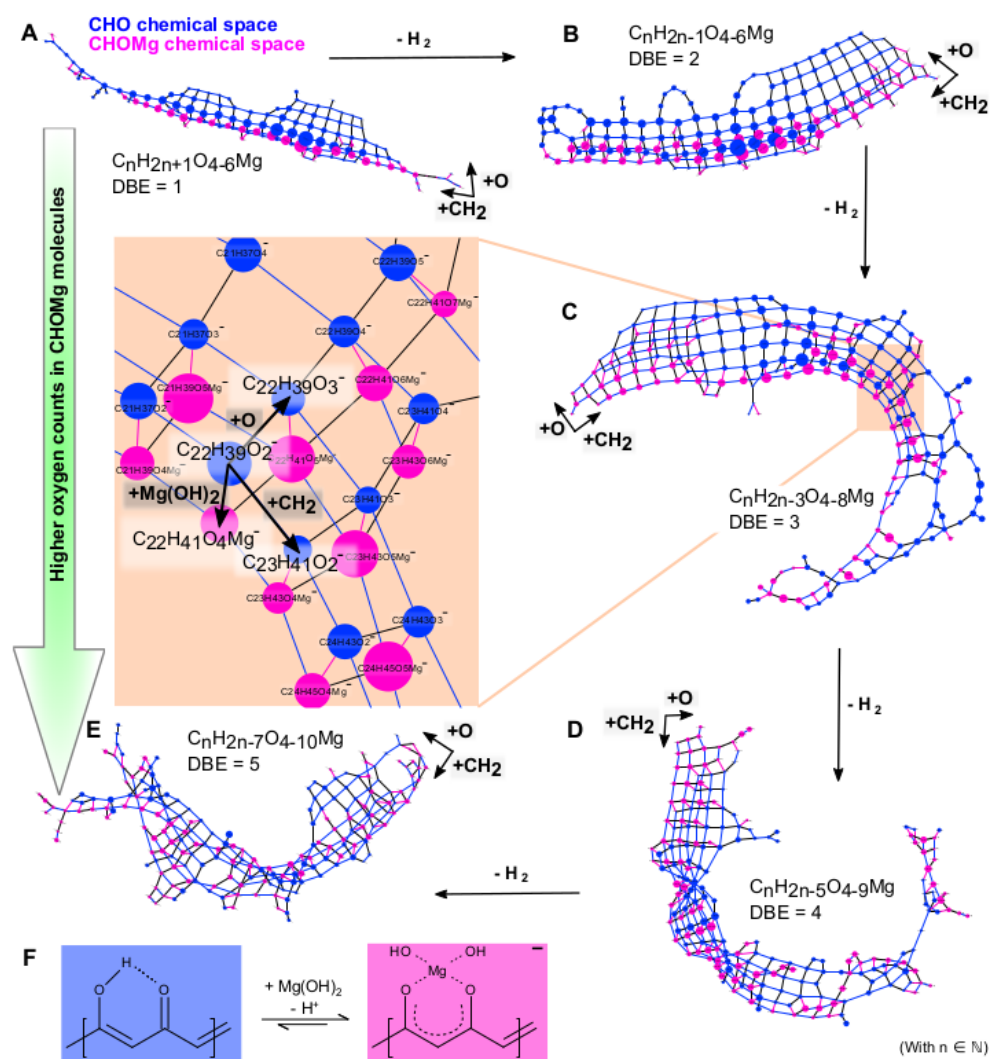


Figure 2.9: Mass difference networks, presenting the chemical complexity/reactivity of the CHOMg space and its connection to CHO compositions. (A–E) Five subnetworks, each representing one distinct degree of unsaturation, as well as a gradual increase in the number of oxygen in CHOMg molecules, are shown for NWA 7325 soluble organic matter. The variance in unsaturation is expressed via DBE values. CHOMg nodes are pink and CHO nodes are blue. The nodal diameter is proportional to the natural logarithm of each mass peak's intensity. Three types of edges are defined, the mass differences of CH_2 and O illustrate the systematic connection within the CHO or CHOMg chemical space, and $\Delta m/z(Mg(OH)_2)$ addresses reaction pairs that connect CHO and CHOMg compositions. (F) Proposed alternative organomagnesium complex formation with unsaturated β -hydroxy ketones as chelate ligands.

2.4 Chemosynthesis of organomagnesium compounds and the link to thermal history

Here, $C_xH_yO + Mg(OH)_2$ reaction pairs (with $\{x,y\} \in \mathbb{N}$) were identified for various degrees of unsaturation and numbers of oxygen atoms. First, highly connected methylenebased homologous series can be observed (CH_2 as an edge) for the CHO and CHOMg compositional spaces, respectively. Second, different sub-series with varying oxygen numbers are present. This functional network is split into five disconnected subnetworks, differing in their saturation states and laid out in the CH_2 vs. O directions. The degree of unsaturation (described via double-bond equivalent values, DBE) affects the reactivity of CHO compounds ($C_xH_yO_z + Mg(OH)_2 \rightarrow C_xH_{y+2}O_{z+2}Mg$ reaction, with $x,y,z \in \mathbb{N}$); the number of possible reactions increases with increasing DBE. Saturated $C_xH_yO_2$ compounds (DBE = 1) almost exclusively react to MgO_4R^- compositions (like dihydroxymagnesium carboxylates, $R = \text{hydrocarbon } C_xH_y$ and $\{x,y\} \in \mathbb{N}$). With increasing numbers of DBE, additional varieties of organomagnesium complex formation become available due to increased numbers of isomers of CHO compounds. On average, the transition from Fig. 2.9A to Fig. 2.9B doubles the number of organomagnesium compounds (pink chains), representing an increase in chemical CHOMg complexity.

The presence of carbonyl and hydroxyl groups in meteoritic soluble organic matter has previously been demonstrated [55, 112]. We propose the additional presence of β hydroxy carbonyl functionalities for unsaturated compounds that are isomeric and vinylogous to carboxylic compositions. Unsaturated β -hydroxy ketones are stabilized via conjugation effects, which enhance the likelihood for alternating σ and π bonds within the aliphatic chain (Fig. 2.9). The enol form is preferred, relative to the keto form, due to the presence of a pseudo ring, driven by hydrogen bonding. Additionally, keto–enol tautomerism explains the acidic character of β -hydroxy ketones. They are able to form chelate complexes [176], similar to organomagnesium coordination compounds. This alternative Mg coordination motif, compared with carboxylate ligands, may explain why highly unsaturated oxygenated CHO molecules react to CHOMg compositions. Further, the presence of two organic ligands enhances the probability of forming organomagnesium complexes, compared with one single organic educt class.

2.4. Chemosynthesis of organomagnesium compounds and the link to thermal history

One might ask about the origin of these organomagnesium compounds and whether the genesis of this compound class is coupled to the individual “history” of the various meteorites, meteoroids, and parent bodies. The effects of shock events, thermal metamorphism, and aqueous alteration play a major role in the classification of meteorites, which are commonly based on petrologic indicators [177]. CM-type meteorites [9, 99] have shown the highest number of CHNOS compositions. The thermally altered Sutter’s Mill shows losses of these signatures with additional new polysulfidic patterns [126]. The recent falls of the ordinary chondrites, such as Novato (L6), Chelyabinsk (LL5), or Vicência (LL3.2), show similar losses in nitrogen and sulfur compounds. Conversely, formation of compounds with high numbers of nitrogen at higher shock levels [98, 100, 124] are observed, suggesting that shock events/thermal metamorphism play a role in this context as well.

The CHOMg signatures relate to shock stage (with S0 being unshocked and S5 highly shocked meteorites, as assigned for examples in Fig. 2.10) and thermal processing among 61 meteorites of various classes, as demonstrated by orthogonal

2.4 Chemosynthesis of organomagnesium compounds and the link to thermal history

partial least square regression analysis (OPLS) (Fig. 2.10, x axis as first component). For example, the thermally altered meteorite Soltmany [97] contains >700 CHOMg compounds. In comparison, the less-altered meteorite Paris (CM) with only weak thermal alteration [178] shows merely 90 CHOMg compounds of low mass peak intensity. The information on the variation of oxygen numbers within CHOMg formulas is revealed by the y axis (orthogonal to the first component) of the OPLS analysis. Based on the mass difference network analysis (Fig. 2.9), we propose that the y axis potentially also represents a discrimination of the degree of unsaturation. High oxygen numbers of CHOMg molecular formulas correspond to a higher degree of unsaturation.

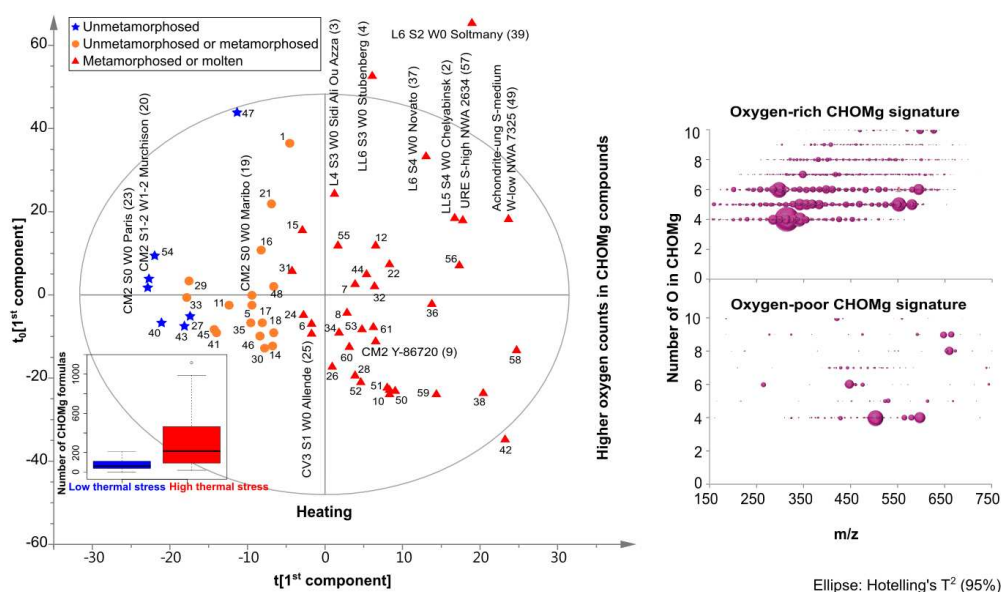


Figure 2.10: Relationship of CHOMg signatures with different thermal processing stages of meteorites. An OPLS score scatter plot for 61 meteorites (CI, CK, CM, CO, CR, CV, EUC, H, L, LL, URE, and achondrite classes) with different inter- and intrameteorite class metamorphism stages is shown, based on the abundance and molecular diversity of CHOMg compounds. Details on the OPLS analysis are given in SI Materials and Methods and meteorite assignments are listed in Table S1. The box plots represent the averaged numbers of CHOMg molecular formulas for low and highly thermally altered meteorites, respectively. Thermal processing states vary from low to high along the x axis (first component), proceeding from negative to positive values. This first component (x axis) is related to the number and intensity of CHOMg molecular formulas, as represented in the box plot. The y axis (orthogonal to the first component) represents the proportion of oxygen atoms within the molecular formulas, as illustrated by modified van Krevelen diagrams of the most relevant loading values. Independent of the specimen, CHOMg signatures were observed with increased Mg-metalorganic diversity for thermally stressed meteorites. The two CM2 chondrites, Y-793321 and Y-86720, reported to be thermally metamorphosed [177], well described meteorites, with respect to their shock history (Chelyabinsk [98] and Novato [124]), as well as the recently classified fall Sidi Ali Ou Azza (L4) and a very new German fall Stubenberg (LL6) were also assigned to the thermally stressed region.

2.4 Chemosynthesis of organomagnesium compounds and the link to thermal history

Parent body thermal metamorphism also imposes a compositional variance of CHOMg compounds. High thermal metamorphism is associated with an elevated saturation (high H/C ratio) and a convergence of oxygen numbers to 4 within the organomagnesium molecules at high thermal stress (Fig. 2.11). By heating Murchison, a meteorite with a low degree of metamorphism, we were able to simulate and follow the effect of short-duration thermal stress in a laboratory experiment. Here, CHOMg-based hierarchical cluster analysis revealed differentiation according to temperature regimes (Fig. 2.12). Similarly, the number of oxygen atoms in CHOMg molecules converges toward $O = 4$ at high temperatures, as expected (Fig. 2.12). A detailed comparison within highly shocked/thermally stressed ureilite meteorites also agrees with the above results (Fig. 2.12).

The production of CHOMg compounds by heating is further demonstrated by analyses of meteorite's fusion crust. Freshly fallen meteorites are found with a glassy coating that formed at $\sim 1,400$ °C surrounding their cold interior. The fusion crust is formed upon atmospheric entry by melting the meteoroid's surface as it enters the Earth's atmosphere at supersonic speed. During the brief melting, the liquid-like crust loses volatile elements and reacts with atmospheric matter faster, relative to the heterogeneous solid-state interior. ESI-FT-ICR mass spectra were acquired for Maribo (CM2) and Allende (CV3) by probing their outer crust and their inner core. Higher numbers and higher molecular diversity of CHOMg compounds were obtained from the crusted surfaces, relative to the core regions (Fig. 2.13). The different thermal conditions experienced by the outer and inner parts of a meteorite lead to different potential chemical activities, which promote the synthesis of these organomagnesium compounds at elevated temperatures within a short time scale. This observation agrees with the above experimental results, demonstrating that reaction energy, namely pressure and temperature, as substantiated by Eq. 2.2, relate with higher abundance of CHOMg molecules.

The role of alteration can also be evaluated from the isotopic signature of the Mg atoms in CHOMg compounds. Isotopic analyses of Mg were performed on both organic extracts and residual fractions of NWA 7325 and Novato (Fig. 2.1). The organic extract of Novato had a $\delta^{26}\text{Mg}$ value of -0.74 ± 0.08 ‰, and the residue had a $\delta^{26}\text{Mg}$ value of -0.29 ± 0.09 ‰. Details on the Mg isotopic analysis are given in SI Materials and Methods. Similarly, the organic extract of NWA 7325 had a $\delta^{26}\text{Mg}$ value of -0.62 ± 0.04 ‰, and the residue had a $\delta^{26}\text{Mg}$ value of -0.35 ± 0.11 ‰. Thus, for both Novato and NWA 7325, the organic extracts were relatively enriched in isotopically light Mg, compared with the isotopic composition of Mg in the bulk rock. This is consistent with the observation by Black et al. [180], who found chelation during intracellular processes enrich light Mg isotopes.

However, Mg isotopic fractionation occurs upon abiotic aqueous alteration as well. Aqueous alteration leads to clay-mineral formation and Mg-rich phases [138]. We did not observe any significant direct correlation between the numbers of organomagnesium compounds and the extent of aqueous alteration within CM2 meteorites, ranging from CM2.7 to CM2.0 (Fig. 2.13). Studies from Wimpenny et al. [181] show that the removal of exchangeable magnesium from alteration phases preferentially liberates isotopically light Mg, compared with the bulk mineral. This suggests that aqueous alteration may have an indirect effect on the synthesis of organomagnesium compounds. If a released Mg educt, produced by aqueous alteration, is consecutively

2.4 Chemosynthesis of organomagnesium compounds and the link to thermal history

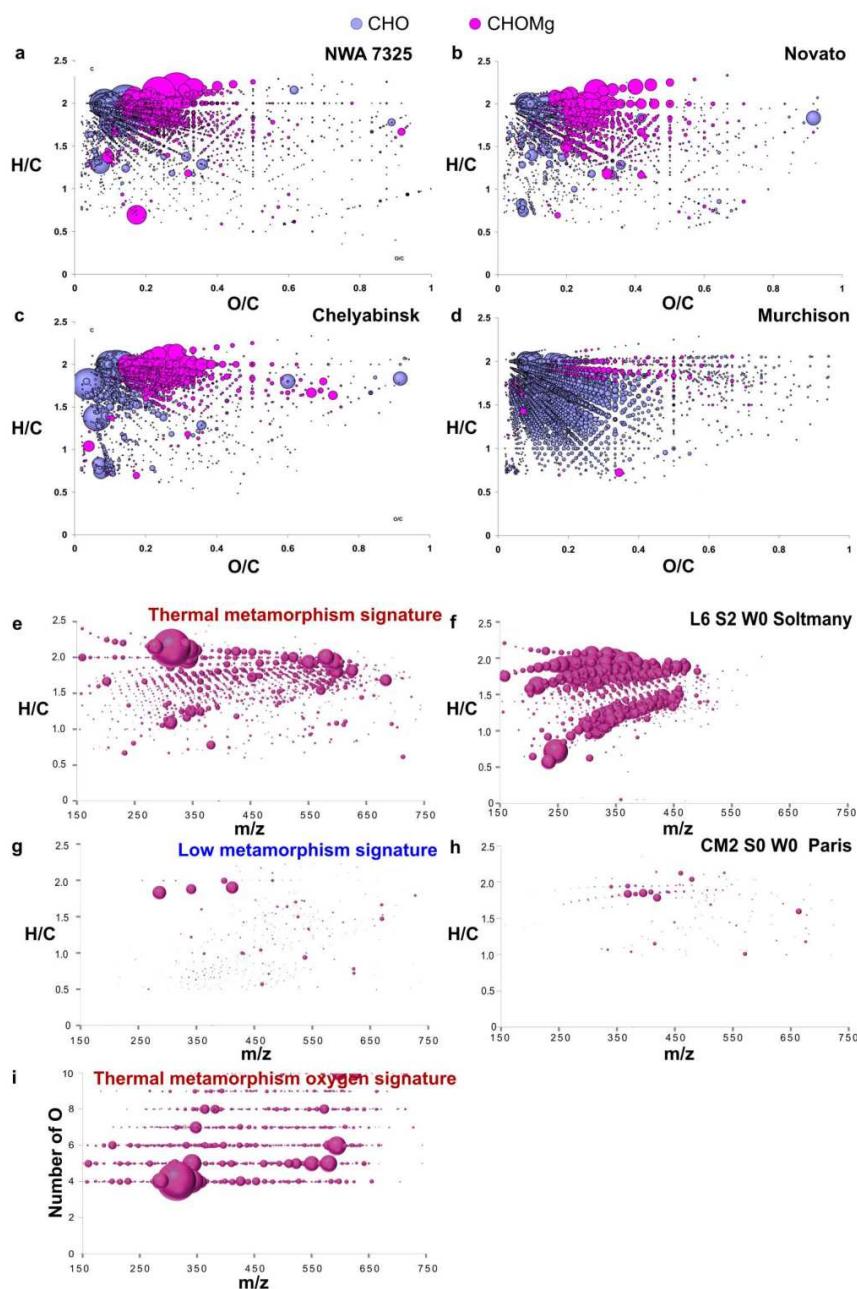


Figure 2.11: Van Krevelen-type diagrams for the comparison of CHO and CHOMg compositions and representing the thermal metamorphism signature. Van Krevelen representations of soluble organic matter in NWA 7325 (A), Novato (B), Chelyabinsk (C), and Murchison (D) are shown. Modified van Krevelen diagrams of the overlapped CHOMg molecules (50th percentile of positive loading values on the x axis) reflect the highly aliphatic structure of the CHOMg compositional space (A) for relevant loadings, which represent high (E) and low (G) thermal metamorphism signatures, as seen in the 61 meteorites studied. The bubble size represents the relative intensity of the mass peaks. (F and H) Mass-edited H/C ratios of two representative examples for low- (Paris) and high-degree thermally processed meteorites (Soltmany) [97]. The convergence of O = 4 in CHOMg molecular formulas for thermal stress loading values is presented by an oxygen number- m/z diagram. (I) Again, these plotted m/z values reflect the 50th percentile of the variables, out of the OPLS score plot (Fig. 2.10).

2.4 Chemosynthesis of organomagnesium compounds and the link to thermal history

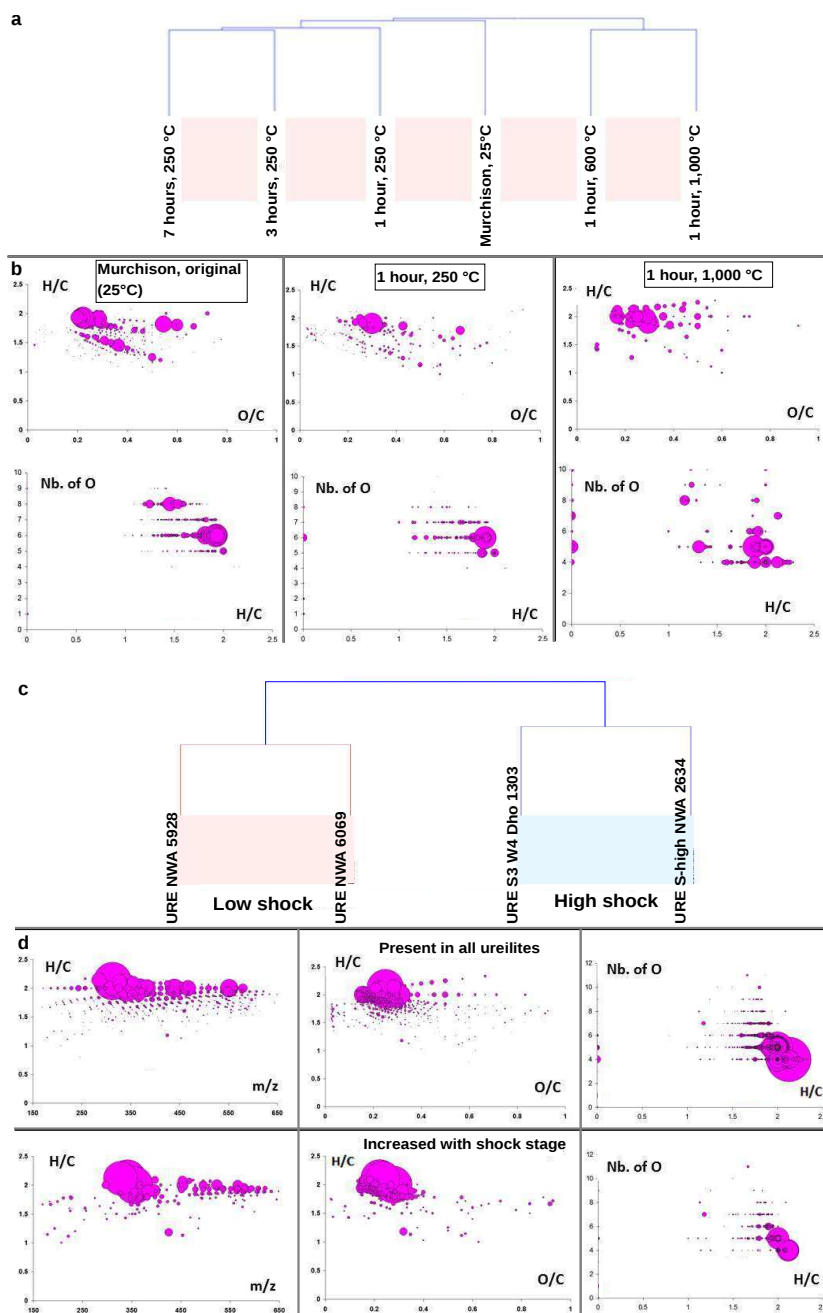


Figure 2.12: Simulated thermal metamorphism of Murchison and CHOMg-based shock stage differentiation. (A) Laboratory experiment, in which a Murchison meteorite sample was heated to selected temperatures for variable durations (25 °C, 250 °C, 600 °C, and 1,000 °C). Number and distribution of organomagnesium compounds enabled reconstruction of thermal exposure by means of HCA. The samples clustered according their elevated temperatures (25 °C, 250 °C, 600 °C, and 1,000 °C). This effect of convergence with increasing temperature is depicted in modified van Krevelen diagrams in B. The bubble size represents the relative intensity of the mass peaks (–)-ESI-FT-ICR-MS). Sampling the effect of time-dependency on the variation of the CHOMg chemical space, three different time points were sampled for temperature 250 °C and clustered together. (C) Four ureilite meteorites were studied, which had experienced high thermal and shock conditions [179]. (D) (Top) CHOMg chemical spaces of four ureilite methanolic extracts (overlapped CHOMg compounds) are shown on top. (Bottom) CHOMg compositions, which increased in abundance in the higher-shocked ureilite meteorites Dho for 1303 and NWA 2634.

2.4 Chemosynthesis of organomagnesium compounds and the link to thermal history



Figure 2.13: Crust-core comparison and their influences on the CHOMg synthesis and dependency of CHOMg formulas on the aqueous alteration. (A) Number of CHOMg compounds in crust and core sections of the Maribo and Allende meteorites. The mass edited H/C ratios (B–E) illustrate the increased coverage within the CHOMg chemical space for the crust, compared with the core (interior) region. Among the specific organomagnesium molecules, some are unique for the crust and for the core regions, respectively, indicative of a preferential spatial accumulation for certain CHOMg (F and G). The bubble size represents the relative intensity of the mass peaks. Pictures of the Maribo and the Allende specimens are shown in H and I, to reflect the different morphology of their outer crusts and their interiors. (J) Number of CHOMg molecular formulas in methanolic extracts of several CM2 meteorites that had been subjected to variable extents of aqueous alteration [classified from CM2.7 (left) to CM2.0 (right)]. No significant correlation between the extent of aqueous alteration of a meteorite and the number of organomagnesium compounds was retrieved, suggesting that the CHOMg synthesis is not directly dependent on the aqueous alteration.

2.5 Conclusions/outlook

exposed to high temperatures, enhanced CHOMg formation would be expected to result by close spatial proximity and intercalation of the mineral and organic phases in CM2 meteoritic materials [138]. Secondary ion mass spectrometric (SIMS) analyses of the Chelyabinsk meteorite indicated a spatial proximity of Mg and organic compounds (Fig. 2.1), which has not been reported previously by this method. Ordinary chondrites do not typically undergo aqueous alteration.

2.5. Conclusions/outlook

The composition of soluble CHOMg compounds is shown to be highly related to the thermal-processing states of meteorites. Molecular complexity of MgO_4R^- compositions ($\text{R} = \text{hydrocarbon } \text{C}_x\text{H}_y \text{ and } \{x,y\} \in \mathbb{N}$) is increasingly diversified, because a meteorite experiences increasing degrees of thermal processing. The most abundant subclass of CHOMg compounds in meteorites is the four-oxygen-containing MgO_4R^- type and represents the previously unreported chemical class of dihydroxymagnesium carboxylates $[(\text{OH})_2\text{MgO}_2\text{CR}]^-$.

The use of CHOMg compound distributions as potential chemical markers, together with the CHNOS chemical space, may help to expand our knowledge of (i) astrochemistry of higher molecular masses and chemical complexity within the solar nebula and/or (ii) postaccretional processes in meteoritic parent body metamorphism. In the context of meteorite classification, CHOMg content and diversity may provide a useful estimate of the degree of thermal alteration reflecting their temporal evolution under high temperature.

Additionally, this work raises the questions of whether these CHOMg compositions are specific for extraterrestrial chemistry and what we can learn from these findings within ongoing studies on natural metalorganic compounds in terrestrial systems and deep carbon sequestration in the Earth interior under high temperature and pressures [182].

Metal ions are essential for the origin of living systems on Earth [183–185]. Metal ions can either support reactions via catalytic effects or stabilize organic molecules, because life-relevant organics are often thermolabile and celestial bodies undergo highenergy gradients through time and space. Here, highly thermostable organomagnesium compounds might have contributed to the stabilization of organic molecules, such as fatty acids, on a geological time scale, being in contact with Mg-bearing minerals at high energetic conditions. These protecting metalorganic motifs might represent important intermediate molecules in the selection history of organic molecules of life. A concentration/fractionation of fatty acids can be accomplished via the stabilization in their organomagnesium motifs, which is highly relevant in the formation of protocells/cells due to compartmentization/vesicle formation in membranes.

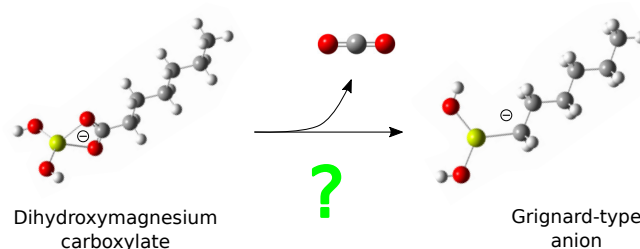
Due to their high abundance [31] and known metalorganic chemistry, Fe, Ni, Al, Zn, and V [133, 186, 187] may also be present as astrobiologically relevant molecular building blocks in meteorites, next to Mg-bearing compounds. No other metalorganics could be experimentally detected yet.

Potential future detections of organometallic compounds (or organics in general) from sample return missions to Mars, asteroids, or the Moon would imply that meteoritic organic compounds might survive some of the high-temperature, early phases of planetary accretion processes. This may not necessarily mean that life

2.5 Conclusions/outlook

existed at a certain point in the histories of these planetary bodies. Insights into potential amplification of abiogenesis probabilities among planetary systems with various chemistries and molecular complexities can be achieved.

3. Do dihydroxymagnesium carboxylates form Grignard-type reagents?



Dihydroxymagnesium carboxylates (CHOMg) represent a novel, previously unreported chemical class. Thus, we assess fundamental chemical properties of these CHOMg molecules. Chemical stability was studied by targeting (i) the polar head group and (ii) the apolar alkyl chain. Here, we probed CHOMg at their polar head group for decarboxylation, both via MP2 and DFT computations. This study is connected to the question whether these CHOMg molecules form Grignard-type molecules. Forward energy barrier for decarboxylation increases linearly as a function of the ligand's chain length, as observed for C_4 and C_{11} . Decarboxylation-type fragmentations of these CHOMg seem to be improbable in non-catalytic, low energetic environments. A high forward energy barrier ($E_{MP2} > 55$ kcal/mol) towards a described transition state restricts the release of CO_2 . Once, this challenging transition state is overcome, a stable Mg-C bond is formed via an intramolecular nucleophilic attack, as studied by NBO analysis. Putatively formed Grignard-type OH-bearing product molecules possess a more polarized Mg-C bond in comparison to RMgCl species. Thus, carbanion formation reactions out of OH-bearing Grignard-type molecules are made feasible.

3.1. Introduction/motivation

As a part of coordination chemistry and inorganic chemistry, organometallic chemistry encompasses a successful research area, ranging from organic synthesis to applications in materials science [188]. In addition, several Nobel prizes were awarded to organometallic scientists, including the prominent works on Grignard reactions [189] or on enantioselective catalysis [190]. The synthesis of diethylzinc by Frankland in the mid nineteenth century [191] and especially the already mentioned remarkable work of Victor Grignard on organomagnesium reagents at the beginning of the twentieth century [192] reflect the basis of modern organometallic chemistry. The Grignard reaction is an important tool for the formation of carbon-carbon bonds [193].

Eventhough, organometallic chemistry is usually defined conservatively to compounds possessing metal-carbon bonds [141, 194]. Organic ligands, which form metal-heteroatom bonds (e.g. towards hydrogen, oxygen or nitrogen) also play important roles in certain organometallic/coordination compound reactions [195]. Especially, carboxylate ligands belong to an important family of binding partners towards metallic central atoms. Particularly in the field of bioinorganic chemistry, carboxylates represent key motifs and bind towards doubly charged cations, like Mg^{2+} , Ca^{2+} (parvalbumins in muscles) [196, 197] or Fe^{2+} (iron-containing methane monooxygenase) [198]. The coordination of the magnesium center is switched between a mono- and bidentate coordination, as been referred as "carboxylate shift" [199, 200]. Another important motif in nature for magnesium-carboxylate interactions is the plant protein RuBisCO's active site, which catalyzes C-C bond formation during the addition of CO_2 towards a carbohydrate substrate [201].

Recently, a previously unreported chemical class, dihydroxymagnesium carboxylates $[(\text{OH})_2\text{MgO}_2\text{CR}]^-$ with $\text{R} = \text{hydrocarbon } \text{C}_x\text{H}_y$ and $\{x,y\} \in \mathbb{N}$, could be observed in meteorites [161] and extended the already extremely high complex astrochemical compositional space [9, 112] to metalorganic species. Their formation is supposed to require high energetic conditions, since the compound's abundance could be related to the thermal processing history of a meteoritic body. Metalorganic compounds are rarely discussed in astrochemistry yet, but are supposed to represent key intermediates for extraterrestrial organic evolution [133]. Exemplarily, the iron interaction with of polyaromatic hydrocarbons (PAH) is discussed, which is supposed to influence their growth in evolved star envelopes [132, 135]. Dihydroxymagnesium carboxylates might have contributed to the selective stabilization of organic molecules on a large time scale, which emphasizes their potential astrobiological relevance [161].

Dihalogenomagnesium carboxylates $[\text{X}_2\text{MgO}_2\text{CR}]^-$ with $\text{R} = \{\text{Me, Et, Pr, iPr, tBu, vinyl, allyl, HC}\equiv\text{C, Ph, PhCH}_2, \text{PhCH}_2\text{CH}_2\}$; $\text{X} = \{\text{Cl, Br, I}\}$, a closely related chemical family, were probed for their gas-phase fragmentations and their transformation towards organomagnesates/Grignard (intermediate) reagents could be successfully observed [202]. Mg-C bonds formation was monitored via decarboxylation reactions in that study and therefore the formation of Grignard reagents (RMgX compositions with $\text{R} = \text{hydrocarbon } \text{C}_x\text{H}_y$ and $\{x,y\} \in \mathbb{N}$ and $\text{X} = \text{Halogen}$) proposed. This motivated us to probe decarboxylation-type fragmentations for the analog, astrochemically/astrobiologically relevant chemical class, dihydroxymagnesium carboxylates. Can $\text{RMg}(\text{OH})$ be used as Grignard reagent analogs for organic

3.2 Decarboxylation of dihydroxymagnesium carboxylates - probing the potential energy surface

synthesis? This questions might has consequences for astrochemical organic evolution or general organic synthesis routes. OH-bearing Grignard molecules seem to be a powerful alternative next to traditional halogen-bearing Grignard molecules in green chemistry and organic synthesis strategies.

Here, we testify whether dihydroxymagnesium carboxylates $[(\text{OH})_2\text{MgO}_2\text{CR}]^-$ with $\text{R} =$ hydrocarbon C_xH_y and $\{x,y\} \in \mathbb{N}$ are able to form Grignard reagent-type (intermediate) molecules. Therefore, we probed the charge-proximal head group to test for decarboxylation-type fragmentations (Fig. 3.1). Charge-proximal fragmentation channels were computed both by means of second-order Møller–Plesset perturbation theory (MP2) and density functional theory (DFT), on 6-311+G(2d,p) // 6-31+G(d,p) level of theory to get orthogonal quantum-chemical information. Different linear alkyl chain lengths between C_4 and C_{11} were computed to extract putative trends to describe differences in stability towards decarboxylation within homologues series of $[(\text{OH})_2\text{MgO}_2\text{CR}]^-$.

In addition, natural bond orbital (NBO) analyses were performed to probe the respective molecule's charge distribution to get insights into the fragmentation mechanism and describe properties of putative OH-bearing Grignard-type molecules. This theoretical work is on the basis of experimental findings, which were published previously [161].

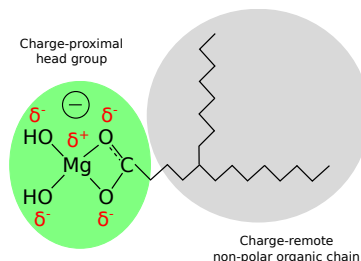


Figure 3.1: Schematic representation of spatial chemical differences within dihydroxymagnesium carboxylates. This molecular class can be majorly classified by a charged head group and a non-polar organic motif.

3.2. Decarboxylation of dihydroxymagnesium carboxylates - probing the potential energy surface

Dihydroxymagnesium carboxylates $[(\text{OH})_2\text{MgO}_2\text{CR}]^-$ with $\text{R} =$ hydrocarbon C_xH_y and $\{x,y\} \in \mathbb{N}$ were probed extensively for decarboxylation-type fragmentations on a theoretical level. By using orthogonal quantum chemical methods, namely second-order Møller–Plesset perturbation theory (MP2) and density functional theory (DFT), insights were given into the stability of this recently introduced metalorganic compound class [161].

To probe the decarboxylation-type fragmentation pathway of dihydroxymagnesium carboxylates in greater detail, the energy profile of $[(\text{OH})_2\text{MgO}_2\text{C}_7\text{H}_{13}]^-$ along decarboxylation intrinsic reaction coordinate (1D potential energy "surface", PES) was investigated. Fig. 3.2 represents the fragmentation channel for the decarboxylation of $[(\text{OH})_2\text{MgO}_2\text{CC}_7\text{H}_{13}]^-$. As reported previously, dihydroxymagnesium carboxylates approach a relaxed, fairly tetrahedral coordination [161]. The carboxylate ligand is bound as a bidentate towards the magnesium coordination center. This bidentate coordination complex represents the local minimum on the PES when considering charge-proximal fragmentations (lowest potential energy along this reaction coordinate).

The bidentate conformation is being transformed towards a monodentate chelate complex. This rearrangement requires an energy barrier of approximately 6 kcal/mol,

3.2 Decarboxylation of dihydroxymagnesium carboxylates - probing the potential energy surface

which needs to be overcome. Both quantum chemical methods are in agreement when describing this transition state on the coordination switch.

The release of CO₂ is only possible from a monodentate coordinated structure, not out of the bidentate coordination. Within the bidentate complex, the angle between CO₂-carbon atom towards Mg and C α (first carbon atom in the chain attached to the carboxyl group) approaches 180°. Starting from the monodentate complex, this triangle is described by an angle of around 100°. This monodentate intermediate is stabilized via a six-membered pseudo-ring structure (O-Mg-O-C-C-C). The reactive center (CO₂-carbon atom, Mg and C α) is characterized on the saddle point/transition state by a fairly equilateral triangle. Anyhow, the high forward energy barrier of transition state #2 ($E_{MP2} > 55$ kcal/mol) is challenging to overcome within natural, non-catalytic environments.

Relative to MP2 level of theory, B3LYP-DFT underestimates the energy barrier for the decarboxylation transition state by a difference of approximately 9 kcal/mol. Details on the computed presented structures are given in supplementary information.

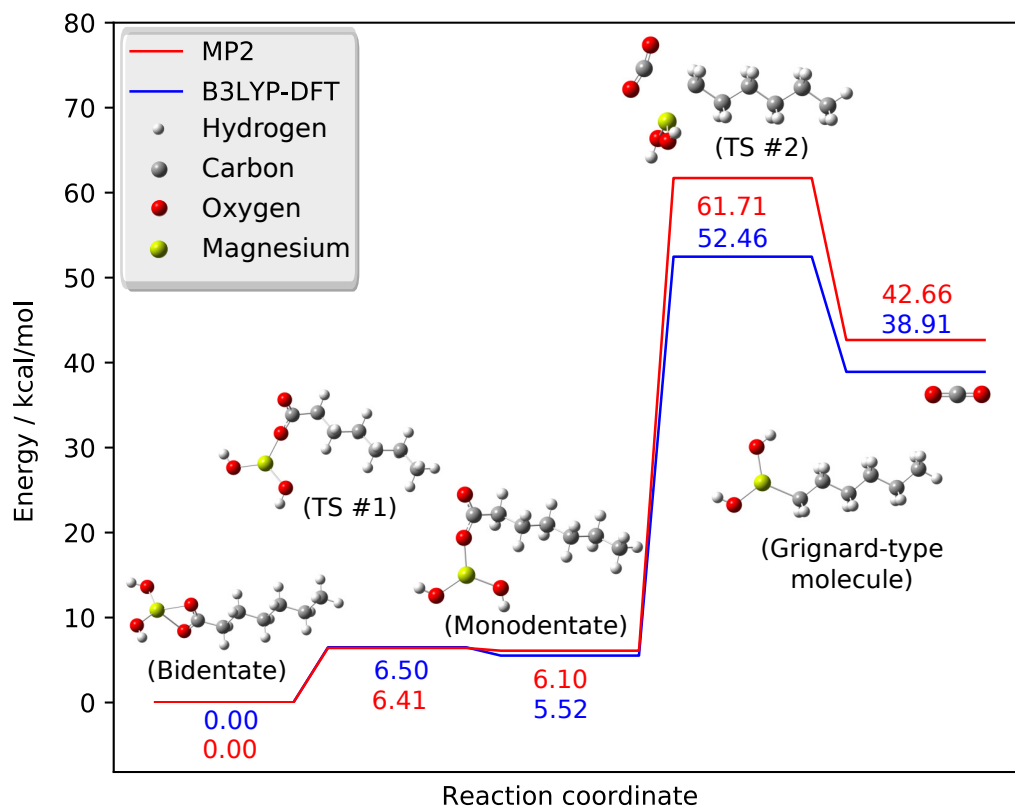


Figure 3.2: Potential energy curve of CO₂ fragmentations out of dihydroxymagnesium carboxylates. The charge-proximal fragmentation of $[(OH)_2MgO_2C_7H_{13}]^-$ is shown. Dihydroxymagnesium carboxylates are present as bi- and mono-chelate complexes ("TS #1"). Starting from a monodentate coordinated geometry, CO₂ can be released ("TS #2"). Fragmentation channels were computed both by means of MP2 (as assigned in red) and B3LYP-DFT (as assigned in blue), both on 6-311+G(2d,p) // 6-31+G(d,p) level of theory.

3.3 Chain length dependence of $[(\text{OH})_2\text{MgO}_2\text{CR}]^-$ decarboxylation

3.3. Chain length dependence of $[(\text{OH})_2\text{MgO}_2\text{CR}]^-$ decarboxylation

Dihydroxymagnesium carboxylates were recently introductory reported [161]. As presented in that study, collision-induced dissociation tandem mass spectrometry experiments (CID-MS/MS) could not experimentally show a loss of CO_2 out of probed $[(\text{OH})_2\text{MgO}_2\text{CR}]^-$ anions. Molecular series from C_{14} to C_{19} were subjected for experimental fragmentation studies. Therefore, we studied here the influence of the ligand's chain length on the decarboxylation of dihydroxymagnesium carboxylates. Is there a trend within the energy barrier of charge-mediated fragmentations as a function of the ligand's chain length?

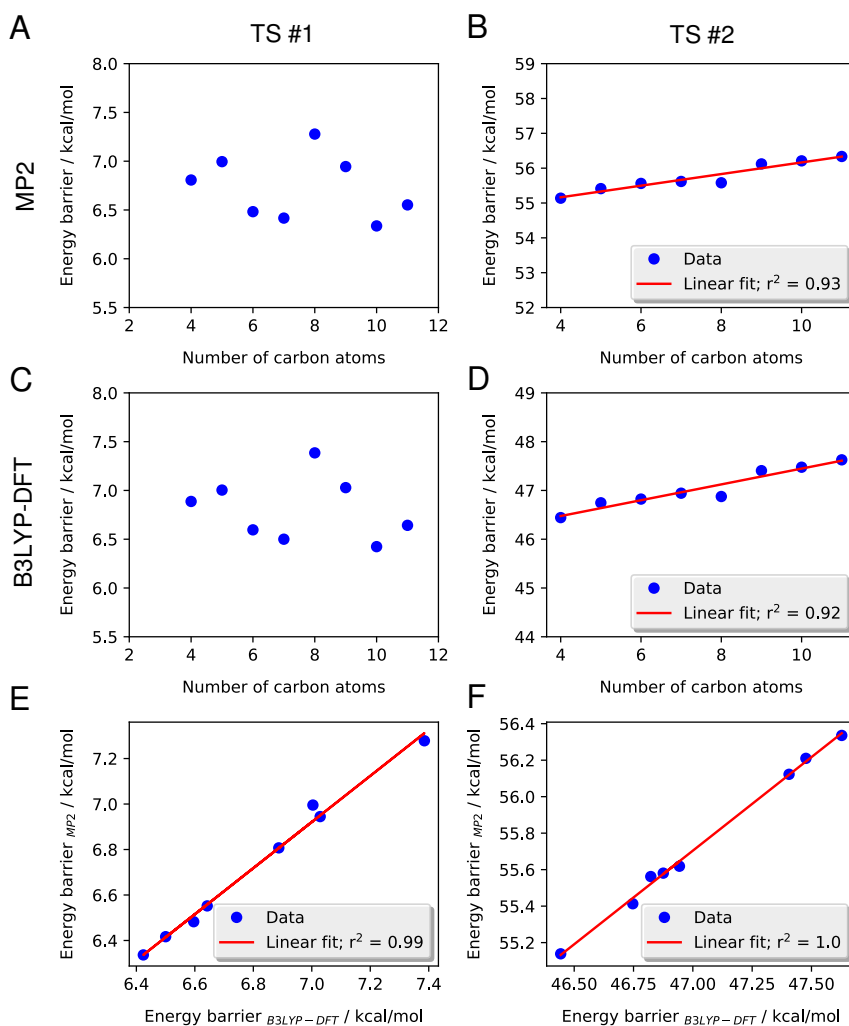


Figure 3.3: Chain length dependence of $[(\text{OH})_2\text{MgO}_2\text{CR}]^-$ decarboxylation. Forward energy barriers are plotted for various carbon atom numbers (C_4 and C_{11}) within the aliphatic chain in dihydroxymagnesium carboxylates. (A,C) The carboxylate coordination shift dependence ("TS #1") was computed both via MP2 and B3LYP-DFT. No trend could be observed here. Otherwise, a linear increase of the forward energy barrier as a function of the ligand chain length could be observed for the loss of CO_2 (panel B,D). The correlation of extracted computed energies for both methods, MP2 and B3LYP-DFT is shown in panel E and F.

3.4 Insights into the decarboxylation-type fragmentation mechanism

To track the influence of the chain length on decarboxylation-type fragmentations, we probed eight species, $[(\text{OH})_2\text{MgO}_2\text{C}_4\text{H}_7]^-$ to $[(\text{OH})_2\text{MgO}_2\text{CC}_{11}\text{H}_{23}]^-$ (C_4 to C_{11}), as representatives of the homologues series of saturated dihydroxymagnesium carboxylates. Therefore, insights can be tracked to observe trends within the energy barrier of decarboxylation for various ligand chain lengths.

As shown in Fig. 3.3, the variation of the forward energy barriers was studied for the respective two transition states, which influence the loss of CO_2 out of a dihydroxymagnesium carboxylate molecule. The notation of the transition state labelling is introduced in Fig. 3.2. The forward transition along "TS #1" represents the conversion of a bidentate towards a monodentate coordination complex and "TS #2" reflects the saddle point, which enables the release of CO_2 from these organomagnesium complexes.

Transition state #1 (carboxylate shift between mono- and bidentate coordination at the magnesium center) is not significantly influenced by the chain length variation of the aliphatic ligand in these organomagnesium complexes. No trend could be observed, neither by MP2 nor by B3LYP-DFT computations. This effect is referred to the active site only, namely the charge-proximal site directly. Therefore, no direct electronic influence (neither inductive nor mesomeric effect) of the ligand's chain can be observed on the energy barrier of the coordination switch.

In contrast, the forward energy barrier for the release of CO_2 from dihydroxymagnesium carboxylates (labelled as "transition state #2") increases linearly with longer carbon chain lengths. This trend is significant (p-value = $6.41\text{e-}05$ for the slope of the forward energy barrier (MP2)). The degree of energy difference between C_4 and C_{11} computations is in range of expectations. In comparison, the variation in nucleophilicity as a function of the carbon chain length was reported in similar energy differences, as obtained in this study [203]. Extracted data points could be fitted via linear regression with resulting correlation coefficients of $r^2 > 0.9$.

This observed chain length dependence gives evidence why no CO_2 loss could be experimentally observed for fairly large dihydroxymagnesium carboxylates (C_{14} to C_{19}) [161]. Additionally, the high absolute value ($E_{\text{MP2}} > 55$ kcal/mol for C_4) of the lowest forward energy barrier argues the difficulty of decarboxylating dihydroxymagnesium carboxylates.

3.4. Insights into the decarboxylation-type fragmentation mechanism

Natural bond orbital analyses (NBO) were performed to extract mechanistic insights for CO_2 fragmentations of dihydroxymagnesium carboxylates. Once the forward energy barrier of TS #2 is overcome, there exists a competition between the intramolecular nucleophilic attack of C_α (labelled as C_1 in Fig. 3.4) atom towards two electrophilic centers, either towards the CO_2 -carbon (C^*) atom or towards the magnesium electrophile. In the first case, the reaction will be directed towards the reversed reaction path, namely towards the monodentately coordinated dihydroxymagnesium carboxylate. In the latter case, CO_2 release is observed towards the formation a Mg-C bond, which means the formation of a Grignard-type molecules.

Fig. 3.4 reflects the charge distribution of these organomagnesium molecules. The aliphatic chain ligand is surrounded by hydrogen atoms, which possess a net charge of fairly 0 and thus, they are unlabelled in Fig. 3.4. On the left side in this representation of dihydroxymagnesium-n-pentanoate $[(\text{OH})_2\text{MgO}_2\text{C}_5\text{H}_9]^-$, a higher

3.5 Properties of putative Grignard-type OH-bearing molecules

degree of electronic polarization can be observed. Within this charge-proximal head group, the active center for decarboxylation is expressed by a triangle between the highlighted atoms C*, Mg and C₁. These atoms represent a fairly equilateral triangle within this transition state geometry ("TS #2"). Here, the CO₂ moiety is described to be almost neutral, which enhances its release from the organomagnesium complex. The formation of a Mg-C bond is directly driven via a nucleophilic attack of C_α (labelled as C₁, charge_{NBO} = -0.964) towards the electrophilic magnesium center (charge_{NBO} = 1.446). Therefore, the nucleophilic attack within this transition state environment is preferred towards the Mg center, relative to the C* electrophilic center, which is less electropositive (charge_{NBO} = 1.026), compared to Mg. Details on the NBO analysis are given in supplementary information.

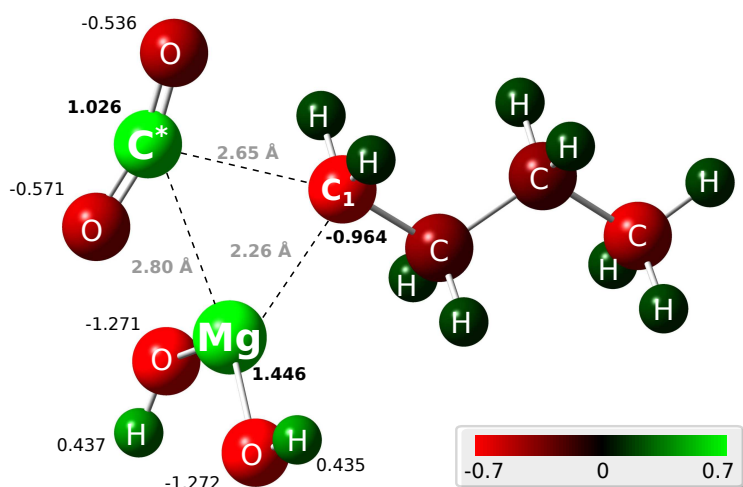


Figure 3.4: Charge population analysis of the C₅-dihydroxymagnesium carboxylate transition state #2. NBO analysis was performed to get insights into the charge distribution of dihydroxymagnesium carboxylates. Resulted charge values for key atoms of the polar head group are depicted, as computed on B3LYP/6-311+G(2d,p) level of theory. Additionally, bond lengths for the active center for decarboxylation are fairly equidistant (triangle between C*, C₁ and Mg) are depicted (in grey font color). Special interest was taken on the charge-proximal head group. Mechanistically, the CO₂ loss is forced by the high negative charge of C_α (charge_{NBO} (C_α) = -0.964) and the released entropy by the loss of CO₂, present as almost electroneutral species. The color code was ranged from charges -0.7 to 0.7.

3.5. Properties of putative Grignard-type OH-bearing molecules

The formation of Grignard-type OH-bearing organomagnesates, starting from dihydroxymagnesium carboxylates, seems to be improbable, as majorly influenced by the presence of two transition barriers. Especially, the high forward energy barrier of transition state #2 ($E_{MP2} > 55$ kcal/mol) is challenging to overcome. Nevertheless, once this barrier is passed, decarboxylation out of dihydroxymagnesium carboxylate, meaning the formation of a Grignard-type OH-bearing organomagnesate molecule, is enabled.

To track properties of putatively formed Grignard-type, natural bond orbital (NBO) analyses for both, anionic and neutral motifs of the Grignard reagent RMgCl and the Grignard-type molecules RMg(OH) were computed. In Fig. 3.5, charge

3.6 Conclusions/outlook

distributions of the respective neutral compounds are presented, while details on the charged organomagnesates are given supplementary information. Formed Mg-C share similar bond lengths, both in the OH and the Cl motif ($\approx 2.10 \text{ \AA}$).

The formation of carbanion intermediates is an important step within C-C bond formation in the Grignard reaction [204]. Therefore, the polarizability of the Mg-C bond within a Grignard reagent is of high interest. The polarizability of the Mg-C bond differs for hydroxy and chloro ligands ($\Delta\text{Charge}_{\text{Mg-C}} = 2.569$ for OH species and $\Delta\text{Charge}_{\text{Mg-C}} = 2.397$ for Cl species). This makes OH-bearing Grignard-type molecules potentially attractive to use them for C-C bond formation reactions, either in their carbanionic or neutral motif, in the field of organic synthesis and green chemistry.

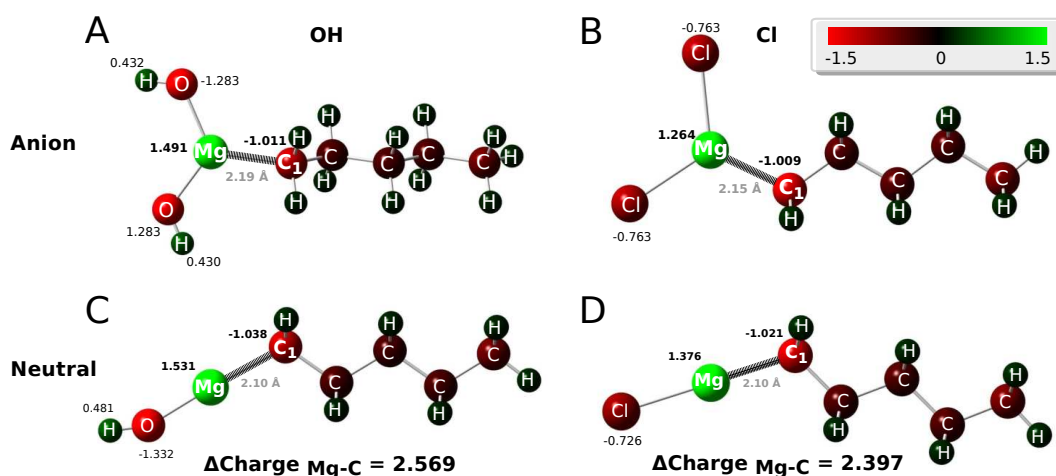


Figure 3.5: Charge population analysis of putative Grignard-type OH- and Cl-bearing molecules. NBO analyses helped in describing chemical properties of potential Grignard-type OH- (A) and Cl-bearing (B) molecules. C_5 compounds were used as representatives, as depicted in their neutral motifs. Resulted charge values for key atoms of the polar head group are depicted, as computed on B3LYP/6-311+G(2d,p) level of theory. Bond lengths of formed Mg-C are highlighted. For both probed species, similar Mg-C bond lengths were observed. The polarizability of the Mg-C bond is increased in the OH case, which prefers a potential carbanion formation out of the OH-bearing Grignard-type molecules. The color code was ranged from charges -1.5 to 1.5.

3.6. Conclusions/outlook

Dihydroxymagnesium carboxylates $[(\text{OH})_2\text{MgO}_2\text{CR}]^-$ with R = hydrocarbon C_xH_y and $\{x,y\} \in \mathbb{N}$ were probed for decarboxylation-type fragmentation on a theoretical level. Both second-order Møller–Plesset perturbation theory (MP2) and density functional theory (B3LYP-DFT) quantum chemical methods were used to decipher the ability of these organomagnesium compounds to form Grignard-type molecules.

Different linear alkyl chain lengths between C_4 and C_{11} were analyzed to extract the influence of the ligand's chain length on the decarboxylation likelihood. The observed slight increase in the forward energy barrier for decarboxylation of dihydroxymagnesium carboxylates suggests that the potential formation of Grignard-type (intermediate) reagent molecules is limited with respect to larger ligand's chain

3.6 Conclusions/outlook

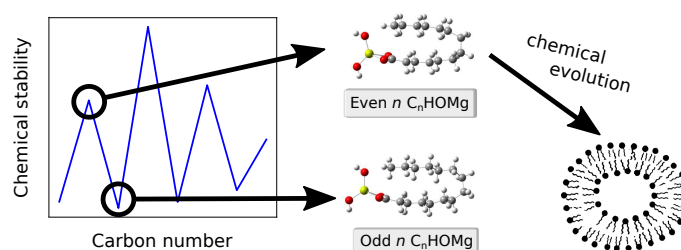
length. Experimentally, no CO₂ could have been observed for C₁₄ and C₁₉ molecules [161], which is in agreement with these theoretical findings. Decarboxylation-type fragmentations of these organomagnesium compounds seem to be improbable. First, a coordination conversion of the relaxed electronic structure from a bidentate towards a monodentate complex is required. Second, the presence of TS #2 with a high forward energy barrier ($E_{MP2} > 55$ kcal/mol) challenges the release of CO₂ in addition.

Nevertheless, an intramolecular nucleophilic attack mechanism enables the release of CO₂, as natural bond orbital (NBO) analysis could reveal. The C α atom is supposed to prefer binding towards the electrophilic magnesium coordination center, relative towards the electrophilic CO₂-carbon atom (C*). Once, the challenging transition state for decarboxylation is overcome, Mg-C can be formed and would be stable. Properties of putatively formed OH-bearing Grignard-type molecules show a tendency to form carbanionic species, which may be used for C-C bond formation reactions.

In conclusion, decarboxylation-type fragmentations of dihydroxymagnesium carboxylates seem to be improbable within non-catalytic, low energetic chemical environments. Nevertheless, we want to stimulate ideas on a theoretical level by this study, eventhough that decarboxylation-type fragmentations of these organomagnesium compounds are endergonic processes including high forward energy barriers. First, it is supposed to require certain catalytic effects to lower the forward energy barrier for the decarboxylation transition state (TS #2) to form OH-bearing Grignard-type molecules. Murray et al. presented a Ruthenium-based catalyst to convert alkenoic fatty acids into alkenes [205].

Second, the endergonic nature of this reaction has to be considered. External energy excess is required to get the system out of equilibrium and to trigger the release of CO₂. It is proposed to use energy propagation properties to make these kind of endergonic processes feasible, or generally a high energy source [206, 207].

4. The role of organomagnesium species within chemical evolution



In addition to probe dihydroxymagnesium carboxylates (CHOMg) for polar head group fragmentation, we assessed chemical stability with respect to their apolar alkyl chain fragmentation. Here, we observed odd/even alternation patterns within CHOMg stability. Odd/even alternation effects among fatty acids play an important role within biochemical systems, e.g. bilayer membranes. Here, we observed both experimentally and theoretically enrichment of even carbon-bearing fatty acids (CHO) and their organomagnesium (CHOMg) counterpart molecules, as compared to their adjacent odd carbon species. In-depth quantum chemical simulations of pseudocyclic organomagnesium conformers give mechanistic insights into the difference in chemical stability between odd and even carbon species. Thus, thermostable CHOMg preserve early information on odd/even alternation signatures within chemical stability and enables fatty acid hydrolytic release. This emphasizes its relevance on chemical evolution within prebiotic vesicles and formation of minimal cells by analog dominance of even carbon-bearing fatty acid within both high energy astrochemical and biochemical environments.

4.1. Introduction/motivation

Odd/even alternation effects within biochemical aliphatic alkyl chains play an important base the metabolic fundamentals of life and is found over role within all living organisms. Especially Lipids as bases for biological membranes preserve amphiphilic molecules like fatty acids as main building blocks, which commonly exist in even carbon number motifs (e.g. C_{14} , C_{16} , C_{18} and C_{20}). Fatty acid biosynthesis is based on a starting C_2 unit, namely acetyl-CoA [208] and governs therefore the resulting biochemical fingerprint. The presence of odd number of carbon metabolism is reserved to some very rare biological processes occurring in bacteria [209]. This phenomenon implies evolutionary aspects as well, because of the ability to form vesicles, protocells and finally cells via lipid membranes [210, 211]. Therefore, repeating molecular sub-unit patterns of even carbon numbers represents a structural biomarker [212].

In context of prebiotic, chemical organic evolution and the search for life's origin, amphiphilic molecules, like dihydroxymagnesium carboxylates or fatty acids, are of high relevance [213]. Amphiphilic molecules within self-assembled microcompartments form vesicles and membrane bilayer structures. Nevertheless, these building blocks of a minimal cell are not strictly biogenic and were also studied in various astrophysical environments. Vesicle formation could be observed out of ice experiments [214], Murchison meteorite extract [215, 216] or hydrothermal vent reactions [217]. Herein, odd/even effects are known to be stronger when inserting chemical functional groups into a carbon-based backbone molecular system [218]. Meteorites contain organic material that are similar, sometimes identical, to those found in the biosphere, such as amino acids, carboxylic acids, and sugar derivatives, which makes meteorites ideally to probe chemical evolution in the laboratory [219]. Fatty acids' concentrations in meteorites were reported to be significantly high (≈ 300 ppm [16]). In addition to small carboxylic acids [72, 73], broad molecular series including various degree of unsaturation could be observed [9]. Studies on small carboxylic acids (C_1 to C_{10}) show a decreasing molecule abundance with increasing number of carbon. Second, an inequality in odd/even patterns can be observed, which was not discussed in further detail previously [72, 73].

Carbon clusters are of high interest in astrochemistry within the formation of linear carbon chains and therefore within carbon chemical evolution [220, 221]. Odd/even effects are well reported for linear and cyclic carbon clusters, doped with various elements [222] including magnesium-carbon clusters [223] or cyanopolynes, which are closely related to complex organic molecules [224]. In addition to biochemical carboxylic acids, also within heteroatom-doped carbon clusters, even carbon chain molecules dominate in stability over odd numbers of carbon, as being present in interstellar medium [222, 223].

Recently, a previously unreported chemical class, dihydroxymagnesium carboxylates $[(OH)_2MgO_2CR]^-$ (CHOMg, $R = \text{hydrocarbon } C_xH_y$ and $\{x,y\} \in \mathbb{N}$), could be observed in meteorites [161]. CHOMg majorly share similar chemical properties with fatty acids (CHO), but are orders of magnitude more thermostable [161]. Previously, we showed the reversibility of the reaction $CHO_4Mg \rightleftharpoons CHO_2$ at low pH and their hydrolysis back into the corresponding fatty acids. Thus, they might have contributed to the selective stabilization of organic carboxylated molecules like fatty acids on a large time scale through high energy gradients within astrophysical environments, which emphasizes their potential astrobiological relevance [161]. This

4.2 Odd/even alternation within meteoritic (metal)organic matter

enables them to preserve early fatty acid fingerprints, including odd/even alternation chain length signatures.

Here, we test dihydroxymagnesium carboxylates for odd/even alternation patterns within their aliphatic chain. Experimental ultrahigh-resolution mass spectrometric data will be discussed next to quantum chemical fragmentation studies. Overall, we elucidate the stability of dihydroxymagnesium carboxylates with respect to different chain lengths and targeting the influence of odd and even chain lengths on a CHOMg/CHO molecule's stability. In addition to observations, we propose an explanation of odd/even alternation within CHOMg alkyl chains. Finally, implications of the results on early fatty acid chemical evolution will be given.

4.2. Odd/even alternation within meteoritic (metal)organic matter

Dihydroxymagnesium carboxylates (CHOMg) and fatty acid molecules (CHO) were tested for odd/even patterns within their aliphatic carbon chain stability. Experimentally, negative ionization electrospray ionization Fourier transform ion cyclotron resonance mass spectrometry (ESI-FT-ICR-MS) was used to get insights into intensity distributions of CHOMg and CHO for meteorite samples. Ultrahigh mass resolving power ($R > 10^6$) and mass accuracy (<200 ppb) was needed to extract unambiguously CHOMg compounds out of highly complex molecular spaces [161].

Fig. 4.1 shows odd/even alternation within dihydroxymagnesium carboxylate and fatty acid intensities, as observed by FT-ICR-MS experiments for methanolic extracts of meteorite specimen (soluble (metal)organic matter). Even carbon number-bearing molecules show higher intensities (local maxima) over a broad molecular range ($C_6 - C_{36}$) relative to their odd carbon number-bearing adjacent molecular neighbours. Additionally, O/C ratios were calculated for all molecular formulas. Two stability maxima were obtained within NWA 7325 CHOMg and CHO FT-ICR mass spectrometric data (Fig. 4.1). Molecules possessing ≈ 16 and ≈ 24 carbon atoms and O/C ratios of ≈ 0.15 and ≈ 0.25 represent the most abundant CHOMg/CHO molecules.

Odd/even alternation varies with meteoritic thermal/shock processing. Four representative samples, Thika L6 S1 W0 [125], Soltmany L6 S2 W0 [225], Ash Creek L6 S3 W0 and Braunschweig L6 S4 W0 [125] were probed, differing in their meteoritic shock history. In addition, NWA 7325 was used as moderately processed meteorite, representing medium shock grade and low weathering grade. All meteorite samples represent metamorphosed L6-type chondrites with almost no terrestrial weathering (W0 value). Therefore, insights are given into shock effects via meteoritic shock grades (ranging from S0 being unshocked towards S5 highly shocked meteorites). Higher degrees of odd/even fluctuation for both CHOMg and CHO could be observed for shocked meteorites (Fig. 4.1). Mass spectrometric were normalized by Euclidean norm prior data evaluation to observe intrinsic odd/even stability alternation (Fig. C.1). Artificial chain length fluctuation amplitudes due to different absolute intensities are ruled out. More stable even- n C_n HOMg/ C_n HO compounds (C_n HOMg/ C_n HO) remain whereas odd- n C_n HOMg/ C_n HO (C_{n-1} HOMg/ C_{n-1} HO) decompose more likely, expressing early chemical differentiation/fractionation of odd/even carbon-bearing molecules, as triggered by high energy astrophysical conditions.

In conclusion, higher abundance of even carbon species compared to their adja-

4.3 Methylene and ethylene release from dihydroxymagnesium carboxylates

cent molecular neighbours suggests higher stability of even carbon number-bearing CHOMg and CHO molecules in meteorites.

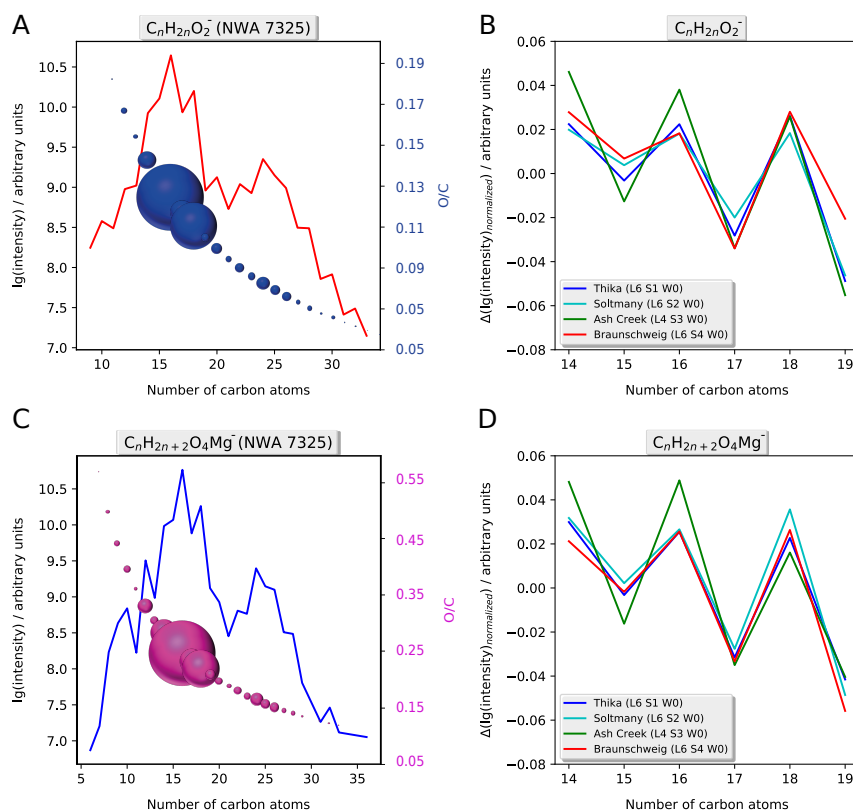


Figure 4.1: Odd/even alternation within meteoritic (metal)organic matter. (A), (C) Experimental negative ionization ESI-FT-ICR-MS intensity distribution of CHO_2^- and CHO_4Mg^- are shown for various carbon numbers, as observed for NWA 7325 meteorite. In addition, O/C ratios are depicted in violet color for CHO (A) and blue for CHOMg (C). Bubble sizes are scaled by the mass spectrometric intensity. (B), (D) Differences in odd/even intensity fluctuations as a function of carbon number are shown for differently shock-processed meteorites, ranging from weakly processed Thika (blue line) to highly shocked Braunschweig meteorite (red line). $\Delta(\lg(\text{intensity}_{\text{normalized}}))$ calculations are defined in supplementary information.

4.3. Methylene and ethylene release from dihydroxymagnesium carboxylates

Next to experimental mass spectrometric data of meteorites, modern computational quantum chemical approaches (density functional theory, DFT) were performed to study in-depth alkyl chain fragmentation of methylene CH_2 and ethylene C_2H_4 . This gives detailed insights into the stability dihydroxymagnesium carboxylates [161]. CHOMg was tested due to their higher thermal stability and therefore higher importance within chemical evolution, as compared to CHO compounds [161].

CH_2 and C_2H_4 releases were modelled on B3LYP-DFT6-311+G(2d,p) // B3LYP-DFT6-31+G(d,p) level of theory. Computational details are given in supplementary information. Different linear alkyl chain lengths were computed to extract information on odd/even alternation $[(\text{OH})_2\text{MgO}_2\text{CR}]^-$ stability regarding alkyl chain fragmentation. Homologous series of C_{12} - C_{19} were chosen, as motivated by two fol-

4.3 Methylene and ethylene release from dihydroxymagnesium carboxylates

lowing aspects. (i) The global intensity/stability maximum was extracted in a range of twelve to nineteen carbon atoms (Fig. 4.1). This allows most sensitive sampling of odd/even stability fluctuations by highest numbers in intensity differences. (ii) C_{12} to C_{19} fatty acids are of biological importance [208]. These amphiphilic molecules have been evolved to be optimal in formation of vesicles, lipid membranes or finally biological cells.

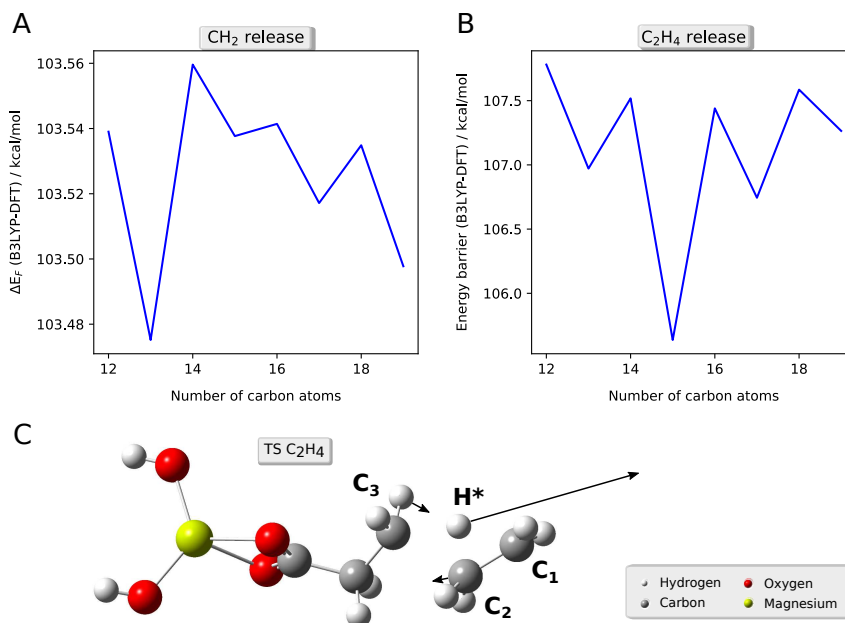


Figure 4.2: Computed alkyl chain fragmentation out of CHOMg. (A) CH_2 release, as modelled by thermodynamic fragmentation energy ΔE_F for varying number of carbon atoms. (B) C_2H_4 fragmentation monitoring by plotting its transition state energy barrier as a function of carbon number. For both cases, odd/even alternation within CHOMg stability is observed. Even- n C_n HOMg were observed to be more stable, relative to their adjacent odd- n species. (C) Transition state geometry of C_2H_4 release. Atom's trajectories within this transition state are indicated by black arrows. All computations were on B3LYP-DFT/6-311+G(2d,p) level of theory.

Fig. 4.2 depicts thermodynamic fragmentation energies for CH_2 fragmentation and transition state (TS) energy barriers for C_2H_4 release from respective CHOMg molecules. Releasing carbene moieties requires higher fragmentation as compared to the entropy-driven loss of C_2H_4 . Collision energy of >20 eV of accelerated CHOMg ions are required to induce carbene CH_2 release, as being experimentally observed from MS/MS fragmentation studies [161]). C_2H_4 release was experimentally observed with significantly lower collision energy (<10 eV [161]). The favorable C_2H_4 fragmentation channel was studied via integrated transition state analysis to compare the stability of odd/even CHOMg ionic systems. CH_2 stability investigations were probed via thermodynamic fragmentation energies to test single carbon changes. This enables direct comparison between odd- n and even- n C_n HOMg molecules.

For both fragmentation channels, odd/even alternation patterns were observed. For CH_2 release, local maxima of computed fragmentation energies were extracted for even carbon number-bearing molecules, as compared to their odd carbon molec-

4.4 Why is there odd/even alternation? Insights from pseudocyclic conformations

ular neighbours. Energy barriers for C_2H_4 release were found to be higher for even- n C_nHOMg molecules. In other words, higher energy is needed to fragment even- n C_nHOMg molecules, as indicated by modelling these fragmentation pathways. The C_2H_4 release transition state, describing C_2-C_3 bond breaking, is characterized via a [1,3] H shift, governed by the hydrogen atom, labeled as H^* . H^* translates in plane with respect to the released ethylene molecule.

In summary, quantum chemical fragmentation studies revealed a higher stability of even carbon-bearing CHOMg species, supporting experimental findings.

4.4. Why is there odd/even alternation? Insights from pseudocyclic conformations

Previous two sections described odd/even alternation effects within (i) meteoritic (metal)organic matter (experimental data) and (ii) for methylene CH_2 and for ethylene C_2H_4 fragmentation (computational simulations). Next, we want to decipher the reason behind this stability alternation effect within dihydroxymagnesium carboxylates.

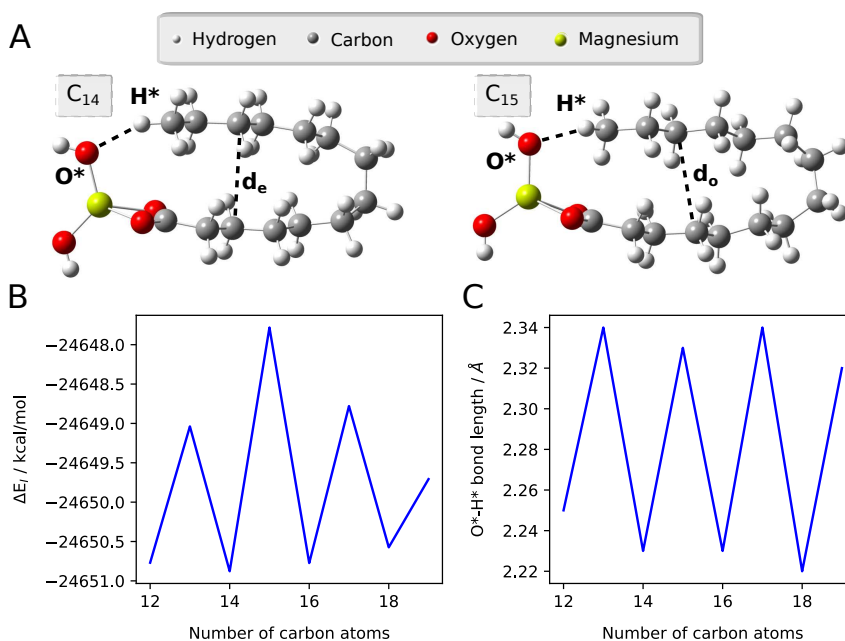


Figure 4.3: Pseudocyclization of dihydroxymagnesium carboxylates. (A) Relaxed pseudocyclic $C_{14}H_{29}MgO_4^-$ and $C_{15}H_{31}MgO_4^-$ geometries, as computed on M06-2X-DFT/def2TZVP-D3 level of theory. Average alkyl chain distances are $d_e \approx 3.7$ Å for even carbon species and $d_o \approx 4.0$ Å for odd carbon species. (B) Incremental binding energy ΔE_I as a function of number of carbon atoms shows odd/even alternation within CHOMg alkyl chain. (C) Bond length fluctuation (O*-H* bond) with varying carbon atoms give insights into structural differences between odd and even carbon-bearing CHOMg species.

Insights into mechanistic understanding for odd/even alternation within CHOMg alkyl chains were enabled by pseudocyclic conformers of dihydroxymagnesium carboxylates. Computations on M06-2X-DFT/def2TZVP-D3 level of theory were performed, considering dispersion effect for pseudocyclic CHOMg geometries [226]. M06-2X functional has been employed as it has been demonstrated to describe noncovalent interactions reliably [227]. van der Waals forces, especially London dispersion

4.4 Why is there odd/even alternation? Insights from pseudocyclic conformations

interactions, were taken into account [228] by using dispersion correction imputations, as introduced by Grimme et al. [226]. Fig. 4.3 shows distances d_o and d_e between two opposing alkyl chains to be in the range of 3.5-4.0 Å. This range of bond distances is sensitive for noncovalent interactions [226]. Details on the computational methodology on probing noncovalent interactions are given in supplementary information. Relative stability of pseudocyclic organomagnesium systems was investigated in analogy to the concept of incremental binding energy [224]. Here, E_I is defined by comparing total Gibbs free energies of adjacent molecules $C_n\text{HOMg}$ and $C_{n-1}\text{HOMg}$ within a homologous series (with integer n). Therefore, insights are given into stability fluctuations as a function the homologous series' sub-unit, like CH_2 here.

Fig. 4.3 shows an alternating effect of the incremental binding energy E_I as a function of carbon atoms. E_I is higher for odd- n $C_n\text{HOMg}$ molecules, as compared to their even- n counterparts, meaning odd- n $C_n\text{HOMg}$ are lower in absolute Gibbs Free energies. This suggests a higher stability of even- n $C_n\text{HOMg}$ relative to the odd- n ones. Two important parameters, which influence the stability of pseudocyclic CHOMg conformers, are bond length between oxygen atom of the $\text{Mg}(\text{OH})_2$ head group (O^* in Fig. 4.3) and the degree of eclipse of two opposed alkyl chains. Polar interactions between the heteratomic head group and the alkyl chain terminus are stronger for even carbon number species, as indicated by smaller $\text{O}^*\text{-H}^*$ bond lengths (Fig. 4.3). Even carbon molecular $\text{O}^*\text{-H}^*$ bond lengths are ≈ 2.2 Å, whereas $\text{O}^*\text{-H}^*$ bond lengths for odd carbon-bearing CHOMg molecules are slightly higher (≈ 2.3 Å). Second, alkyl chains are more completely eclipsed for even carbon number species (Fig. 4.4), which enhances attractive London force interactions. The distance between two alkyl chains are shorter for even carbon number-bearing molecules (Fig. 4.3, $d_e \approx 3.7$ Å for even carbon species and $d_o \approx 4.0$ Å). Both parameters argue for increased stability of even- n $C_n\text{HOMg}$, as compared to their odd carbon-bearing homologous.

Higher stability, as deduced from both experimental and computed data, of even- n $C_n\text{HOMg}$ species in relation to odd- n molecules is better understood when considering intramolecular interactions of pseudocyclic dihydroxymagnesium carboxylate conformers.

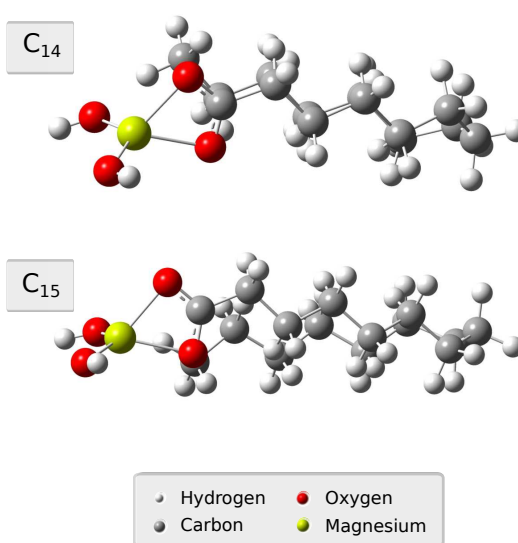


Figure 4.4: Pseudocyclic geometries for odd and even CHOMg species. Relaxed geometries, as computed on M06-2X-DFT/def2TZVP-D3 level of theory, for $C_{14}\text{H}_{29}\text{MgO}_4^-$ and $C_{15}\text{H}_{31}\text{MgO}_4^-$. Both structures are eclipsed, but the even carbon-bearing molecule eclipse more complete than the odd carbon-chain. This gives insights into stability difference based on varying strengths of van der Waals forces between opposed carbon chain increments.

4.5 Implications for fatty acid chemical evolution

4.5. Implications for fatty acid chemical evolution

Dihydroxymagnesium carboxylates (CHOMg) were found to show odd/even alternation effects in their chemical stability. CHOMg molecules are chemically similar to fatty acids [161], but are much more thermostable than fatty acids. This proposes them to be astrobiologically relevant due to putative stabilization of fatty acids within organic chemical evolution on a geological time scale.

FT-ICR mass spectrometry experiments provide insights on meteoritic fatty acid abundance distributions over a broad molecular range. Odd/even alternation patterns are observed for also fatty acids next to CHOMg intensity fluctuations (Fig. 4.1). Fig. 4.5 shows the ratio of organomagnesium molecules over fatty acid molecules for different carbon atoms. These data were obtained for NWA 7325 meteorite. Small chain lengths (< 14 carbon atoms) are dominated by CHOMg motifs (CHOMg/CHO ratio > 1), whereas chain lengths between 15 and 29 carbon atoms are fairly equally distributed between CHOMg and CHO motifs (CHOMg/CHO \approx 1). This indicates molecular sequestration for small carbon fatty acids and a moderate effect for long alkyl carboxylates as being present as CHOMg motifs.

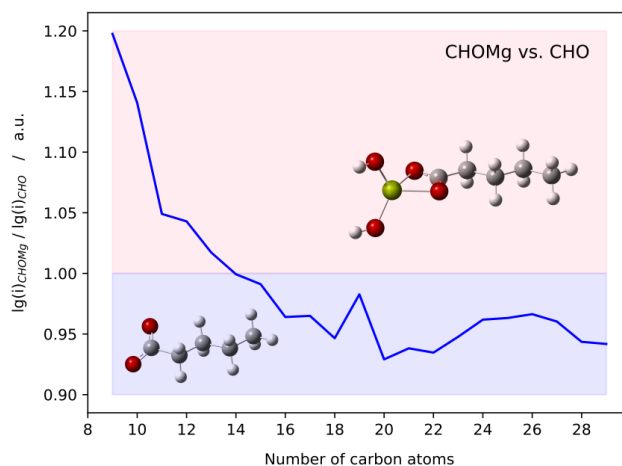


Figure 4.5: Distribution of fatty acids and their organomagnesium counterparts. This plot shows the ratio of logarithmic FT-ICR mass spectrometric intensities i of CHOMg over CHO compounds within NWA 7325 meteoritic soluble (metal)organic matter, represented in arbitrary units (a.u.) over the number of carbon atoms. Here, both depicted chemical species are only saturated carboxylate molecules, meaning $C_nH_{2n+2}O_4$ and $C_nH_{2n}O_2$, as illustrated by two C_5 representative structures.

Odd/even CHOMg stability alternation suggests an importance of amphiphilic organomagnesium molecules within fatty acids chemical evolution and finally within the evolution of prebiotic membranes. CHOMg molecules possess a higher molecular asymmetry relative to fatty acids, which enhances their attractive interactions between the polar head group and the apolar alkyl chain terminus. Second, thermostability of CHOMg enables preservation of thermolabile fatty acids within high energy astrophysical environments [153, 161]. Dihydroxymagnesium carboxylates store early information on odd/even alternation signatures within chemical stability and enable fatty acid release via hydrolysis [161]. This underlines astrobiological relevance and its influence in early prebiotic molecular selection processes within the evolution of vesicles of protocellular biological systems.

4.6. Conclusions/outlook

Odd/even alternation within chemical stability of both, fatty acid CHO and dihydroxymagnesium carboxylates CHOMg molecules could be observed on both experimental and theoretical level. Meteoritic FT-ICR-MS analysis provided additional insights into meteoritic shock grade dependence on the amplification of even carbon-bearing alkyl chain species. In-depth quantum chemical computations propose mechanistic insights via pseudocyclic CHOMg conformers to understand the effect of enrichment of even- n C_n HOMg molecules, as compared to their adjacent odd carbon species. Therefore, thermostable CHOMg preserve early information on odd/even alternation signatures within chemical stability and enables fatty acid hydrolytic release. The pairwise dominance of even carbon-bearing CHO and CHOMg species within both high energy astrochemical and biochemical environments emphasize its relevance on chemical evolution within prebiotic vesicles and formation of minimal cells. This chemical route may be one out of various mechanisms, which has lead to amplification of even carbon-bearing fatty acid molecules during chemical evolution.

5. Conclusions and outlook

This thesis reports on findings on organomagnesium-based metalorganic molecules (CHOMg) in astrochemical context (section 2). CHOMg compounds were experimentally found in meteorites via ultrahigh-resolving mass spectrometric techniques (FT-ICR-MS analysis). The necessity of ultrahigh mass spectrometric resolution was shown to enable unambiguous detection in complex organic mixtures. High resolving power $R > 10^6$ and high mass accuracy < 200 ppb was required to resolve mass peaks, which differ in mass difference by less than the mass of an electron (CHOMg-CHO isobaric problem). These results underline the power of data-driven astrochemical research for in-depth studies of meteoritic organic matter.

In addition, dihydroxymagnesium carboxylates were probed for fundamental chemical stability, as those molecular properties have been not reported previously. Chemical stability was studied by targeting two molecular regimes, (i) the polar head group and its resistance towards release of CO_2 . (ii) The apolar alkyl chain was investigated for charge-remote fragmentation.

Release of carbon dioxide from dihydroxymagnesium carboxylates may open new pathways of Grignard reactions, based on non-halogenated compounds. The potential on the formation of Grignard-type organomagnesate were probed via quantum chemical computations (section 3). Therefore, catalytic C-C coupling reactions in context of green chemistry might be enabled.

Probing alkyl chain fragmentations within CHOMg molecules showed odd/even alternation effects in chemical stability (section 4). Even carbon-bearing CHOMg compounds were found to be more stable, as compared to their adjacent odd carbon species. The chemical relationships between CHOMg and CHO analog species suggested implications within context of chemical evolution. The preferred presence of even over odd carbon-bearing molecules might shed light into early mechanism of vesicle formation.

The finding of dihydroxymagnesium carboxylates (CHOMg) enable subsequent research possibilities, which are listed in the following:

-
- **Extensive CHOMg screening within meteoritic and natural Earth samples.** As presented in section 2, CHOMg were found to relate with thermal processing in meteorites. In general scope, thermal processing can be extended to natural Earth samples as well. Project objectives are fundamental learning on formation mechanisms of CHOMg, as spatially resolved. Additionally, insights on early deep carbon sequestration within chondrules and their implications on the formation of complex organic molecules within chondrules may be gained.
 - **CHOMg-Grignard reactions.** A mid-term research aim is the application of laboratory-synthesized dihydroxymagnesium carboxylates and their modifications towards Grignard-type organomagnesates. To-date, we assume the requirement of high energy for synthesising dihydroxymagnesium carboxylates. This hypothesis is based on the relation of CHOMg to meteoritic thermal processing. The formation of halogen-free Grignard-type is a twofold challenging investigation, finding (i) a catalytic system lowering the forward reaction energy barrier and (ii) to find a smart way to set the chemical system out of equilibrium to enable the endergonic reaction of carbon dioxide release. Even though, this project is a challenging task, the main project objective of enabling green Grignard chemistry within C-C coupling reactions give motivations for studying this problem.
 - **Experimental studies on CHOMg vesicle formation.** Similar to the described project on CHOMg-based Grignard chemistry, challenging synthesis of dihydroxymagnesium carboxylates is required prior studying CHOMg vesicle formation. The increased thermostability of CHOMg compounds relative to their analogous CHO counterparts [153] drives research questions to experimentally probe CHOMg for early odd/even aliphatic chain alternation. Project objectives are implications of differentiated odd/even carbon-bearing CHOMg molecules within vesicle formation and their consequences for chemical evolution.

A. Appendix Chapter 2

A.1. ICP-MS Experiments

Methanolic extracts and residues of the meteorites were analyzed for total elemental composition. Extracts were diluted appropriately 10- or 26-fold to achieve the necessary sample volume. Extract residues were pressuredigested. Samples were exactly weighed within quartz vessels, to which 1 mL HNO₃, Suprapur, subboiling distilled (Merck), was added. The vessels were closed and introduced into a pressure digestion system (Seif) for 10 h at 170 °C. The resulting clear solutions were filled up exactly to the mark at 10 mL with Milli-Q H₂O and were then ready for element determination.

An ELEMENT 2 Thermo-Electron inductively coupled plasma sector field mass spectrometry instrument was used for determination of the elements. A solution of ¹⁰³Rh was added as an internal standard to each sample at a concentration of 1 μg/L. Sample introduction was carried out using a peristaltic pump connected to a Meinhard nebulizer with a cyclon spray chamber. The rf power was adjusted to 1,300 W, the plasma gas was 15 (L Ar)/min, whereas the nebulizer gas was ~0.9 (L Ar)/min after daily optimization. Measured element isotopes were as follows: ⁹Be, ¹¹⁴Cd, ⁵⁹Co, ⁵²Cr, ⁵⁶Fe, ²⁰²Hg, ¹⁹³Ir, ⁵⁵Mn, ⁹⁸Mo, ⁶⁰Ni, ²⁰⁸Pb, ¹²¹Sb, ⁷⁸Se, ⁵¹V, and ¹⁸⁴W.

Each determination method has been validated previously by regular laboratory intercomparison studies and by regular analyses of adequate certified reference materials, the latest directly before this study. Routinely, every 10 measurements, three blank determinations and a control determination of a certified standard for

This chapter has been published in *Proceedings of the National Academy of Sciences* **2017** 114, 2819–2824. [161].

A.2 SIMS Experiments

all mentioned elements were performed. Calculation of results was carried out on a computerized laboratory-data management system, relating the sample measurements to calibration curves, blank determinations, control standards, and the weight of the digested sample.

The solid-state meteorite sample was scanned using a commercial laser ablation system coupled to inductively coupled plasma mass spectrometry (LA-ICP-MS). The laser ablation system was a NWR 213 instrument from New Wave Research/ ESI, equipped with a beam expander, yielding laser spot sizes between 4 and 250 μm . The laser system was coupled to a PerkinElmer NexIon 300 ICP-mass spectrometer (Sciex). The ICPMS was synchronized with the LA unit in external triggering mode. The meteorite piece was mounted into the standard sample cell of the LA system with laboratory plasticine between the sample holder and the lower side in such a way that the flat upper side surface of the meteorite was placed on a level, where the laser would be focused. The exact position for ablation lines was defined by using the dual microscope of the LA system. The laser settings were as follows: energy, 30 J/cm²; power output, 100%; pulse repetition rate, 10 Hz; scan speed, 20 $\mu\text{m/s}$; spot size, 100 μm ; and ablation pattern, lines. The Ar-gas flow to ICPMS was 1.14 L/min. The ICP-MS settings were as follows: rf power, 1,200 W; plasma gas, 15 (L Ar) /min; and dwell time per isotope, 15 ms. The following isotopes have been selected for analysis: ²⁴Mg, ²⁷Al, ²⁸Si, ³⁵Cl, ⁵¹V, ⁵⁵Mn, ⁵⁷Fe, ⁵⁹Co, ⁶⁰Ni, ⁶³Cu, ⁶⁶Zn, ⁹⁸Mo, and ¹³⁸Ba. ICP-MS data were exported to Microsoft Excel, where signal intensities were color-coded.

A.2. SIMS Experiments

Measurements were performed using an IMS-4f Cameca secondary ion mass spectrometer. Etching in oxygen plasma for 10 min was performed to remove carbon contamination on the sample surface after grinding and polishing. These conditions were used to study a glassy vein of Chelyabinsk meteorite as selected target.

The sample target is a good insulator and charged during analysis. A normal incidence electron gun was used to compensate the positive charge on the sample surface. This gun has been effectively applied to detect negative secondary ions. In this case, the field accelerating the secondary ions was decelerating for electrons and therefore a cloud of electrons was created above the sample surface. This cloud discharges the charging areas of the sample surface, which was coated additionally with thin a layer of gold (~ 10 nm) to improve the discharge.

Because negatively charged secondary ions were selected for analysis, it was necessary to provide a high yield. This technique is well-known and consists of using Cs⁺ as the primary ions with impact energy of 14.5 keV to ablate analyte atoms/molecules. In contrast to the positive secondary ions, the detection of negative secondary ions has its own characteristics. Not all chemical elements have strong electron affinity. For example N, Ca, Mn, and Mg have electron affinity values close to zero. However, the analyzed sample was a mixture of oxides. To determine the elements of these oxides, molecular ions of MgO⁻ as well as C⁻, H⁻, and Si⁻ ions were detected and mapped.

Mass spectral resolution of 5,000 was used to overcome interference problems. The map of element distributions was performed using a dynamic transfer system. Lateral resolution was determined by the field-of-view aperture and equals 5 μm

A.3 ESI-FT-ICR-MS experiments

with a raster of 250 x 250 μm . Output data of the SIMS results were the signal intensities at the coordinates (x,y) analysis at a certain depth. The software, using the obtained coordinates and the intensities of the analyzed element signal, allows visualizing the data as a 2D distribution, where each point is assigned as a color depending intensity at that point.

A.3. ESI-FT-ICR-MS experiments

Fragments of fresh interior samples were first washed by stirring for a few seconds within the extraction solvent (methanol, LC-MS grade; Fluka) before crushing in 1 mL solvent poured into the corresponding agate mortar. This procedure was shown to limit the number of peaks resulting from terrestrial and human contamination, for example fatty acids arising from sample handling. The mixture (suspension) was transferred into an Eppendorf vial and underwent ultrasonic cleaning for <10 min and then was centrifuged. The supernatant liquid was removed with a microsyringe, ready for flow injection into the ESI source. A solvent methanolic blank was measured in accordance to be able to detect indigenous meteoritic (metal)organic matter in each sample. Organomagnesium compounds were absent in blank spectra.

The experimental study was performed on a high-field FT-ICR mass spectrometer from Bruker Daltonics with a 12-T magnet from Magnex. A time-domain transient with 4 MWords was obtained and Fouriertransformed into a frequency domain spectrum. The frequency domain was afterward converted to a mass spectrum by the solariX control program of Bruker Daltonics. The ion excitations were generated in broadband mode (frequency sweep radial ion excitation) and 3,000 scans were accumulated for each mass spectrum in a mass range of 147-1,000 amu. Ions were accumulated for 300 ms before ICR ion detection. The pressure in the quadrupole/hexapole and ICR vacuum chamber was 3×10^{-6} mbar and 6×10^{-10} mbar, respectively. For CID-MS/MS, ions were accumulated for 3 s.

The ESI source (Apollo II; Bruker Daltonics) was used in negative ionization mode. The methanolic solutions were injected directly into the ionization source by means of a microliter pump at a flow rate of $120 \mu\text{L} \cdot \text{h}^{-1}$. A source heating temperature of 200 °C was maintained and no nozzle-skimmer fragmentation was performed in the ionization source. The instrument was previously externally calibrated by using arginine negative cluster ions ($5 \text{ mg} \cdot \text{L}^{-1}$ arginine in methanol).

FT-ICR mass spectra with m/z from 147 to 1,000 amu were calibrated externally and internally to preclude alignment errors. Subsequently, the mass spectra were exported to peak lists at a signal-to-noise ratio ≥ 3 . Elemental formulas were calculated combinatorially within a mass accuracy window of ± 0.2 ppm for each peak in batch mode by an in-house software tool and validated via the senior-rule approach/cyclomatic number [92], assuming valence 2 for S and valence 4 (coordination number) for Mg.

A.4. Computations

The electronic structure simulations were performed on a stand-alone computer by ab initio quantum mechanical computations, based on density functional theory (DFT), as implemented in Gaussian 03 [229]. The hybrid DFT-functional B3LYP was implemented with d-polarization functions for each heavy atom and 1p for each hydrogen atom in all single-point energy calculations. All geometry optimizations

A.5 Correlation Between the Experimental and Computed Fragmentation Energies

were performed with the 6-31+G(d,p) basis set. Frequency calculations were done for each optimized geometry with the same 6-31+G(d,p) basis set to obtain the zero point vibrational energy. This value was multiplied by a scaling factor of 0.9804 to correct for vibrational anharmonicities [230]. Another intention for performing the frequency analysis is the identification of transition states. Detecting negative frequencies (imaginary frequencies) implies that the optimized geometry is not fully relaxed as a stationary point on the potential energy surface. The single point energy calculations were done at the 6-311+G(2d,p) level of theory. The use of diffuse functions was important to represent the correct geometry and thermodynamic properties of anionic species [231]. Stability tests were performed in critical cases (significantly different energy values relative to the homologous series of treated attachment systems) to ensure that the used wave function represents the lowest energy solution of the selfconsistent field equations.

For geometry optimization, the Bery analytical gradient optimization routines [232, 233] were used in combination with the GDIIS algorithm [234]. The requested convergence value in the density matrix was 10^{-8} , the threshold value for maximum displacement was 0.0018 Å, and the threshold value for the maximum force was 0.00045 Hartree Bohr⁻¹. The nature of the stationary points was established by calculating and diagonalizing the Hessian matrix (force-constant matrix). All geometries of electronic structures calculated were viewed with the GaussView or Avogadro program.

The Gibbs free energy ΔG between each neutral Mg(OH)₂ and the anionic carboxylate anion in the gas phase was calculated as Eq. A.1, satisfying the reaction of Eq. 2.1:

$$\Delta G = -BE = E_{Complex} - (E_{Mg(OH)_2} + E_{RCOO^-}) \quad (A.1)$$

$E(x)$ are the single-point energies of respective species x and $R = \text{hydrocarbon } C_xH_y$ and $\{x,y\} \in$. Therefore, the two educts were first optimized in the absence of the reaction partner (step 1). Afterward, the charged complex was relaxed (step 2). The mentioned energies in Eq. A.1 are the single-point energies of steps 1 and 2. All computations are referred to gas-phase conditions.

A.5. Correlation Between the Experimental and Computed Fragmentation Energies

The minimum collision energy of 10 eV, required to initiate dissociation of the C₁₆-dihydroxymagnesium carboxylate complex anion, had to be scaled because the magnitude of internal energy deposition from kinetic acceleration in an electric field in a quadrupole can be estimated to reach 20% [235]. The corresponding energy of 193.3 kJ/mol is in the range of the DFT-computed binding energy (BE) for [(OH)₂MgO₂CR]⁻ for the reaction of Mg(OH)₂ with the carboxylate anion (BE_{computed} = 206.7 kJ/mol).

A.6. Calculation of the Measured Equilibrium Constant K'

The equilibrium constant K for the reaction in Eq. A.2 is given as

$$K = \frac{a([(OH)_2MgO_2CR]^-)}{a(RCOO^-) \cdot a(Mg(OH)_2)} \approx \frac{c([(OH)_2MgO_2CR]^-)}{c(RCOO^-) \cdot c(Mg(OH)_2)} \quad (A.2)$$

A.7 Mass Difference Network Reconstruction

with R = hydrocarbon C_xH_y and $\{x,y\} \in$. Thermodynamic activities $a(x)$ can be approximated by concentrations $c(x)$ for different molecules x , when ideal behavior is assumed. $c(x)$ is expressed as the compound's mass spectrometric intensity I , which is proportional to the compound's abundances [236]. For K , a measured equilibrium constant K' is used with the assumption that $c(\text{Mg}(\text{OH})_2) \gg c(\text{RCOO}^-)$ because of the much higher amount of mineral compounds relative to the organic compounds [237]. Therefore, the reaction is considered as a pseudo-first-order reaction, where $d(c(\text{Mg}(\text{OH})_2))/dt \approx 0$. Thus, K' is calculated with Eq. A.3 instead:

$$K' = \frac{I([\text{(OH)}_2\text{MgO}_2\text{CR}]^-)}{I(\text{RCOO}^-)} \quad (\text{A.3})$$

A.7. Mass Difference Network Reconstruction

Theoretical ion masses of the above assigned molecular formulas were used for mass difference network reconstruction. Theoretical ion masses (nodes) were connected by edges if their mass differences were equal (± 0 ppm) to the theoretical mass differences of ΔCH_2 (14.015650 amu), ΔO (15.994915 amu), or $\Delta\text{Mg}(\text{OH})_2$ (57.990521 amu). Mass difference networks were laid out using the Cytoscape software (Allegro version 3.2.1 layout) (55).

A.8. Statistical Evaluation of Meteorite Samples

CHOMg mass lists were aligned with an in-house software [238]. To stabilize the variance, only m/z values present in more than 5% of all samples were further considered in the statistical elaboration to remove unique compounds. The peak intensities were scaled to unit variance and logarithm-transformed.

To evaluate the data, several multivariate models were set up. Orthogonal partial least square discriminant analysis (OPLS-DA) and OPLS regression models were performed by the sevenfold cross-validation procedure, as implemented in the software SIMCA, and then verified with CV-ANOVA (cross-validation ANOVA), to exclude overfitting. Relevant indicators, such as P value, $R^2(\text{Y})$, and $Q^2(\text{cum})$, were subsequently reported to indicate the significance, the goodness of the fit, and the quality of the model prediction. Moreover, potential discriminating variables were chosen by examining the loading plot. The software tools, used for the statistical elaboration, were SIMCA 13.0.3.0 (Umetrics) and RStudio (version 0.98.1103; RStudio, Inc.).

First, a classification model was set up via OPLS-DA using a meteorite subset, formed by samples with assigned information about their thermal stress level. All samples were correctly classified with a Fisher probability of $5e^{-81}$ and the model was valid ($P < 0.001$). Based on this model, properties were predicted for additional samples without any available thermal stress information. Based on the classification, a gradient for the thermal stress was set up among all samples from low- to high-thermally stressed meteorites. This gradient was used as Y variable in an OPLS model to reveal a possible relation between the m/z variables and Y. The OPLS score scatter plot (Fig. 2.10) was robust to overfitting ($P = 0.004$) with $R^2(\text{Y}) = 0.91$ and $Q^2(\text{cum}) = 0.27$. The ellipse represents the Hotelling's T^2 confidence region (95%). The first axis (x axis) is the so-called first component with the new samples coordinate. It can be seen as the best-fit line that traverses the geometric origin of

A.9 Mg Isotope Measurements

the dataset accounting for the greatest amount of variance of the data. The second greatest variance is explained by the second component, orthogonal to the first, and so on. All of the components have to be uncorrelated each other and cumulatively all together account for the 100% of the variance. The aforementioned coordinates of data points on the first component are the first principal component values, or component scores; they are computed as the product of (centered) data matrix and the eigenvector.

The most relevant masses, 50th percentile of loading values of the y axis (oxygen variation in CHOMg formulas), were visualized in modified van Krevelen diagrams, as depicted in Fig. 2.10. Concerning the thermal stress variation, the most relevant masses, 50th percentile of loading values of the x axis, were visualized in modified van Krevelen diagrams, as depicted in Fig. 2.11. The box plot was set up by counting CHOMg formulas for negative and positive loading values on the x axis, respectively.

Hierarchical cluster analysis (HCA) was performed using the average linkage method (UPGMA) for the distance between clusters and the Pearson correlation coefficient as criteria to cluster the variables. The HCA was done by the Hierarchical Clustering Explorer 3.0 (Human-Computer Interaction Lab, University of Maryland). Hierarchical cluster analysis organizes the samples, as a graphical output, into a dendrogram (cluster tree) whose branches are the desired clusters. Based on different similarity rules the clusters are defined. Similar samples are within a cluster.

A.9. Mg Isotope Measurements

All samples (both the methanolic extracts and residues) were dissolved subsequently using a standard 3:1 HF:HNO₃ dissolution technique in Savillex 3-mL vials (hexagonal cap, square body type) [239]. After dissolution, ca. ~1% aliquot of the solution was saved for ²⁷Al/²⁴Mg analyses. The remainder was centrifuged and processed through a cation exchange column to separate Mg from the sample matrix and potential isobaric interferences. The column procedure was first calibrated to separate Mg from matrix elements, such as Na, Al, K, and Ca. In particular, separation of Mg and Ca is important because this has been shown to cause fractionation of Mg isotope ratios by up to 1‰ [240]. Standards and unknowns were dried down (~20 μg of Mg) and redissolved in 0.5 mL of 1 N HNO₃ before eluting through 0.75 mL of BioRad AG50W-X12 resin (200–400 mesh). We added a rinse step involving 3 mL of 0.15 M HF, which causes removal of Al and Ti from the column but leaves Mg unaffected. The Mg cut was collected in 12 mL of 1 N HNO₃. Once eluted, the Mg fraction was collected and dried down and the residue was redissolved in 20 μL of concentrated HNO₃ to oxidize any organic molecules derived from the resin. After repeating this column chemistry, the final Mg fraction was dried down and redissolved in 1 mL of 2% HNO₃. After sample processing, the resin was cleaned by repeated elutions of 7 M double-distilled HNO₃ and Milli-Q ultrapure H₂O. Both Mg isotope compositions and ²⁷Al/²⁴Mg ratios were measured on a Thermo Neptune Plus HR-MC-ICP-MS in the Department of Earth and Planetary Sciences at the University of California, Davis.

Isotopic analyses of Mg were bracketed using the DSM-3 pure Mg standard [241] to account for instrumental mass bias and drift throughout the analysis period. Mg isotope ratios are expressed using delta notation as parts per thousand (‰)

A.9 Mg Isotope Measurements

differences from DSM-3. Each sample was initially prescreened using 1% of the final Mg solution to ensure accurate dilution of the sample to match the signal intensity of the bracketing standard to within 10%. Samples were analyzed under dry plasma conditions using an ESI Apex IR desolvating nebulizer, which suppresses oxide interferences. The samples were analyzed in medium resolution to avoid the CN+ peak on ^{26}Mg , which cannot be resolved at low resolution. Using a high-sensitivity “x” skimmer cone the typical intensities for a 500-ppb solution at medium resolution were between 20–25 V of ^{24}Mg (amplified with a 1011-ohm register board). Blank intensities on ^{24}Mg were typically 0.003-0.005 V. To assess the accuracy of our measurements, the pure Mg standard CAM-1 was routinely measured throughout each analytical session. In total, CAM-1 was measured 78 times with an average $\delta^{26}\text{Mg}$ value of $-2.61 \pm 0.08 \text{ ‰}$, which is within error of the accepted value ($-2.59 \pm 0.14 \text{ ‰}$) [241]. To assess the accuracy of the column chemistry and our external reproducibility, the USGS basalt standard BCR-2 was processed with every batch of column chemistry. A total of 26 separate analyses from eight separate chemical separations were performed on this standard. On average, BCR2 had a $\delta^{26}\text{Mg}$ value of $-0.20 \pm 0.07 \text{ ‰}$ and $\delta^{25}\text{Mg}$ value of $-0.10 \pm 0.04 \text{ ‰}$, which is within error of the estimated average composition of the upper continental crust ($\delta^{26}\text{Mg} = -0.22 \text{ ‰}$) [242] and other recent published values for basalts [243].

A.10. Information on 61 meteorite samples, used in the statistical analysis

Assignment of 61 meteorite samples, used in the statistical multivariate analysis. CHOMg molecular signatures were found in all these meteorites (Fig. 2.10).

Table A.1: Information on 61 meteorite samples, used in the statistical analysis

Sample ID	Meteorite description	Type class	Number of CHOMg formulas	Mean CHOMg intensities
49	Achondrite-ung S-medium W-low NWA 7325	Achondrite-ung	1154	1.82E+08
14	CI1 Orgueil	CI	514	8.71E+07
15	CK4 S2 W0 NWA 7310	CK	888	1.00E+08
5	CM2 WA Y-74662	CM	286	2.35E+07
9	CM2 Y-86720		991	7.27E+06
11	CM2 Y-791198		273	2.81E+07
13	CM2 Y-793321		762	4.42E+06
16	CM1 Moapa Valley		1102	1.55E+09
17	CM1/2 W-low NWA 8534		676	1.22E+07
18	CM2 S0 W1 Jbilet Winselwan		396	1.64E+07
19	CM2 S0 W0 Maribo		552	1.61E+07
20	CM2 S1-2 W1-2 Murchison		610	1.53E+07
21	CM2 Murray		902	3.55E+07
22	CM2-an W1 NWA 3340		470	2.94E+08
23	CM2 S0 W0 Paris		521	9.59E+06
27	CM2 DOM 08003		387	4.38E+06
28	CM2 EET 87522		194	3.31E+06
30	CM2 EET 96029		213	3.76E+06
40	CM2 LEW 85311		320	2.79E+06
41	CM2 WB LEW 85312		317	4.54E+06
43	CM2 WB MCY 05230		432	3.61E+06
45	CM1 MET 01070		218	4.48E+06
46	CM2 WA MIL 07700		209	9.23E+06
48	CM2 S2 W-low NWA 7131		331	1.74E+08
50	CM2 WB PCA 02010		255	6.24E+06

51	CM2 WB PCA 02012		253	4.64E+06
52	CM2 WB PCA 91008		110	1.00E+07
53	CM2 WA/Be QUE 93005		287	1.62E+07
61	CM2 WA/BeWIS 91600		333	3.06E+07
6	CO3.0 Y-81020	CO	186	3.98E+07
7	CO3.2 Y-82050		1157	6.75E+07
8	CO3.5 Y-82094		610	1.21E+08
12	CO3.3 Y-791717		1315	1.63E+08
24	CO3.6 S2 W0 Moss		1019	3.71E+08
29	CR2 EET 92042	CR	270	2.10E+07
32	CR2 GRA 06100		445	5.30E+07
33	CR2 GRA 95229		214	1.69E+07
34	CR2 GRO 03116		251	1.20E+07
35	CR1 GRO 95577		173	1.70E+07
54	CR2 WBE QUE 99177		392	2.90E+07
10	CV3 Y-86751	CV	837	5.47E+06
25	CV3 S1 W0 Allende		361	1.10E+07
26	CV3 Vigarano		259	1.78E+08
31	EUC W0 Tihert	EUC	787	3.33E+08
47	H4 Grüneberg	H	920	7.06E+07
1	Howardite S3 W-low Saricicek (Recent Turkish Fall, September 2015)	Howardite	1090	1.10E+08
3	L4 S3 W0 Sidi Ali Ou Azza	L	738	1.94E+08
36	L6 S4 W0 Braunschweig		504	7.15E+07
37	L6 S4 W0 Novato		1023	1.77E+08
38	L6 S4 W0 Battle Mountain		566	6.71E+07
39	L6 S2 W0 Soltmany		1363	1.74E+08
44	L(LL)3.05 WB/C MET 00526		497	2.79E+07
55	L6 S1 W0 Thika		777	1.08E+07
60	L5 S4 W0 Varre-Sai		276	5.59E+07
2	LL5 S4 W0 Chelyabinsk	LL	1111	1.32E+08
4	LL6 S3 W0 Stubenberg (Recent German fall, March 2016)		1412	1.13E+08
42	LL6 Kilabo		636	1.40E+06

A.10 Information on 61 meteorite samples, used in the statistical analysis

A.10 Information on 61 meteorite samples, used in the statistical analysis

56	URE S3 W4 Dho 1303	URE	935	6.10E+08
57	URE S-high NWA 2634		1015	6.69E+08
58	URE NWA 5928		858	7.79E+08
59	URE Sahara 98505		156	2.64E+07

A.11 Mass list of significantly enriched compounds in thermal processed meteorites

A.11. Mass list of significantly enriched compounds in thermal processed meteorites

Mass list of significantly enriched compounds in thermal processed meteorites, plotted in Fig. 2.11. These plotted m/z values reflect the 50th percentile of the variables, which are unique for the positive values of the first component (x-axis) of the OPLS score plot (Fig. 2.10).

Table A.2: Mass list of significantly enriched compounds in thermal processed meteorites

m/z (exp)	m/z (theo)	Error (m/z) / ppm	Molecular formula	O/C	H/C
143.02002	143.02003	-0.066	C4H7O4Mg1-	1.00	2.00
144.99928	144.99929	-0.076	C3H5O5Mg1-	1.67	2.00
145.03565	145.03568	-0.163	C4H9O4Mg1-	1.00	2.50
154.98364	154.98364	-0.007	C4H3O5Mg1-	1.25	1.00
156.99929	156.99929	-0.034	C4H5O5Mg1-	1.25	1.50
157.03567	157.03568	-0.03	C5H9O4Mg1-	0.80	2.00
158.97854	158.97856	-0.101	C3H3O6Mg1-	2.00	1.33
159.01494	159.01494	-0.018	C4H7O5Mg1-	1.25	2.00
159.05132	159.05133	-0.05	C5H11O4Mg1-	0.80	2.40
168.99931	168.99929	0.112	C5H5O5Mg1-	1.00	1.20
171.01495	171.01494	0.057	C5H7O5Mg1-	1.00	1.60
171.05133	171.05133	-0.001	C6H11O4Mg1-	0.67	2.00
172.9942	172.99421	-0.029	C4H5O6Mg1-	1.50	1.50
173.03059	173.03059	0.012	C5H9O5Mg1-	1.00	2.00
173.06698	173.06698	0.048	C6H13O4Mg1-	0.67	2.33
179.02003	179.02003	-0.005	C7H7O4Mg1-	0.57	1.14
180.94765	180.94765	-0.006	C1H1O9Mg1-	9.00	2.00
183.05134	183.05133	0.056	C7H11O4Mg1-	0.57	1.71
185.03059	185.03059	-0.023	C6H9O5Mg1-	0.83	1.67
185.06697	185.06698	-0.018	C7H13O4Mg1-	0.57	2.00
187.00986	187.00986	0.036	C5H7O6Mg1-	1.20	1.60
187.04624	187.04624	0.001	C6H11O5Mg1-	0.83	2.00
187.08263	187.08263	0.026	C7H15O4Mg1-	0.57	2.29
189.02553	189.02551	0.109	C5H9O6Mg1-	1.20	2.00
193.03567	193.03568	-0.028	C8H9O4Mg1-	0.50	1.25
197.06698	197.06698	0.015	C8H13O4Mg1-	0.50	1.75
199.00985	199.00986	-0.008	C6H7O6Mg1-	1.00	1.33
199.08262	199.08263	-0.014	C8H15O4Mg1-	0.50	2.00
201.02551	201.02551	0	C6H9O6Mg1-	1.00	1.67
201.09828	201.09828	-0.005	C8H17O4Mg1-	0.50	2.25
203.00477	203.00477	0.011	C5H7O7Mg1-	1.40	1.60
203.02003	203.02003	0.011	C9H7O4Mg1-	0.44	0.89
203.04116	203.04116	0.019	C6H11O6Mg1-	1.00	2.00
203.07756	203.07754	0.117	C7H15O5Mg1-	0.71	2.29
207.01493	207.01494	-0.054	C8H7O5Mg1-	0.63	1.00
207.05133	207.05133	0.002	C9H11O4Mg1-	0.44	1.33
208.97896	208.97895	0.019	C3H5O9Mg1-	3.00	2.00
209.0306	209.03059	0.036	C8H9O5Mg1-	0.63	1.25
209.06698	209.06698	0.007	C9H13O4Mg1-	0.44	1.56
211.00988	211.00986	0.125	C7H7O6Mg1-	0.86	1.14
211.04623	211.04624	-0.029	C8H11O5Mg1-	0.63	1.50
211.08263	211.08263	0.008	C9H15O4Mg1-	0.44	1.78
213.0255	213.02551	-0.015	C7H9O6Mg1-	0.86	1.43
213.09827	213.09828	-0.035	C9H17O4Mg1-	0.44	2.00

A.11 Mass list of significantly enriched compounds in thermal processed meteorites

215.07755	215.07754	0.026	C8H15O5Mg1-	0.63	2.00
215.11393	215.11393	-0.002	C9H19O4Mg1-	0.44	2.22
217.02042	217.02042	0.018	C6H9O7Mg1-	1.17	1.67
217.09319	217.09319	-0.029	C8H17O5Mg1-	0.63	2.25
219.01495	219.01494	0.047	C9H7O5Mg1-	0.56	0.89
221.03059	221.03059	-0.007	C9H9O5Mg1-	0.56	1.11
223.04625	223.04624	0.049	C9H11O5Mg1-	0.56	1.33
223.08264	223.08263	0.043	C10H15O4Mg1-	0.40	1.60
225.02555	225.02551	0.195	C8H9O6Mg1-	0.75	1.25
225.06189	225.06189	-0.024	C9H13O5Mg1-	0.56	1.56
225.09828	225.09828	0.019	C10H17O4Mg1-	0.40	1.80
227.04116	227.04116	0.033	C8H11O6Mg1-	0.75	1.50
227.11393	227.11393	0	C10H19O4Mg1-	0.40	2.00
229.09318	229.09319	-0.04	C9H17O5Mg1-	0.56	2.00
229.12958	229.12958	0.031	C10H21O4Mg1-	0.40	2.20
231.03607	231.03607	-0.008	C7H11O7Mg1-	1.00	1.71
231.07247	231.07246	0.074	C8H15O6Mg1-	0.75	2.00
231.10881	231.10884	-0.121	C9H19O5Mg1-	0.56	2.22
233.03059	233.03059	-0.013	C10H9O5Mg1-	0.50	1.00
233.06698	233.06698	0.03	C11H13O4Mg1-	0.36	1.27
233.08807	233.08811	-0.156	C8H17O6Mg1-	0.75	2.25
235.04624	235.04624	0.008	C10H11O5Mg1-	0.50	1.20
235.08263	235.08263	0.004	C11H15O4Mg1-	0.36	1.45
237.0619	237.06189	0.048	C10H13O5Mg1-	0.50	1.40
237.09829	237.09828	0.073	C11H17O4Mg1-	0.36	1.64
239.04117	239.04116	0.037	C9H11O6Mg1-	0.67	1.33
239.07754	239.07754	-0.012	C10H15O5Mg1-	0.50	1.60
239.11394	239.11393	0.038	C11H19O4Mg1-	0.36	1.82
241.05681	241.05681	0.013	C9H13O6Mg1-	0.67	1.56
241.09319	241.09319	0.004	C10H17O5Mg1-	0.50	1.80
241.12958	241.12958	-0.005	C11H21O4Mg1-	0.36	2.00
245.05173	245.05172	0.027	C8H13O7Mg1-	0.88	1.75
245.0881	245.08811	-0.01	C9H17O6Mg1-	0.67	2.00
247.00986	247.00986	0.002	C10H7O6Mg1-	0.60	0.80
247.04624	247.04624	0.011	C11H11O5Mg1-	0.45	1.09
249.0255	249.02551	-0.032	C10H9O6Mg1-	0.60	1.00
249.0619	249.06189	0.019	C11H13O5Mg1-	0.45	1.27
249.09827	249.09828	-0.025	C12H17O4Mg1-	0.33	1.50
251.04116	251.04116	0.028	C10H11O6Mg1-	0.60	1.20
251.07755	251.07754	0.017	C11H15O5Mg1-	0.45	1.45
251.11394	251.11393	0.064	C12H19O4Mg1-	0.33	1.67
253.05681	253.05681	0.02	C10H13O6Mg1-	0.60	1.40
253.09319	253.09319	-0.002	C11H17O5Mg1-	0.45	1.64
253.12958	253.12958	0.017	C12H21O4Mg1-	0.33	1.83
255.03607	255.03607	-0.012	C9H11O7Mg1-	0.78	1.33
255.07246	255.07246	0.016	C10H15O6Mg1-	0.60	1.60
255.14523	255.14523	0.001	C12H23O4Mg1-	0.33	2.00
257.05173	257.05172	0.016	C9H13O7Mg1-	0.78	1.56
259.03101	259.03099	0.076	C8H11O8Mg1-	1.00	1.50
259.06737	259.06737	0.013	C9H15O7Mg1-	0.78	1.78
259.10376	259.10376	0.014	C10H19O6Mg1-	0.60	2.00
259.14016	259.14014	0.072	C11H23O5Mg1-	0.45	2.18
261.02551	261.02551	-0.002	C11H9O6Mg1-	0.55	0.91
261.04665	261.04664	0.047	C8H13O8Mg1-	1.00	1.75
261.06189	261.06189	0.006	C12H13O5Mg1-	0.42	1.17

A.11 Mass list of significantly enriched compounds in thermal processed meteorites

261.09829	261.09828	0.038	C13H17O4Mg1-	0.31	1.38
261.11942	261.11941	0.045	C10H21O6Mg1-	0.60	2.20
263.04116	263.04116	0.01	C11H11O6Mg1-	0.55	1.09
263.07753	263.07754	-0.058	C12H15O5Mg1-	0.42	1.33
263.11393	263.11393	0.003	C13H19O4Mg1-	0.31	1.54
265.05681	265.05681	0.031	C11H13O6Mg1-	0.55	1.27
265.0932	265.09319	0.016	C12H17O5Mg1-	0.42	1.50
265.12957	265.12958	-0.027	C13H21O4Mg1-	0.31	1.69
267.03607	267.03607	0.002	C10H11O7Mg1-	0.70	1.20
267.05723	267.0572	0.095	C7H15O9Mg1-	1.29	2.29
267.07246	267.07246	-0.003	C11H15O6Mg1-	0.55	1.45
267.10885	267.10884	0.039	C12H19O5Mg1-	0.42	1.67
269.05173	269.05172	0.018	C10H13O7Mg1-	0.70	1.40
269.08811	269.08811	0.006	C11H17O6Mg1-	0.55	1.64
269.16089	269.16088	0.06	C13H25O4Mg1-	0.31	2.00
271.06736	271.06737	-0.031	C10H15O7Mg1-	0.70	1.60
271.17653	271.17653	-0.001	C13H27O4Mg1-	0.31	2.15
273.04665	273.04664	0.054	C9H13O8Mg1-	0.89	1.56
273.1194	273.11941	-0.013	C11H21O6Mg1-	0.55	2.00
275.04115	275.04116	-0.032	C12H11O6Mg1-	0.50	1.00
275.0623	275.06229	0.061	C9H15O8Mg1-	0.89	1.78
275.07756	275.07754	0.062	C13H15O5Mg1-	0.38	1.23
275.09866	275.09867	-0.041	C10H19O7Mg1-	0.70	2.00
275.11388	275.11393	-0.182	C14H19O4Mg1-	0.29	1.43
277.02042	277.02042	0.005	C11H9O7Mg1-	0.64	0.91
277.05682	277.05681	0.05	C12H13O6Mg1-	0.50	1.17
277.0932	277.09319	0.014	C13H17O5Mg1-	0.38	1.38
277.12959	277.12958	0.059	C14H21O4Mg1-	0.29	1.57
279.03607	279.03607	-0.016	C11H11O7Mg1-	0.64	1.09
279.07248	279.07246	0.078	C12H15O6Mg1-	0.50	1.33
279.10884	279.10884	-0.017	C13H19O5Mg1-	0.38	1.54
279.14523	279.14523	0.02	C14H23O4Mg1-	0.29	1.71
281.05175	281.05172	0.102	C11H13O7Mg1-	0.64	1.27
281.08813	281.08811	0.09	C12H17O6Mg1-	0.50	1.50
281.1245	281.12449	0.026	C13H21O5Mg1-	0.38	1.69
281.16086	281.16088	-0.043	C14H25O4Mg1-	0.29	1.86
283.04624	283.04624	-0.022	C14H11O5Mg1-	0.36	0.86
283.06736	283.06737	-0.052	C11H15O7Mg1-	0.64	1.45
283.10376	283.10376	0.028	C12H19O6Mg1-	0.50	1.67
283.17654	283.17653	0.034	C14H27O4Mg1-	0.29	2.00
285.04664	285.04664	-0.001	C10H13O8Mg1-	0.80	1.40
285.08303	285.08302	0.029	C11H17O7Mg1-	0.64	1.64
285.09825	285.09828	-0.098	C15H17O4Mg1-	0.27	1.20
285.19219	285.19218	0.033	C14H29O4Mg1-	0.29	2.14
287.06231	287.06229	0.066	C10H15O8Mg1-	0.80	1.60
287.07756	287.07754	0.05	C14H15O5Mg1-	0.36	1.14
287.09867	287.09867	0.002	C11H19O7Mg1-	0.64	1.82
287.11388	287.11393	-0.179	C15H19O4Mg1-	0.27	1.33
287.13507	287.13506	0.037	C12H23O6Mg1-	0.50	2.00
287.17149	287.17144	0.16	C13H27O5Mg1-	0.38	2.15
289.04156	289.04155	0.037	C9H13O9Mg1-	1.00	1.56
289.05681	289.05681	0.03	C13H13O6Mg1-	0.46	1.08
289.0932	289.09319	0.016	C14H17O5Mg1-	0.36	1.29
289.1143	289.11432	-0.074	C11H21O7Mg1-	0.64	2.00
289.15076	289.15071	0.174	C12H25O6Mg1-	0.50	2.17

A.11 Mass list of significantly enriched compounds in thermal processed meteorites

291.03607	291.03607	0.01	C12H11O7Mg1-	0.58	1.00
291.07246	291.07246	0.021	C13H15O6Mg1-	0.46	1.23
291.10884	291.10884	0.009	C14H19O5Mg1-	0.36	1.43
291.14524	291.14523	0.037	C15H23O4Mg1-	0.27	1.60
292.91206	292.91206	0.014	C1H1O16Mg1-	16.00	2.00
293.05171	293.05172	-0.044	C12H13O7Mg1-	0.58	1.17
293.08811	293.08811	0.017	C13H17O6Mg1-	0.46	1.38
293.12451	293.12449	0.047	C14H21O5Mg1-	0.36	1.57
293.16089	293.16088	0.033	C15H25O4Mg1-	0.27	1.73
295.06739	295.06737	0.076	C12H15O7Mg1-	0.58	1.33
295.10375	295.10376	-0.006	C13H19O6Mg1-	0.46	1.54
295.14015	295.14014	0.028	C14H23O5Mg1-	0.36	1.71
295.17654	295.17653	0.058	C15H27O4Mg1-	0.27	1.87
297.08305	297.08302	0.099	C12H17O7Mg1-	0.58	1.50
297.11941	297.11941	0.014	C13H21O6Mg1-	0.46	1.69
299.06229	299.06229	0.019	C11H15O8Mg1-	0.73	1.45
299.09868	299.09867	0.037	C12H19O7Mg1-	0.58	1.67
301.07794	301.07794	0.02	C11H17O8Mg1-	0.73	1.64
301.09319	301.09319	0.009	C15H17O5Mg1-	0.33	1.20
301.1871	301.18709	0.023	C14H29O5Mg1-	0.36	2.14
303.05722	303.0572	0.065	C10H15O9Mg1-	0.90	1.60
303.07247	303.07246	0.045	C14H15O6Mg1-	0.43	1.14
303.09358	303.09359	-0.007	C11H19O8Mg1-	0.73	1.82
303.10884	303.10884	-0.004	C15H19O5Mg1-	0.33	1.33
305.05172	305.05172	0.008	C13H13O7Mg1-	0.54	1.08
305.08811	305.08811	-0.003	C14H17O6Mg1-	0.43	1.29
305.1245	305.12449	0.017	C15H21O5Mg1-	0.33	1.47
305.16088	305.16088	0.015	C16H25O4Mg1-	0.25	1.63
307.06736	307.06737	-0.048	C13H15O7Mg1-	0.54	1.23
307.10376	307.10376	0.009	C14H19O6Mg1-	0.43	1.43
307.14015	307.14014	0.044	C15H23O5Mg1-	0.33	1.60
307.17654	307.17653	0.049	C16H27O4Mg1-	0.25	1.75
309.08303	309.08302	0.032	C13H17O7Mg1-	0.54	1.38
309.11942	309.11941	0.057	C14H21O6Mg1-	0.43	1.57
309.1558	309.15579	0.012	C15H25O5Mg1-	0.33	1.73
309.19219	309.19218	0.031	C16H29O4Mg1-	0.25	1.88
311.09867	311.09867	-0.007	C13H19O7Mg1-	0.54	1.54
311.13506	311.13506	0.008	C14H23O6Mg1-	0.43	1.71
311.17143	311.17144	-0.021	C15H27O5Mg1-	0.33	1.87
311.20783	311.20783	0.026	C16H31O4Mg1-	0.25	2.00
313.11432	313.11432	0.009	C13H21O7Mg1-	0.54	1.69
313.12954	313.12958	-0.116	C17H21O4Mg1-	0.24	1.29
313.22348	313.22348	0.017	C16H33O4Mg1-	0.25	2.13
315.07247	315.07246	0.044	C15H15O6Mg1-	0.40	1.07
315.09361	315.09359	0.079	C12H19O8Mg1-	0.67	1.67
315.16636	315.16636	0.009	C14H27O6Mg1-	0.43	2.00
315.20276	315.20274	0.059	C15H31O5Mg1-	0.33	2.13
317.05173	317.05172	0.028	C14H13O7Mg1-	0.50	1.00
317.08808	317.08811	-0.078	C15H17O6Mg1-	0.40	1.20
317.16085	317.16088	-0.083	C17H25O4Mg1-	0.24	1.53
319031	319.03099	0.043	C13H11O8Mg1-	0.62	0.92
319.06736	319.06737	-0.043	C14H15O7Mg1-	0.50	1.14
319.10376	319.10376	0.002	C15H19O6Mg1-	0.40	1.33
319.14015	319.14014	0.028	C16H23O5Mg1-	0.31	1.50
319.17654	319.17653	0.058	C17H27O4Mg1-	0.24	1.65

A.11 Mass list of significantly enriched compounds in thermal processed meteorites

321.08301	321.08302	-0.041	C14H17O7Mg1-	0.50	1.29
321.11944	321.11941	0.103	C15H21O6Mg1-	0.40	1.47
321.1558	321.15579	0.033	C16H25O5Mg1-	0.31	1.63
321.19219	321.19218	0.038	C17H29O4Mg1-	0.24	1.76
323.13503	323.13506	-0.071	C15H23O6Mg1-	0.40	1.60
323.17145	323.17144	0.021	C16H27O5Mg1-	0.31	1.75
323.20783	323.20783	0.02	C17H31O4Mg1-	0.24	1.88
325.11431	325.11432	-0.045	C14H21O7Mg1-	0.50	1.57
325.15069	325.15071	-0.052	C15H25O6Mg1-	0.40	1.73
327.09357	327.09359	-0.041	C13H19O8Mg1-	0.62	1.54
327.10884	327.10884	0.002	C17H19O5Mg1-	0.29	1.18
327.12996	327.12997	-0.021	C14H23O7Mg1-	0.50	1.71
329.10921	329.10924	-0.071	C13H21O8Mg1-	0.62	1.69
329.14563	329.14562	0.022	C14H25O7Mg1-	0.50	1.86
329.16084	329.16088	-0.103	C18H25O4Mg1-	0.22	1.44
329.18199	329.18201	-0.057	C15H29O6Mg1-	0.40	2.00
329.21842	329.21839	0.076	C16H33O5Mg1-	0.31	2.13
331.0885	331.0885	-0.004	C12H19O9Mg1-	0.75	1.67
331.10375	331.10376	-0.034	C16H19O6Mg1-	0.38	1.25
331.16126	331.16127	-0.03	C14H27O7Mg1-	0.50	2.00
331.17652	331.17653	-0.013	C18H27O4Mg1-	0.22	1.56
333083	333.08302	-0.061	C15H17O7Mg1-	0.47	1.20
333.11941	333.11941	0.011	C16H21O6Mg1-	0.38	1.38
333.15579	333.15579	-0.008	C17H25O5Mg1-	0.29	1.53
333.19219	333.19218	0.048	C18H29O4Mg1-	0.22	1.67
335.09866	335.09867	-0.038	C15H19O7Mg1-	0.47	1.33
335.13507	335.13506	0.037	C16H23O6Mg1-	0.38	1.50
335.17144	335.17144	0.001	C17H27O5Mg1-	0.29	1.65
335.20783	335.20783	0.015	C18H31O4Mg1-	0.22	1.78
337.1143	337.11432	-0.066	C15H21O7Mg1-	0.47	1.47
337.1507	337.15071	-0.033	C16H25O6Mg1-	0.38	1.63
337.18708	337.18709	-0.035	C17H29O5Mg1-	0.29	1.76
339.11478	339.11472	0.188	C11H23O10Mg1-	0.91	2.18
339.12995	339.12997	-0.063	C15H23O7Mg1-	0.47	1.60
339.16636	339.16636	0.008	C16H27O6Mg1-	0.38	1.75
339.23913	339.23913	0.014	C18H35O4Mg1-	0.22	2.00
341.05172	341.05172	0.011	C16H13O7Mg1-	0.44	0.88
341.21839	341.21839	-0.011	C17H33O5Mg1-	0.29	2.00
341.25477	341.25478	-0.022	C18H37O4Mg1-	0.22	2.11
343.12491	343.12489	0.06	C14H23O8Mg1-	0.57	1.71
343.14015	343.14014	0.013	C18H23O5Mg1-	0.28	1.33
343.17651	343.17653	-0.063	C19H27O4Mg1-	0.21	1.47
343.19766	343.19766	0.01	C16H31O6Mg1-	0.38	2.00
345.06777	345.06777	0.016	C12H17O10Mg1-	0.83	1.50
345.1042	345.10415	0.141	C13H21O9Mg1-	0.69	1.69
345.11941	345.11941	0.005	C17H21O6Mg1-	0.35	1.29
345.15581	345.15579	0.041	C18H25O5Mg1-	0.28	1.44
345.19212	345.19218	-0.16	C19H29O4Mg1-	0.21	1.58
347.09867	347.09867	0.006	C16H19O7Mg1-	0.44	1.25
347.13505	347.13506	-0.005	C17H23O6Mg1-	0.35	1.41
347.17144	347.17144	0.004	C18H27O5Mg1-	0.28	1.56
347.20779	347.20783	-0.118	C19H31O4Mg1-	0.21	1.68
349.07794	349.07794	-0.004	C15H17O8Mg1-	0.53	1.20
349.11429	349.11432	-0.098	C16H21O7Mg1-	0.44	1.38
349.1507	349.15071	-0.028	C17H25O6Mg1-	0.35	1.53

A.11 Mass list of significantly enriched compounds in thermal processed meteorites

349.18709	349.18709	0.004	C18H29O5Mg1-	0.28	1.67
349.22349	349.22348	0.031	C19H33O4Mg1-	0.21	1.79
351.09357	351.09359	-0.032	C15H19O8Mg1-	0.53	1.33
351.12995	351.12997	-0.047	C16H23O7Mg1-	0.44	1.50
351.15112	351.1511	0.039	C13H27O9Mg1-	0.69	2.15
351.16636	351.16636	0.005	C17H27O6Mg1-	0.35	1.65
351.20275	351.20274	0.03	C18H31O5Mg1-	0.28	1.78
351.23915	351.23913	0.056	C19H35O4Mg1-	0.21	1.89
353.10926	353.10924	0.073	C15H21O8Mg1-	0.53	1.47
353.14563	353.14562	0.038	C16H25O7Mg1-	0.44	1.63
353.18202	353.18201	0.043	C17H29O6Mg1-	0.35	1.76
353.25477	353.25478	-0.012	C19H37O4Mg1-	0.21	2.00
355.14601	355.14602	-0.018	C12H27O10Mg1-	0.83	2.33
355.16128	355.16127	0.025	C16H27O7Mg1-	0.44	1.75
355.27043	355.27043	0.016	C19H39O4Mg1-	0.21	2.11
357.14056	357.14054	0.066	C15H25O8Mg1-	0.53	1.73
357.15576	357.15579	-0.076	C19H25O5Mg1-	0.26	1.37
357.21329	357.21331	-0.051	C17H33O6Mg1-	0.35	2.00
359.13505	359.13506	-0.009	C18H23O6Mg1-	0.33	1.33
361.07792	361.07794	-0.031	C16H17O8Mg1-	0.50	1.13
361.15072	361.15071	0.032	C18H25O6Mg1-	0.33	1.44
361.18708	361.18709	-0.036	C19H29O5Mg1-	0.26	1.58
361.22347	361.22348	-0.007	C20H33O4Mg1-	0.20	1.70
363.07835	363.07833	0.041	C12H19O11Mg1-	0.92	1.67
363.09358	363.09359	-0.028	C16H19O8Mg1-	0.50	1.25
363.12997	363.12997	-0.009	C17H23O7Mg1-	0.41	1.41
363.16635	363.16636	-0.013	C18H27O6Mg1-	0.33	1.56
363.20273	363.20274	-0.043	C19H31O5Mg1-	0.26	1.68
363.23914	363.23913	0.042	C20H35O4Mg1-	0.20	1.80
365.07288	365.07285	0.092	C15H17O9Mg1-	0.60	1.20
365.10922	365.10924	-0.045	C16H21O8Mg1-	0.50	1.38
365.14562	365.14562	-0.01	C17H25O7Mg1-	0.41	1.53
365.18201	365.18201	-0.001	C18H29O6Mg1-	0.33	1.67
365.21839	365.21839	0.001	C19H33O5Mg1-	0.26	1.79
365.25478	365.25478	0.016	C20H37O4Mg1-	0.20	1.90
367.12487	367.12489	-0.048	C16H23O8Mg1-	0.50	1.50
367.16127	367.16127	0	C17H27O7Mg1-	0.41	1.65
367.19766	367.19766	0.008	C18H31O6Mg1-	0.33	1.78
367.27045	367.27043	0.074	C20H39O4Mg1-	0.20	2.00
369.10414	369.10415	-0.031	C15H21O9Mg1-	0.60	1.47
369.12527	369.12528	-0.024	C12H25O11Mg1-	0.92	2.17
369.14052	369.14054	-0.057	C16H25O8Mg1-	0.50	1.63
369.17692	369.17692	0.008	C17H29O7Mg1-	0.41	1.76
371.1198	371.1198	-0.017	C15H23O9Mg1-	0.60	1.60
371.13506	371.13506	0.01	C19H23O6Mg1-	0.32	1.26
371.17143	371.17144	-0.031	C20H27O5Mg1-	0.25	1.40
371.22899	371.22896	0.077	C18H35O6Mg1-	0.33	2.00
373.12015	373.1202	-0.124	C11H25O12Mg1-	1.09	2.36
373.13547	373.13545	0.056	C15H25O9Mg1-	0.60	1.73
373.15071	373.15071	-0.004	C19H25O6Mg1-	0.32	1.37
373.18708	373.18709	-0.023	C20H29O5Mg1-	0.25	1.50
373.2234	373.22348	-0.2	C21H33O4Mg1-	0.19	1.62
375.1664	375.16636	0.107	C19H27O6Mg1-	0.32	1.47
375.20273	375.20274	-0.04	C20H31O5Mg1-	0.25	1.60
375.23914	375.23913	0.033	C21H35O4Mg1-	0.19	1.71

A.11 Mass list of significantly enriched compounds in thermal processed meteorites

377.00598	377.00596	0.063	C7H13O16Mg1-	2.29	2.00
377.07872	377.07873	-0.022	C9H21O14Mg1-	1.56	2.44
377.10923	377.10924	-0.007	C17H21O8Mg1-	0.47	1.29
377.14561	377.14562	-0.029	C18H25O7Mg1-	0.39	1.44
377.18201	377.18201	0.02	C19H29O6Mg1-	0.32	1.58
377.21839	377.21839	0.009	C20H33O5Mg1-	0.25	1.70
377.25477	377.25478	-0.014	C21H37O4Mg1-	0.19	1.81
379.12485	379.12489	-0.088	C17H23O8Mg1-	0.47	1.41
379.1613	379.16127	0.063	C18H27O7Mg1-	0.39	1.56
379.17653	379.17653	0.003	C22H27O4Mg1-	0.18	1.27
379.19766	379.19766	0.017	C19H31O6Mg1-	0.32	1.68
379.27045	379.27043	0.062	C21H39O4Mg1-	0.19	1.90
381.04662	381.04664	-0.037	C18H13O8Mg1-	0.44	0.78
381.14055	381.14054	0.029	C17H25O8Mg1-	0.47	1.53
381.17691	381.17692	-0.018	C18H29O7Mg1-	0.39	1.67
381.21331	381.21331	0	C19H33O6Mg1-	0.32	1.79
381.28609	381.28608	0.024	C21H41O4Mg1-	0.19	2.00
383.06228	383.06229	-0.016	C18H15O8Mg1-	0.44	0.89
383.15615	383.15619	-0.087	C17H27O8Mg1-	0.47	1.65
383.19258	383.19257	0.021	C18H31O7Mg1-	0.39	1.78
383.30176	383.30173	0.08	C21H43O4Mg1-	0.19	2.10
385.17184	385.17184	0.005	C17H29O8Mg1-	0.47	1.76
385.18708	385.18709	-0.019	C21H29O5Mg1-	0.24	1.43
385.22345	385.22348	-0.062	C22H33O4Mg1-	0.18	1.55
385.2446	385.24461	-0.015	C19H37O6Mg1-	0.32	2.00
387.1511	387.1511	0.009	C16H27O9Mg1-	0.56	1.75
387.16637	387.16636	0.037	C20H27O6Mg1-	0.30	1.40
387.20274	387.20274	0.006	C21H31O5Mg1-	0.24	1.52
387.22386	387.22387	-0.043	C18H35O7Mg1-	0.39	2.00
389.14562	389.14562	-0.004	C19H25O7Mg1-	0.37	1.37
389.18204	389.18201	0.093	C20H29O6Mg1-	0.30	1.50
389.21837	389.21839	-0.062	C21H33O5Mg1-	0.24	1.62
389.25477	389.25478	-0.029	C22H37O4Mg1-	0.18	1.73
391.1096	391.10963	-0.067	C14H23O11Mg1-	0.79	1.71
391.12488	391.12489	-0.011	C18H23O8Mg1-	0.44	1.33
391.16124	391.16127	-0.084	C19H27O7Mg1-	0.37	1.47
391.19764	391.19766	-0.042	C20H31O6Mg1-	0.30	1.60
391.23402	391.23404	-0.063	C21H35O5Mg1-	0.24	1.71
391.27039	391.27043	-0.089	C22H39O4Mg1-	0.18	1.82
393.10412	393.10415	-0.088	C17H21O9Mg1-	0.53	1.29
393.14052	393.14054	-0.045	C18H25O8Mg1-	0.44	1.44
393.17691	393.17692	-0.02	C19H29O7Mg1-	0.37	1.58
393.21331	393.21331	0.001	C20H33O6Mg1-	0.30	1.70
393.24968	393.24969	-0.024	C21H37O5Mg1-	0.24	1.81
393.28609	393.28608	0.021	C22H41O4Mg1-	0.18	1.91
395.1562	395.15619	0.034	C18H27O8Mg1-	0.44	1.56
395.19257	395.19257	-0.014	C19H31O7Mg1-	0.37	1.68
395.22896	395.22896	0.004	C20H35O6Mg1-	0.30	1.80
395.30175	395.30173	0.051	C22H43O4Mg1-	0.18	2.00
397.13547	397.13545	0.038	C17H25O9Mg1-	0.53	1.53
397.17183	397.17184	-0.006	C18H29O8Mg1-	0.44	1.67
397.20824	397.20822	0.036	C19H33O7Mg1-	0.37	1.79
397.3174	397.31738	0.048	C22H45O4Mg1-	0.18	2.09
399.0995	399.09946	0.097	C12H23O13Mg1-	1.08	2.00
399.15109	399.1511	-0.029	C17H27O9Mg1-	0.53	1.65

A.11 Mass list of significantly enriched compounds in thermal processed meteorites

399.20275	399.20274	0.032	C22H31O5Mg1-	0.23	1.45
399.23918	399.23913	0.127	C23H35O4Mg1-	0.17	1.57
401.16671	401.16675	-0.112	C17H29O9Mg1-	0.53	1.76
401.21838	401.21839	-0.031	C22H33O5Mg1-	0.23	1.55
403.14603	403.14602	0.025	C16H27O10Mg1-	0.63	1.75
403.23403	403.23404	-0.03	C22H35O5Mg1-	0.23	1.64
403.27038	403.27043	-0.116	C23H39O4Mg1-	0.17	1.74
405.17692	405.17692	-0.006	C20H29O7Mg1-	0.35	1.50
405.2133	405.21331	-0.019	C21H33O6Mg1-	0.29	1.62
405.2497	405.24969	0.01	C22H37O5Mg1-	0.23	1.73
405.27087	405.27082	0.132	C19H41O7Mg1-	0.37	2.21
405286	405.28608	-0.179	C23H41O4Mg1-	0.17	1.83
407.14097	407.14093	0.095	C15H27O11Mg1-	0.73	1.87
407.19259	407.19257	0.035	C20H31O7Mg1-	0.35	1.60
407.22894	407.22896	-0.029	C21H35O6Mg1-	0.29	1.71
407.26535	407.26534	0.018	C22H39O5Mg1-	0.23	1.82
407.30173	407.30173	0.001	C23H43O4Mg1-	0.17	1.91
409.07795	409.07794	0.027	C20H17O8Mg1-	0.40	0.90
409.08385	409.08381	0.085	C13H21O13Mg1-	1.00	1.69
409.13542	409.13545	-0.089	C18H25O9Mg1-	0.50	1.44
409.17183	409.17184	-0.012	C19H29O8Mg1-	0.42	1.58
409.20822	409.20822	-0.001	C20H33O7Mg1-	0.35	1.70
409281	409.28099	0.031	C22H41O5Mg1-	0.23	1.91
409.31742	409.31738	0.101	C23H45O4Mg1-	0.17	2.00
411.09358	411.09359	-0.023	C20H19O8Mg1-	0.40	1.00
411.15111	411.1511	0.017	C18H27O9Mg1-	0.50	1.56
411.1875	411.18749	0.021	C19H31O8Mg1-	0.42	1.68
411.22387	411.22387	-0.012	C20H35O7Mg1-	0.35	1.80
411.33304	411.33303	0.034	C23H47O4Mg1-	0.17	2.09
413.20315	413.20314	0.02	C19H33O8Mg1-	0.42	1.79
413.21838	413.21839	-0.018	C23H33O5Mg1-	0.22	1.48
413.27591	413.27591	0.008	C21H41O6Mg1-	0.29	2.00
415.18244	415.1824	0.082	C18H31O9Mg1-	0.50	1.78
415.19767	415.19766	0.022	C22H31O6Mg1-	0.27	1.45
415.23403	415.23404	-0.032	C23H35O5Mg1-	0.22	1.57
415.25515	415.25517	-0.052	C20H39O7Mg1-	0.35	2.00
417.16166	417.16167	-0.016	C17H29O10Mg1-	0.59	1.76
417.19805	417.19805	-0.008	C18H33O9Mg1-	0.50	1.89
417.24969	417.24969	0.002	C23H37O5Mg1-	0.22	1.65
417.28607	417.28608	-0.015	C24H41O4Mg1-	0.17	1.75
419.19256	419.19257	-0.022	C21H31O7Mg1-	0.33	1.52
419.26533	419.26534	-0.036	C23H39O5Mg1-	0.22	1.74
421.17186	421.17184	0.062	C20H29O8Mg1-	0.40	1.50
421.24463	421.24461	0.052	C22H37O6Mg1-	0.27	1.73
421.31738	421.31738	0	C24H45O4Mg1-	0.17	1.92
423.09947	423.09946	0.02	C14H23O13Mg1-	0.93	1.71
423.13588	423.13585	0.091	C15H27O12Mg1-	0.80	1.87
423.18747	423.18749	-0.044	C20H31O8Mg1-	0.40	1.60
423.22388	423.22387	0.031	C21H35O7Mg1-	0.33	1.71
423.26027	423.26026	0.021	C22H39O6Mg1-	0.27	1.82
423.33308	423.33303	0.128	C24H47O4Mg1-	0.17	2.00
425.14563	425.14562	0.012	C22H25O7Mg1-	0.32	1.18
425.18202	425.18201	0.04	C23H29O6Mg1-	0.26	1.30
425.20315	425.20314	0.036	C20H33O8Mg1-	0.40	1.70
425.21837	425.21839	-0.062	C24H33O5Mg1-	0.21	1.42

A.11 Mass list of significantly enriched compounds in thermal processed meteorites

425.34871	425.34868	0.067	C24H49O4Mg1-	0.17	2.08
427.05798	427.05799	-0.015	C12H19O15Mg1-	1.25	1.67
427.18241	427.1824	0.014	C19H31O9Mg1-	0.47	1.68
427.19772	427.19766	0.149	C23H31O6Mg1-	0.26	1.39
427.2188	427.21879	0.037	C20H35O8Mg1-	0.40	1.80
427.23402	427.23404	-0.057	C24H35O5Mg1-	0.21	1.50
427.29155	427.29156	-0.006	C22H43O6Mg1-	0.27	2.00
429.16162	429.16167	-0.108	C18H29O10Mg1-	0.56	1.67
429.2133	429.21331	-0.015	C23H33O6Mg1-	0.26	1.48
429.2497	429.24969	0.014	C24H37O5Mg1-	0.21	1.58
429.27083	429.27082	0.015	C21H41O7Mg1-	0.33	2.00
431.14092	431.14093	-0.027	C17H27O11Mg1-	0.65	1.65
431.26534	431.26534	-0.012	C24H39O5Mg1-	0.21	1.67
433.19296	433.19297	-0.023	C18H33O10Mg1-	0.56	1.89
433281	433.28099	0.021	C24H41O5Mg1-	0.21	1.75
433.31731	433.31738	-0.146	C25H45O4Mg1-	0.16	1.84
435.1511	435.1511	-0.013	C20H27O9Mg1-	0.45	1.40
435.18752	435.18749	0.065	C21H31O8Mg1-	0.38	1.52
435.22386	435.22387	-0.02	C22H35O7Mg1-	0.32	1.64
435.26024	435.26026	-0.044	C23H39O6Mg1-	0.26	1.74
435.29663	435.29664	-0.021	C24H43O5Mg1-	0.21	1.83
435.33303	435.33303	0.017	C25H47O4Mg1-	0.16	1.92
437.20315	437.20314	0.022	C21H33O8Mg1-	0.38	1.62
437.23951	437.23952	-0.028	C22H37O7Mg1-	0.32	1.73
437.2759	437.27591	-0.004	C23H41O6Mg1-	0.26	1.83
437.3487	437.34868	0.045	C25H49O4Mg1-	0.16	2.00
438.94882	438.94884	-0.047	C10H7O18Mg1-	1.80	0.80
439.1824	439.1824	-0.006	C20H31O9Mg1-	0.45	1.60
439.2552	439.25517	0.065	C22H39O7Mg1-	0.32	1.82
439.36437	439.36433	0.098	C25H51O4Mg1-	0.16	2.08
441.19805	441.19805	-0.004	C20H33O9Mg1-	0.45	1.70
441.23447	441.23444	0.07	C21H37O8Mg1-	0.38	1.81
441.27084	441.27082	0.043	C22H41O7Mg1-	0.32	1.91
441.30719	441.30721	-0.032	C23H45O6Mg1-	0.26	2.00
443.21368	443.2137	-0.053	C20H35O9Mg1-	0.45	1.80
443.22897	443.22896	0.021	C24H35O6Mg1-	0.25	1.50
443.26533	443.26534	-0.016	C25H39O5Mg1-	0.20	1.60
445.15064	445.15071	-0.155	C25H25O6Mg1-	0.24	1.04
447.15107	447.1511	-0.07	C21H27O9Mg1-	0.43	1.33
447.29663	447.29664	-0.025	C25H43O5Mg1-	0.20	1.76
447.33294	447.33303	-0.19	C26H47O4Mg1-	0.15	1.85
449.06347	449.06347	-0.003	C11H21O17Mg1-	1.55	2.00
449.16676	449.16675	0.019	C21H29O9Mg1-	0.43	1.43
449.18791	449.18788	0.052	C18H33O11Mg1-	0.61	1.89
449.23953	449.23952	0.017	C23H37O7Mg1-	0.30	1.65
449.2548	449.25478	0.059	C27H37O4Mg1-	0.15	1.41
449.27593	449.27591	0.051	C24H41O6Mg1-	0.25	1.75
449.3486	449.34868	-0.168	C26H49O4Mg1-	0.15	1.92
451.05797	451.05799	-0.036	C14H19O15Mg1-	1.07	1.43
451.25517	451.25517	0.003	C23H39O7Mg1-	0.30	1.74
451.29158	451.29156	0.049	C24H43O6Mg1-	0.25	1.83
451.36434	451.36433	0.029	C26H51O4Mg1-	0.15	2.00
453.11005	453.11003	0.041	C15H25O14Mg1-	0.93	1.73
453.14056	453.14054	0.063	C23H25O8Mg1-	0.35	1.13
453.19806	453.19805	0.019	C21H33O9Mg1-	0.43	1.62

A.11 Mass list of significantly enriched compounds in thermal processed meteorites

453.23448	453.23444	0.086	C22H37O8Mg1-	0.36	1.73
453.38002	453.37998	0.106	C26H53O4Mg1-	0.15	2.08
455.26531	455.26534	-0.062	C26H39O5Mg1-	0.19	1.54
455.30167	455.30173	-0.117	C27H43O4Mg1-	0.15	1.63
455.32286	455.32286	0.016	C24H47O6Mg1-	0.25	2.00
457.15655	457.15658	-0.069	C19H29O11Mg1-	0.58	1.58
457.19294	457.19297	-0.051	C20H33O10Mg1-	0.50	1.70
457.24462	457.24461	0.019	C25H37O6Mg1-	0.24	1.52
457.28096	457.28099	-0.066	C26H41O5Mg1-	0.19	1.62
461.31229	461.31229	0.002	C26H45O5Mg1-	0.19	1.77
463.16124	463.16127	-0.061	C25H27O7Mg1-	0.28	1.12
463.25519	463.25517	0.048	C24H39O7Mg1-	0.29	1.67
463.29157	463.29156	0.035	C25H43O6Mg1-	0.24	1.76
463.32795	463.32794	0.014	C26H47O5Mg1-	0.19	1.85
463.36437	463.36433	0.084	C27H51O4Mg1-	0.15	1.93
464.89768	464.89759	0.191	C3H5O25Mg1-	8.33	2.00
465.18277	465.1828	-0.052	C18H33O12Mg1-	0.67	1.89
465.23447	465.23444	0.081	C23H37O8Mg1-	0.35	1.65
465.27085	465.27082	0.066	C24H41O7Mg1-	0.29	1.75
465.28606	465.28608	-0.033	C28H41O4Mg1-	0.14	1.50
465.34362	465.34359	0.058	C26H49O5Mg1-	0.19	1.92
465.38002	465.37998	0.1	C27H53O4Mg1-	0.15	2.00
467.14096	467.14093	0.05	C20H27O11Mg1-	0.55	1.40
467.22896	467.22896	0.014	C26H35O6Mg1-	0.23	1.38
467.25007	467.25009	-0.028	C23H39O8Mg1-	0.35	1.74
467.2865	467.28647	0.054	C24H43O7Mg1-	0.29	1.83
467.39567	467.39563	0.083	C27H55O4Mg1-	0.15	2.07
469.20828	469.20822	0.125	C25H33O7Mg1-	0.28	1.36
469.2294	469.22935	0.103	C22H37O9Mg1-	0.41	1.73
469.26578	469.26574	0.094	C23H41O8Mg1-	0.35	1.83
469.30212	469.30212	-0.004	C24H45O7Mg1-	0.29	1.92
469.33853	469.33851	0.044	C25H49O6Mg1-	0.24	2.00
470.97508	470.97505	0.061	C11H11O19Mg1-	1.73	1.09
471.20864	471.20862	0.039	C21H35O10Mg1-	0.48	1.71
471.22387	471.22387	0.002	C25H35O7Mg1-	0.28	1.44
471.24502	471.245	0.033	C22H39O9Mg1-	0.41	1.82
471.26026	471.26026	0.004	C26H39O6Mg1-	0.23	1.54
471.29661	471.29664	-0.067	C27H43O5Mg1-	0.19	1.63
473.3123	473.31229	0.024	C27H45O5Mg1-	0.19	1.70
473.34867	473.34868	-0.021	C28H49O4Mg1-	0.14	1.79
475.17658	475.17653	0.113	C30H27O4Mg1-	0.13	0.93
475.29158	475.29156	0.049	C26H43O6Mg1-	0.23	1.69
475.31264	475.31269	-0.098	C23H47O8Mg1-	0.35	2.09
475.32794	475.32794	-0.008	C27H47O5Mg1-	0.19	1.78
475.36431	475.36433	-0.041	C28H51O4Mg1-	0.14	1.86
477.18284	477.1828	0.091	C19H33O12Mg1-	0.63	1.79
477.21326	477.21331	-0.108	C27H33O6Mg1-	0.22	1.26
477.21911	477.21918	-0.161	C20H37O11Mg1-	0.55	1.90
477.27083	477.27082	0.007	C25H41O7Mg1-	0.28	1.68
477.30722	477.30721	0.022	C26H45O6Mg1-	0.23	1.77
477.37992	477.37998	-0.125	C28H53O4Mg1-	0.14	1.93
479.14088	479.14093	-0.107	C21H27O11Mg1-	0.52	1.33
479.16204	479.16206	-0.034	C18H31O13Mg1-	0.72	1.78
479.23492	479.23483	0.174	C20H39O11Mg1-	0.55	2.00
479.26533	479.26534	-0.024	C28H39O5Mg1-	0.18	1.43

A.11 Mass list of significantly enriched compounds in thermal processed meteorites

479.28647	479.28647	0.003	C25H43O7Mg1-	0.28	1.76
479.35929	479.35924	0.11	C27H51O5Mg1-	0.19	1.93
479.39566	479.39563	0.073	C28H55O4Mg1-	0.14	2.00
480.92891	480.92889	0.039	C4H9O25Mg1-	6.25	2.50
481.09905	481.09907	-0.034	C23H21O10Mg1-	0.43	0.96
481.22935	481.22935	0.003	C23H37O9Mg1-	0.39	1.65
481.26573	481.26574	-0.004	C24H41O8Mg1-	0.33	1.75
481.30214	481.30212	0.038	C25H45O7Mg1-	0.28	1.84
481.41135	481.41128	0.148	C28H57O4Mg1-	0.14	2.07
483.2814	483.28139	0.035	C24H43O8Mg1-	0.33	1.83
483.29659	483.29664	-0.111	C28H43O5Mg1-	0.18	1.57
483.35416	483.35416	0.006	C26H51O6Mg1-	0.23	2.00
485.16674	485.16675	-0.029	C24H29O9Mg1-	0.38	1.25
485.22422	485.22427	-0.086	C22H37O10Mg1-	0.45	1.73
485.23951	485.23952	-0.02	C26H37O7Mg1-	0.27	1.46
485.26067	485.26065	0.038	C23H41O9Mg1-	0.39	1.83
486.93352	486.93358	-0.115	C10H7O21Mg1-	2.10	0.80
487.20356	487.20353	0.058	C21H35O11Mg1-	0.52	1.71
487.21883	487.21879	0.096	C25H35O8Mg1-	0.32	1.44
487.29156	487.29156	0.017	C27H43O6Mg1-	0.22	1.63
487.32794	487.32794	-0.001	C28H47O5Mg1-	0.18	1.71
487.36433	487.36433	0.002	C29H51O4Mg1-	0.14	1.79
489.23444	489.23444	0.007	C25H37O8Mg1-	0.32	1.52
489.34361	489.34359	0.039	C28H49O5Mg1-	0.18	1.79
491.2501	491.25009	0.027	C25H39O8Mg1-	0.32	1.60
491.28647	491.28647	-0.001	C26H43O7Mg1-	0.27	1.69
491.32287	491.32286	0.024	C27H47O6Mg1-	0.22	1.78
491.35924	491.35924	0.002	C28H51O5Mg1-	0.18	1.86
491.39556	491.39563	-0.126	C29H55O4Mg1-	0.14	1.93
493.26572	493.26574	-0.038	C25H41O8Mg1-	0.32	1.68
493.28105	493.28099	0.113	C29H41O5Mg1-	0.17	1.45
493.30215	493.30212	0.053	C26H45O7Mg1-	0.27	1.77
493.37491	493.37489	0.037	C28H53O5Mg1-	0.18	1.93
493.41128	493.41128	0.006	C29H57O4Mg1-	0.14	2.00
495.13579	495.13585	-0.114	C21H27O12Mg1-	0.57	1.33
495.24497	495.245	-0.073	C24H39O9Mg1-	0.38	1.67
495.26023	495.26026	-0.054	C28H39O6Mg1-	0.21	1.43
495.28135	495.28139	-0.076	C25H43O8Mg1-	0.32	1.76
495.31781	495.31777	0.071	C26H47O7Mg1-	0.27	1.85
495.42691	495.42693	-0.026	C29H59O4Mg1-	0.14	2.07
497.16675	497.16675	-0.003	C25H29O9Mg1-	0.36	1.20
497.20311	497.20314	-0.053	C26H33O8Mg1-	0.31	1.31
497.27584	497.27591	-0.13	C28H41O6Mg1-	0.21	1.50
497.29706	497.29704	0.047	C25H45O8Mg1-	0.32	1.84
497.33345	497.33342	0.057	C26H49O7Mg1-	0.27	1.92
497.36986	497.36981	0.107	C27H53O6Mg1-	0.22	2.00
499.23986	499.23992	-0.11	C23H39O10Mg1-	0.43	1.74
499.2552	499.25517	0.052	C27H39O7Mg1-	0.26	1.48
499.32786	499.32794	-0.158	C29H47O5Mg1-	0.17	1.66
501.23448	501.23444	0.082	C26H37O8Mg1-	0.31	1.46
501.25562	501.25557	0.106	C23H41O10Mg1-	0.43	1.83
501.34357	501.34359	-0.041	C29H49O5Mg1-	0.17	1.72
501.37991	501.37998	-0.142	C30H53O4Mg1-	0.13	1.80
503.21375	503.2137	0.096	C25H35O9Mg1-	0.36	1.44
503.25011	503.25009	0.046	C26H39O8Mg1-	0.31	1.54

A.11 Mass list of significantly enriched compounds in thermal processed meteorites

503.28649	503.28647	0.026	C27H43O7Mg1-	0.26	1.63
503.32283	503.32286	-0.058	C28H47O6Mg1-	0.21	1.71
503.35926	503.35924	0.033	C29H51O5Mg1-	0.17	1.79
503.39569	503.39563	0.117	C30H55O4Mg1-	0.13	1.87
505.19292	505.19297	-0.102	C24H33O10Mg1-	0.42	1.42
505.30212	505.30212	0	C27H45O7Mg1-	0.26	1.70
505.37491	505.37489	0.034	C29H53O5Mg1-	0.17	1.86
505.41124	505.41128	-0.081	C30H57O4Mg1-	0.13	1.93
507.1418	507.14172	0.148	C15H31O17Mg1-	1.13	2.13
507.17226	507.17223	0.063	C23H31O11Mg1-	0.48	1.39
507.26024	507.26026	-0.033	C29H39O6Mg1-	0.21	1.38
507.28136	507.28139	-0.058	C26H43O8Mg1-	0.31	1.69
507.333	507.33303	-0.053	C31H47O4Mg1-	0.13	1.55
507.39054	507.39054	0.005	C29H55O5Mg1-	0.17	1.93
507.42695	507.42693	0.05	C30H59O4Mg1-	0.13	2.00
509.2759	509.27591	-0.013	C29H41O6Mg1-	0.21	1.45
509.29699	509.29704	-0.095	C26H45O8Mg1-	0.31	1.77
509.33341	509.33342	-0.018	C27H49O7Mg1-	0.26	1.85
509.4062	509.40619	0.014	C29H57O5Mg1-	0.17	2.00
509.44261	509.44258	0.075	C30H61O4Mg1-	0.13	2.07
511.27639	511.2763	0.182	C25H43O9Mg1-	0.36	1.76
511.3127	511.31269	0.019	C26H47O8Mg1-	0.31	1.85
511.3491	511.34907	0.048	C27H51O7Mg1-	0.26	1.93
513.25554	513.25557	-0.052	C24H41O10Mg1-	0.42	1.75
513.27084	513.27082	0.041	C28H41O7Mg1-	0.25	1.50
514.96489	514.96488	0.027	C12H11O21Mg1-	1.75	1.00
515.21367	515.2137	-0.061	C26H35O9Mg1-	0.35	1.38
515.28649	515.28647	0.031	C28H43O7Mg1-	0.25	1.57
515.32287	515.32286	0.029	C29H47O6Mg1-	0.21	1.66
515.35921	515.35924	-0.06	C30H51O5Mg1-	0.17	1.73
515.39562	515.39563	-0.01	C31H55O4Mg1-	0.13	1.81
517.3021	517.30212	-0.042	C28H45O7Mg1-	0.25	1.64
517.31737	517.31738	-0.003	C32H45O4Mg1-	0.13	1.44
517.33851	517.33851	0.003	C29H49O6Mg1-	0.21	1.72
517.37492	517.37489	0.05	C30H53O5Mg1-	0.17	1.80
517.41126	517.41128	-0.033	C31H57O4Mg1-	0.13	1.87
519.20862	519.20862	0.016	C25H35O10Mg1-	0.40	1.44
519.31777	519.31777	-0.003	C28H47O7Mg1-	0.25	1.71
519.33298	519.33303	-0.09	C32H47O4Mg1-	0.13	1.50
519.35416	519.35416	0.015	C29H51O6Mg1-	0.21	1.79
519.39057	519.39054	0.058	C30H55O5Mg1-	0.17	1.87
519.42696	519.42693	0.059	C31H59O4Mg1-	0.13	1.94
520.87221	520.87217	0.094	C1H5O30Mg1-	30.00	6.00
521.1879	521.18788	0.035	C24H33O11Mg1-	0.46	1.42
521.24531	521.2454	-0.166	C22H41O12Mg1-	0.55	1.91
521.29701	521.29704	-0.042	C27H45O8Mg1-	0.30	1.70
521.33346	521.33342	0.064	C28H49O7Mg1-	0.25	1.79
521.44262	521.44258	0.076	C31H61O4Mg1-	0.13	2.00
523.12492	523.12489	0.069	C29H23O8Mg1-	0.28	0.83
523.31267	523.31269	-0.024	C27H47O8Mg1-	0.30	1.78
523.32793	523.32794	-0.027	C31H47O5Mg1-	0.16	1.55
523.34905	523.34907	-0.039	C28H51O7Mg1-	0.25	1.86
523.42186	523.42184	0.034	C30H59O5Mg1-	0.17	2.00
523.45827	523.45823	0.082	C31H63O4Mg1-	0.13	2.06
525.13118	525.13116	0.05	C18H29O16Mg1-	0.89	1.67

A.11 Mass list of significantly enriched compounds in thermal processed meteorites

525.27082	525.27082	-0.003	C29H41O7Mg1-	0.24	1.45
525.29195	525.29195	-0.009	C26H45O9Mg1-	0.35	1.77
525.30723	525.30721	0.054	C30H45O6Mg1-	0.20	1.53
525.32837	525.32834	0.069	C27H49O8Mg1-	0.30	1.85
525.36472	525.36472	0.003	C28H53O7Mg1-	0.25	1.93
527.13148	527.13155	-0.136	C14H31O19Mg1-	1.36	2.29
527.1773	527.17732	-0.031	C26H31O10Mg1-	0.38	1.23
527.25005	527.25009	-0.07	C28H39O8Mg1-	0.29	1.43
527.28642	527.28647	-0.098	C29H43O7Mg1-	0.24	1.52
527.3228	527.32286	-0.11	C30H47O6Mg1-	0.20	1.60
527.35914	527.35924	-0.195	C31H51O5Mg1-	0.16	1.68
527.39557	527.39563	-0.105	C32H55O4Mg1-	0.13	1.75
529.03808	529.03805	0.057	C11H21O22Mg1-	2.00	2.00
529.30217	529.30212	0.085	C29H45O7Mg1-	0.24	1.59
529.3385	529.33851	-0.017	C30H49O6Mg1-	0.20	1.67
529.37489	529.37489	-0.007	C31H53O5Mg1-	0.16	1.74
531.31776	531.31777	-0.014	C29H47O7Mg1-	0.24	1.66
531.39052	531.39054	-0.033	C31H55O5Mg1-	0.16	1.81
531.42685	531.42693	-0.145	C32H59O4Mg1-	0.13	1.88
532.93904	532.93906	-0.03	C11H9O23Mg1-	2.09	0.91
533.29705	533.29704	0.025	C28H45O8Mg1-	0.29	1.64
533.33346	533.33342	0.065	C29H49O7Mg1-	0.24	1.72
533.36985	533.36981	0.081	C30H53O6Mg1-	0.20	1.80
533.40621	533.40619	0.039	C31H57O5Mg1-	0.16	1.87
533.44262	533.44258	0.081	C32H61O4Mg1-	0.13	1.94
535.17299	535.17302	-0.059	C17H35O17Mg1-	1.00	2.12
535.2036	535.20353	0.128	C25H35O11Mg1-	0.44	1.44
535.27627	535.2763	-0.059	C27H43O9Mg1-	0.33	1.63
535.32787	535.32794	-0.134	C32H47O5Mg1-	0.16	1.50
535.34912	535.34907	0.097	C29H51O7Mg1-	0.24	1.79
535.38549	535.38546	0.058	C30H55O6Mg1-	0.20	1.87
535.42187	535.42184	0.044	C31H59O5Mg1-	0.16	1.94
535.45826	535.45823	0.061	C32H63O4Mg1-	0.13	2.00
537.32835	537.32834	0.023	C28H49O8Mg1-	0.29	1.79
537.36472	537.36472	-0.004	C29H53O7Mg1-	0.24	1.86
537.40111	537.40111	0.006	C30H57O6Mg1-	0.20	1.93
537.47396	537.47388	0.16	C32H65O4Mg1-	0.13	2.06
539.17738	539.17732	0.118	C27H31O10Mg1-	0.37	1.19
539.1984	539.19845	-0.086	C24H35O12Mg1-	0.50	1.50
539.34404	539.34399	0.093	C28H51O8Mg1-	0.29	1.86
539.35922	539.35924	-0.044	C32H51O5Mg1-	0.16	1.63
539.38033	539.38037	-0.082	C29H55O7Mg1-	0.24	1.93
539.39559	539.39563	-0.068	C33H55O4Mg1-	0.12	1.70
541.13548	541.13545	0.045	C29H25O9Mg1-	0.31	0.90
541.15658	541.15658	-0.003	C26H29O11Mg1-	0.42	1.15
541.28685	541.28687	-0.022	C26H45O10Mg1-	0.38	1.77
541.31738	541.31738	0.012	C34H45O4Mg1-	0.12	1.35
541.37481	541.37489	-0.151	C32H53O5Mg1-	0.16	1.69
543.29662	543.29664	-0.046	C33H43O5Mg1-	0.15	1.33
543.30255	543.30252	0.052	C26H47O10Mg1-	0.38	1.85
543.35414	543.35416	-0.037	C31H51O6Mg1-	0.19	1.68
543.39044	543.39054	-0.182	C32H55O5Mg1-	0.16	1.75
545.29708	545.29704	0.079	C29H45O8Mg1-	0.28	1.59
545.33342	545.33342	-0.007	C30H49O7Mg1-	0.23	1.67
545.40617	545.40619	-0.046	C32H57O5Mg1-	0.16	1.81

A.11 Mass list of significantly enriched compounds in thermal processed meteorites

547.31269	547.31269	0.01	C29H47O8Mg1-	0.28	1.66
547.34908	547.34907	0.017	C30H51O7Mg1-	0.23	1.73
547.38544	547.38546	-0.027	C31H55O6Mg1-	0.19	1.81
549.32827	549.32834	-0.129	C29H49O8Mg1-	0.28	1.72
549.36473	549.36472	0.006	C30H53O7Mg1-	0.23	1.80
549.40111	549.40111	-0.001	C31H57O6Mg1-	0.19	1.87
549.43747	549.43749	-0.04	C32H61O5Mg1-	0.16	1.94
549.47388	549.47388	0.005	C33H65O4Mg1-	0.12	2.00
551.141	551.14093	0.118	C27H27O11Mg1-	0.41	1.04
551.19849	551.19845	0.088	C25H35O12Mg1-	0.48	1.44
551.30763	551.3076	0.051	C28H47O9Mg1-	0.32	1.71
551.34393	551.34399	-0.095	C29H51O8Mg1-	0.28	1.79
551.38038	551.38037	0.016	C30H55O7Mg1-	0.23	1.87
553.30214	553.30212	0.027	C31H45O7Mg1-	0.23	1.48
553.32326	553.32325	0.017	C28H49O9Mg1-	0.32	1.79
553.35958	553.35964	-0.098	C29H53O8Mg1-	0.28	1.86
553.3749	553.37489	0.01	C33H53O5Mg1-	0.15	1.64
553.39599	553.39602	-0.058	C30H57O7Mg1-	0.23	1.93
555.1511	555.1511	-0.003	C30H27O9Mg1-	0.30	0.93
555.35411	555.35416	-0.088	C32H51O6Mg1-	0.19	1.63
555.37528	555.37529	-0.018	C29H55O8Mg1-	0.28	1.93
555.3905	555.39054	-0.069	C33H55O5Mg1-	0.15	1.70
555.4269	555.42693	-0.049	C34H59O4Mg1-	0.12	1.76
557.33342	557.33342	-0.009	C31H49O7Mg1-	0.23	1.61
557.36979	557.36981	-0.034	C32H53O6Mg1-	0.19	1.69
557.40621	557.40619	0.025	C33H57O5Mg1-	0.15	1.76
557.44259	557.44258	0.027	C34H61O4Mg1-	0.12	1.82
559.26112	559.26105	0.122	C25H43O12Mg1-	0.48	1.76
559.27633	559.2763	0.042	C29H43O9Mg1-	0.31	1.52
559.31274	559.31269	0.088	C30H47O8Mg1-	0.27	1.60
559.38549	559.38546	0.056	C32H55O6Mg1-	0.19	1.75
559.42187	559.42184	0.043	C33H59O5Mg1-	0.15	1.82
559.4582	559.45823	-0.048	C34H63O4Mg1-	0.12	1.88
561.26138	561.26144	-0.104	C21H45O15Mg1-	0.71	2.19
561.32831	561.32834	-0.043	C30H49O8Mg1-	0.27	1.67
561.40114	561.40111	0.052	C32H57O6Mg1-	0.19	1.81
561.43746	561.43749	-0.05	C33H61O5Mg1-	0.15	1.88
561.47391	561.47388	0.064	C34H65O4Mg1-	0.12	1.94
563.344	563.34399	0.026	C30H51O8Mg1-	0.27	1.73
563.3804	563.38037	0.047	C31H55O7Mg1-	0.23	1.81
563.39554	563.39563	-0.145	C35H55O4Mg1-	0.11	1.60
563.41679	563.41676	0.056	C32H59O6Mg1-	0.19	1.88
563.45316	563.45314	0.032	C33H63O5Mg1-	0.15	1.94
563.48952	563.48953	-0.013	C34H67O4Mg1-	0.12	2.00
565.35964	565.35964	-0.001	C30H53O8Mg1-	0.27	1.80
565.39597	565.39602	-0.084	C31H57O7Mg1-	0.23	1.87
567.2087	567.20862	0.147	C29H35O10Mg1-	0.34	1.24
567.37531	567.37529	0.043	C30H55O8Mg1-	0.27	1.87
567.39054	567.39054	0.005	C34H55O5Mg1-	0.15	1.65
567.41169	567.41167	0.029	C31H59O7Mg1-	0.23	1.94
569.22429	569.22427	0.05	C29H37O10Mg1-	0.34	1.31
569.31813	569.31817	-0.073	C28H49O10Mg1-	0.36	1.79
569.33343	569.33342	0.007	C32H49O7Mg1-	0.22	1.56
569.36979	569.36981	-0.028	C33H53O6Mg1-	0.18	1.64
569.40612	569.40619	-0.118	C34H57O5Mg1-	0.15	1.71

A.11 Mass list of significantly enriched compounds in thermal processed meteorites

571.31271	571.31269	0.044	C31H47O8Mg1-	0.26	1.55
571.33389	571.33382	0.119	C28H51O10Mg1-	0.36	1.86
571.34909	571.34907	0.035	C32H51O7Mg1-	0.22	1.63
571.38547	571.38546	0.03	C33H55O6Mg1-	0.18	1.70
571.42185	571.42184	0.009	C34H59O5Mg1-	0.15	1.76
571.4582	571.45823	-0.053	C35H63O4Mg1-	0.11	1.83
573.29195	573.29195	-0.003	C30H45O9Mg1-	0.30	1.53
573.36476	573.36472	0.066	C32H53O7Mg1-	0.22	1.69
573.40109	573.40111	-0.037	C33H57O6Mg1-	0.18	1.76
573.43753	573.43749	0.066	C34H61O5Mg1-	0.15	1.82
575.30761	575.3076	0.007	C30H47O9Mg1-	0.30	1.60
575.38043	575.38037	0.104	C32H55O7Mg1-	0.22	1.75
575.3956	575.39563	-0.053	C36H55O4Mg1-	0.11	1.56
575.41676	575.41676	0.011	C33H59O6Mg1-	0.18	1.82
575.45314	575.45314	-0.01	C34H63O5Mg1-	0.15	1.88
575.48952	575.48953	-0.004	C35H67O4Mg1-	0.11	1.94
577.28683	577.28687	-0.072	C29H45O10Mg1-	0.34	1.59
577.32328	577.32325	0.056	C30H49O9Mg1-	0.30	1.67
577.35964	577.35964	0.01	C31H53O8Mg1-	0.26	1.74
577.39603	577.39602	0.017	C32H57O7Mg1-	0.22	1.81
577.4324	577.43241	-0.008	C33H61O6Mg1-	0.18	1.88
577.46878	577.46879	-0.018	C34H65O5Mg1-	0.15	1.94
579.2814	579.28139	0.019	C32H43O8Mg1-	0.25	1.38
579.33887	579.3389	-0.05	C30H51O9Mg1-	0.30	1.73
579.41168	579.41167	0.011	C32H59O7Mg1-	0.22	1.88
579.44805	579.44806	-0.004	C33H63O6Mg1-	0.18	1.94
579.48446	579.48444	0.035	C34H67O5Mg1-	0.15	2.00
581.24542	581.2454	0.04	C27H41O12Mg1-	0.44	1.56
581.35458	581.35455	0.054	C30H53O9Mg1-	0.30	1.80
581.40622	581.40619	0.057	C35H57O5Mg1-	0.14	1.66
581.42734	581.42732	0.036	C32H61O7Mg1-	0.22	1.94
583.33373	583.33382	-0.146	C29H51O10Mg1-	0.34	1.79
583.34905	583.34907	-0.046	C33H51O7Mg1-	0.21	1.58
583.37026	583.3702	0.091	C30H55O9Mg1-	0.30	1.87
583.45823	583.45823	0.005	C36H63O4Mg1-	0.11	1.78
585.34359	585.34359	-0.007	C36H49O5Mg1-	0.14	1.39
585.36466	585.36472	-0.111	C33H53O7Mg1-	0.21	1.64
585.40109	585.40111	-0.026	C34H57O6Mg1-	0.18	1.71
585.47385	585.47388	-0.044	C36H65O4Mg1-	0.11	1.83
587.25596	587.25596	-0.003	C26H43O13Mg1-	0.50	1.69
587.3076	587.3076	0.005	C31H47O9Mg1-	0.29	1.55
587.34393	587.34399	-0.088	C32H51O8Mg1-	0.25	1.63
587.38027	587.38037	-0.168	C33H55O7Mg1-	0.21	1.70
587.41669	587.41676	-0.12	C34H59O6Mg1-	0.18	1.76
587.4532	587.45314	0.104	C35H63O5Mg1-	0.14	1.83
589.32321	589.32325	-0.065	C31H49O9Mg1-	0.29	1.61
589.35963	589.35964	-0.006	C32H53O8Mg1-	0.25	1.69
589.46883	589.46879	0.057	C35H65O5Mg1-	0.14	1.89
591.26617	591.26613	0.073	C29H43O11Mg1-	0.38	1.52
591.3753	591.37529	0.018	C32H55O8Mg1-	0.25	1.75
591.39063	591.39054	0.149	C36H55O5Mg1-	0.14	1.56
591.41164	591.41167	-0.051	C33H59O7Mg1-	0.21	1.82
591.42688	591.42693	-0.079	C37H59O4Mg1-	0.11	1.62
593.24549	593.2454	0.157	C28H41O12Mg1-	0.43	1.50
593.35447	593.35455	-0.145	C31H53O9Mg1-	0.29	1.74

A.11 Mass list of significantly enriched compounds in thermal processed meteorites

593.39087	593.39094	-0.107	C32H57O8Mg1-	0.25	1.81
593.4637	593.46371	-0.013	C34H65O6Mg1-	0.18	1.94
595.33385	595.33382	0.052	C30H51O10Mg1-	0.33	1.73
595.355	595.35495	0.081	C27H55O12Mg1-	0.44	2.07
595.40658	595.40659	-0.009	C32H59O8Mg1-	0.25	1.88
595.45817	595.45823	-0.104	C37H63O4Mg1-	0.11	1.73
597.34938	597.34947	-0.147	C30H53O10Mg1-	0.33	1.80
597.40106	597.40111	-0.087	C35H57O6Mg1-	0.17	1.66
597.42222	597.42224	-0.033	C32H61O8Mg1-	0.25	1.94
597.47383	597.47388	-0.087	C37H65O4Mg1-	0.11	1.78
599.38042	599.38037	0.074	C34H55O7Mg1-	0.21	1.65
599.41674	599.41676	-0.026	C35H59O6Mg1-	0.17	1.71
599.45316	599.45314	0.026	C36H63O5Mg1-	0.14	1.78
601.32327	601.32325	0.039	C32H49O9Mg1-	0.28	1.56
601.43243	601.43241	0.044	C35H61O6Mg1-	0.17	1.77
601.46883	601.46879	0.07	C36H65O5Mg1-	0.14	1.83
603.37533	603.37529	0.071	C33H55O8Mg1-	0.24	1.70
603.41167	603.41167	-0.007	C34H59O7Mg1-	0.21	1.76
603.4481	603.44806	0.068	C35H63O6Mg1-	0.17	1.83
603.48442	603.48444	-0.039	C36H67O5Mg1-	0.14	1.89
605.35456	605.35455	0.007	C32H53O9Mg1-	0.28	1.69
605.39093	605.39094	-0.02	C33H57O8Mg1-	0.24	1.76
605.42731	605.42732	-0.025	C34H61O7Mg1-	0.21	1.82
605.46366	605.46371	-0.076	C35H65O6Mg1-	0.17	1.89
607.32792	607.32794	-0.036	C38H47O5Mg1-	0.13	1.26
607.3702	607.3702	-0.003	C32H55O9Mg1-	0.28	1.75
607.40664	607.40659	0.094	C33H59O8Mg1-	0.24	1.82
607.44301	607.44297	0.068	C34H63O7Mg1-	0.21	1.88
607.47934	607.47936	-0.028	C35H67O6Mg1-	0.17	1.94
609.34941	609.34947	-0.1	C31H53O10Mg1-	0.32	1.74
609.42222	609.42224	-0.035	C33H61O8Mg1-	0.24	1.88
609.43742	609.43749	-0.121	C37H61O5Mg1-	0.14	1.68
609.4586	609.45862	-0.034	C34H65O7Mg1-	0.21	1.94
611.41674	611.41676	-0.031	C36H59O6Mg1-	0.17	1.67
611.45314	611.45314	-0.003	C37H63O5Mg1-	0.14	1.73
611.48947	611.48953	-0.085	C38H67O4Mg1-	0.11	1.79
613.35963	613.35964	-0.017	C34H53O8Mg1-	0.24	1.59
613.37488	613.37489	-0.019	C38H53O5Mg1-	0.13	1.42
613.43241	613.43241	-0.002	C36H61O6Mg1-	0.17	1.72
615.339	615.3389	0.159	C33H51O9Mg1-	0.27	1.58
615.37526	615.37529	-0.044	C34H55O8Mg1-	0.24	1.65
615.41169	615.41167	0.021	C35H59O7Mg1-	0.20	1.71
617.39096	617.39094	0.043	C34H57O8Mg1-	0.24	1.71
617.46372	617.46371	0.021	C36H65O6Mg1-	0.17	1.83
619.31849	619.31856	-0.111	C28H51O13Mg1-	0.46	1.86
619.37021	619.3702	0.018	C33H55O9Mg1-	0.27	1.70
619.47937	619.47936	0.016	C36H67O6Mg1-	0.17	1.89
621.42222	621.42224	-0.023	C34H61O8Mg1-	0.24	1.82
621.43751	621.43749	0.037	C38H61O5Mg1-	0.13	1.63
621.49504	621.49501	0.053	C36H69O6Mg1-	0.17	1.94
623.36516	623.36512	0.074	C32H55O10Mg1-	0.31	1.75
623.47425	623.47427	-0.036	C35H67O7Mg1-	0.20	1.94
623.48956	623.48953	0.053	C39H67O4Mg1-	0.10	1.74
625.38072	625.38077	-0.077	C32H57O10Mg1-	0.31	1.81
625.43239	625.43241	-0.024	C37H61O6Mg1-	0.16	1.68

A.11 Mass list of significantly enriched compounds in thermal processed meteorites

627.37534	627.37529	0.09	C35H55O8Mg1-	0.23	1.60
627.39057	627.39054	0.041	C39H55O5Mg1-	0.13	1.44
627.44804	627.44806	-0.027	C37H63O6Mg1-	0.16	1.73
627.48444	627.48444	-0.003	C38H67O5Mg1-	0.13	1.79
629.39098	629.39094	0.06	C35H57O8Mg1-	0.23	1.66
631.40652	631.40659	-0.098	C35H59O8Mg1-	0.23	1.71
633.31306	633.31308	-0.034	C32H49O11Mg1-	0.34	1.56
633.45867	633.45862	0.071	C36H65O7Mg1-	0.19	1.83
633.49498	633.49501	-0.037	C37H69O6Mg1-	0.16	1.89
635.2619	635.26184	0.107	C23H47O18Mg1-	0.78	2.09
635.47432	635.47427	0.067	C36H67O7Mg1-	0.19	1.89
639.44799	639.44806	-0.112	C38H63O6Mg1-	0.16	1.68
639.48438	639.48444	-0.092	C39H67O5Mg1-	0.13	1.74
641.39096	641.39094	0.036	C36H57O8Mg1-	0.22	1.61
641.40622	641.40619	0.048	C40H57O5Mg1-	0.13	1.45
645.4434	645.44337	0.043	C33H65O10Mg1-	0.30	2.00
645495	645.49501	-0.009	C38H69O6Mg1-	0.16	1.84
647.20436	647.20432	0.059	C26H39O17Mg1-	0.65	1.54
647.34988	647.34986	0.028	C30H55O13Mg1-	0.43	1.87
649.46874	649.46879	-0.08	C40H65O5Mg1-	0.13	1.65
649.48995	649.48992	0.043	C37H69O7Mg1-	0.19	1.89
651.46916	651.46919	-0.036	C36H67O8Mg1-	0.22	1.89
655.47938	655.47936	0.035	C39H67O6Mg1-	0.15	1.74
657.42226	657.42224	0.041	C37H61O8Mg1-	0.22	1.68
661.4899	661.48992	-0.039	C38H69O7Mg1-	0.18	1.84
662.91406	662.91403	0.043	C11H11O31Mg1-	2.82	1.09
663.37533	663.37529	0.065	C38H55O8Mg1-	0.21	1.47
663.4692	663.46919	0.016	C37H67O8Mg1-	0.22	1.84
665.21478	665.21489	-0.16	C26H41O18Mg1-	0.69	1.62
665.4485	665.44845	0.075	C36H65O9Mg1-	0.25	1.83
665.4848	665.48484	-0.049	C37H69O8Mg1-	0.22	1.89
667.42193	667.42184	0.132	C42H59O5Mg1-	0.12	1.43
667.44297	667.44297	-0.001	C39H63O7Mg1-	0.18	1.64
667.46418	667.4641	0.112	C36H67O9Mg1-	0.25	1.89
667.47934	667.47936	-0.026	C40H67O6Mg1-	0.15	1.70
671.3862	671.38625	-0.07	C33H59O12Mg1-	0.36	1.82
671.41679	671.41676	0.042	C41H59O6Mg1-	0.15	1.46
671.43796	671.43789	0.109	C38H63O8Mg1-	0.21	1.68
681.47969	681.47975	-0.099	C37H69O9Mg1-	0.24	1.89
683.10106	683.10104	0.031	C19H31O25Mg1-	1.32	1.68
685.48994	685.48992	0.021	C40H69O7Mg1-	0.18	1.75
691.33393	691.33382	0.156	C38H51O10Mg1-	0.26	1.37
695.08587	695.08579	0.113	C16H31O28Mg1-	1.75	2.00
699.46925	699.46919	0.083	C40H67O8Mg1-	0.20	1.70
701.48483	701.48484	-0.003	C40H69O8Mg1-	0.20	1.75
703.18828	703.18828	0.012	C35H35O14Mg1-	0.40	1.03
707.45908	707.45902	0.096	C38H67O10Mg1-	0.26	1.79
711.13244	711.13234	0.138	C21H35O25Mg1-	1.19	1.71
713.48486	713.48484	0.025	C41H69O8Mg1-	0.20	1.71
715.12728	715.12726	0.026	C20H35O26Mg1-	1.30	1.80
725.14793	725.14799	-0.085	C22H37O25Mg1-	1.14	1.73
727.44294	727.44297	-0.044	C44H63O7Mg1-	0.16	1.45
743.41687	743.41676	0.145	C47H59O6Mg1-	0.13	1.28
743.45315	743.45314	0.015	C48H63O5Mg1-	0.10	1.33
763.44295	763.44297	-0.029	C47H63O7Mg1-	0.15	1.36

A.12 Coordinates of the relaxed, computed geometry of C₁₆-dihydroxymagnesium carboxylate

787.25765	787.25754	0.137	C26H51O25Mg1-	0.96	2.00
809.25719	809.25715	0.047	C32H49O22Mg1-	0.69	1.56
815.12795	815.12805	-0.123	C20H39O32Mg1-	1.60	2.00
830.76502	830.76499	0.041	C3H3O48Mg1-	16.00	1.33
874.85816	874.8581	0.073	C14H11O42Mg1-	3.00	0.86
884.87875	884.87883	-0.092	C16H13O41Mg1-	2.56	0.88
887.37686	887.37687	-0.008	C40H63O20Mg1-	0.50	1.60

A.12. Coordinates of the relaxed, computed geometry of C₁₆-dihydroxymagnesium carboxylate

Coordinates of the relaxed geometry of C₁₆-dihydroxymagnesium carboxylate complex anion, presented as xyz coordinates. All atoms are labeled with atom numbers.

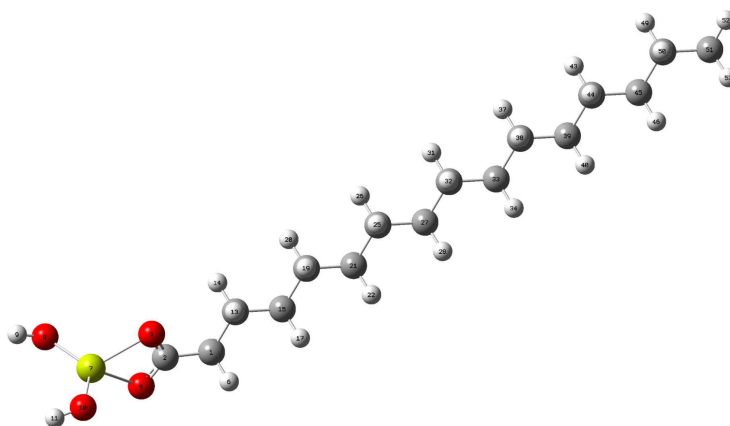


Table A.3: Coordinates of the relaxed, computed geometries - C₁₆-dihydroxymagnesium carboxylate

Atom	xyz coordinates
1 C	5.36862 1.17566 -0.12707
2 C	6.72747 0.48060 -0.06198
3 O	6.80091 -0.74818 0.24731
4 O	7.76737 1.16891 -0.30519
5 H	5.36006 1.79618 -1.03195
6 H	5.33706 1.87997 0.71664
7 Mg	8.93792 -0.58040 0.08000
8 O	9.68341 -1.33207 -1.51151
9 H	10.42420 -1.94355 -1.46784
10 O	9.79590 -0.61696 1.78750
11 H	10.72988 -0.83040 1.86874
12 C	4.15806 0.24048 -0.08521
13 H	4.22848 -0.39351 0.80628
14 H	4.20252 -0.44517 -0.94126
15 C	2.81950 0.99078 -0.09338
16 H	2.76374 1.63353 -0.98529
17 H	2.77664 1.67004 0.77172
18 C	1.59611 0.06468 -0.06563
19 H	1.65065 -0.57848 0.82480
20 H	1.63669 -0.61281 -0.93109
21 C	0.25493 0.81039 -0.06978
22 H	0.21443 1.48693 0.79687
23 H	0.20148 1.45473 -0.95999
24 C	-0.96845 -0.11562 -0.04362

A.13 Coordinates of the relaxed, computed geometries - C₁₆-carboxylate

25	H	-0.91374	-0.76233	0.84440
26	H	-0.93075	-0.78958	-0.91206
27	C	-2.30891	0.63146	-0.04195
28	H	-2.34727	1.30366	0.82795
29	H	-2.36293	1.27992	-0.92892
30	C	-3.53245	-0.29433	-0.01860
31	H	-3.49551	-0.96509	-0.88952
32	H	-3.47794	-0.94412	0.86719
33	C	-4.87232	0.45375	-0.01398
34	H	-4.90994	1.12320	0.85797
35	H	-4.92627	1.10483	-0.89894
36	C	-6.09599	-0.47187	0.00700
37	H	-6.05915	-1.14056	-0.86549
38	H	-6.04189	-1.12365	0.89133
39	C	-7.43551	0.27679	0.01305
40	H	-7.47280	0.94485	0.88603
41	H	-7.48943	0.92915	-0.87090
42	C	-8.65925	-0.64879	0.03286
43	H	-8.62207	-1.31679	-0.84016
44	H	-8.60553	-1.30118	0.91677
45	C	-9.99874	0.09970	0.03885
46	H	-10.03738	0.76745	0.91218
47	H	-10.05345	0.75256	-0.84483
48	C	-11.22282	-0.82545	0.05787
49	H	-11.18488	-1.49230	-0.81484
50	H	-11.16894	-1.47743	0.94093
51	C	-12.55658	-0.06925	0.06370
52	H	-13.40857	-0.75812	0.07807
53	H	-12.63917	0.58080	0.94309
54	H	-12.65610	0.56480	-0.82557

A.13. Coordinates of the relaxed, computed geometries - C₁₆-carboxylate

Coordinates of the relaxed geometry of C₁₆-carboxylate anion, presented as xyz coordinates. All atoms are labeled with atom numbers.

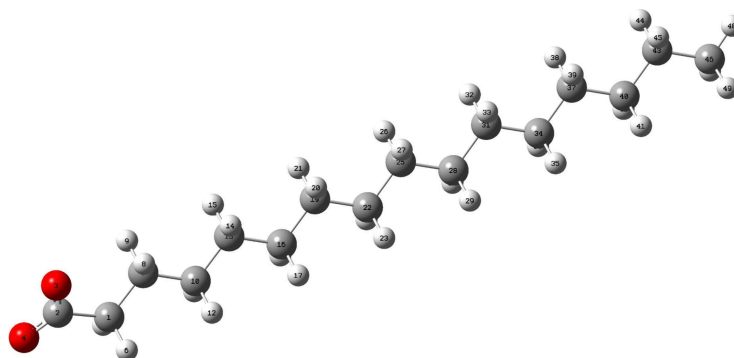


Table A.4: Coordinates of the relaxed, computed geometries - C₁₆-carboxylate

Atom	xyz coordinates			
1	C	7.41994	-0.63693	-0.01295
2	C	8.76062	0.17837	-0.02513
3	O	8.68785	1.36462	-0.44960

A.14 Coordinates of the relaxed, computed geometries - C₅-dihydroxymagnesium carboxylate

4	O	9.77762	-0.45851	0.36275
5	H	7.48038	-1.38914	0.78447
6	H	7.38540	-1.19669	-0.96181
7	C	6.14981	0.20744	0.12210
8	H	6.20605	1.02378	-0.60781
9	H	6.14185	0.69188	1.11009
10	C	4.84724	-0.58484	-0.06115
11	H	4.81665	-1.41951	0.65694
12	H	4.84305	-1.04756	-1.06049
13	C	3.57675	0.26147	0.10467
14	H	3.60742	1.10008	-0.60665
15	H	3.57572	0.71593	1.10684
16	C	2.27241	-0.52261	-0.09377
17	H	2.26407	-0.96140	-1.10284
18	H	2.25070	-1.37217	0.60548
19	C	1.00423	0.31976	0.10016
20	H	1.02872	1.17527	-0.59107
21	H	1.00769	0.74912	1.11304
22	C	-0.29892	-0.46243	-0.11163
23	H	-0.30860	-0.88027	-1.12926
24	H	-0.31779	-1.32560	0.57034
25	C	-1.56650	0.37564	0.10218
26	H	-1.55996	0.78660	1.12253
27	H	-1.54564	1.24314	-0.57394
28	C	-2.86884	-0.40513	-0.11891
29	H	-2.88071	-0.80659	-1.14295
30	H	-2.88474	-1.27881	0.54941
31	C	-4.13629	0.42854	0.11165
32	H	-4.12574	0.82637	1.13708
33	H	-4.11987	1.30445	-0.55359
34	C	-5.43812	-0.35186	-0.11342
35	H	-5.45177	-0.74463	-1.14074
36	H	-5.45178	-1.23100	0.54763
37	C	-6.70563	0.47907	0.12647
38	H	-6.69197	0.87126	1.15402
39	H	-6.69252	1.35852	-0.53415
40	C	-8.00723	-0.30157	-0.09828
41	H	-8.02279	-0.69301	-1.12622
42	H	-8.02085	-1.18178	0.56155
43	C	-9.27524	0.52798	0.14359
44	H	-9.25955	0.92048	1.16999
45	H	-9.26390	1.40599	-0.51741
46	C	-10.57051	-0.26114	-0.08032
47	H	-10.62986	-1.12439	0.59354
48	H	-11.45529	0.36053	0.09688
49	H	-10.63035	-0.64033	-1.10764

A.14. Coordinates of the relaxed, computed geometries - C₅-dihydroxymagnesium carboxylate

Coordinates of the relaxed geometry of C₅-dihydroxymagnesium carboxylate complex anion, presented as xyz coordinates. All atoms are labeled with atom numbers.

A.14 Coordinates of the relaxed, computed geometries - C₅-dihydroxymagnesium carboxylate

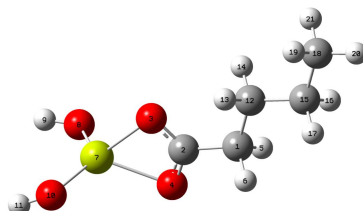


Table A.5: Coordinates of the relaxed, computed geometries - C₅-dihydroxymagnesium carboxylate

Atom	xyz coordinates			
1	C	-1.33614	-0.14736	0.92428
2	C	0.12785	-0.07298	0.49407
3	O	0.42935	0.01626	-0.73545
4	O	1.02103	-0.11254	1.39715
5	H	-1.47867	0.59894	1.71677
6	H	-1.47355	-1.12353	1.41020
7	Mg	2.49767	0.02410	-0.14482
8	O	3.34216	1.73780	-0.20673
9	H	4.18827	1.85530	-0.64814
10	O	3.37773	-1.61957	-0.56636
11	H	4.33519	-1.66400	-0.64221
12	C	-2.35744	0.04288	-0.19893
13	H	-2.17101	-0.70047	-0.98345
14	H	-2.19506	1.01942	-0.67263
15	C	-3.80981	-0.06153	0.28526
16	H	-3.98733	0.68497	1.07329
17	H	-3.96745	-1.04238	0.75737
18	C	-4.83813	0.13202	-0.83639
19	H	-4.70913	-0.62179	-1.62268
20	H	-5.86664	0.05378	-0.46297
21	H	-4.72665	1.11685	-1.30635

B. Appendix Chapter 3

B.1. Computational methods

The electronic structure simulations were performed on a stand-alone computer (one node server system) by state-of-the-art quantum mechanical computations, based on *ab initio* second-order Møller–Plesset perturbation theory (MP2) and density functional theory (DFT), as implemented within the Gaussian 09 program [244]. These orthogonal quantum chemical methods were used to gain unbiased insights into the stability of dihydroxymagnesium carboxylates regarding the release of CO₂. The hybrid DFT-functional B3LYP and post-Hartree-Fock many-body wave function description were implemented with d-polarization functions for each heavy atom and 1p for each hydrogen atom in all single-point energy (SPE) calculations.

For geometry optimization, the Berny analytical gradient optimization routines [232, 233] were used in combination with the GDIIS algorithm [234]. The requested convergence value in the density matrix was 10^{-8} , the threshold value for maximum displacement was 0.0018 Å, and the threshold value for the maximum force was 0.00045 Hartree Bohr⁻¹. The nature of the stationary points was established by calculating and diagonalizing the Hessian matrix (force-constant matrix). All geometry optimizations were performed via a 6-31+G(d,p) basis set.

Additionally, frequency calculations were computed for each optimized geometry, also with a 6-31+G(d,p) basis set to identify transition states (1st order saddle points on the potential energy surface, PES). Detecting imaginary frequencies implies that the optimized geometry is not fully relaxed as a stationary point on the PES. Transition structures were characterized in detail through normal-mode analysis (frequency analysis). The transition

B.2 Coordinates of computed structures regarding the potential energy curve

vector, which is associated with the unique imaginary frequency has been determined in each transition state found. This vector represents the eigenvector, which is associated with the unique negative eigenvalue of the force constant matrix. This indicates that the found structure corresponds to a first order saddle point (transition state). In order to further check that the transition state found actually connects two energy minima structures with each other (reactant with product), intrinsic reaction coordinate (IRC) calculations [245] in all the transition state geometries found were performed in mass-weighted internal coordinates [246].

All geometries of computed electronic structures were visualized either via the GaussView [247] program.

Energy barriers between a transition state and its connected relaxed local minimum on the potential energy curve along decarboxylation intrinsic reaction coordinate in the gas phase were calculated as Eq. C.4:

$$\text{Energy barrier} = E_{\text{transition state}} - E_{\text{local minimum structure}} \quad (\text{B.1})$$

$E(x)$ represents the sum of electronic and thermal free energies ($\varepsilon_0 + G_{\text{corr}}$, corrected by a scaled zero-point vibrational energy, ZPVE) of respective C-, H-, O-, Mg-bearing species. ZPVE was obtained by performing frequency analysis computations. Resulted ZPE values were multiplied by a scaling factor of 0.9804 to correct for vibrational anharmonicities [230]. ε_0 were computed via single point energy calculations, at 6-311+G(2d,p) level of theory. The use of diffuse functions was important to represent the correct geometry and thermodynamic properties of anionic species [231]. Stability tests were performed in all cases to ensure that the used wave function represents the lowest energy solution of the self-consistent field (SCF) equations.

Natural bond orbital (NBO) analyses were run, as implemented within the Gaussian 09 program [244], on 6-311+G(2d,p) level of theory. Respective charge distribution results were visualized using the GaussView program [247].

All computations are referred to gas-phase conditions.

B.2. Coordinates of computed structures regarding the potential energy curve

Table B.1: Coordinates of the relaxed geometries of bidentate C₇-dihydroxymagnesium carboxylate, as computed on B3LYP/6-311+G(2d,p) level of theory

Atom	xyz coordinates		
C	0.14498	-0.78121	-0.77091
C	-1.28349	-0.39720	-0.38595
O	-1.49189	0.42899	0.55417
O	-2.24046	-0.93152	-1.02877
H	0.23471	-0.63768	-1.85568
H	0.23890	-1.86420	-0.60912
Mg	-3.61100	0.20582	0.17803
C	1.24786	-0.02595	-0.02626
H	1.12287	1.05072	-0.19560
H	1.11786	-0.17208	1.05288
C	2.65916	-0.45806	-0.44653
H	2.77909	-0.31203	-1.53090
H	2.77816	-1.53852	-0.27238
O	-4.38208	1.70229	-0.71467

B.2 Coordinates of computed structures regarding the potential energy curve

H	-5.28886	1.95230	-0.51357
O	-4.56238	-0.81081	1.48521
H	-4.16912	-1.58488	1.89879
C	3.77762	0.29425	0.28702
H	3.66164	1.37406	0.11274
H	3.66104	0.14895	1.37112
C	5.19094	-0.13433	-0.12971
H	5.30735	0.01038	-1.21322
H	5.30802	-1.21311	0.04656
C	6.30168	0.62473	0.60661
H	7.29723	0.29520	0.28637
H	6.23216	1.70366	0.42179
H	6.23272	0.47240	1.69067

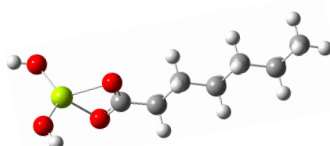


Table B.2: Coordinates of the relaxed geometries of the transition state of the coordinate switch from bi- and monodentate C₇-dihydroxymagnesium carboxylate, as computed on B3LYP/6-311+G(2d,p) level of theory

Atom	xyz coordinates		
C	-0.05743	1.82145	-0.40746
C	-1.49144	1.70036	0.13680
O	-2.12610	0.65353	-0.27728
O	-1.93491	2.56197	0.90739
H	0.32525	2.82170	-0.17572
H	-0.09162	1.70739	-1.49962
Mg	-3.01141	-1.04231	-0.03567
C	0.86828	0.74248	0.18156
H	0.93353	0.88491	1.26958
H	0.41296	-0.24275	0.02651
C	2.28121	0.76280	-0.41663
H	2.72378	1.76272	-0.28616
H	2.21447	0.59862	-1.50293
O	-1.87338	-2.40900	0.61118
H	-2.20242	-3.30247	0.74559
O	-4.80668	-1.28131	-0.58230
H	-5.34445	-0.52780	-0.84323
C	3.21939	-0.28727	0.19370
H	2.76743	-1.28278	0.08050
H	3.30072	-0.11381	1.27702
C	4.62517	-0.29456	-0.42155
H	5.07430	0.70334	-0.31241
H	4.54448	-0.47421	-1.50312
C	5.55776	-1.34235	0.19894
H	5.15188	-2.35363	0.07509
H	6.55279	-1.32268	-0.26199
H	5.68485	-1.16982	1.27482

B.2 Coordinates of computed structures regarding the potential energy curve



Table B.3: Coordinates of the relaxed geometries of monodentate C₇-dihydroxymagnesium carboxylate, as computed on B3LYP/6-311+G(2d,p) level of theory

Atom	xyz coordinates		
C	0.39276	1.63444	0.64223
C	1.74726	1.78910	-0.07309
O	2.45743	0.70950	-0.18173
O	2.08404	2.89927	-0.50451
H	0.00764	2.63724	0.85960
H	0.55400	1.11458	1.59685
Mg	2.60709	-1.20809	-0.01832
C	-0.63009	0.83655	-0.18682
H	-0.76791	1.33521	-1.15774
H	-0.23643	-0.16803	-0.38034
C	-1.99069	0.70522	0.51068
H	-2.40197	1.70468	0.72433
H	-1.84456	0.21531	1.48467
O	0.95969	-2.14516	0.03250
H	0.93876	-3.10500	0.08833
O	4.31360	-2.01068	0.08699
H	5.11441	-1.48193	0.02350
C	-3.01135	-0.10123	-0.30344
H	-2.58905	-1.09286	-0.51610
H	-3.16191	0.38457	-1.27965
C	-4.37031	-0.26365	0.39054
H	-4.78781	0.72977	0.61079
H	-4.22124	-0.75334	1.36328
C	-5.38371	-1.06897	-0.43260
H	-5.00895	-2.07894	-0.63856
H	-6.34343	-1.16842	0.08929
H	-5.57794	-0.58788	-1.39940

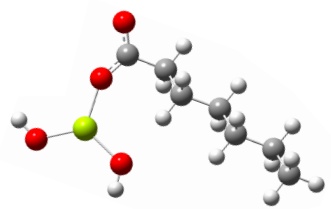


Table B.4: Coordinates of the relaxed geometries of the transition state of decarboxylation of C₇-dihydroxymagnesium carboxylate, as computed on B3LYP/6-311+G(2d,p) level of theory

Atom	xyz coordinates		
C	-0.57195	0.75585	0.02706

B.2 Coordinates of computed structures regarding the potential energy curve

C	-3.09266	1.55770	-0.02566
O	-3.74751	0.56619	-0.02150
O	-2.77264	2.68907	-0.03092
H	-0.54064	1.40034	0.91909
H	-0.54143	1.42707	-0.84340
Mg	-1.98684	-1.01032	0.00070
O	-2.24363	-1.93230	1.65682
H	-2.03360	-1.51817	2.49909
O	-2.15051	-1.84306	-1.70734
H	-2.46431	-2.74953	-1.77907
C	0.70352	-0.11903	0.00780
H	0.71362	-0.80025	0.87428
H	0.70150	-0.76868	-0.88145
C	2.03023	0.67094	0.01521
H	2.05126	1.32046	0.90371
H	2.04415	1.34522	-0.85436
C	3.28846	-0.21000	-0.00233
H	3.26170	-0.86098	-0.88907
H	3.27076	-0.88448	0.86715
C	4.60541	0.57875	0.00165
H	4.62526	1.25186	-0.86743
H	4.63423	1.22865	0.88811
C	5.85461	-0.31181	-0.01660
H	5.87967	-0.97350	0.85817
H	5.87096	-0.94921	-0.90937
H	6.77759	0.28132	-0.01302

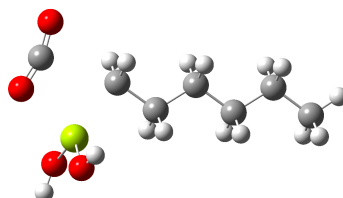


Table B.5: Coordinates of the relaxed geometries of C₆-dihydroxyorganomangesate, a Grignard-type molecule, as computed on B3LYP/6-311+G(2d,p) level of theory

Atom	xyz coordinates		
C	-1.07980	0.87934	0.00042
H	-1.02401	1.55285	0.87616
H	-1.02393	1.55344	-0.87486
Mg	-3.06350	-0.04474	0.00002
O	-3.30302	-1.95146	0.00008
H	-2.54478	-2.54397	0.00033
O	-4.61836	1.07371	-0.00051
H	-5.48378	0.65155	-0.00064
C	0.15336	-0.03759	0.00015
H	0.12299	-0.70844	0.87521
H	0.12293	-0.70799	-0.87525
C	1.52476	0.67253	0.00028
H	1.57926	1.33386	0.87889
H	1.57916	1.33432	-0.87799
C	2.73565	-0.27265	-0.00004

B.2 Coordinates of computed structures regarding the potential energy curve

H	2.67917	-0.93394	-0.87854
H	2.67935	-0.93431	0.87820
C	4.09340	0.44363	-0.00003
H	4.15261	1.10338	-0.87754
H	4.15280	1.10304	0.87772
C	5.29441	-0.51113	-0.00034
H	5.28145	-1.16094	-0.88438
H	6.24740	0.03260	-0.00030
H	5.28160	-1.16132	0.88343

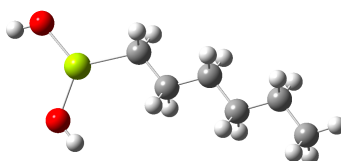


Table B.6: Coordinates of the relaxed geometries of CO₂, as computed on B3LYP/6-311+G(2d,p) level of theory

Atom	xyz coordinates		
C	0.00000	0.00000	0.00000
O	0.00000	0.00000	1.16938
O	0.00000	0.00000	-1.16938



B.3 Natural bond orbital analysis - coordinates of the computed C₅-dihydroxymagnesium carboxylate transition state geometry

B.3. Natural bond orbital analysis - coordinates of the computed C₅-dihydroxymagnesium carboxylate transition state geometry

Table B.7: Summary of Natural Population Analysis (NBO) for C₅-dihydroxymagnesium carboxylate, as computed on B3LYP/6-311+G(2d,p) level of theory

Atom	No	Natural Charge	Core	Valence	Natural Population	
					Rydberg	Total
C	1	-0.96393	1.99926	4.93221	0.03245	6.96393
C	2	1.02590	1.99957	2.93112	0.04340	4.97410
O	3	-0.57058	1.99973	6.53637	0.03448	8.57058
O	4	-0.53578	1.99971	6.50594	0.03012	8.53578
H	5	0.17310	0.00000	0.82480	0.00210	0.82690
H	6	0.17826	0.00000	0.81962	0.00212	0.82174
Mg	7	1.44628	9.99778	0.53595	0.01999	10.55372
O	8	-1.27206	1.99985	7.26171	0.01050	9.27206
H	9	0.43509	0.00000	0.56165	0.00326	0.56491
O	10	-1.27122	1.99985	7.26098	0.01039	9.27122
H	11	0.43691	0.00000	0.55985	0.00324	0.56309
C	12	-0.41218	1.99933	4.39546	0.01739	6.41218
H	13	0.18088	0.00000	0.81711	0.00201	0.81912
H	14	0.18960	0.00000	0.80851	0.00189	0.81040
C	15	-0.37644	1.99933	4.36071	0.01639	6.37644
H	16	0.17604	0.00000	0.82148	0.00248	0.82396
H	17	0.17837	0.00000	0.81919	0.00244	0.82163
C	18	-0.57172	1.99938	4.56159	0.01076	6.57172
H	19	0.18747	0.00000	0.81047	0.00207	0.81253
H	20	0.18024	0.00000	0.81820	0.00156	0.81976
H	21	0.18578	0.00000	0.81215	0.00207	0.81422
* Total *		-1.00000	27.99380	57.75509	0.25111	86.00000

B.4 Natural bond orbital analysis - coordinates of the computed OH- and Cl-bearing putative Grignard-type molecules

B.4. Natural bond orbital analysis - coordinates of the computed OH- and Cl-bearing putative Grignard-type molecules

Table B.8: Summary of Natural Population Analysis (NBO) for C₅-dihydroxymagnesium organomagnesate, as computed on B3LYP/6-311+G(2d,p) level of theory

Atom	No	Natural Charge	Core	Valence	Natural Population	
					Rydberg	Total
C	1	-1.01074	1.99936	4.97975	0.03163	7.01074
H	2	0.16464	0.00000	0.83318	0.00218	0.83536
H	3	0.16959	0.00000	0.82828	0.00214	0.83041
Mg	4	1.49060	9.99820	0.49820	0.01300	10.50940
O	5	-1.28330	1.99987	7.27230	0.01113	9.28330
H	6	0.43008	0.00000	0.56605	0.00387	0.56992
O	7	-1.28282	1.99987	7.27202	0.01093	9.28282
H	8	0.43247	0.00000	0.56375	0.00379	0.56753
C	9	-0.38500	1.99934	4.36747	0.01820	6.38500
H	10	0.16580	0.00000	0.83178	0.00242	0.83420
H	11	0.17265	0.00000	0.82501	0.00234	0.82735
C	12	-0.38110	1.99929	4.36348	0.01833	6.38110
H	13	0.17562	0.00000	0.82175	0.00263	0.82438
H	14	0.17749	0.00000	0.81989	0.00262	0.82251
C	15	-0.38310	1.99932	4.36810	0.01568	6.38310
H	16	0.18077	0.00000	0.81656	0.00266	0.81923
H	17	0.17939	0.00000	0.81792	0.00269	0.82061
C	18	-0.56738	1.99938	4.55737	0.01063	6.56738
H	19	0.18312	0.00000	0.81538	0.00150	0.81688
H	20	0.18592	0.00000	0.81211	0.00197	0.81408
H	21	0.18531	0.00000	0.81272	0.00198	0.81469
* Total *		-1.00000	23.99463	47.84307	0.16231	72.00000

B.4 Natural bond orbital analysis - coordinates of the computed OH- and Cl-bearing putative Grignard-type molecules

Table B.9: Summary of Natural Population Analysis (NBO) for C₅-organomagnesiumhydroxid, a putative Grignard-type molecule, as computed on B3LYP/6-311+G(2d,p) level of theory

Atom	No	Natural Charge	Core	Valence	Natural Population	
					Rydberg	Total
C	1	-1.03763	1.99930	5.01191	0.02642	7.03763
H	2	0.19916	0.00000	0.79882	0.00201	0.80084
H	3	0.19918	0.00000	0.79881	0.00201	0.80082
Mg	4	1.53077	9.99655	0.46380	0.00888	10.46923
O	5	-1.33190	1.99984	7.32263	0.00944	9.33190
H	6	0.48100	0.00000	0.51609	0.00291	0.51900
C	7	-0.38954	1.99932	4.37298	0.01724	6.38954
H	8	0.17912	0.00000	0.81869	0.00219	0.82088
H	9	0.17913	0.00000	0.81869	0.00219	0.82087
C	10	-0.38035	1.99928	4.36343	0.01764	6.38035
H	11	0.18553	0.00000	0.81237	0.00210	0.81447
H	12	0.18553	0.00000	0.81237	0.00210	0.81447
C	13	-0.38253	1.99932	4.36814	0.01507	6.38253
H	14	0.18554	0.00000	0.81217	0.00229	0.81446
H	15	0.18553	0.00000	0.81218	0.00229	0.81447
C	16	-0.56889	1.99938	4.55868	0.01084	6.56889
H	17	0.19734	0.00000	0.80148	0.00118	0.80266
H	18	0.19151	0.00000	0.80681	0.00169	0.80849
H	19	0.19150	0.00000	0.80681	0.00169	0.80850
* Total *		0.00000	21.99299	39.87685	0.13016	62.00000

Table B.10: Summary of Natural Population Analysis (NBO) for C₅-dichloromagnesium organomagnesate, as computed on B3LYP/6-311+G(2d,p) level of theory

Atom	No	Natural Charge	Core	Valence	Natural Population	
					Rydberg	Total
C	1	-1.00936	1.99930	4.97990	0.03017	7.00936
H	2	0.17840	0.00000	0.81967	0.00193	0.82160
H	3	0.17840	0.00000	0.81967	0.00193	0.82160
Mg	4	1.26354	9.99853	0.71770	0.02024	10.73646
Cl	5	-0.76324	9.99978	7.75514	0.00832	17.76324
Cl	6	-0.76327	9.99978	7.75489	0.00859	17.76327
C	7	-0.38408	1.99934	4.36666	0.01808	6.38408
H	8	0.17585	0.00000	0.82200	0.00215	0.82415
H	9	0.17584	0.00000	0.82201	0.00215	0.82416
C	10	-0.38137	1.99929	4.36417	0.01791	6.38137
H	11	0.17755	0.00000	0.82002	0.00243	0.82245
H	12	0.17755	0.00000	0.82002	0.00243	0.82245
C	13	-0.37419	1.99934	4.36001	0.01484	6.37419
H	14	0.17996	0.00000	0.81748	0.00256	0.82004
H	15	0.17996	0.00000	0.81748	0.00256	0.82004
C	16	-0.56061	1.99936	4.55114	0.01011	6.56061
H	17	0.18195	0.00000	0.81657	0.00148	0.81805
H	18	0.18355	0.00000	0.81444	0.00200	0.81645
H	19	0.18355	0.00000	0.81444	0.00200	0.81645
* Total *		-1.00000	39.99472	47.85340	0.15188	88.00000

B.4 Natural bond orbital analysis - coordinates of the computed OH- and Cl-bearing putative Grignard-type molecules

Table B.11: Summary of Natural Population Analysis (NBO) for C₅-organomagnesiumchlorid, a putative Grignard-type molecule, as computed on B3LYP/6-311+G(2d,p) level of theory

Atom	No	Natural Charge	Core	Valence	Natural Population	
					Rydberg	Total
C	1	-1.02129	1.99925	4.99323	0.02880	7.02129
H	2	0.20290	0.00000	0.79518	0.00192	0.79710
H	3	0.20290	0.00000	0.79518	0.00192	0.79710
Mg	4	1.37584	9.99825	0.60940	0.01650	10.62416
Cl	5	-0.72591	9.99976	7.71177	0.01438	17.72591
C	6	-0.39099	1.99932	4.37423	0.01744	6.39099
H	7	0.18033	0.00000	0.81753	0.00214	0.81967
H	8	0.18033	0.00000	0.81753	0.00214	0.81967
C	9	-0.38002	1.99929	4.36272	0.01801	6.38002
H	10	0.18649	0.00000	0.81144	0.00207	0.81351
H	11	0.18649	0.00000	0.81144	0.00207	0.81351
C	12	-0.38260	1.99932	4.36827	0.01501	6.38260
H	13	0.18609	0.00000	0.81165	0.00226	0.81391
H	14	0.18609	0.00000	0.81165	0.00226	0.81391
C	15	-0.56909	1.99938	4.55883	0.01088	6.56909
H	16	0.19839	0.00000	0.80045	0.00116	0.80161
H	17	0.19201	0.00000	0.80632	0.00167	0.80799
H	18	0.19201	0.00000	0.80632	0.00167	0.80799
* Total *		0.00000	29.99458	39.86313	0.14230	70.00000

C. Appendix Chapter 4

C.1. ESI-FT-ICR-MS experiments

ESI-FT-ICR-MS measurements/data acquisition. Fragments of fresh meteoritic NWA 7325, Maribo, Soltmany and Chelyabinsk interior were first washed by stirring for a few seconds within the extraction solvent (methanol, LC-MS grade; Fluka) before crushing in 1 mL solvent poured into the corresponding agate mortar. This procedure was shown to limit the number of peaks resulting from terrestrial and human contamination, for example fatty acids arising from sample handling. The mixture (suspension) was transferred into an Eppendorf vial and underwent ultrasonic cleaning for <10 min and then was centrifuged. The supernatant liquid was removed with a microsyringe, ready for flow injection into the ESI source. A solvent methanolic blank was measured in accordance to be able to detect indigenous meteoritic (metal)organic matter in each sample. Organomagnesium compounds were absent in blank spectra.

The experimental study was performed on a high-field FT-ICR mass spectrometer from Bruker Daltonics with a 12-T magnet from Magnex. A time-domain transient with 4 MWords was obtained and Fourier-transformed into a frequency domain spectrum. The frequency domain was afterward converted to a mass spectrum by the solariX control program of Bruker Daltonics. The ion excitations were generated in broadband mode (frequency sweep radial ion excitation) and 3,000 scans were accumulated for each mass spectrum in a mass range of 147-1,000 amu. Ions were accumulated for 300 ms before ICR ion detection. The pressure in the quadrupole/hexapole and ICR vacuum chamber was 3×10^{-6} mbar and 6×10^{-10} mbar, respectively. For CID-MS/MS, ions were accumulated for 3 s.

This chapter has been submitted for publication.

C.1 ESI-FT-ICR-MS experiments

The ESI source (Apollo II; Bruker Daltonics) was used in negative ionization mode. The methanolic solutions were injected directly into the ionization source by means of a microliter pump at a flow rate of $120 \mu\text{L} \cdot \text{h}^{-1}$. A source heating temperature of 200°C was maintained and no nozzle-skimmer fragmentation was performed in the ionization source. The instrument was previously externally calibrated by using arginine negative cluster ions ($5 \text{ mg} \cdot \text{L}^{-1}$ arginine in methanol).

FT-ICR-MS data analysis. FT-ICR mass spectra with m/z from 147 to 1,000 amu were calibrated externally and internally to preclude alignment errors. Subsequently, the mass spectra were exported to peak lists at a signal-to-noise ratio ≥ 3 . Elemental formulas were calculated combinatorially within a mass accuracy window of ± 0.2 ppm for each peak in batch mode by an in-house software tool and validated via the senior-rule approach/cyclomatic number [92], assuming valence 4 (coordination number) for Mg.

The investigation of odd/even fluctuation of experimental mass spectrometric CHOMg and CHO intensities (Fig. 4.1) requires extensive data analytical treatment. First, m/z intensities were lg-transformed and second, $\lg(\text{intensity})$ was normalized according Euclidean norm. This enables valid comparison of odd/even chain length alternation. Therefore, artificial odd/even fluctuations based on different absolute values of MS intensities can be ruled when extracting stability alternation effects for differently processed meteorites. Data analytical transformations is shown in Fig. C.1. Fig. 4.1 discusses the experimental odd/even alternation within alkyl chains for CHO and CHOMg. Therein, $\Delta(\lg(\text{intensity}_{\text{normalized}}))$ is calculated in analogy to concept of incremental binding energy [224]. $\Delta(\lg(\text{intensity}_{\text{normalized}}))$ is calculated by subtracting logarithmic mass spectrometric intensities, as normalized to Euclidean norm, of adjacent C_nHO and C_{n-1} molecules (and $\text{HO C}_n\text{HOMg}$ and $\text{C}_{n-1}\text{HOMg}$, respectively), as shown in Eq. C.1.

$$\Delta(\lg(\text{intensity}_{\text{normalized}})) = \lg(i_{\text{normalized}(\text{C}_n\text{HO})}) - \lg(i_{\text{normalized}(\text{C}_{n-1}\text{HO})}) \quad (\text{C.1})$$

C.1 ESI-FT-ICR-MS experiments

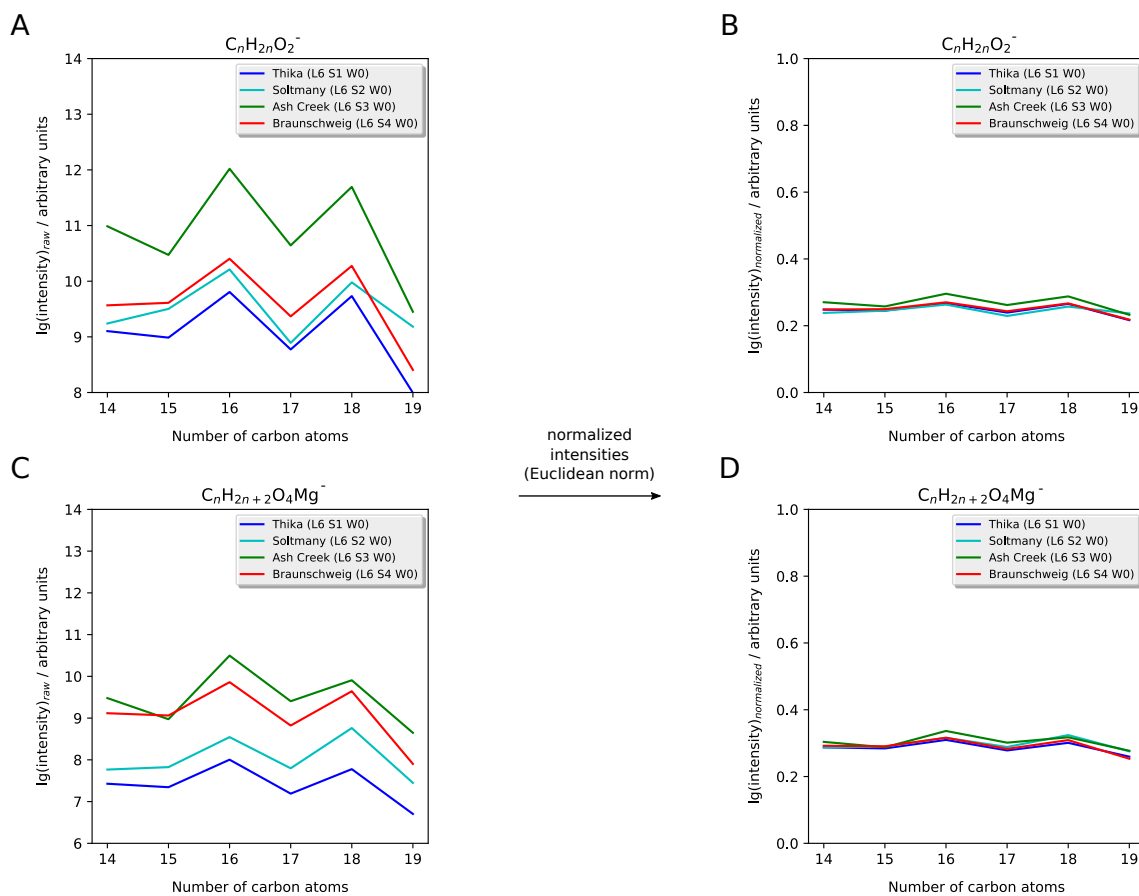


Figure C.1: Data analysis of experimental meteoritic FT-ICR-MS data. $CHOMg$ (A, B) and CHO homologues series were normalized according the Euclidean norm to enable valid comparison of odd/even chain length alternation.

C.2. Computational methods

Linear relaxed and transition states geometries. The electronic structure computations were performed on a stand-alone computer (one node server system) by state-of-the-art quantum chemical computations, based on density functional theory (DFT, hybrid functional B3LYP) level of theory, as implemented within the Gaussian 09 program [244]. These orthogonal quantum chemical methods were used to gain unbiased insights into the stability of dihydroxymagnesium carboxylates regarding the carbon chain fragmentation.

For geometry optimization, the Berny analytical gradient optimization routines [232, 233] were used in combination with the GDIIS algorithm [234]. The requested convergence value in the density matrix was 10^{-8} , the threshold value for maximum displacement was 0.0018 Å, and the threshold value for the maximum force was 0.00045 Hartree Bohr⁻¹. The nature of the stationary points was established by calculating and diagonalizing the Hessian matrix (force-constant matrix). All geometry optimizations were performed with 6-31+G(d,p) basis set. Additionally, frequency calculations were computed for each optimized geometry to identify both, local relaxed energy minima and transition state geometries, also with 6-31+G(d,p) basis set. Detecting imaginary frequencies implies that the optimized geometry is not fully relaxed as a stationary point on the potential energy surface (PES). Transition structures were characterized in detail through normal-mode analysis (frequency analysis). The transition vector, which is associated to a single imaginary frequency has been determined in each found transition state (1st order saddle points on the PES). This vector represents the eigenvector, which is associated with the unique negative eigenvalue of the force constant matrix. This indicates that the found structure corresponds to a first order saddle point (transition state). In order to further check that the transition state found actually connects two energy minima structures with each other (reactant with product), intrinsic reaction coordinate (IRC) analyses [245] in all the transition state geometries found were performed in mass-weighted internal coordinates [246]. C₂H₄ fragmentation was computed with 6-311+G(2d,p) // 6-31+G(d,p) basis set.

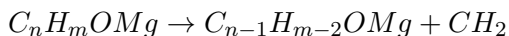
Total Gibbs free energies G of each molecular system was computed as sum of thermal and electronic free energies, corrected by a scaled zero-point vibrational energy, ZPVE, expressed as Zero-point corrections, ZPC) of respective C-, H-, O-, Mg-bearing species (Equation C.2).

$$G = G_{corr} - ZPC + ZPC \cdot f_{anharmonicities} + SPE \quad (C.2)$$

ZPC was obtained by performing frequency analysis computations. Resulting ZPC values were scaled by a factor $f_{anharmonicities}$ of 0.9804 to correct for vibrational anharmonicities [230]. Single-point energies (SPE) were computed via implementing d-polarization functions for each heavy atom and 1p for each hydrogen atom in all B3LYP-DFT computations (6-311+G(2d,p) basis set). The use of diffuse functions was important to represent the correct geometry and thermodynamic properties of anionic species [231]. Stability tests were performed in all cases to ensure that the used wave function represents the lowest energy solution of the self-consistent field (SCF) equations. All molecular systems were treated as restricted shell systems.

Thermodynamic fragmentation energy ΔE_F for methylene release fragmentation

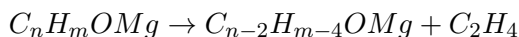
C.2 Computational methods



was defined according to Eq.C.3, namely the difference between the sum of infinitely separated products and the reactant. Products were CH_2 and $CHOMg$ ($-CH_2$), whereas reactants were $CHOMg$ molecules probed for their stability.

$$\Delta E_F = \sum G_{products} - G_{reactant} \quad (C.3)$$

Transition state energy barriers for C_2H_4 fragmentation



between a transition state and its connected relaxed local minimum on the potential energy surface along ethylene release intrinsic reaction coordinate in the gas phase were calculated as Eq. C.4:

$$Energy\ barrier = E_{transition\ state} - E_{local\ minimum\ structure} \quad (C.4)$$

Pseudocyclic geometries. Pseudocyclic geometries were optimized via DFT, at M06-2X/def2TZVP level of theory. Additionally, pseudocyclic systems were corrected for dispersion effects after Grimme et al. [226] with the original D3 damping function. M06-2X functional has been employed as it has been demonstrated to describe noncovalent interactions reliably [227]. Actually, the implementation of noncovalent-considering functional with dispersion correction is necessary, since B3LYP-DFT/6-311+G(2d,p) results failed to describe accurate odd/even alternation effects for pseudocyclic $CHOMg$ molecular systems. Resulting total Gibbs free energies G were computed, according Eq. C.2. Thermal and electronic free energies were computed on M06-2X/def2TZVP-D3 level of theory.

To probe the investigated pseudocyclic systems for stability, we adopted the concept of incremental binding energy [224], labeled as ΔE_I . Here, ΔE_I is defined by comparing total Gibbs free energies of adjacent molecules C_nHOMg and $C_{n-1}HOMg$ within a homologous series and gives therefore insights into stability fluctuations as a function the homologous series' sub-unit, like CH_2 here. For simplification and clarity, dihydroxymagnesium carboxylates $[(OH)_2MgO_2CR]^-$ with $R = \text{hydrocarbon } C_xH_y$ and $\{x,y\} \in \mathbb{N}$ are acronymed as C_nHOMg with integer n . ΔE_I is calculated by subtracting total Gibbs free energy differences of adjacent C_nHOMg and $C_{n-1}HOMg$ molecules, as shown in Eq. C.5.

$$\Delta E_I = G(C_nHOMg) - G(C_{n-1}HOMg) \quad (C.5)$$

All geometries of computed electronic structures were visualized either via the GaussView [247] program and all computations are referred to gas-phase conditions.

C.3 Coordinates of representative computed pseudocyclic organomagnesium structures

C.3. Coordinates of representative computed pseudocyclic organomagnesium structures

Table C.1: Coordinates of the relaxed geometry of pseudocyclic C₁₄-dihydroxymagnesium carboxylate, as computed on M06-2X/def2TZVP-D3 level of theory

Atom	xyz coordinates		
C	-5.1925	-1.13963	0.49052
C	-0.1844	-1.55447	-0.04983
C	-5.38809	0.38092	0.40789
C	-0.70557	2.05106	-0.61948
H	-6.14203	-1.6036	0.20863
H	-6.282	0.62371	0.98938
H	-5.61784	0.65218	-0.62921
H	-0.22051	-0.59839	0.47896
H	-0.68312	1.11335	-1.18936
H	-0.94505	2.83845	-1.34449
H	0.01934	-2.30625	0.71759
H	-5.01642	-1.41781	1.53609
C	-1.53422	-1.81822	-0.70524
H	-1.54281	-2.80235	-1.188
H	-1.68344	-1.08665	-1.5087
C	-1.81101	1.96121	0.42602
H	-1.50643	1.24124	1.19475
H	-1.91752	2.92238	0.94154
C	0.96459	-1.50866	-1.04151
C	2.28233	-1.04329	-0.44432
O	2.32066	-0.66448	0.75435
O	3.30256	-1.03215	-1.17849
H	1.13741	-2.48054	-1.51115
H	0.73743	-0.8174	-1.86041
Mg	4.35486	-0.21735	0.45369
O	5.59276	-1.37038	1.25028
H	5.46851	-2.31815	1.25148
O	4.62229	1.63718	0.33816
H	5.43069	2.0027	0.69605
C	0.67968	2.29188	-0.03056
H	0.90988	1.49912	0.68769
H	0.67507	3.2303	0.53446
C	-2.69113	-1.70528	0.28132
H	-2.62785	-2.51087	1.02022
H	-2.56251	-0.78073	0.84647
C	-3.15203	1.52733	-0.15503
H	-2.98836	0.63581	-0.76295
H	-3.52225	2.29061	-0.84809
C	-4.07283	-1.73057	-0.3757
H	-4.31821	-2.76568	-0.63054
H	-4.03809	-1.19199	-1.32885
C	-4.22315	1.24801	0.90174
H	-3.76512	0.76893	1.77329
H	-4.61101	2.2048	1.26312
C	1.77605	2.32765	-1.0867
H	2.76783	2.40747	-0.63434
H	1.76999	1.40716	-1.67781
H	1.62361	3.1615	-1.77923

C.3 Coordinates of representative computed pseudocyclic organomagnesium structures

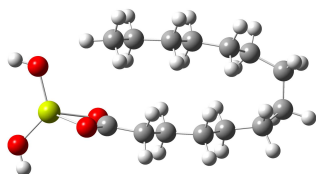
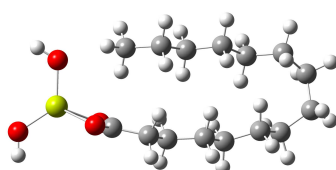


Table C.2: Coordinates of the relaxed geometry of pseudocyclic C₁₅-dihydroxymagnesium carboxylate, as computed on M06-2X/def2TZVP-D3 level of theory

Atom	xyz coordinates		
C	5.77032	-0.90798	-0.14308
C	-0.52816	-1.64158	-0.12923
C	5.82546	0.62542	-0.20275
C	-0.35692	2.11096	0.44891
H	5.85444	-1.22542	0.90285
H	5.82368	0.938	-1.25349
H	6.7947	0.92988	0.2021
H	-0.54906	-0.67432	-0.63869
H	-0.48843	1.17111	0.99785
H	-0.28735	2.89929	1.20648
H	-0.70884	-2.39179	-0.90453
H	6.66604	-1.2828	-0.64623
C	0.83784	-1.85273	0.50952
H	0.85217	-2.79287	1.07294
H	0.99558	-1.0573	1.24793
C	0.95004	2.04542	-0.33313
H	0.89331	1.20376	-1.03393
H	1.04693	2.94472	-0.95267
C	-1.64919	-1.67241	0.89588
C	-2.97484	-1.11375	0.4086
O	-3.05327	-0.60108	-0.7365
O	-3.95601	-1.14587	1.19407
H	-1.8285	-2.68239	1.27317
H	-1.37945	-1.0733	1.77187
Mg	-4.96601	0.08469	-0.17322
O	-6.47173	-0.63304	-1.01389
H	-6.55563	-1.56641	-1.20115
O	-4.7862	1.88685	0.31271
H	-5.52656	2.48475	0.21992
C	-1.56208	2.34986	-0.45159
H	-1.63805	1.56295	-1.20552
H	-2.51195	2.34894	0.08853
H	-1.46154	3.30845	-0.96934
C	1.99401	-1.8325	-0.48386
H	1.98047	-2.73948	-1.09798
H	1.848	-0.99632	-1.17697
C	2.19731	1.89046	0.52965
H	2.03754	1.07845	1.24896
H	2.35273	2.79613	1.12704
C	3.3463	-1.67546	0.19925
H	3.51442	-2.51243	0.8859
H	3.3031	-0.78557	0.82957

C.4 Coordinates of representative computed structures regarding thermodynamic fragmentation energy simulations

C	4.53313	-1.57178	-0.7613
H	4.79305	-2.57695	-1.10486
H	4.24019	-1.01924	-1.65977
C	3.44393	1.58519	-0.29173
H	3.24326	0.69592	-0.89124
H	3.61476	2.39134	-1.01358
C	4.71438	1.38282	0.53688
H	5.0872	2.3641	0.84399
H	4.47447	0.85599	1.46618



C.4. Coordinates of representative computed structures regarding thermodynamic fragmentation energy simulations

Table C.3: Coordinates of the relaxed geometry of linear C₁₄-dihydroxymagnesium carboxylate, as computed on B3LYP/6-311+G(2d,p) level of theory

Atom	xyz coordinates		
C	4.12316	1.17954	-0.17714
C	5.49220	0.50747	-0.08887
O	5.58565	-0.70124	0.28719
O	6.52011	1.19544	-0.37916
H	4.10548	1.77102	-1.10097
H	4.08048	1.90900	0.64456
Mg	7.71883	-0.51279	0.09503
O	8.46656	-1.34092	-1.45693
H	9.21603	-1.93886	-1.38380
O	8.58679	-0.43847	1.79619
H	9.52490	-0.63006	1.88396
C	2.92681	0.22794	-0.10444
H	3.01011	-0.37910	0.80444
H	2.97856	-0.48093	-0.94108
C	1.57733	0.95797	-0.12903
H	1.50975	1.57562	-1.03771
H	1.52695	1.65953	0.71766
C	0.36737	0.01561	-0.07268
H	0.43478	-0.60416	0.83332
H	0.41391	-0.68265	-0.92115
C	-0.98407	0.74237	-0.08920
H	-1.03056	1.43893	0.76111
H	-1.04991	1.36430	-0.99441
C	-2.19465	-0.19921	-0.03574
H	-2.12715	-0.82434	0.86675
H	-2.15180	-0.89250	-0.88857
C	-3.54495	0.52986	-0.04473
H	-3.58852	1.22095	0.80998

C.4 Coordinates of representative computed structures regarding thermodynamic fragmentation energy simulations

H	-3.61145	1.15735	-0.94583
C	-4.75613	-0.41105	0.00502
H	-4.71441	-1.10038	-0.85105
H	-4.68908	-1.04026	0.90471
C	-6.10554	0.31964	-0.00037
H	-6.14810	1.00728	0.85707
H	-6.17177	0.95062	-0.89894
C	-7.31720	-0.62080	0.04616
H	-7.27549	-1.30760	-0.81194
H	-7.25086	-1.25259	0.94410
C	-8.66624	0.11034	0.04228
H	-8.70964	0.79633	0.90114
H	-8.73329	0.74319	-0.85506
C	-9.87843	-0.82949	0.08693
H	-9.83588	-1.51445	-0.77143
H	-9.81242	-1.46161	0.98352
C	-11.22176	-0.09034	0.08280
H	-12.06497	-0.78939	0.11616
H	-11.30860	0.57761	0.94829
H	-11.33334	0.52305	-0.81947

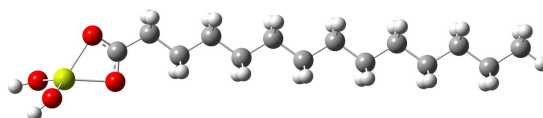


Table C.4: Coordinates of the relaxed geometry of linear C₁₅-dihydroxymagnesium carboxylate, as computed on B3LYP/6-311+G(2d,p) level of theory

Atom	xyz coordinates		
C	4.75137	1.17475	-0.12907
C	6.11036	0.47989	-0.06482
O	6.18429	-0.74853	0.2458
O	7.14989	1.16804	-0.31003
H	4.74191	1.79475	-1.03429
H	4.72049	1.87952	0.71427
Mg	8.3211	-0.58066	0.07599
O	9.06531	-1.33355	-1.51554
H	9.80581	-1.94537	-1.47181
O	9.18071	-0.61555	1.7827
H	10.11538	-0.82626	1.86309
C	3.54089	0.23952	-0.08557
H	3.6122	-0.39404	0.80615
H	3.5845	-0.44651	-0.94137
C	2.20235	0.9899	-0.09277
H	2.14591	1.63247	-0.98477
H	2.16033	1.66936	0.77222
C	0.97881	0.06403	-0.06377
H	1.03424	-0.57933	0.82646
H	1.01818	-0.61327	-0.92942
C	-0.36214	0.81017	-0.06615
H	-0.40134	1.48657	0.80067
H	-0.41641	1.4547	-0.95617

C.4 Coordinates of representative computed structures regarding thermodynamic fragmentation energy simulations

C	-1.58591	-0.1153	-0.03873
H	-1.53063	-0.76203	0.84925
H	-1.54944	-0.78927	-0.90721
C	-2.92594	0.63254	-0.03571
H	-2.96298	1.30486	0.83415
H	-2.98049	1.28095	-0.92268
C	-4.15011	-0.2924	-0.01098
H	-4.11444	-0.96346	-0.88171
H	-4.09533	-0.94193	0.87497
C	-5.48936	0.45679	-0.00545
H	-5.5257	1.12652	0.86634
H	-5.54349	1.10767	-0.89054
C	-6.71386	-0.46772	0.01678
H	-6.67826	-1.13677	-0.85547
H	-6.65976	-1.11921	0.90131
C	-8.05271	0.28219	0.02347
H	-8.08879	0.9505	0.89634
H	-8.10648	0.93439	-0.86064
C	-9.27741	-0.64189	0.04419
H	-9.24246	-1.31038	-0.82871
H	-9.22489	-1.29447	0.9282
C	-10.61656	0.10744	0.05085
H	-10.65245	0.77455	0.92349
H	-10.66959	0.75942	-0.83231
C	-11.83414	-0.82411	0.07063
H	-12.77277	-0.25874	0.07484
H	-11.84445	-1.48025	-0.80806
H	-11.82751	-1.46517	0.96043

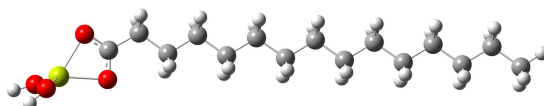


Table C.5: Coordinates of the relaxed geometry of methylene CH_2 , as computed on B3LYP/6-311+G(2d,p) level of theory

Atom	xyz coordinates		
C	0.00000	0.17680	0.00000
H	0.86304	-0.53039	0.00000
H	-0.86304	-0.53039	0.00000



Table C.6: Coordinates of the relaxed geometry of ethylene C_2H_4 , as computed on B3LYP/6-311+G(2d,p) level of theory

Atom	xyz coordinates		
C	0.66716	0.00000	-0.00000
H	1.23836	-0.92471	0.00000

C.4 Coordinates of representative computed structures regarding thermodynamic fragmentation energy simulations

H	1.23835	0.92471	0.00000
C	-0.66717	0.00000	0.00000
H	-1.23834	-0.92472	0.00000
H	-1.23834	0.92472	0.00000



Table C.7: Coordinates of the transition state geometry of ethylene C_2H_4 release out of C_5 -dihydroxymagnesium carboxylate, as computed on B3LYP/6-31+G(d,p) level of theory

Atom	xyz coordinates		
C	4.07193	-0.44866	0.11791
H	3.91653	-0.90033	-0.85878
H	3.76984	-1.08229	0.94847
C	5.27939	0.35819	0.28755
H	5.76564	0.79002	-0.57793
H	3.82287	0.73532	0.19212
H	5.6125	0.63384	1.28003
C	-0.16558	-0.25301	-0.30784
O	-0.96679	-0.37256	-1.28249
O	-0.56393	0.04963	0.85814
Mg	-2.56903	0.07953	0.08417
O	-3.59022	-1.47282	0.51974
H	-4.48925	-1.4063	0.85361
O	-3.27189	1.84691	-0.06949
H	-4.2193	2.00763	-0.09749
C	2.23396	0.50095	0.11513
H	2.27763	1.45254	-0.43256
H	1.99621	0.67032	1.16751
C	1.32862	-0.51881	-0.53928
H	1.52599	-1.51602	-0.11513
H	1.50245	-0.5805	-1.61793



Bibliography

- (1) De Becker, M. *arXiv preprint arXiv:1305.6243* **2013**.
- (2) Molecules in the Interstellar Medium or Circumstellar Shells., <http://www.astro.uni-koeln.de/cdms/molecules/> (accessed 11/24/2017).
- (3) Atacama Large Millimeter/submillimeter Array., <http://almascience.eso.org/> (accessed 11/25/2017).
- (4) Anglada, G.; Amado, P. J.; Ortiz, J. L.; Gómez, J. F.; Macías, E.; Alberdi, A.; Osorio, M.; Gómez, J. L.; de Gregorio-Monsalvo, I.; Pérez-Torres, M. A., et al. *The Astrophysical Journal Letters* **2017**, *850*, L6.
- (5) Cordiner, M.; Biver, N.; Crovisier, J.; Bockelée-Morvan, D.; Mumma, M.; Charnley, S.; Villanueva, G.; Paganini, L.; Lis, D.; Milam, S., et al. *The Astrophysical Journal* **2017**, *837*, 177.
- (6) Andrews, S. M.; Wilner, D. J.; Zhu, Z.; Birnstiel, T.; Carpenter, J. M.; Pérez, L. M.; Bai, X.-N.; Öberg, K. I.; Hughes, A. M.; Isella, A., et al. *The Astrophysical Journal Letters* **2016**, *820*, L40.
- (7) Herschel Space Observatory., <http://sci.esa.int/herschel/> (accessed 11/25/2017).
- (8) Bergin, E. A.; Cleeves, L. I.; Gorti, U.; Zhang, K.; Blake, G. A.; Green, J. D.; Andrews, S. M.; Evans II, N. J.; Henning, T.; Öberg, K., et al. *Nature* **2013**, *493*, 644–646.
- (9) Schmitt-Kopplin, P.; Gabelica, Z.; Gougeon, R. D.; Fekete, A.; Kanawati, B.; Harir, M.; Gebefuegi, I.; Eckel, G.; Hertkorn, N. *Proceedings of the National Academy of Sciences* **2010**, *107*, 2763–2768.
- (10) Schmitt-Kopplin, P.; Harir, M.; Kanawati, B.; Gougeon, R.; Moritz, F.; Hertkorn, N.; Clary, S.; Gebefügi, I.; Gabelica, Z. *Astrobiology: an evolutionary approach*. CRC Press, Florida **2014**, 63–80.
- (11) Cordes, E. H., *The tao of chemistry and life: a scientific journey*; Oxford University Press: 2009.
- (12) Markert, B.; Fränzle, S.; Wünschmann, S., *Chemical Evolution: The Biological System of the Elements*; Springer: 2015.
- (13) Gerner, T.; Beuther, H.; Semenov, D.; Linz, H.; Vasyunina, T.; Bihr, S; Shirley, Y.; Henning, T. *Astronomy & Astrophysics* **2014**, *563*, A97.
- (14) Cronin, J.; Cooper, G.; Pizzarello, S *Advances in Space Research* **1995**, *15*, 91–97.
- (15) Sephton, M. A. *Astronomy & Geophysics* **2004**, *45*, 2–8.
- (16) Lauretta, D. S.; McSween, H. Y., *Meteorites and the early solar system II*; University of Arizona Press: 2006.
- (17) Pizzarello, S.; Shock, E. *Cold Spring Harbor perspectives in biology* **2010**, *2*, a002105.
- (18) Shaw, A. M., *Astrochemistry: from astronomy to astrobiology*; John Wiley & Sons: 2007.
- (19) Rosetta - rendezvous with a comet., <http://rosetta.esa.int/> (accessed 11/25/2017).
- (20) Altwegg, K.; Balsiger, H.; Bar-Nun, A.; Berthelier, J.-J.; Bieler, A.; Bochsler, P.; Briois, C.; Calmonte, U.; Combi, M. R.; Cottin, H., et al. *Science advances* **2016**, *2*, e1600285.
- (21) Fray, N.; Bardyn, A.; Cottin, H.; Altwegg, K.; Baklouti, D.; Briois, C.; Colangeli, L.; Engrand, C.; Fischer, H.; Glasmachers, A., et al. *Nature* **2016**, *538*, 72–74.
- (22) Gerlich, D; Smith, M *Physica Scripta* **2005**, *73*, C25.
- (23) Danger, G.; Bossa, J.-B.; De Marcellus, P.; Borget, F.; Duvernay, F.; Theulé, P.; Chiavassa, T.; d'Hendecourt, L. *Astronomy & Astrophysics* **2011**, *525*, A30.
- (24) Borget, F.; Duvernay, F.; Danger, G.; Theulé, P.; Vinogradoff, V.; Mispelaer, F.; Müller, S.; Grote, D.; Chiavassa, T.; Bossa, J.-B. *Journal of Physical Organic Chemistry* **2015**, *28*, 163–169.
- (25) Sellgren, K. *Spectrochimica Acta Part A: Molecular and Biomolecular Spectroscopy* **2001**, *57*, 627–642.
- (26) Fresneau, A; Mrad, N. A.; d'Hendecourt, L. L.; Duvernay, F; Flandinet, L; Orthous-Daunay, F.-R.; Vuitton, V; Thissen, R; Chiavassa, T; Danger, G *The Astrophysical Journal* **2017**, *837*, 168.

Bibliography

- (27) Marov, M. Y., *Fundamentals of Modern Astrophysics*; Springer: 2016.
- (28) Cabrit, S Shocks in Astrophysics, ed. TJ Millar, & AC Raga., 1995.
- (29) Pizzarello, S.; Davidowski, S. K.; Holland, G. P.; Williams, L. B. *Proceedings of the National Academy of Sciences* **2013**, *110*, 15614–15619.
- (30) Remusat, L. *European Astronomical Society Publications Series* **2012**, *58*, 175–186.
- (31) Lodders, K. *The Astrophysical Journal* **2003**, *591*, 1220.
- (32) Alexander, C. M.; Howard, K. T.; Bowden, R.; Fogel, M. L. *Geochimica et Cosmochimica Acta* **2013**, *123*, 244–260.
- (33) Swindle, T. D.; Campins, H. *Meteoritics & Planetary Science* **2004**, *39*, 1733–1740.
- (34) Campins, H.; Swindle, T. D. *Meteoritics & Planetary Science* **1998**, *33*, 1201–1211.
- (35) Anders, E. *Icarus* **1975**, *24*, 363–371.
- (36) Campins, H; Swindle, T. In *Lunar and Planetary Science Conference*, 1998; Vol. 29.
- (37) Taylor, A.; Baggaley, W.; Steel, D. *Nature* **1996**, *380*, 323–325.
- (38) Greenberg, J. M.; Hage, J. *The Astrophysical Journal* **1990**, *361*, 260–274.
- (39) Gounelle, M.; Morbidelli, A.; Bland, P. A.; Spurny, P; Young, E. D.; Sephton, M. *The solar system beyond Neptune* **2008**, 525–541.
- (40) Weisberg, M. K.; McCoy, T. J.; Krot, A. N. *Meteorites and the early solar system II* **2006**, *19*.
- (41) Bouvier, A.; Wadhwa, M. *Nature geoscience* **2010**, *3*, 637–641.
- (42) Robert, F. *Meteorites and the early solar system II* **2006**, *943*, 341–351.
- (43) UNGROUPED MAFIC ACHONDRITE NORTHWEST AFRICA 7325: A REDUCED, IRON-POOR CUMULATE OLIVINE GABBRO FROM A DIFFERENTIATED PLANETARY PARENT BODY, 44th Lunar and Planetary Science Conference (2013)., <https://www.lpi.usra.edu/meetings/lpsc2013/pdf/2164.pdf> (accessed 11/26/2017).
- (44) Green Meteorite's Age Casts Doubt on Possible Mercury Origin., <https://www.space.com/20547-mercury-meteorite-mystery-age.html> (accessed 11/26/2017).
- (45) Greenish rock may be first meteorite from Mercury., http://www.nbcnews.com/id/50712511/ns/technology_and_science-space/t/greenish-rock-may-be-first-meteorite-mercury/#.Whr_MXWGOP8 (accessed 11/26/2017).
- (46) Murchison fall - Meteoritical Bulletin Database., <https://www.lpi.usra.edu/meteor/metbull.php?code=16875> (accessed 11/26/2017).
- (47) Cronin, J. R.; Pizzarello, S.; Frye, J. S. *Geochimica et Cosmochimica Acta* **1987**, *51*, 299–303.
- (48) Remusat, L.; Palhol, F.; Robert, F.; Derenne, S.; France-Lanord, C. *Earth and Planetary Science Letters* **2006**, *243*, 15–25.
- (49) Cody, G. D.; Alexander, C. M. *Geochimica et Cosmochimica Acta* **2005**, *69*, 1085–1097.
- (50) Busemann, H.; Alexander, M.; Nittler, L. R. *Meteoritics & Planetary Science* **2007**, *42*, 1387–1416.
- (51) Quirico, E.; Orthous-Daunay, F.-R.; Beck, P.; Bonal, L.; Brunetto, R.; Dartois, E.; Pino, T.; Montagnac, G.; Rouzaud, J.-N.; Engrand, C., et al. *Geochimica et Cosmochimica Acta* **2014**, *136*, 80–99.
- (52) Derenne, S.; Robert, F. *Meteoritics & Planetary Science* **2010**, *45*, 1461–1475.
- (53) Bonal, L.; Quirico, E.; Bourot-Denise, M.; Montagnac, G. *Geochimica et Cosmochimica Acta* **2006**, *70*, 1849–1863.
- (54) Bonal, L.; Quirico, E.; Flandinet, L.; Montagnac, G. *Geochimica et Cosmochimica Acta* **2016**, *189*, 312–337.
- (55) Sephton, M. A. *Natural product reports* **2002**, *19*, 292–311.
- (56) Watson, J. S.; Pearson, V. K.; Gilmour, I.; Sephton, M. A. *Organic Geochemistry* **2003**, *34*, 37–47.

Bibliography

- (57) Aerts, J.; Elsaesser, A.; Röling, W.; Ehrenfreund, P. *Meteoritics & Planetary Science* **2016**, *51*, 920–931.
- (58) Kebukawa, Y.; Nakashima, S.; Otsuka, T.; NAKAMURA-MESSENGER, K.; Zolensky, M. E. *Meteoritics & Planetary Science* **2009**, *44*, 545–557.
- (59) Elsila, J. E.; Callahan, M. P.; Glavin, D. P.; Dworkin, J. P.; Brückner, H. *Astrobiology* **2011**, *11*, 123–133.
- (60) Martins, Z.; Botta, O.; Fogel, M. L.; Sephton, M. A.; Glavin, D. P.; Watson, J. S.; Dworkin, J. P.; Schwartz, A. W.; Ehrenfreund, P. *Earth and planetary science Letters* **2008**, *270*, 130–136.
- (61) President Clinton Statment Regarding Mars Meteorite Discovery., <https://www2.jpl.nasa.gov/snc/clinton.html> (accessed 11/26/2017).
- (62) McKay, D. S.; Gibson, E. K.; Thomas-Keprta, K. L.; Vali, H.; Romanek, C. S.; Clemett, S. J.; Chillier, X. D. F.; Maechling, C. R.; Zare, R. N. *Science* **1996**, *273*, 924–930, DOI: 10.1126/science.273.5277.924.
- (63) Barrat, J.; Gillet, P.; Lesourd, M.; BLICHERT-TOFT, J.; Poupeau, G. *Meteoritics & Planetary Science* **1999**, *34*, 91–97.
- (64) Kvenvolden, K.; Lawless, J.; Pering, K.; Peterson, E.; Flores, J.; Ponnampertuma, C.; Kaplan, I. R.; Moore, C. *Nature* **1970**, *228*, 923–926.
- (65) Callahan, M. P.; Smith, K. E.; Cleaves, H. J.; Ruzicka, J.; Stern, J. C.; Glavin, D. P.; House, C. H.; Dworkin, J. P. *Proceedings of the National Academy of Sciences* **2011**, *108*, 13995–13998.
- (66) Cooper, G.; Kimmich, N.; Belisle, W.; Sarinana, J.; Brabham, K.; Garrel, L. *Nature* **2001**, *414*, 879–883.
- (67) Pasek, M. A. *Proceedings of the National Academy of Sciences* **2008**, *105*, 853–858.
- (68) Pasek, M. A.; Lauretta, D. S. *Astrobiology* **2005**, *5*, 515–535.
- (69) De Graaf, R.; Visscher, J.; Schwartz, A. W. *Journal of molecular evolution* **1997**, *44*, 237–241.
- (70) Pasek, M. A.; Dworkin, J. P.; Lauretta, D. S. *Geochimica et Cosmochimica Acta* **2007**, *71*, 1721–1736.
- (71) Pasek, M.; Herschy, B.; Kee, T. P. *Origins of Life and Evolution of Biospheres* **2015**, *45*, 207–218.
- (72) Naraoka, H.; Shimoyama, A.; Harada, K. *Origins of Life and Evolution of the Biosphere* **1999**, *29*, 187–201.
- (73) Huang, Y.; Wang, Y.; Alexandre, M. R.; Lee, T.; Rose-Petruck, C.; Fuller, M.; Pizzarello, S. *Geochimica et Cosmochimica Acta* **2005**, *69*, 1073–1084.
- (74) Bailey, J. *Acta Astronautica* **2000**, *46*, 627–631.
- (75) Pizzarello, S.; Zolensky, M.; Turk, K. A. *Geochimica et Cosmochimica Acta* **2003**, *67*, 1589–1595.
- (76) Cooper, G.; Rios, A. C. *Proceedings of the National Academy of Sciences* **2016**, *113*, E3322–E3331.
- (77) Bonner, W. A. *Origins of Life and Evolution of Biospheres* **1991**, *21*, 59–111.
- (78) Blackmond, D. G. *Cold Spring Harbor perspectives in biology* **2010**, *2*, a002147.
- (79) Bonner, W. A.; Greenberg, J. M.; Rubenstein, E. *Origins of Life and Evolution of the Biosphere* **1999**, *29*, 215–219.
- (80) Meierhenrich, U., *Amino acids and the asymmetry of life: caught in the act of formation*; Springer Science & Business Media: 2008.
- (81) Meinert, C.; Myrgorodska, I.; De Marcellus, P.; Buhse, T.; Nahon, L.; Hoffmann, S. V.; d’Hendecourt, L. L. S.; Meierhenrich, U. J. *Science* **2016**, *352*, 208–212.
- (82) Marshall, A. G.; Hendrickson, C. L.; Jackson, G. S. *Mass spectrometry reviews* **1998**, *17*, 1–35.
- (83) Nikolaev, E. N.; Kostyukevich, Y. I.; Vladimirov, G. N. *Mass spectrometry reviews* **2016**, *35*, 219–258.
- (84) Makarov, A.; Denisov, E.; Kholomeev, A.; Balschun, W.; Lange, O.; Strupat, K.; Horning, S. *Analytical chemistry* **2006**, *78*, 2113–2120.

Bibliography

- (85) Makarov, A.; Denisov, E.; Lange, O.; Horning, S. *Journal of the American Society for Mass Spectrometry* **2006**, *17*, 977–982.
- (86) Vuitton, V.; Bonnet, J.-Y.; Frisari, M.; Thissen, R.; Quirico, E.; Dutuit, O.; Schmitt, B.; Le Roy, L.; Fray, N.; Cottin, H., et al. *Faraday discussions* **2010**, *147*, 495–508.
- (87) Danger, G.; Fresneau, A.; Mrad, N. A.; De Marcellus, P.; Orthous-Daunay, F.-R.; Duvernay, F.; Vuitton, V.; d'Hendecourt, L. L. S.; Thissen, R.; Chiavassa, T. *Geochimica et Cosmochimica Acta* **2016**, *189*, 184–196.
- (88) Yamashita, Y.; Naraoka, H. *Geochemical Journal* **2014**, *48*, 519–525.
- (89) Orthous-Daunay, F.; Thissen, R.; Vuitton, V.; Moynier, F.; Zinner, E. *Meteoritics and Planetary Science Supplement* **2013**, *76*.
- (90) Naraoka, H.; Yamashita, Y.; Yamaguchi, M.; Orthous-Daunay, F.-R. *ACS Earth and Space Chemistry* **2017**.
- (91) Briois, C.; Thissen, R.; Thirkell, L.; Aradj, K.; Bouabdellah, A.; Boukrara, A.; Carrasco, N.; Chalumeau, G.; Chapelon, O.; Colin, F., et al. *Planetary and Space Science* **2016**, *131*, 33–45.
- (92) Senior, J. K. *American Journal of Mathematics* **1951**, *73*, 663–689.
- (93) Kind, T.; Fiehn, O. *BMC bioinformatics* **2007**, *8*, 105.
- (94) Pellegrin, V. *J. Chem. Educ* **1983**, *60*, 626.
- (95) Koch, B.; Dittmar, T. *Rapid communications in mass spectrometry* **2006**, *20*, 926–932.
- (96) Yassine, M. M.; Harir, M.; Dabek-Zlotorzynska, E.; Schmitt-Kopplin, P. *Rapid Communications in Mass Spectrometry* **2014**, *28*, 2445–2454.
- (97) Schmitt-Kopplin, P.; Harir, M.; Kanawati, B.; Tziozis, D.; Hertkorn, N.; Gabelica, Z. *Meteorites* **2012**, *2*.
- (98) Popova, O. P.; Jenniskens, P.; Emel'yanenko, V.; Kartashova, A.; Biryukov, E.; Khaibrakhmanov, S.; Shuvalov, V.; Rybnov, Y.; Dudorov, A.; Grokhovsky, V. I.; Badyukov, D. D.; Yin, Q.-Z.; Gural, P. S.; Albers, J.; Granvik, M.; Evers, L. G.; Kuiper, J.; Kharlamov, V.; Solovyov, A.; Rusakov, Y. S.; Korotkiy, S.; Serdyuk, I.; Korochantsev, A. V.; Larionov, M. Y.; Glazachev, D.; Mayer, A. E.; Gisler, G.; Gladkovsky, S. V.; Wimpenny, J.; Sanborn, M. E.; Yamakawa, A.; Verosub, K. L.; Rowland, D. J.; Roeske, S.; Botto, N. W.; Friedrich, J. M.; Zolensky, M. E.; Le, L.; Ross, D.; Ziegler, K.; Nakamura, T.; Ahn, I.; Lee, J. I.; Zhou, Q.; Li, X.-H.; Li, Q.-L.; Liu, Y.; Tang, G.-Q.; Hiroi, T.; Sears, D.; Weinstein, I. A.; Vokhmintsev, A. S.; Ishchenko, A. V.; Schmitt-Kopplin, P.; Hertkorn, N.; Nagao, K.; Haba, M. K.; Komatsu, M.; Mikouchi, T.; (the Chelyabinsk Airburst Consortium) en *Science* **Nov. 2013**, *342*, 1069–1073, DOI: 10.1126/science.1242642.
- (99) Haack, H.; Grau, T.; Bischoff, A.; Horstmann, M.; Wasson, J.; SøRensen, A.; Laubenstein, M.; Ott, U.; Palme, H.; Gellissen, M.; Greenwood, R. C.; Pearson, V. K.; Franchi, I. A.; Gabelica, Z.; Schmitt-Kopplin, P. en *Meteoritics & Planetary Science* **Jan. 2012**, *47*, 30–50, DOI: 10.1111/j.1945-5100.2011.01311.x.
- (100) Keil, K.; Zucolotto, M. E.; Krot, A. N.; Doyle, P. M.; Telus, M.; Krot, T. V.; Greenwood, R. C.; Franchi, I. A.; Wasson, J. T.; Welten, K. C.; Caffee, M. W.; Sears, D. W. G.; Riebe, M.; Wieler, R.; dos Santos, E.; Scorzelli, R. B.; Gattacceca, J.; Lagroix, F.; Laubenstein, M.; Mendes, J. C.; Schmitt-Kopplin, P.; Harir, M.; Moutinho, A. L. R. en *Meteoritics & Planetary Science* **June 2015**, *50*, 1089–1111, DOI: 10.1111/maps.12456.
- (101) Van Krevelen, D. *Fuel* **1950**, *29*, 269–284.
- (102) Tziotis, D.; Hertkorn, N.; Schmitt-Kopplin, P. *European Journal of Mass Spectrometry* **2011**, *17*, 415–421.
- (103) Forcisi, S.; Moritz, F.; Lucio, M.; Lehmann, R.; Stefan, N.; Schmitt-Kopplin, P. *Analytical chemistry* **2015**, *87*, 8917–8924.
- (104) Moritz, F.; Kaling, M.; Schnitzler, J.-P.; Schmitt-Kopplin, P. *Plant, cell & environment* **2017**, *40*, 1057–1073.
- (105) Hemmler, D.; Roullier-Gall, C.; Marshall, J. W.; Rychlik, M.; Taylor, A. J.; Schmitt-Kopplin, P. *Scientific Reports* **2017**, *7*.

Bibliography

- (106) Bastian, M.; Heymann, S.; Jacomy, M. **2009**.
- (107) Hayashi, C. In *Data Science, Classification, and Related Methods*; Springer: 1998, pp 40–51.
- (108) Pyne, S.; Rao, B. P.; Rao, S. B., *Big Data Analytics: Methods and Applications*; Springer: 2016.
- (109) Somogyi, Á.; Thissen, R.; Orthous-Daunay, F.-R.; Vuitton, V. *International journal of molecular sciences* **2016**, *17*, 439.
- (110) Liger-Belair, G.; Cilindre, C.; Gougeon, R. D.; Lucio, M.; Gebefügi, I.; Jeandet, P.; Schmitt-Kopplin, P. *Proceedings of the National Academy of Sciences* **2009**, *106*, 16545–16549.
- (111) Rossello-Mora, R.; Lucio, M.; Peña, A.; Brito-Echeverría, J.; López-López, A.; Valens-Vadell, M.; Frommberger, M.; Antón, J.; Schmitt-Kopplin, P. *The ISME journal* **2008**, *2*, 242–253.
- (112) Hertkorn, N.; Harir, M.; Schmitt-Kopplin, P. *Magnetic Resonance in Chemistry* **2015**, *53*, 754–768.
- (113) Calvin, M.; Vaughn, S. K. *Lawrence Berkeley National Laboratory* **1959**.
- (114) Nagy, B.; Meinschein, W. G.; Hennessy, D. J. *Annals of the New York Academy of Sciences* **1963**, *108*, 534–552.
- (115) Kebukawa, Y.; Alexander, C. M.; Cody, G. D. *Geochimica et Cosmochimica Acta* **2011**, *75*, 3530–3541.
- (116) Hutt, L. D.; Glavin, D. P.; Bada, J. L.; Mathies, R. A. *Analytical chemistry* **1999**, *71*, 4000–4006.
- (117) Cooper, G.; Kimmich, N.; Belisle, W.; Sarinana, J.; Brabham, K.; Garrel, L. *Nature* **2001**, *414*, 879–883.
- (118) Meierhenrich, U. J.; Caro, G. M. M.; Bredehöft, J. H.; Jessberger, E. K.; Thiemann, W. H.-P. *Proceedings of the National Academy of Sciences of the United States of America* **2004**, *101*, 9182–9186.
- (119) Cronin, J. R.; Pizzarello, S. *Science* **1997**, *275*, 951–955.
- (120) Cody, G. D.; Alexander, C. O.; Tera, F. *Geochimica et Cosmochimica Acta* **2002**, *66*, 1851–1865.
- (121) Danzer, K., *Analytical chemistry: theoretical and metrological fundamentals*; Springer Science & Business Media: 2007.
- (122) Theodor W. Hänsch - Nobel Lecture: Passion for Precision". Nobelprize.org. Nobel Media AB 2014. Web., http://www.nobelprize.org/nobel_prizes/physics/laureates/2005/hansch-lecture.html (accessed 11/27/2017).
- (123) Moritz, F. Deep Metabotyping of exhaled breath condensate (EBC) – characterization of surrogate markers for systemic metabolism and non-invasive diagnostics in Diabetes., Dissertation, München: Technische Universität München, 2014.
- (124) Jenniskens, P.; Rubin, A. E.; Yin, Q.-Z.; Sears, D. W. G.; Sandford, S. A.; Zolensky, M. E.; Krot, A. N.; Blair, L.; Kane, D.; Utas, J.; Verish, R.; Friedrich, J. M.; Wimpenny, J.; Eppich, G. R.; Ziegler, K.; Verosub, K. L.; Rowland, D. J.; Albers, J.; Gural, P. S.; Grigsby, B.; Fries, M. D.; Matson, R.; Johnston, M.; Silber, E.; Brown, P.; Yamakawa, A.; Sanborn, M. E.; Laubenstein, M.; Welten, K. C.; Nishiizumi, K.; Meier, M. M. M.; Busemann, H.; Clay, P.; Caffee, M. W.; Schmitt-Kopplin, P.; Hertkorn, N.; Glavin, D. P.; Callahan, M. P.; Dworkin, J. P.; Wu, Q.; Zare, R. N.; Grady, M.; Verchovsky, S.; Emel'Yanenko, V.; Naroenkov, S.; Clark, D. L.; Girten, B.; Worden, P. S.; (The Novato Meteorite Consortium) en *Meteorit Planet Sci* **Aug. 2014**, *49*, 1388–1425, DOI: 10.1111/maps.12323.
- (125) Bartoschewitz, R.; Appel, P.; Barrat, J.-A.; Bischoff, A.; Caffee, M. W.; Franchi, I. A.; Gabelica, Z.; Greenwood, R. C.; Harir, M.; Harries, D.; Hochleitner, R.; Hopp, J.; Laubenstein, M.; Mader, B.; Marques, R.; Morlok, A.; Nolze, G.; Prudêncio, M. I.; Rochette, P.; Ruf, A.; Schmitt-Kopplin, P.; Seemann, E.; Szurgot, M.; Tagle, R.; Wach, R. A.; Welten, K. C.; Weyrauch, M.; Wimmer, K. *Chemie der Erde - Geochemistry* **2017**, *77*, 207–224, DOI: <https://doi.org/10.1016/j.chemer.2016.10.004>.

Bibliography

- (126) Jenniskens, P.; Fries, M. D.; Yin, Q.-Z.; Zolensky, M.; Krot, A. N.; Sandford, S. A.; Sears, D.; Beauford, R.; Ebel, D. S.; Friedrich, J. M.; Nagashima, K.; Wimpenny, J.; Yamakawa, A.; Nishizumi, K.; Hamajima, Y.; Caffee, M. W.; Welten, K. C.; Laubenstein, M.; Davis, A. M.; Simon, S. B.; Heck, P. R.; Young, E. D.; Kohl, I. E.; Thiemens, M. H.; Nunn, M. H.; Mikouchi, T.; Hagiya, K.; Ohsumi, K.; Cahill, T. A.; Lawton, J. A.; Barnes, D.; Steele, A.; Rochette, P.; Verosub, K. L.; Gattacceca, J.; Cooper, G.; Glavin, D. P.; Burton, A. S.; Dworkin, J. P.; Elsil, J. E.; Pizzarello, S.; Ogliore, R.; Schmitt-Kopplin, P.; Harir, M.; Hertkorn, N.; Verchovsky, A.; Grady, M.; Nagao, K.; Okazaki, R.; Takechi, H.; Hiroi, T.; Smith, K.; Silber, E. A.; Brown, P. G.; Albers, J.; Klotz, D.; Hankey, M.; Matson, R.; Fries, J. A.; Walker, R. J.; Puchtel, I.; Lee, C.-T. A.; Erdman, M. E.; Eppich, G. R.; Roeske, S.; Gabelica, Z.; Lerche, M.; Nuevo, M.; Girten, B.; Worden, S. P.; (the Sutter's Mill Meteorite Consortium) en *Science* **Dec. 2012**, *338*, 1583–1587, DOI: 10.1126/science.1227163.
- (127) Barone, V.; Biczysko, M.; Puzzarini, C. *Accounts of chemical research* **2015**, *48*, 1413–1422.
- (128) Mendoza, C; Ruetter, F; Martorell, G; Rodriguez, L. *The Astrophysical Journal Letters* **2004**, *601*, L59.
- (129) Fortenberry, R. C. *The Journal of Physical Chemistry A* **2015**, *119*, 9941–9953.
- (130) Koch, W.; Holthausen, M. C., *A chemist's guide to density functional theory*; John Wiley & Sons: 2015.
- (131) Jensen, F., *Introduction to computational chemistry*; John Wiley & Sons: 2017.
- (132) Serra, G; Chaudret, B; Saillard, Y; Le Beuze, A; Rabaa, H; Ristorcelli, I; Klotz, A *Astronomy and Astrophysics* **1992**, *260*, 489–493.
- (133) Fioroni, M. *Computational and Theoretical Chemistry* **2016**, *1084*, 196–212.
- (134) Henning, T., *Astromineralogy*; Springer: 2010; Vol. 815.
- (135) Marty, P.; de Parseval, P.; Klotz, A.; Chaudret, B.; Serra, G.; Boissel, P. *Chemical physics letters* **1996**, *256*, 669–674.
- (136) Bohme, D. K. *Chemical reviews* **1992**, *92*, 1487–1508.
- (137) Prasad, S.; Huntress Jr, W. *The Astrophysical Journal Supplement Series* **1980**, *43*, 1–35.
- (138) Le Guillou, C.; Bernard, S.; Brearley, A. J.; Remusat, L. *Geochimica et Cosmochimica Acta* **2014**, *131*, 368–392.
- (139) Pearson, V. K.; Sephton, M. A.; Kearsley, A. T.; Bland, P. A.; Franchi, I. A.; Gilmour, I. *Meteoritics & Planetary Science* **2002**, *37*, 1829–1833.
- (140) Yesiltas, M.; Kebukawa, Y. *Meteoritics & Planetary Science* **2016**, *51*, 584–595.
- (141) Elschenbroich, C., *Organometallics*; John Wiley & Sons: 2016.
- (142) Schulte, M.; Shock, E. *Meteoritics & Planetary Science* **2004**, *39*, 1577–1590.
- (143) Ehrenfreund, P.; Irvine, W; Becker, L; Blank, J; Brucato, J.; Colangeli, L; Derenne, S; Despois, D; Dutrey, A; Fraaije, H, et al. *Reports on progress in physics* **2002**, *65*, 1427.
- (144) Sephton, M. A.; Botta, O. *International Journal of Astrobiology* **2005**, *4*, 269–276.
- (145) Pizzarello, S. *Chemistry & biodiversity* **2007**, *4*, 680–693.
- (146) Schulze-Makuch, D.; Irwin, L. N., *Life in the universe: expectations and constraints*; Springer Science & Business Media: 2008.
- (147) Schrödinger, E., *Was ist Leben?: die lebende Zelle mit den Augen des Physikers betrachtet*; Piper ebooks: 2017.
- (148) Benner, S. A. *Astrobiology* **2010**, *10*, 1021–1030.
- (149) Cleland, C. E.; Chyba, C. F. *Origins of Life and Evolution of the Biosphere* **2002**, *32*, 387–393.
- (150) Benner, S. A.; Ricardo, A.; Carrigan, M. A. *Current opinion in chemical biology* **2004**, *8*, 672–689.
- (151) McDonough, W. F.; Sun, S.-S. *Chemical geology* **1995**, *120*, 223–253.
- (152) Williams, R. J. *Concepts Models Bioinorg. Chem.* **2006**.

Bibliography

- (153) Moldoveanu, S. In *Pyrolysis of Organic Molecules with Applications to Health and Environmental Issues*, Moldoveanu, S. C., Ed.; Techniques and Instrumentation in Analytical Chemistry Supplement C, Vol. 28; Elsevier: 2010, pp 471–526, DOI: [https://doi.org/10.1016/S0167-9244\(09\)02817-0](https://doi.org/10.1016/S0167-9244(09)02817-0).
- (154) Navarro-González, R; Ponnampereuma, C *Advances in Space Research* **1995**, *15*, 357–364.
- (155) Williams, R. *Journal of inorganic biochemistry* **2012**, *111*, 104–109.
- (156) Feig, A. L.; Uhlenbeck, O. C. *COLD SPRING HARBOR MONOGRAPH SERIES* **1999**, *37*, 287–320.
- (157) Lawless, J. G.; Levi, N. *Journal of molecular evolution* **1979**, *13*, 281–286.
- (158) Da Silva, J. F.; Williams, R. J. P., *The biological chemistry of the elements: the inorganic chemistry of life*; Oxford University Press: 2001.
- (159) Williams, R. J. *Biological Reviews* **1953**, *28*, 381–412.
- (160) Highberger, J.; Savage, C; Biegging, J.; Ziurys, L. *The Astrophysical Journal* **2001**, *562*, 790.
- (161) Ruf, A.; Kanawati, B.; Hertkorn, N.; Yin, Q.-Z.; Moritz, F.; Harir, M.; Lucio, M.; Michalke, B.; Wimpenny, J.; Shilobreeva, S.; Bronsky, B.; Saraykin, V.; Gabelica, Z.; Gougeon, R. D.; Quirico, E.; Ralew, S.; Jakubowski, T.; Haack, H.; Gonsior, M.; Jenniskens, P.; Hinman, N. W.; Schmitt-Kopplin, P. *Proceedings of the National Academy of Sciences* **2017**, *114*, 2819–2824, DOI: 10.1073/pnas.1616019114.
- (162) Burton, A. S.; Stern, J. C.; Elsila, J. E.; Glavin, D. P.; Dworkin, J. P. *Chemical Society Reviews* **2012**, *41*, 5459–5472.
- (163) Ehrenfreund, P.; Glavin, D. P.; Botta, O.; Cooper, G.; Bada, J. L. *Proceedings of the National Academy of Sciences* **2001**, *98*, 2138–2141.
- (164) Elschenbroich, C.; Salzer, A., *Organometallics; VCH: New York, 1989*.
- (165) Khairallah, G. N.; Thum, C. C.; Lesage, D.; Tabet, J.-C.; O’Hair, R. A. *Organometallics* **2013**, *32*, 2319–2328.
- (166) Bock, C. W.; Kaufman, A.; Glusker, J. P. *Inorganic Chemistry* **1994**, *33*, 419–427.
- (167) Hazen, R. M.; Jones, A. P.; Baross, J. A. **2013**.
- (168) Ferralis, N.; Matys, E. D.; Knoll, A. H.; Hallmann, C.; Summons, R. E. *Carbon* **2016**, *108*, 440–449.
- (169) Johnson, N. M.; Elsila, J. E.; Kopstein, M.; Nuth, J. A. *Meteoritics & Planetary Science* **2012**, *47*, 1029–1034.
- (170) Hill, H. G.; Grady, C. A.; Nuth, J. A.; Hallenbeck, S. L.; Sitko, M. L. *Proceedings of the National Academy of Sciences* **2001**, *98*, 2182–2187.
- (171) Irving, A. J.; Kuehner, S. M.; Bunch, T. E.; Ziegler, K.; Chen, G.; Herd, C. D. K.; Conrey, R. M.; Ralew, S. In *Lunar and Planetary Science Conference*, 2013; Vol. 44, p 2164.
- (172) Summons, R. E.; Albrecht, P.; McDonald, G.; Moldowan, J. M. *Space Science Reviews* **2008**, *135*, 133–159.
- (173) Wakil, S. J. *Biochemistry* **1989**, *28*, 4523–4530.
- (174) Cheng, C.; Gross, M. L. *Mass spectrometry reviews* **2000**, *19*, 398–420.
- (175) Dove, A. P.; Gibson, V. C.; Hormnirun, P.; Marshall, E. L.; Segal, J. A.; White, A. J.; Williams, D. J. *Dalton Transactions* **2003**, 3088–3097.
- (176) Stary, J.; Liljenzin, J. O. *Pure and applied chemistry* **1982**, *54*, 2557–2592.
- (177) Huss, G. R.; Rubin, A. E.; Grossman, J. N. *Meteorites and the early solar system II* **2006**, 567–586.
- (178) Martins, Z.; Modica, P.; Zanda, B.; d’Hendecourt, L. L. S. *Meteoritics & Planetary Science* **2015**, *50*, 926–943.
- (179) Rubin, A. E. *Meteoritics & Planetary Science* **2006**, *41*, 125–133.

Bibliography

- (180) Black, J. R.; Yin, Q.-z.; Casey, W. H. *Geochimica et cosmochimica acta* **2006**, *70*, 4072–4079.
- (181) Wimpenny, J.; Colla, C. A.; Yin, Q.-Z.; Rustad, J. R.; Casey, W. H. *Geochimica et Cosmochimica Acta* **2014**, *128*, 178–194.
- (182) Hazen, R. M.; Filley, T. R.; Goodfriend, G. A. *Proceedings of the National Academy of Sciences* **2001**, *98*, 5487–5490.
- (183) Williams, R. J. *BioMetals* **2007**, *20*, 107–112.
- (184) Martin, W.; Russell, M. J. *Philosophical Transactions of the Royal Society of London B: Biological Sciences* **2003**, *358*, 59–85.
- (185) Saladino, R.; Botta, G.; Bizzarri, B. M.; Di Mauro, E.; Garcia Ruiz, J. M. *Biochemistry* **2016**, *55*, 2806–2811.
- (186) Witt, M.; Roesky, H. W. *Curr. Sci* **2000**, *78*, 410–430.
- (187) Rehder, D. *Organic & biomolecular chemistry* **2008**, *6*, 957–964.
- (188) Rappoport, Z.; Marek, I., *The Chemistry of Organomagnesium Compounds, 2 Volume Set*; John Wiley & Sons: 2008; Vol. 173.
- (189) The Nobel Prize in Chemistry 1912., http://www.nobelprize.org/nobel_prizes/chemistry/laureates/1912/ (accessed 06/05/2017).
- (190) The Nobel Prize in Chemistry 2001., http://www.nobelprize.org/nobel_prizes/chemistry/laureates/2001/ (accessed 06/05/2017).
- (191) Frankland, E; Ann, J. L. *J. Chem. Soc* **1850**, *2*, 263–296.
- (192) Grignard, V *Ann. Chim* **1901**, *24*, 433–490.
- (193) Shirley, D. A. *Organic reactions* **1954**.
- (194) Astruc, D., *Organometallic chemistry and catalysis*; Springer: 2007; Vol. 291.
- (195) Hartwig, J. F. *Nature* **2008**, *455*, 314–322.
- (196) Kaim, W.; Schwederski, B.; Klein, A., *Bioinorganic Chemistry–Inorganic Elements in the Chemistry of Life: An Introduction and Guide*; John Wiley & Sons: 2013.
- (197) Haiech, J.; Derancourt, J.; Pechere, J. F.; Demaille, J. G. *Biochemistry* **1979**, *18*, 2752–2758.
- (198) Rosenzweig, A.; Frederick, C.; Lippard, S.; Nordlund, P *Nature* **1993**, *366*, 537–543.
- (199) Sousa, S. F.; Fernandes, P. A.; Ramos, M. J. *Journal of the American Chemical Society* **2007**, *129*, 1378–1385.
- (200) Ducháčková, L.; Schröder, D.; Roithová, J. *Inorganic chemistry* **2011**, *50*, 3153–3158.
- (201) Andersson, I. *Journal of experimental botany* **2008**, *59*, 1555–1568.
- (202) Khairallah, G. N.; Thum, C. C.; Lesage, D.; Tabet, J.-C.; O’Hair, R. A. *Organometallics* **2013**, *32*, 2319–2328.
- (203) Chamorro, E.; Duque-Noreña, M.; Pérez, P. *Journal of Molecular Structure: THEOCHEM* **2009**, *896*, 73–79.
- (204) Van Klink, G. P.; de Boer, H. J.; Schat, G.; Akkerman, O. S.; Bickelhaupt, F.; Spek, A. L. *Organometallics* **2002**, *21*, 2119–2135.
- (205) Murray, R. E.; Walter, E. L.; Doll, K. M. *ACS Catalysis* **2014**, *4*, 3517–3520.
- (206) Le Saux, T.; Plasson, R.; Jullien, L. *Chemical Communications* **2014**, *50*, 6189–6195.
- (207) Schlesener, C.; Amatore, C; Kochi, J. *Journal of the American Chemical Society* **1984**, *106*, 3567–3577.
- (208) Summons, R. E.; Albrecht, P.; McDonald, G.; Moldowan, J. M. *Space Science Reviews* **2008**, *135*, 133–159.
- (209) Řezanka, T.; Sigler, K. *Progress in lipid research* **2009**, *48*, 206–238.
- (210) Deamer, D.; Chakrabarti, A *Handbook of non-medical Applications of Liposomes. Models for Biological Phenomena*, *2*, 303–313.

Bibliography

- (211) Luisi, P. L.; Varela, F. J. *Origins of Life and Evolution of Biospheres* **1989**, *19*, 633–643.
- (212) Georgiou, C. D.; Deamer, D. W. *Astrobiology* **2014**, *14*, 541–549.
- (213) Deamer, D. W. *Origins of Life and Evolution of Biospheres* **1986**, *17*, 3–25.
- (214) Dworkin, J. P.; Deamer, D. W.; Sandford, S. A.; Allamandola, L. J. *Proceedings of the National Academy of Sciences* **2001**, *98*, 815–819.
- (215) Deamer, D. W. *Nature* **1985**, *317*, 792–794.
- (216) Deamer, D. W.; Pashley, R. *Origins of Life and Evolution of the Biosphere* **1989**, *19*, 21–38.
- (217) Hazen, R. M.; Deamer, D. W. *Origins of Life and Evolution of Biospheres* **2007**, *37*, 143–152.
- (218) Tao, F.; Bernasek, S. L. *Chemical reviews* **2007**, *107*, 1408–1453.
- (219) Pizzarello, S. *Origins of Life and Evolution of Biospheres* **2004**, *34*, 25–34.
- (220) Hinkle, K. W.; Keady, J. J.; Bernath, P. F. *Science* **1988**, *241*, 1319.
- (221) Bernath, P. F.; Hinkle, K. H.; Keady, J. J. *Science* **1989**, 562–564.
- (222) Li, G.; Tang, Z. *The Journal of Physical Chemistry A* **2003**, *107*, 5317–5326.
- (223) Redondo, P.; Barrientos, C.; Cimas, A.; Largo, A. *The Journal of Physical Chemistry A* **2003**, *107*, 6317–6325.
- (224) Qi, J.; Chen, M.; Wu, W.; Zhang, Q.; Au, C. *Chemical Physics* **2009**, *364*, 31–38.
- (225) Schmitt-Kopplin, P.; Harir, M.; Kanawati, B.; Tziozis, D.; Hertkorn, N.; Gabelica, Z. *Meteorites* **2012**, *2*.
- (226) Grimme, S.; Antony, J.; Ehrlich, S.; Krieg, H. *The Journal of chemical physics* **2010**, *132*, 154104.
- (227) Zhao, Y.; Truhlar, D. G. *Theoretical Chemistry Accounts: Theory, Computation, and Modeling (Theoretica Chimica Acta)* **2008**, *120*, 215–241.
- (228) Grimme, S.; Steinmetz, M. *Physical Chemistry Chemical Physics* **2013**, *15*, 16031–16042.
- (229) Frisch, M. J.; Trucks, G. W.; Schlegel, H. B.; Scuseria, G. E.; Robb, M. A.; Cheeseman, J. R.; Montgomery Jr., J. A.; Vreven, T.; Kudin, K. N.; Burant, J. C.; Millam, J. M.; Iyengar, S. S.; Tomasi, J.; Barone, V.; Mennucci, B.; Cossi, M.; Scalmani, G.; Rega, N.; Petersson, G. A.; Nakatsuji, H.; Hada, M.; Ehara, M.; Toyota, K.; Fukuda, R.; Hasegawa, J.; Ishida, M.; Nakajima, T.; Honda, Y.; Kitao, O.; Nakai, H.; Klene, M.; Li, X.; Knox, J. E.; Hratchian, H. P.; Cross, J. B.; Bakken, V.; Adamo, C.; Jaramillo, J.; Gomperts, R.; Stratmann, R. E.; Yazyev, O.; Austin, A. J.; Cammi, R.; Pomelli, C.; Ochterski, J. W.; Ayala, P. Y.; Morokuma, K.; Voth, G. A.; Salvador, P.; Dannenberg, J. J.; Zakrzewski, V. G.; Dapprich, S.; Daniels, A. D.; Strain, M. C.; Farkas, O.; Malick, D. K.; Rabuck, A. D.; Raghavachari, K.; Foresman, J. B.; Ortiz, J. V.; Cui, Q.; Baboul, A. G.; Clifford, S.; Cioslowski, J.; Stefanov, B. B.; Liu, G.; Liashenko, A.; Piskorz, P.; Komaromi, I.; Martin, R. L.; Fox, D. J.; Keith, T.; Al-Laham, M. A.; Peng, C. Y.; Nanayakkara, A.; Challacombe, M.; Gill, P. M. W.; Johnson, B.; Chen, W.; Wong, M. W.; Gonzalez, C.; Pople, J. A. Gaussian 03, revision c. 02; Gaussian., \uppercaseGaussian, Inc., Wallingford, CT, 2004.
- (230) Foresman, J. B.; Frisch, A., *Exploring chemistry with electronic structure methods: a guide to using Gaussian*; Gaussian, Incorporated: 1993.
- (231) Jensen, F. *The Journal of chemical physics* **2002**, *117*, 9234–9240.
- (232) Schlegel, H. B. *Journal of Computational Chemistry* **1982**, *3*, 214–218.
- (233) Schlegel, H. B. *Theoretica chimica acta* **1984**, *66*, 333–340.
- (234) Császár, P.; Pulay, P. *Journal of Molecular Structure* **1984**, *114*, 31–34.
- (235) Kanawati, B.; Joniec, S.; Winterhalter, R.; Moortgat, G. K. *International Journal of Mass Spectrometry* **2007**, *266*, 97–113.
- (236) Gabelica, V.; Galic, N.; Rosu, F.; Houssier, C.; De Pauw, E. *Journal of mass spectrometry* **2003**, *38*, 491–501.

Bibliography

- (237) Davis, A. M., *Meteorites, Comets, and Planets: Treatise on Geochemistry, Second Edition*, en; Elsevier: Nov. 2005.
- (238) Lucio, M.; Fekete, A.; Frommberger, M.; Schmitt-Kopplin, P. *Handbook of Molecular Microbial Ecology I: Metagenomics and Complementary Approaches* **2011**, 683–695.
- (239) Jacobsen, B.; Yin, Q.-z.; Moynier, F.; Amelin, Y.; Krot, A. N.; Nagashima, K.; Hutcheon, I. D.; Palme, H. en *Earth and Planetary Science Letters* **July 2008**, *272*, 353–364, DOI: 10.1016/j.epsl.2008.05.003.
- (240) Young, E. D.; Galy, A. *Reviews in Mineralogy and Geochemistry* **2004**, *55*, 197–230.
- (241) Galy, A.; Yoffe, O.; Janney, P. E.; Williams, R. W.; Cloquet, C.; Alard, O.; Halicz, L.; Wadhwa, M.; Hutcheon, I. D.; Ramon, E.; Carignan, J. en *Journal of Analytical Atomic Spectrometry* **2003**, *18*, 1352, DOI: 10.1039/b309273a.
- (242) Li, W.-Y.; Teng, F.-Z.; Ke, S.; Rudnick, R. L.; Gao, S.; Wu, F.-Y.; Chappell, B. W. *Geochimica et Cosmochimica Acta* **2010**, *74*, 6867–6884.
- (243) Bourdon, B.; Tipper, E. T.; Fitoussi, C.; Stracke, A. *Geochimica et Cosmochimica Acta* **2010**, *74*, 5069–5083.
- (244) Frisch, M. J.; Trucks, G. W.; Schlegel, H. B.; Scuseria, G. E.; Robb, M. A.; Cheeseman, J. R.; Scalmani, G.; Barone, V.; Mennucci, B.; Petersson, G. A.; Nakatsuji, H.; Caricato, M.; Li, X.; Hratchian, H. P.; Izmaylov, A. F.; Bloino, J.; Zheng, G.; Sonnenberg, J. L.; Hada, M.; Ehara, M.; Toyota, K.; Fukuda, R.; Hasegawa, J.; Ishida, M.; Nakajima, T.; Honda, Y.; Kitao, O.; Nakai, H.; Vreven, T.; Montgomery Jr., J. A.; Peralta, J. E.; Ogliaro, F.; Bearpark, M.; Heyd, J. J.; Brothers, E.; Kudin, K. N.; Staroverov, V. N.; Kobayashi, R.; Normand, J.; Raghavachari, K.; Rendell, A.; Burant, J. C.; Iyengar, S. S.; Tomasi, J.; Cossi, M.; Rega, N.; Millam, J. M.; Klene, M.; Knox, J. E.; Cross, J. B.; Bakken, V.; Adamo, C.; Jaramillo, J.; Gomperts, R.; Stratmann, R. E.; Yazyev, O.; Austin, A. J.; Cammi, R.; Pomelli, C.; Ochterski, J. W.; Martin, R. L.; Morokuma, K.; Zakrzewski, V. G.; Voth, G. A.; Salvador, P.; Dannenberg, J. J.; Dapprich, S.; Daniels, A. D.; Farkas, O.; Foresman, J. B.; Ortiz, J. V.; Cioslowski, J.; Fox, D. J. Gaussian 09 Revision A.1., Gaussian Inc. Wallingford CT 2009.
- (245) Gonzalez, C; Schlegel, H. *The Journal of Chemical Physics* **1989**, *90*, 2154, DOI: 10.1063/1.456010.
- (246) Gonzalez, C; Schlegel, H. *Journal of Physical Chemistry* **1990**, *94*, 5523, DOI: 10.1021/j100377a021.
- (247) Dennington, R.; Keith, T. A.; Millam, J. M. GaussView Version 3., Semichem Inc. Shawnee Mission KS, 2016.

List of Figures

1.1. Sketching chemical evolution in terms of molecular diversity and molecular complexity	5
1.2. Classification of meteorites	8
1.3. Model of molecular structure of Murchison insoluble organic matter	10
1.4. van Krevelen diagram of Murchison soluble organic matter	13
1.5. Mass difference network of Murchison soluble organic matter	14
1.6. Model of molecular structure of Murchison soluble organic matter	15
1.7. Curiosity-driven research	17
1.8. Metal distributions for meteorites, Earth and a biological system	21
1.9. Outline of this thesis	24
2.1. Elemental analysis of meteorites	27
2.2. Detection of the CHOMg chemical space	28
2.3. Isotopic fine structure for the molecule ion $[C_{16}H_{33}MgO_4]^-$	29
2.4. Characteristics of the CHOMg chemical space	30
2.5. Complexity of the CHOMg chemical space	31
2.6. Fragmentation experiments to characterize dihydroxymagnesium carboxylates	33
2.7. Characterization of dihydroxymagnesium carboxylates	34
2.8. General CHOMg reactivity and verification of DFT simulations with MP2 level of theory	35
2.9. Mass difference networks, presenting the chemical complexity/reactivity of the CHOMg space	36
2.10. Relationship of CHOMg signatures with different thermal processing stages of meteorites	38
2.11. Van Krevelen diagrams for the comparison of CHO and CHOMg compositions for several meteorites and modified van Krevelen diagrams representing the thermal metamorphism signature	40
2.12. Simulated thermal metamorphism of Murchison and CHOMg-based shock stage differentiation	41
2.13. Crust-core comparison and their influences on the CHOMg synthesis and dependency of CHOMg formulas on the aqueous alteration	42
3.1. Schematic representation of spatial chemical differences within dihydroxymagnesium carboxylates	47
3.2. Potential energy curve of CO_2 fragmentations out of dihydroxymagnesium carboxylates	48
3.3. Chain length dependence of $[(OH)_2MgO_2CR]^-$ ecarboxylation	49
3.4. Charge population analysis of the C_5 dihydroxymagnesium carboxylate transition state #2	51
3.5. Charge population analysis of putative Grignard-type OH- and Cl-bearing molecules	52
4.1. Odd/even alternation within meteoritic (metal)organic matter	58
4.2. Computed alkyl chain fragmentation out of CHOMg	59

List of Figures

4.3. Pseudocyclization of dihydroxymagnesium carboxylates	60
4.4. Pseudocyclic geometries for odd and even CHOMg species	61
4.5. Distribution of fatty acids and their organomagnesium counterparts	62
C.1. Data analysis of experimental meteoritic FT-ICR-MS data	111

List of Tables

1.1. Molecules in the Interstellar Medium or Circumstellar Shells	3
A.1. Information on 61 meteorite samples, used in the statistical analysis	74
A.2. Mass list of significantly enriched compounds in thermal processed meteorites	77
A.3. Coordinates of the relaxed, computed geometries - C ₁₆ -dihydroxymagnesium carboxylate	94
A.4. Coordinates of the relaxed, computed geometries - C ₁₆ -carboxylate	95
A.5. Coordinates of the relaxed, computed geometries - C ₅ -dihydroxymagnesium carboxylate	97
B.1. Coordinates of the relaxed geometries of bidentate C ₇ -dihydroxymagnesium carboxylate	100
B.2. Coordinates of the relaxed geometries of the transition state of the coordi- nate switch from bi- and monodentate C ₇ -dihydroxymagnesium carboxylate	101
B.3. Coordinates of the relaxed geometries of monodentate C ₇ -dihydroxymagnesium carboxylate	102
B.4. Coordinates of the relaxed geometries of the transition state of decarboxy- lation of C ₇ -dihydroxymagnesium carboxylate	102
B.5. Coordinates of the relaxed geometries of C ₆ -dihydroxyorganomagnesate . .	103
B.6. Coordinates of the relaxed geometries of CO ₂	104
B.7. Summary of Natural Population Analysis (NBO) for C ₅ -dihydroxymagnesium carboxylate	105
B.8. Summary of Natural Population Analysis (NBO) for C ₅ -dihydroxymagnesium organomagnesate	106
B.9. Summary of Natural Population Analysis (NBO) for C ₅ -organomagnesiumhydroxid	107
B.10. Summary of Natural Population Analysis (NBO) for C ₅ -dichloromagnesium organomagnesate	107
B.11. Summary of Natural Population Analysis (NBO) for C ₅ -organomagnesiumchlorid	108
C.1. Coordinates of the relaxed geometry of pseudocyclic C ₁₄ -dihydroxymagnesium carboxylate	114
C.2. Coordinates of the relaxed geometry of pseudocyclic C ₁₅ -dihydroxymagnesium carboxylate	115
C.3. Coordinates of the relaxed geometry of linear C ₁₄ -dihydroxymagnesium car- boxylate	116
C.4. Coordinates of the relaxed geometry of linear C ₁₅ -dihydroxymagnesium car- boxylate	117
C.5. Coordinates of the relaxed geometry of methylene CH ₂	118
C.6. Coordinates of the relaxed geometry of ethylene C ₂ H ₄	118
C.7. Coordinates of the transition state geometry of ethylene C ₂ H ₄ release out of C ₅ -dihydroxymagnesium carboxylate	119

Eidesstattliche Erklärung

Ich erkläre an Eides statt, dass ich die bei der promotionsführenden Einrichtung Wissenschaftszentrum Weihenstephan für Ernährung, Landnutzung und Umwelt der Technischen Universität München zur Promotionsprüfung vorgelegte Arbeit mit dem Titel:

Previously unknown organomagnesium compounds in astrochemical context
in Chemie am Lehrstuhl für Analytische Lebensmittelchemie unter der Anleitung und Betreuung durch apl.-Prof. Dr. Dr. Philippe Schmitt-Kopplin ohne sonstige Hilfe erstellt und bei der Abfassung nur die gemäß § 6 Abs. 6 und 7 Satz 2 angegebenen Hilfsmittel benutzt habe.

(x) Ich habe keine Organisation eingeschaltet, die gegen Entgelt Betreuerinnen und Betreuer für die Anfertigung von Dissertationen sucht, oder die mir obliegenden Pflichten hinsichtlich der Prüfungsleistungen für mich ganz oder teilweise erledigt.

(x) Ich habe die Dissertation in dieser oder ähnlicher Form in keinem anderen Prüfungsverfahren als Prüfungsleistung vorgelegt.

(x) Ich habe den angestrebten Doktorgrad noch nicht erworben und bin nicht in einem früheren Promotionsverfahren für den angestrebten Doktorgrad endgültig gescheitert.

Die öffentlich zugängliche Promotionsordnung der TUM ist mir bekannt, insbesondere habe ich die Bedeutung von § 28 (Nichtigkeit der Promotion) und § 9 (Entzug des Doktorgrades) zur Kenntnis genommen. Ich bin mir der Konsequenzen einer falschen eidesstattlichen Erklärung bewusst.

München, den 12.03.2018

A handwritten signature in black ink, appearing to be 'Klaus J.', written in a cursive style.

Short curriculum vitae - Alexander Ruf

PERSONAL DETAILS

Date of birth 31/10/1986
Place of birth Neuburg an der Donau
Nationality German
Affiliation Postdoctoral Researcher /
Aix-Marseille Université (AMU)
Contact a.ruf@tum.de, google scholar



POSITIONS

from 04/2018

Postdoctoral Researcher at Aix-Marseille Université (AMU), research group "Astrochimie, Spectroscopie, Théorie, Réactivité, Origine", Grégoire Danger

09/2009 - 02/2010

Internship in NMR and MS analytics with supervision of an apprentice at Sanofi-Aventis Deutschland GmbH, Abteilung R&D CAS Discovery Analytics FFM, Frankfurt am Main

07/2008 - 09/2008

Chemical lab assistant in analytical chemistry at SystemKosmetik GmbH, Münster am Lech, research group

08/2007 - 09/2007

Chemical lab assistant in organometallic synthesis at Huntsman Textile Effects (Germany) GmbH, research & development group silicones, Langweid am Lech

07/2006 - 08/2006

Chemical lab assistant in organometallic synthesis at Huntsman Textile Effects (Germany) GmbH, research & development group silicones, Langweid am Lech

09/2003 - 06/2006

Apprenticeship as chemical lab assistant at Ciba Spezialitätenchemie Pfersee GmbH, Langweid am Lech

STUDIES

11/2013 - 12/2017

Ph.D. in Chemistry, Helmholtz Zentrum München/Technical University of Munich, Advisor apl. Prof. Dr. P. Schmitt-Kopplin (thesis title: Previously unknown organomagnesium compounds in astrochemical context)

10/2012 - 03/2014

Participation at Linear Algebra for physicists and Analysis 1-3 for physicists, Technical University of Munich

10/2012 - 03/2013

Introduction to philosophy of Karl R. Popper, Technical University of Munich

10/2011 - 09/2013

Master of Science in Chemistry (M.Sc.), Technical University of Munich (major subject: physical chemistry, minor subject: theoretical chemistry, thesis title: Enhancing detection sensitivity in mass spectrometry by anionic dopants)

09/2007 - 08/2011

Undergraduate studies in Chemistry (B.Sc.), University of Applied Science Aalen (major subject: analytical chemistry, accredited studies by ZEvA, thesis title: Optimization of methods for studying the metabolome of *Caenorhabditis elegans*)

TEACHING

2012/13

- Tutorial **physical chemistry** (chemical thermodynamics and kinetics, undergraduate level), Technical University of Munich
- Practical course **inorganic chemistry** (undergraduate level), Technical University of Munich

2011/12

- Tutorial **physical chemistry** (chemical thermodynamics and kinetics, undergraduate level), Technical University of Munich
- Practical course **inorganic chemistry** (undergraduate level), Technical University of Munich
- Tutorial **physical chemistry** (chemical thermodynamics and kinetics, undergraduate level) Technical University of Munich
- Practical course **inorganic chemistry** (undergraduate level), Technical University of Munich

2008/09

- Seminar practical course **experimental physics** (undergraduate level), Hochschule für Technik und Wirtschaft Aalen

A handwritten signature in black ink, appearing to be 'And J'.